



University  
of Glasgow

Alotaiq, Nasser Abdullah S. (2019) *Cavin-1-mediated regulation of suppressor of cytokine signalling 3 (SOCS3) function*. PhD thesis.

<https://theses.gla.ac.uk/8875/>

Copyright and moral rights for this work are retained by the author

A copy can be downloaded for personal non-commercial research or study, without prior permission or charge

This work cannot be reproduced or quoted extensively from without first obtaining permission in writing from the author

The content must not be changed in any way or sold commercially in any format or medium without the formal permission of the author

When referring to this work, full bibliographic details including the author, title, awarding institution and date of the thesis must be given

Enlighten: Theses

<https://theses.gla.ac.uk/>  
[research-enlighten@glasgow.ac.uk](mailto:research-enlighten@glasgow.ac.uk)



**CAVIN-1-MEDIATED REGULATION OF SUPPRESSOR OF  
CYTOKINE SIGNALLING 3 (SOCS3) FUNCTION**

by

NASSER ABDULLAH S ALOTAIQ, M.Sc.

THESIS SUBMITTED IN FULFILMENT OF THE REQUIREMENTS FOR THE DEGREE OF  
*Doctor of Philosophy*

SCHOOL OF MEDICAL, VETERINARY AND LIFE SCIENCES  
INSTITUTE OF CARDIOVASCULAR AND MEDICAL SCIENCES  
UNIVERSITY OF GLASGOW

JANUARY 2019

## Summary

A distinctive feature of many cell types, such as endothelial cells (ECs), is abundant population of small plasma membrane invaginations termed caveolae. These structures represent a distinct membrane microenvironment that are involved in regulating multiple signalling pathways. Several diseases in human, such as heart failure, degenerative muscular illness, and vascular diseases, might result due to the disruption of caveolar integrity. The main caveolar structural membrane protein is cavin-1 and it has been shown to play a major role in caveolae assembly as shown by caveolae destabilisation due to cavin-1 deletion. However, the exact cellular process that regulate the functionality of cavin-1 has not been fully elucidated. One of the signalling pathways that have been found localised and distributed within caveolae is the JAK/STAT signalling, which is downregulated via the suppressor of cytokine signalling-3 (SOCS3). Studies based on proteomic screening and biochemical analysis have revealed an interaction between cavin-1 and SOCS3. As such, we hypothesised that SOCS3/cavin-1 interaction is an important controlling element in caveolae stability and/or the pro-inflammatory signalling pathway mediated by IL-6 in the endothelial cells. In support of this hypothesis, cavin-1 protein levels were significantly reduced in SOCS3<sup>-/-</sup> murine embryonic fibroblasts (MEFs) and human endothelial angiosarcoma (AS-M.5) cells compared with their WT counterparts in the absence of any changes in cavin-1 mRNA. This was associated with a reduced stability of the cavin-1 protein in SOCS3<sup>-/-</sup> AS-M.5 cells (t<sub>1/2</sub>=3 hr) versus WT AS-M.5 cells (t<sub>1/2</sub>>8 hr), significantly reduced levels of caveolin-1 and a parallel decrease in the number of caveolae detectable in SOCS3<sup>-/-</sup> MEFs and AS-M.5 cells by transmission electron microscopy. Confocal imaging experiments also revealed that cavin-1 was required for SOCS3 localisation to the plasma membrane and effective SOCS3-mediated inhibition of IL-6 signalling. Our data suggest a novel role for SOCS3 in regulating caveolae assembly while cavin-1, acting as a scaffold-protein, might aid SOCS3-dependent regulation of JAK/STAT signalling. This is the first indication of a novel role for SOCS3 in caveola homeostasis and suggests that loss of caveolae represents a novel mechanism by which chronic activation of pro-inflammatory JAK/STAT signalling could be triggered in disease. Together, these data demonstrate an important interaction between cavin-1 and SOCS3 responsible for reciprocal regulation of their respective functions.

# Table of Contents

<b>Summary</b>	<b>I</b>
<b>List of Tables</b>	<b>IV</b>
<b>List of Figures</b>	<b>V</b>
<b>Acknowledgements</b>	<b>VII</b>
<b>Author's Declaration</b>	<b>VIII</b>
<b>Abbreviations</b>	<b>IX</b>
<b>1 Introduction</b>	<b>1</b>
1.1 <i>Plasma membrane organisation and function</i>	1
1.1.1 Lipid rafts	1
1.2 <i>Caveolae</i>	4
1.2.1 Caveolins	6
1.2.2 Cavins	12
1.2.3 Caveolae biogenesis	23
1.2.4 Functions of caveolae	26
1.2.5 Potential caveolae-targeting therapeutics	32
1.3 <i>Cytokine Signalling</i>	33
1.3.1 The JAK/STAT pathway and its regulation	36
1.3.2 Suppressor of cytokine signalling proteins	39
1.4 <i>SOCS3</i>	43
1.4.1 SOCS3 structure	45
1.4.2 SOCS3 expression and regulation	48
1.4.3 SOCS3 as an inhibitory protein through KIR-JAK2 interaction	49
1.4.4 SOCS3 and E3 Ubiquitin Ligase activity	49
1.4.5 Identifying cavin-1 as an interactor SOCS-3	51
1.5 <i>Hypothesis</i>	55
1.6 <i>Aims</i>	55
<b>2 Materials and Methods</b>	<b>57</b>
2.1 <i>Materials</i>	57
2.2 <i>Methods</i>	63
2.2.1 Cell culture	63
2.2.2 Protein concentration determination	64
2.2.3 SDS-Polyacrylamide Gel Electrophoresis	65
2.2.4 Immunoblotting for proteins	66
2.2.5 Cell Transfection	69
2.2.6 RNA Extraction, Purification and Quantification	70
2.2.7 Ultrastructural analysis	72
2.2.8 Immunofluorescent Confocal Microscopy	73
2.2.9 Production of SOCS3 Knockout AS-M.5 via CRISPR	74
2.2.10 Statistical analysis	76
<b>3 Generation and characterisation of endothelial SOCS3KO cells for the further examination of the working hypothesis</b>	<b>77</b>
3.1 <i>Perturbation of Target Gene Expression</i>	77

3.1.1	Advances in the development of the CRISPR/Cas9 system	80
3.1.2	Experimental cell lines	81
3.1.3	Aims	82
3.2	<i>Results and discussion</i>	82
3.2.1	CRISPR/Cas9 Constructs	83
3.2.2	Transfection of CRISPR/Cas9 Constructs	85
3.2.3	Puromycin selection	87
3.2.4	Cell assay to confirm complete allelic knockouts	89
3.2.5	Phenotypic Differences in SOCS3 <sup>-/-</sup> Endothelial Cells	89
3.3	<i>Conclusion</i>	94
<b>4</b>	<b>Characterisation of cavin-1/SOCS3 interaction</b>	<b>95</b>
4.1	<i>Introduction</i>	95
4.1.1	Aims	96
4.2	<i>The effect of SOCS3 on cavin-1 stability in fibroblasts and endothelial cells</i>	96
4.3	<i>The effect of SOCS3 induction by cAMP elevation on cavin-1</i>	103
4.3.1	SOCS3 induction by cAMP stabilises cavin-1	104
4.3.2	Examining cAMP-dependent regulation of cavin-1	107
4.3.3	Examining phosphorylation status of cavin-1 following cAMP elevation	111
4.4	<i>Discussion</i>	113
4.4.1	Role of SOCS3 in stabilising cavin-1	113
4.4.2	Role of cAMP elevation in cavin-1 stabilisation	113
<b>5</b>	<b>Functional investigation of cavin-1/SOCS3 interaction</b>	<b>115</b>
5.1	<i>Introduction</i>	115
5.1.1	Aims	116
5.2	<i>Results</i>	116
5.2.1	Effect of SOCS3 deletion on caveolae abundance	116
5.2.2	Using confocal microscopy to characterise SOCS3/cavin-1 interaction	123
5.2.3	Examining SOCS3 and cavin-1 in lipid rafts Isolated from WT and Cavin-1 KO MEFs	134
5.2.4	Characterisation the regions within SOCS3 that interact with cavin-1	136
5.3	<i>Investigating roles for cavin-1 in regulating pro-inflammatory IL-6 signalling</i>	139
5.4	<i>Discussion</i>	145
<b>6.</b>	<b>Final Discussion</b>	<b>150</b>
6.1	<i>Therapeutic possibilities</i>	152
6.1.1	Modulation of caveolae	152
6.1.2	Regulation of JAK–STAT signalling pathway	154
6.2	<i>Limitations of the study</i>	157
6.3	<i>Future work</i>	157
	<b>Appendices</b>	<b>158</b>
	<b>References</b>	<b>159</b>

## List of Tables

Table 1–1: Known SOCS3 substrates	52
Table 2–1 List of general materials and reagents	57
Table 2–2 Reagents and materials used in cell culture applications	59
Table 2–3 Plasmid constructs	61
Table 2–4 Primary antibodies used for western blotting	61
Table 2–5 Secondary detection agents for western blotting	62
Table 2–6 Resolving gel components	66
Table 2–7 Stacking gel components	66
Table 2–8 List of primer sequences used for qRT-PCR analysis in this study	72
Table 3–1 Guide RNA sequences used for constructing knockout cells.	83

## List of Figures

Figure 1–1: The morphology and composition of caveolae. ....	5
Figure 1–2: The different subdomains of caveolin proteins. ....	7
Figure 1–3: The basic structures and posttranslational modifications of CAV-1 and CAV-3. ....	8
Figure 1–4: Cavin family proteins ....	13
Figure 1–5: Caveolae biogenesis. ....	25
Figure 1–6: Caveola-Mediated Endocytosis. ....	28
Figure 1–7: The role of cytokines during atherosclerosis development. ....	34
Figure 1–8: A schematic representation of the JAK/STAT pathway. ....	38
Figure 1–9: The structural domains of the SOCS family proteins and their perceived interaction in cellular signalling. ....	41
Figure 1–10: Inhibition of IL-6 signalling via SOCS3. ....	44
Figure 1–11: Structural organisation of the SOCS3 domains ....	45
Figure 1–12: WT and SOCS3 <sup>-/-</sup> MEFs proteomics screen. ....	54
Figure 2–1 Flowchart outlining the experimental procedures to generate SOCS3 KO AS-M.5 cell lines. ....	75
Figure 3–1 Nuclease-induced genome editing ....	79
Figure 3–2: Design of the CRISPR/CAS9 system for SOCS3 gene deletion. ....	84
Figure 3–3: Fluorescence expression in AS-M.5 cells transfected with a CRISPR/Cas9 plasmid that expresses enhanced GFP. ....	86
Figure 3–4: The effect of puromycin treatment on CRISPR/Cas9-transfected AS-M.5 cells. ....	88
Figure 3–5 CRISPR/Cas9 mediated disruption of SOCS3 locus generated complete gene knockouts. ....	91
Figure 3–6 Immunoblot screening of CRISPR/Cas9-mediated SOCS3 gene knockout in AS-M.5 cells ....	92
Figure 3–7 Phase contrast photomicrographs of the parental AS-M.5 human angiosarcoma-derived ECs and clonal cell lines in culture. ....	93
Figure 4–1 SOCS3 deletion significantly reduces endogenous protein levels of cavin-1 and caveolin-1 in AS-M.5 cells. ....	99
Figure 4–2 SOCS3 deletion significantly reduces endogenous protein levels of cavin-1 and caveolin-1 in MEFs. ....	100

Figure 4–3 Real-time qPCR revealed that the mRNA expression level of cavin-1 is significantly increased in SOCS3 <sup>-/-</sup> MEFs as compared to WT (SOCS3 <sup>+/+</sup> ) controls. ....	101
Figure 4–4 Destabilisation of cavin-1 in SOCS3- deficient endothelial cells.....	102
Figure 4–5 The effect of SOCS3 deletion on Fsk-mediated regulation of cavin-1 and Nur77 expression levels in MEFs. ....	106
Figure 4–6 Stabilisation of cavin-1 following cAMP elevation is PKA-independent. ....	109
Figure 4–7 Effect of protein synthesis inhibitor emetine on Fsk-mediated changes in cavin-1 immunoreactivity. ....	110
Figure 4–8 Effect of phosphatase treatment on cavin-1 immunoreactivity. ....	112
Figure 5–1 Detection of caveolae .....	119
Figure 5–2 Ultrastructural analysis of caveolae on the WT, SOCS3 <sup>-/-</sup> , and cavin-1 <sup>-/-</sup> MEF surface.....	120
Figure 5–3 Ultrastructural analysis of caveolae on the WT and SOCS3-null AS-M.5 endothelial cell surface. ....	122
Figure 5–4 Evaluation the expression of GFP and SOCS3-GFP in WT MEFs.....	125
Figure 5–5 Subcellular localisation of SOCS3-GFP and cavin-1 in WT and cavin-1-null MEFs. ....	131
Figure 5–6 Distribution of GFP in WT and <i>cavin-1</i> <sup>-/-</sup> MEFs.....	133
Figure 5–7 Localisation and expression of SOCS3 and cavin-1 in lipid rafts. ....	135
Figure 5–8 Localisation of SOCS3 mutants in WT MEFs. ....	138
Figure 5–9 Cavin-1 deletion enhances Tyr705 STAT3 phosphorylation. ....	141
Figure 5–10 Cavin-1 <sup>-/-</sup> MEFs stably expression GFP and cavin-1-GFP. ....	143
Figure 5–11 Tyr705 phosphorylation of STAT3 is limited by cavin-1.....	144
Figure 6–1 The proposed interaction between cavin-1 and SOCS3 to inhibit cytokine signalling. ....	151
Figure 6–2: The physiological functions of SOCS3 .....	156

## Acknowledgements

All my praises be to Allah, the almighty, for granting me the strength and patience to complete this research successfully.

I would like to express my gratitude and appreciation to my supervisor, Professor. Tim Palmer for his guidance and scientific expertise throughout this PhD project. I also extend my gratitude to co-supervisor Dr. Tom Van Agtmael for his encouragements, guidance, and support.

I would like to thank the following people who helped me with this project: Dr. Jamie Williams for passing on his experience and organising skills. Mrs Margaret Mullin for assistance with TEM. Dr John Pediani for assistance with confocal imaging.

I am also grateful to my sponsor, Al Imam Mohammad Ibn Saud Islamic University in Riyadh, Saudi Arabia for funding this PhD research.

Finally and most importantly, I offer my gratefulness to my loving wife, Haya, and my loving children for their constant care, encouragement, support and patience.

## **Author's Declaration**

I hereby declare that this thesis, which follows, is my own, original composition and that all work has been performed by me unless otherwise acknowledged. Furthermore, none of this work has been previously presented as part of an application for a higher degree.

Nasser Abdullah S Alotaiq

January 2019

## Abbreviations

AC	Adenylyl cyclase
BCA	Bicinchoninic acid
BSA	Bovine serum albumin
BSCL	Berardinelli-Seip congenital lipodystrophy
cAMP	3'-5'-cyclic adenosine monophosphate
CAV	Caveolin
CIS	Cytokine-inducible protein with an SH2 domain
CNTF	Ciliary neurotrophic factor
COPII	Coat protein 2
CRAC	Cholesterol recognition amino acid consensus
CREB	CRE-binding protein
CSD	Scaffolding domain
CSF	Colony stimulating factors
CTD	C-terminal domain
DMD	Duchenne muscular dystrophy
DRM	Detergent-resistant membrane
ECS	Elongin-cullin-SOCS
ECs	Endothelial cells
EGFR	Epidermal growth factor receptor
eNOS	Endothelial nitric oxide synthase
Epac-1	Exchange protein directly activated by cAMP 1
EPOR	Erythropoietin receptor
ER	Endoplasmic reticulum
ERES	Endoplasmic reticulum exit site

ERK	Extracellular signal–regulated kinase
ESS	Extended SH2 subdomain
FAK	Focal adhesion kinase
FcεRI	High-affinity IgE receptor
FSK	Forskolin
FTMS	Fourier transform mass spectrometer
G-CSFR	Granulocyte colony-stimulating factor receptor
GFP	Green fluorescent protein
Gp130	Glycoprotein 130
GPCR	G-protein-coupled receptor
HB-Ub	(His) <sub>6</sub> +biotin-tagged Ub
HRP	Horseradish peroxidase
HUVEC	Human umbilical vein endothelial cells
IFN	Interferons
IgE	Immunoglobulin E
IL-6	Interleukin-6
IMD	Intramembrane domain
IRS	Insulin receptor substrate
JAK	Janus Kinase
JNK	c-Jun N-terminal kinase
KIR	Kinase inhibitory region
LC	Liquid chromatography
LGMD	Limb-girdle muscular dystrophy
LIF	Leukemia inhibitory factor
LPS	Lipopolysaccharide

MAPK	Mitogen-activated protein kinase
MEF	Mouse embryonic fibroblasts
MKK	MAP kinase kinase
MMP-9	Matrix metalloproteinase-9
MURC	Muscle-restricted coiled-coil protein
NTD	N-terminal domain
PALM	Photoactivated localisation microscopy
PDGF	Platelet-derived growth factor
PI3K	Phosphatidylinositol-3-kinase
PIAS	Protein inhibitor of activated STAT
PKC	Protein kinase C
PM	Plasma membrane
PTM	Post-translational modification
PTP	Protein tyrosine phosphatases
PTP	Protein tyrosine phosphatase
PTRF	Polymerase I and transcript release factor
PTyr	Phosphorylated tyrosine
RING	Really Interesting New Gene
RMD	Rippling muscle disease
ROS	Reactive oxygen species
RTK	Receptor tyrosine kinase
SDPR	Serum deprivation protein response
SDS-PAGE	Sodium dodecyl sulphate polyacrylamide gel electrophoresis
SH2	SRC homology 2
SHP	SH2-containing PTP

SIGLEC	Sialic acid-binding Ig-like lectin 7
SILAC	Stable isotopic labelling of amino acids in cell culture
SOCS	Suppressor of cytokine signalling
STAT	Signal transducer and activator of transcription proteins
STED	Stimulated emission depletion
STORM	Stochastic optical reconstruction microscopy
TGF	Transforming growth factors
TNF	Tumour necrosis factors
TTF	Transcription termination factor
TYK2	Non-receptor tyrosine kinase
UPS	Ubiquitin proteasome system
VEGF	Vascular endothelial growth factor
WT	Wild type

# 1 Introduction

## 1.1 Plasma membrane organisation and function

### 1.1.1 Lipid rafts

The fluid mosaic model of Singer and Nicolson [1] is the most accepted representation of the cell membrane organisation and dynamics. According to this model, the lipid bilayer is a neutral two-dimensional fluid construct that allows free diffusion of membrane constituents [2]. Later, a series of experimental findings revealed that partial restriction of most proteins within the plasma membrane over the nanometre scale, and the hypothesis of membrane microdomain 'lipid rafts' was formulated.

Lipid rafts include a variety of nanoscale, transient, relatively ordered assemblies with distinct compositions and properties [3]. They are defined as small (10-200 nm), heterogeneous, highly dynamic, sterol- and sphingolipid-enriched domains that compartmentalise cellular processes [4]. Specific protein-lipid and protein-protein interactions are proposed to enlarge and stabilise functional membrane rafts complexes [5-7]. Furthermore, disrupting lipid raft integrity is associated with the pathogenesis of cardiovascular diseases, such as cardiac hypertrophy and atherosclerosis [8], and chronic inflammatory diseases, such as systemic lupus erythematosus and rheumatoid arthritis [9]. Therefore, pharmacological modulation of membrane rafts and perturbing their interactions with signalling molecules may hold potential therapeutic significance in devising new treatments or many human diseases.

The plasma membrane includes two types of microdomain: planar lipid rafts and a subset of rafts known as caveolae. Flotillin-rich planar lipid rafts are flat non-invaginated microdomains that lack distinguishing morphological features [10]. Caveolin-rich caveolae, on the other hand, are spherical or flask-shaped invaginations of the plasma membrane and represent a subset of membrane lipid rafts with specific functions conferred by the presence of caveolin proteins [11] (Section 1.2). Lipid rafts and caveolae share the similar lipid composition. Nevertheless, caveolae do not seem to occur in all cells compared to lipid rafts

although both rafts and caveolae can co-exist in a given cell type [11]. Flotillin-1 and flotillin-2 have been generally considered as marker proteins of planar lipid rafts. They are thought to function as scaffolding proteins within lipid microdomains by promoting the co-assembly of activated and specific glycosylphosphatidylinositol GPI-anchored proteins in plasma membrane microdomains to allow interaction with specific signalling molecules, such as the high-affinity IgE receptor (FcεRI), epidermal growth factor receptor (EGFR), and Ephrin-B1 receptors [12, 13].

#### **1.1.1.1 Development of the raft model of the cell membrane**

The common biochemical methods for studying the membrane lipid rafts include: 1) isolation of detergent-resistant membrane fractions (DRMs) by antibiotics (e.g. Nystatin) or pore-forming agents (e.g. Saponin) and 2) cholesterol depletion by methyl-β-cyclodextrin [13]. Recently, the existence of dynamic cholesterol-dependent nano-clusters in the cell membrane has been demonstrated by advanced super-resolution microscopy techniques such as photoactivated localisation microscopy (PALM), stimulated emission depletion (STED) fluorescence microscopy and stochastic optical reconstruction microscopy (STORM) [14]. Although an enormous amount of direct and indirect evidence indicates the lipid rafts presence in cell membranes, the concept of lipid rafts is still evolving and a matter of debate. Thus, research in the field has grown in the past decade as hundreds of papers were published annually to discuss the lipid raft hypothesis (for an authoritative review of caveolae and lipid raft structures and functions, see ref.[15]).

#### **1.1.1.2 Signalling through Lipid Rafts**

Accumulating evidence suggests that lipid rafts play an important role in receptor-mediated signal transduction, providing a distinct platform for the functioning of receptors and intracellular molecules [16]. Such data were obtained via several helpful methodological approaches despite their potential pitfalls. For example, simple non-ionic detergent extraction is considered a useful means for the detection of floating lipid rafts although the detection process can be affected by the changes in extraction and detergents conditions

as well as the existence of non-floating rafts which might be connected to the cytoskeleton [17-19]. Another common approach which is used to identify putative raft association is the antibody patching and immunofluorescence microscopy [20]. However, quantification of rafts by using this method may be difficult due to cell-cell variability [19]. In addition, more advanced techniques that require technical expertise and specialised equipment include immunoelectron microscopy, photonic microscopy and fluorescence resonance energy transfer [21-23]. Importantly, chemical cross-linking enables adequate identification of native raft protein complexes although the selection of appropriate reagents and conditions may be semi-empirical [24]. Collectively, these techniques led to the proposal that rafts are indeed dynamic in nature rather than static in situ and that specific signals might affect the distribution of membrane proteins in raft domains [25].

From an historical perspective, these microscopic cholesterol-enriched lipid rafts were initially implicated in various innate and adaptive immune responses. Specifically, Immunoglobulin E (IgE)-mediated signal transduction was the first signalling pathway that highlighted the association of lipid rafts during parasitic and allergic immune responses [26]. Since then, key immune receptors such as T-cell antigen receptor and B-cell antigen receptor were found in membrane rafts following receptor activation [27, 28]. In neuronal cells, lipid rafts are associated with the three components of the ciliary neurotrophic factor (CNTF) receptor complex, namely the CNTF-R itself and its signal transducers the leukaemia inhibitory factor (LIF) receptor and the interleukin-6 (IL-6) signal transducer glycoprotein (gp130) [29]. In addition to their involvement in immune and neuronal signalling, lipid rafts are also critical for haemostasis and thrombosis. Lipid rafts are required for fibrin clot retraction and platelet aggregation via the collagen receptor GPVI, the ADP receptor P2Y<sub>12</sub>, the Fcγ receptor FcγRIIa, and the thromboxane A<sub>2</sub> receptor [30]. Furthermore, lipid rafts-dependent signalling has also been reported in other receptors that have intrinsic tyrosine kinase activity (e.g., insulin receptor, EGFR, and Kit receptor tyrosine kinase) [30, 31]. Additionally, signal transduction of certain G-protein-coupled receptors (GPCR) depends on the interaction with lipid rafts. For example, dopamine D1 receptors were found to preferentially regulate the

activity of specific adenylyl cyclase isoforms (AC 3, 5, and 6) in a lipid rafts-dependant manner [32].

## 1.2 Caveolae

The earliest research on caveolae was conducted by Yamada and Palade in the 1950s [33, 34]. Ultrastructural investigations of the plasma membrane by transmission electron microscopy revealed the presence of distinct 'cave-like' intracellular organelles. Caveolae were first identified in the continuous endothelium of the heart and then in the gall bladder epithelium. These structures exhibit the following characteristic features: 1) Flask-shaped membrane invaginations that are typically associated with the plasma membrane and occasionally seen with narrow neck or a diaphragm; 2) Typical sizes are 50-100 nm without an apparent electron-dense region found in larger "coated" vesicles-i.e., clathrin-coated pits [35, 36]. Morphologically identifiable caveolae have since been found in a variety of cell types. They are particularly abundant in smooth muscle cells, endothelial cells and adipocytes where they comprise up to 35% of the cell surface [37]. In contrast, they are reportedly absent in most neural tissues [38], lymphocytes, red blood cells, and platelets [39].

The discovery of the protein composition of caveolae marked a significant breakthrough in understanding the nature and importance of these organelles [40]. Caveolae are comprised of two classes of proteins, the integral membrane caveolins (caveolin 1-3) and caveola-associated cavins, (cavin 1-4) [41]. Mutation of caveolar proteins in mammals is associated with a broad range of diseases, such as lipodystrophy, muscular dystrophy, cardiovascular diseases and cancers [42-46].

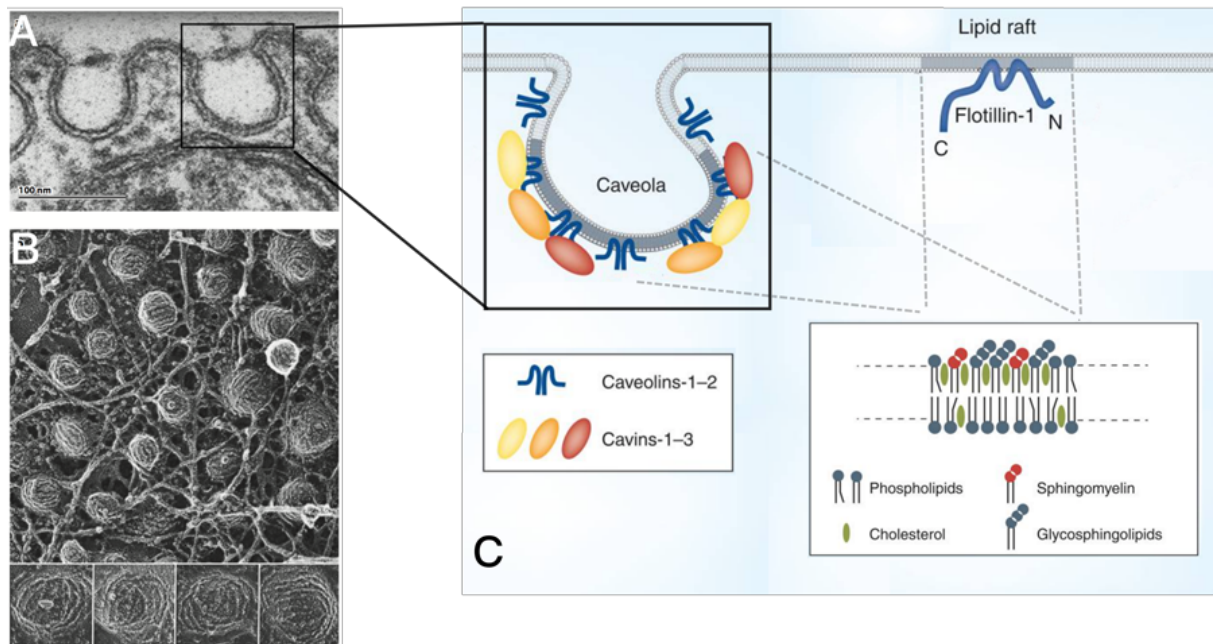


**Figure 1–1: The morphology and composition of caveolae.**

(A) An endothelial cell showing the flask-like invaginations by electron microscopy. (B) Caveolin filaments are shown on the caveolae surface as viewed by rapid-freeze deep-etch electron microscope in the cytoplasm of a human fibroblast cell. Individual caveolae are depicted in the lower panel (C) An individual caveolae with caveolar proteins and lipid species. Additionally, DRMs (lipid rafts) are shown with flotillin-1 protein. Adapted from Shibata et al. [39] and Pilch et al. [47].

### 1.2.1 Caveolins

Caveolins (CAV) are a family of three (caveolins-1-3) small ~18-22kDa proteins characterized by marked homology to each other despite their dissimilarity to other typical proteins. They include membrane integral proteins that resemble hairpins having cytoplasmic NH<sub>2</sub> and COOH-termini [48]. The four major domains of caveolins are the: scaffolding domain (CSD), N-terminal domain (NTD), C-terminal domain (CTD), and intramembrane domain (IMD) [49-51] (Figure 1–2). The family of caveolin genes consists of three caveolins (1, 2, and 3). While many cell types express CAV-1 and CAV-2 (such as the endothelial cells, fibroblasts and adipocytes), CAV-3 is exclusively expressed in skeletal, cardiac, and smooth muscles [52, 53]. Both CAV-1 and CAV-3 are closely related to each other based on protein sequence homology; they are 85% similar and 65% identical [54]. Further, there is a close proximity between CAV-1 and CAV-2 on the chromosome 7 (q31.1), while CAV-3 is found on chromosome (3p25) [55]. Additionally, CAV-2 complexes that subsequently form caveolae are assembled depending on the expression and oligomerisation of CAV 1/3. Actually, this property is exclusive for CAV-2 rather than CAV 1/3. As such, CAV-2 fails to leave the Golgi complex and undergoes rapid degradation in the absence of CAV-1 [56]. In addition, phosphorylation of CAV-1 and CAV-2 can occur on multiple residues, while all caveolins are palmitoylated on three cysteine residues [57-60] (Figure 1–2 and Figure 1–3).

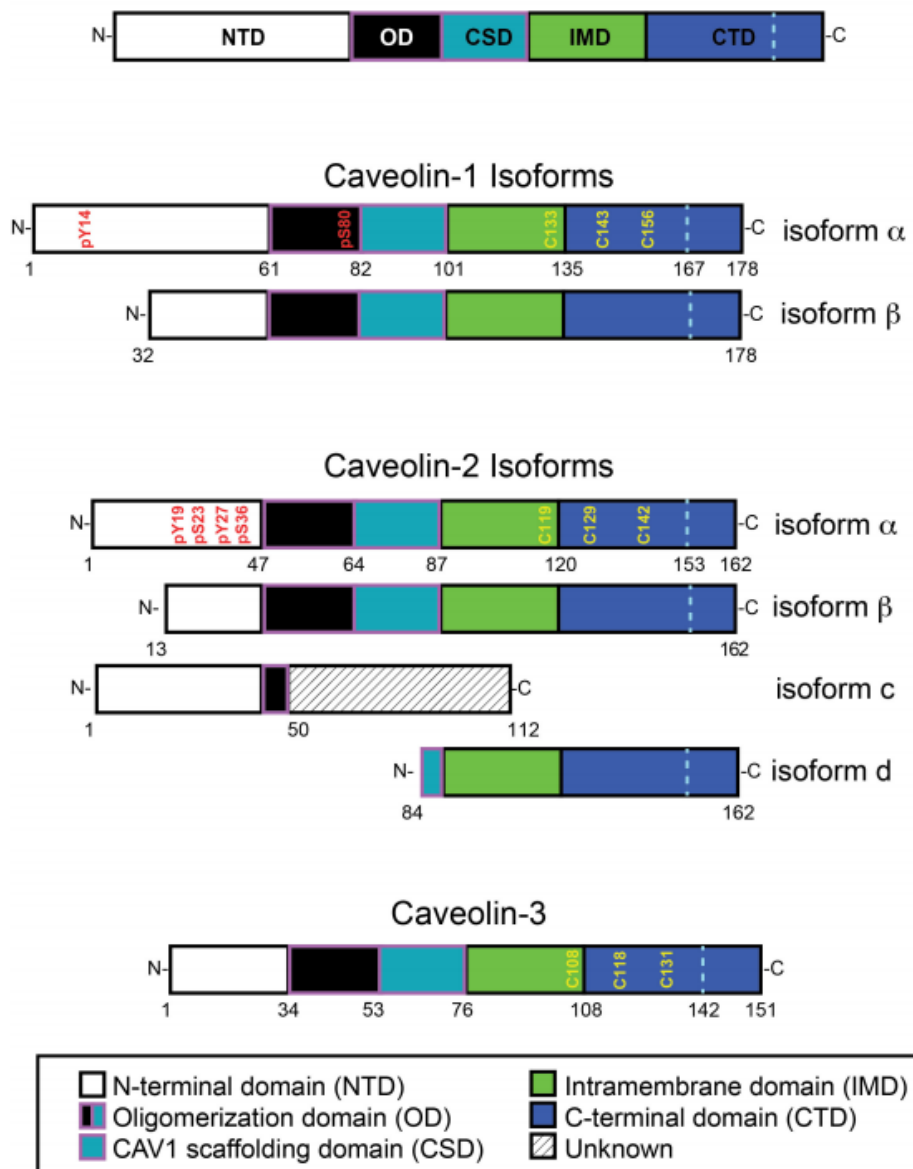


**Figure 1–2: The different subdomains of caveolin proteins.**

Phosphorylation sites and the palmitoylated cysteine residues are shown in red and yellow text, respectively. Adapted from Sverdlov et al. [61]

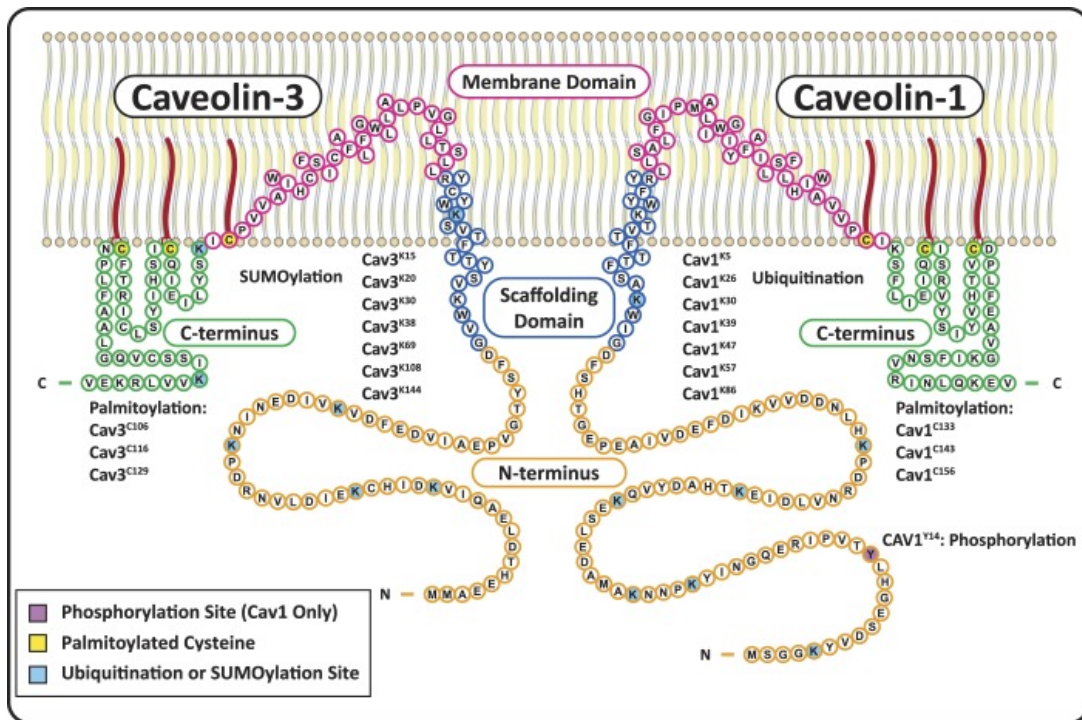


**Figure 1–3: The basic structures and posttranslational modifications of CAV-1 and CAV-3.**

Both proteins have four domains: The N-terminal domain (orange) with several ubiquitination sites as well as exclusive phosphorylation sites on CAV-1, scaffolding domain (blue) which forms alpha helices, intramembrane domain (fuchsia) which moves out of the membrane at a palmitoylation site, and C-terminal domain (green). Adapted from Busija et al. [48]

### 1.2.1.1 Caveolin-1

CAV-1 is a 22kDa protein comprised of 178 amino acids. Alternatively-spliced CAV-1 transcripts encode two distinct isoforms: CAV-1 alpha (CAV-1 $\alpha$ ) and CAV-1 beta (CAV-1 $\beta$ ; 32-178), in which the first 31 amino acids are absent [62, 63]. Such isoforms have specific differences in their impact on the structure and depth of caveolae and how they affect the functions of cytokine receptors [62, 64-66]. For example, studies have demonstrated that deep caveolae are associated with CAV-1 $\alpha$ , while CAV-1 $\beta$  has the ability to inhibit the signals of cytokines [64-66].

Human CAV-1 molecule contains nine tyrosine residues, three of which are located only in CAV-1 $\alpha$ . Such residues might act as potential substrates for Src [67]. Studies have shown that CAV-1 $\alpha$  is selectively phosphorylated in cells expressing viral Src (v-Src) and the basic phosphorylation site of cellular Src (c-Src) is Tyr-14 [68]. CAV-1 phosphorylation by Src family kinases would possibly have an impact on caveolar functions through distinct morphological changes, such as aggregation, flattening, and fusion of caveolae [68]. Gottlieb-Abraham et al. [69] found that Src-mediated CAV-1 phosphorylation at Tyr-14 resulted in modulation of focal adhesion dynamics via accumulation of Src kinases in focal adhesions.

Within the full-length protein (Figure 1–2), the CAV-1 NTD (residues 1–81) is responsible for the assembly of complexes that build caveolae by the integrated oligomerization domain [70]. Additionally, the interaction of CAV-1 with the CSD (residues 82-101) may be involved in the downregulation of many signalling molecules although the presence of specific binding sites to such domains remains unclear [71, 72]. The IMD (residues 102-134) is composed of two  $\alpha$ -helices separated by a unique three residue linker region containing a proline (P110) that induces a  $\sim 50^\circ$  angle between the helical regions [73, 74]. This pattern gives CAV-1 the hairpin topology, with the C- and N- termini directed towards the cellular cytoplasm [73, 75, 76]. Caveolin-1 oligomer/oligomer interactions require CTD (residues 135–178) that also contains three sites of cysteine palmitoylation (C133, C143 and C156) mediating membrane

attachment. Nonetheless, palmitoylation of caveolin is not necessary to target this protein to caveolae [77].

### **1.2.1.2 Caveolin-2**

Two distinct isoforms of caveolin-2 (CAV-2 $\alpha$  and CAV-2 $\beta$ ) have been identified. The full-length protein is encoded by CAV-2 alpha (CAV-2 $\alpha$ ), while the beta isoform lacks the N-terminus. In addition to the transcript variants which encode CAV-2 isoforms, using alternate in-frame initiation codons would encode CAV-2 isoforms, particularly the  $\beta$  isoforms, that are preferentially located in lipid droplets [78]. Nonetheless, Fujimoto et al. [78] reported variations in the subcellular distribution of both isoforms although the detailed knowledge pertinent to them is still insufficient.

The assembly of CAV-2 can be established in the form of homo-dimers or hetero-oligomers with CAV-1 [79, 80]. The expression of CAV-1 is necessary for CAV-2 expression, trafficking, and targeting of caveolae. For instance, In CAV-1 knock-out mice, the expression of CAV-2 is not sufficient to form caveolae and CAV-2 remains trapped in the Golgi. However, caveolae formation is not affected in CAV-2-deficient mice despite the reported reduction in CAV-1 expression (by 50%) observed in pulmonary abnormalities, including hypercellularity of lung parenchyma, thickening of alveolar septa and abundance of the endothelial cells expressing vascular endothelial growth factor receptors [80, 81]. Seemingly, it is unclear that CAV-2 could exert its functions independent of caveolae and CAV-1 on the cellular and tissue levels [80]. However, some reports have shown that CAV-2 has some roles in enhancing caveolae formation [82], inhibit pulmonary fibrosis caused by medications [83], downregulation of cellular proliferation [84, 85], insulin signalling, stimulate blood vessel formation in the tumours [86], and prevent gastrointestinal cellular injury or hyperpermeability [87]. Thus, CAV-2 appears to be involved in CAV-1 functionality to a specific extent, while the independent action of CAV-2 needs to be better elucidated.

### 1.2.1.3 Caveolin-3

CAV-3 forms most of the caveolae present in muscle cells [88]. In addition to their predominance in the skeletal and cardiac muscle cells, there is an evidence of their presence in smooth muscle cells [89]. Unlike CAV-1 and CAV-2, there are no isoforms of CAV-3. The biochemical characterisation of immortalised murine CAV-3<sup>-/-</sup> myoblasts suggested novel roles for CAV-3 during myoblastic development at the step of myoblast fusion into myotubes and in the formation of transverse tubules during the differentiation of muscle cells [90-92]. In mature muscle fibres, CAV-3 has a remarkable post-maturation role as it is found in the sarcolemma, affecting muscular metabolic processes, such as glucose uptake and energy metabolism [93], activation of signalling pathways that mediate the cardiac hypertrophic response [94], and muscular contractility [95]. Talukder et al. [96] revealed that there was a significant change in muscular insulin signalling that was associated with changes in CAV-3 expression. Mutations in CAV-3 have been associated with abnormal elevations of the levels of serum creatine kinase and they were found in several muscular diseases, such as Duchenne muscular dystrophy (DMD), rippling muscle disease (RMD), and limb-girdle muscular dystrophy (LGMD) [92, 97-99].

Experimental animal models that lack CAV-3 exhibit skeletal muscle abnormalities, including muscular dystrophy and cardiac muscle abnormalities, such as progressive cardiomyopathy, hypertrophy, dilation, and reduction of fractional shortening [92, 94]. It has been reported that CAV-3 null mice display impaired insulin resistance and lipid metabolism [100, 101]. In spite of such perceived roles of CAV-3, the exact pathophysiological mechanisms implicated in disease progression are not fully elucidated. Overall, CAV-3 plays an important role in muscle tissue as indicated by a variety of muscle disease that could develop as a result of CAV-3 gene mutations. Challenging aspects related to the identification of potential modifying factors or genetic mutations need to be revealed.

## 1.2.2 Cavins

Although CAV-1 is a vital protein necessary for caveolae formation, it may not be sufficient for their formation [102]. A distinct class of caveolae-associated proteins called cavins (Cavin-1 and -4) was subsequently identified that have significant roles in the biological functions, formation and localisation of caveolae. Cavin1 was formerly known as “polymerase I and transcript release factor” (PTRF) [103], cavin-2 as serum deprivation protein response (SDPR) [104], cavin3 as SDPR-related gene product that binds to C kinase [105], and cavin4 as muscle-restricted coiled-coil protein (MURC) [106]. Kovtun et al. [107] performed a combined sequence of all cavin proteins in mouse and zebrafish Cavin4, revealing two strongly-predicted positively-charged  $\alpha$  helical regions called HR1 and HR2 with a high degree of sequence conservation (HR1 is more consistently similar among cavin proteins than HR2) (Figure 1–4). HR1 and HR2 domains are flanked by negatively-charged, acidic, disordered and poorly conserved regions termed DR1-3. A coiled-coil domain exists in the HR1 domain as confirmed by crystallography analysis and it is involved in the interactions between different cavin proteins [108]. In addition, a leucine zipper-like motif (LZD), which helps in protein-protein interaction, is located in the HR1 of cavin1-3 and HR2 of cavin-1. Furthermore, all cavin proteins have distinct domains, rich in proline (P), glutamic acid (E), serine (S) and threonine (T), termed PEST motifs [109]. Despite their apparent role in proteolytic degradation through the  $\mu$ -calpain and 26S proteasome system that might lead to the shortening of the half-life of cavins, the exact function of the PEST domains in the cavin proteins has not been defined [110, 111]. A membrane association domain (which mediates the attachment to the membrane) is a basic domain located at the C terminus of cavins [112]. Cavin proteins map to different human chromosomes, unlike CAV-1 and CAV-2. Thus cavin-1 is located on chromosome 17 (q21.2), cavin-2 in on chromosome 2 (q32.3), cavin-3 in chromosome 11 (p15.4) and cavin-4 in on chromosome 9 (q31.1) [112].

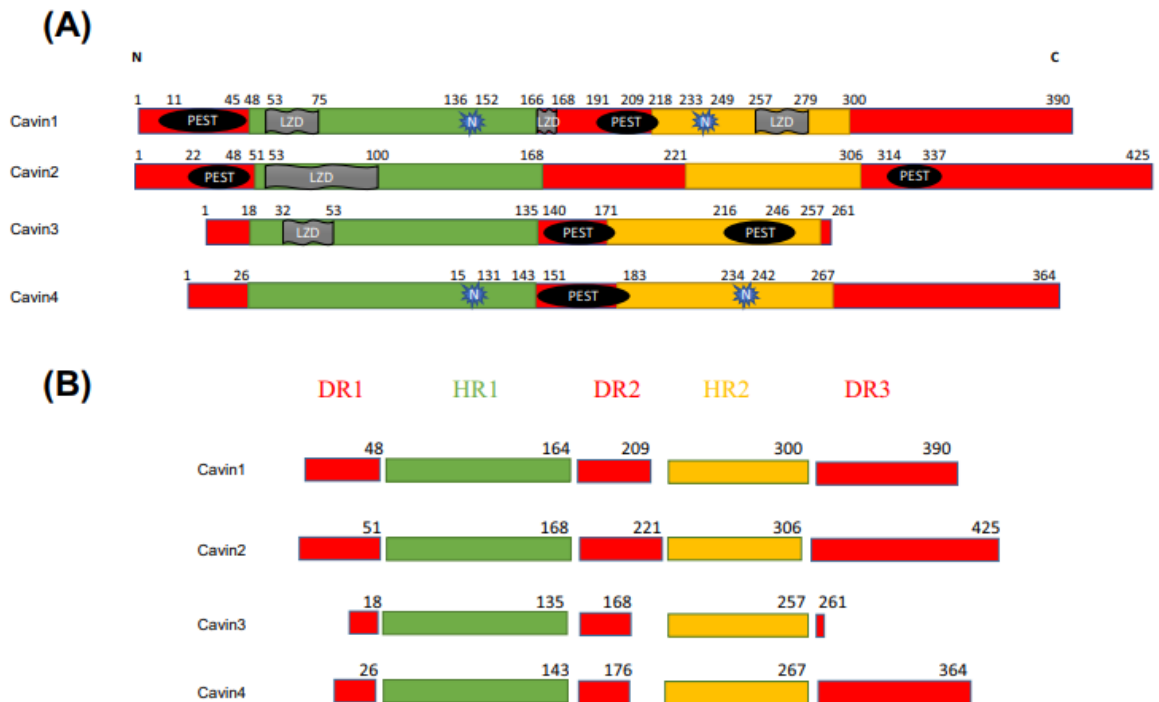


**Figure 1–4: Cavin family proteins**

(A) Structure of different cavin proteins in human. (B) The combined sequence revealed two positively-charged helical regions (HR1 and HR2) which are separated by non-conserved regions named DR1-3. N, Nuclear localization signals, LZD; Leucine zipper-like motif; HR, Helical regions; and DR, Disordered region. Adapted from Nassar and Parat [108]

A putative nuclear localisation signal was originally linked to Cavin-1. Indeed, this is consistent with the former identification of cavin-1 as an RNA-polymerase I regulator as it plays an important role in the process of loop formation which is required for activation of ribosome transcription [113]. However, there is a growing body of evidence that showed an important role of cavin-1 outside the nucleus [114]. Post-translational modification of cavins, results in a 10-15kDa higher migration than expected from their primary structure during fractionation by sodium dodecyl sulphate polyacrylamide gel electrophoresis (SDS-PAGE). Such modifications include multiple aspects of an unclear functional significance. The abundance of PEST motifs in the DR domains of cavins affects their proteolysis and might modulate cavin localisation, given the removal of the C-terminus DR3 results in association with microtubules [115] and the involvement of DRs in cavin oligomerisation [107]. Ubiquitylation has been also reported in cavins consistent with the identification of SUMOylation and ubiquitylation sites [116] and the acceleration of proteasome-dependent proteolysis of non-caveolar cavin-2 [117]. Phosphorylation is another commonly reported modification of cavins. As with caveolins, all cavin proteins have one or more phosphorylation sites, with dozens of reported sites within the DRs [107, 114]. Studies have shown that cavins might undergo rapid phosphorylation following stimulation of adipocytes, indicating a possible linkage between their regulation and the signalling pathways [118-120]. However, the effect of such extensive phosphorylation on the functions of cavins has not been discerned [114].

Cavin 1-3 are found in the body with the same distribution as CAV-1 [102, 121]. In addition, Cavin-1 is present also in skeletal muscle while cavin-3 is found in liver and brain. cavin-4 is exclusively located in the skeletal muscles [106]. Cavin-1 genetic deletion causes a remarkable loss of CAV-1-3 proteins in approximately 80-90% of tissue [121]. Such genetic loss results also in reduction of cavin-2 and -3 levels, but to a less extent, with no effect on cavin-4 expression. Overall, the expression of CAV-1 and cavin-1 is essential for caveolae formation, while the stability and function of caveolae are preserved by cavin-2 and cavin-3. Co-immunoprecipitation data have shown that members of the cavin family interact in a multimeric complex in the cytosol and

plasma membrane fractions yet a clear connection of such interaction to caveolins has not been uncovered [106].

In general, cavin proteins in human and mice show strong homology, with the strongest homology in cavin-1 (93%), while cavin-2, -3, and -4 share homologies of 83%, 78%, and 89%, respectively. Within the murine species, cavin-4 shows a homology of 29% to cavin-1, 24% to cavin-2, and 20% to cavin-3, while it shows a similarity of 49%, 42%, and 39% to cavin-1, cavin-2, and cavin-3, respectively [106]. Compared to caveolins, cavin proteins are larger, with cavin-1 comprising 390 amino acids, cavin-2 425 amino acids, cavin-3 261 amino acids in, and 364 amino acids in cavin-4 (Figure 1–4) [112].

Immunogold labelling technique showed that the expression patterns of cavin proteins are generally demonstrated in a uniform manner around the caveolar bulb [122]. As per single-molecule fluorescence microscopy findings, cavin monomers are composed of 50 molecules with specific patterns of interaction between all cavin family members in a given caveolae [123]. Changes in the membrane tension (membrane stretch) can cause disassembly of the cavin coat into distinct subcomplexes containing cavin-1 and cavin-2 or cavin-1 and cavin-3 [123].

### **1.2.2.1 Cavin-1**

Cavin-1 was first identified by a yeast two-hybrid screening assay [124]. Cavin-1 was named as polymerase I and transcript release factor (PTRF) because it enables the dissociation of RNA polymerase I transcripts and the tertiary structures [125]. Given that the transcription termination factor (TTF)-I is involved in the transcription process of ribosomal mRNA (mediated by polymerase I), the PTRF-related investigations were conducted using the TTF-I as a bait in the yeast two hybrid screen. PTRF was then reclassified following its identification in specific enriched fractions with distinct localisation patterns in caveolae as shown by immunogold labelling [125]. Bastiani et al. [106] reported that cavin-1 is 66% homologous to cavin-2 and 59% homologous to Cavin3 and Cavin4. In terms of tissue distribution, cavin-1 expression has been reported in the heart, lungs, and adipose tissue [121]. The role of cavin-1 is

clearly demonstrated by the failure of caveolae formation in the lung epithelium, smooth muscles of the intestine, and cardiac muscle cells along with metabolic and adipocyte dysfunction when cavin-1 gene is deleted in mice [121, 126].

Notably, cavin-1 depletion is associated with a significant reduction in protein expression of all cavins and caveolins [102, 106]. Even though Liu et al. [121] found that cavin-1 deficiency triggered an upregulation of expression levels for caveolin isoforms. In addition, it has been shown that the consequences of cavin-1 mutations or gene knockout are reduced adipose tissue, muscular dystrophy, cardiomyopathy, hypertriglyceridemia, hyperinsulinemia, and glucose intolerance [121, 126, 127]. Indeed, these patterns were typically reported CAV-1/CAV-3 double knockout mice [128]. This is consistent with the fact that the tissue distribution of combined CAV-1/CAV-3 mimics that of cavin-1.

Akin to caveolin proteins, the pathophysiological consequences of cavin-1 deficiency in animal models have been replicated in rare human genetic disorders [129]. For example, genetic screening on more than 2,700 muscular dystrophy specimens showed that five patients with Berardinelli-Seip congenital lipodystrophy (BSCL), characterized by a marked reduction of the adipose tissue along with severe dyslipidaemia and insulin resistance, were deficient in CAV-3 in the absence of any CAV-3 mutations [127]. However, cavin-1 protein in all BSCL patients had remarkable frame-shift mutations that yielded severely truncated proteins. Furthermore, such BSCL patients suffered also from a generalised muscular dystrophy [127].

In addition, cavin-1 has been involved in lipodystrophy. Several studies have shown that cavin-1 had potentially a major role in the pathogenesis of the near total loss of adipose tissue and multiple myopathic abnormalities in patients with congenital generalized lipodystrophy subtype 4 [43, 44, 130]. Therefore, the outcomes of these studies confirm that cavin-1 produces similar pathological pictures in human and mice.

The location of cavin-1 at the 17q21.2 region on the human genome have been linked with multiple human diseases. For instance, Barrett et al. [131] revealed that cavin-1 was widely reported in patients with type I diabetes, whereas another study conducted by Ikram et al. [132] showed a possible correlation between the variants at 17q21.2 and the intracranial volume. This would eventually lead to inability to attain maximal brain size. However, there is a lack of confirmed evidence regarding a possible role of cavin-1 in these conditions. It worthy to note that the BRCA1 gene (breast cancer gene 1), the well-known tumour suppressor gene, is located at the 17q21.31 locus [133]. Interestingly, there has been a controversy regarding the cancer-related effects of cavin-1. Some studies have proved that cavin-1 is a tumour suppressor in multiple studies, including colorectal [134], prostate [135], breast [45], and lung cancer [136]. In contrast, a recent study proved that cavin-1 promotes the proliferation of glioma cells, thus acting as a tumour promoter [137]. This is because cavin-1 was enriched in glioblastoma subtypes and its increased expression with advanced tumour grades indicated a possible correlation with poor prognosis [137]. In sum, it seems that cavin-1 has a dual role in cancer.

#### **1.2.2.2 Cavin-1 as a regulator of caveolae**

The apparent role of cavin-1 proteins in the regulation of caveolae was first identified by the fact that reduced cavin-1 levels were associated with a reduction of CAV-1 protein recruitment into lipid raft fractions, while an increase of CAV-1 incorporation in lipid rafts was observed in human kidney embryonic kidney (HEK) HEK293-caveolin-1-cavin overexpressing cells [121]. Given the important linkage between caveolae and the actin cytoskeleton which is of an important implication for cellular response to mechanical stress [138], such linkage may be accomplished by cavin-1 since it has been reported that a truncation mutant of this protein localised to a cytoskeletal-like structure rather than the plasma membrane [139]. In contrast, Verma et al. [140] showed that CAV-1 was localised to long branched tubules derived from the plasma membrane (up to 50  $\mu\text{m}$ ) when it was expressed in certain cancer cells, while CAV-1 was appropriately localised to the plasma membrane when cavin-1 was co-expressed with CAV-1. As such, adequate proportions of cavins and

caveolins are required so that they could be appropriately localised to the plasma membrane and subsequently form caveolae.

Indeed, in addition to decreasing the amounts of CAV-1, knockdown of cavin-1 can also lead to a significant reduction in caveola density as demonstrated by electron microscopy due to an increase in the lateral motility and excessive lysosomal degradation of CAV-1 [102]. Moreover, genetic deletion of cavin-1 in mice resulted in a significant instability of all three caveolin proteins [121]. Besides, while cavin-1 exhibits a generally stable expression (like CAV-1), cavin-1 gene can be also induced by stress conditions, such as starvation [118], oxidative stress, and exposure to catecholamines which could ultimately lead to an increase in caveolae number [141].

As mentioned above, a lipodystrophic phenotype is seen in mice in which both copies of the cavin-1 gene are knocked-out. This might be related to a lack of caveolae which impairs triacylglycerol uptake and storage in adipocytes [121]. In humans with cavin-1 mutations, cardiovascular and pulmonary disorders appear to evolve along with the lipodystrophic phenotype as these mutations result in either the loss of cavin-1 expression or the generation of non-functional C-terminally truncated cavin-1 proteins, leading to loss of caveolae in myocytes and fibroblasts [43, 44, 127]. However, diet-induced atherosclerosis caused a remarkable disruption of the positive association between CAV-1 and cavin-1 [142]. In mice fed on a high-fat diet, the DRMs in the lung endothelial cells showed upregulation of CAV-1 despite reduced cavin-1 levels. As a consequence, caveolae were lost and caveolae-dependent signalling was impaired, providing one potential explanation for the association between cardiovascular and pulmonary disorders [142].

It has also been shown that cavin-1 silencing and cholesterol-depleting drugs which disrupt caveolae can limit CAV-1 localisation to lysoendosomal compartments, where it is eventually degraded [143]. Such CAV-1 degradation is prevented by neutralisation of lysosomal pH and partially blocked by proteasome inhibitor MG132 suggesting that the endosomal system could possess a proteasomal activity that modulates CAV-1 turnover [143]. Although

these data reveal the necessity of cavin-1 for an adequate expression of normal amounts of caveolins, the exact details of such mechanism remain unclear. The contribution of cavin-1 has been shown in the process of CAV-1 trafficking and caveolae formation. Once CAV-1 moves to the Golgi after its synthesis in the endoplasmic reticulum (ER), it interacts with cholesterol and its mobility in the plasma membrane is lost. Following cholesterol-CAV-1 interaction, caveolae assembly is inhibited and CAV-1 degradation is accelerated [130, 143].

### **1.2.2.3 Cavin-2**

Cavin-2, formerly known as SDPR, was discovered by Gustincich and Schneider in the early 1990s as an mRNA that was intensively induced in response to serum deprivation in 3T3 fibroblasts [104]. The relationship between caveolae and cavin-2 was subsequently determined following its identification as a protein that mediates caveolae binding to the signalling enzyme protein kinase C (PKC) alpha [144]. In addition, it was recognised as a binding protein to phosphatidylserine in human platelets. This protein was re-named as cavin-2 following detection of its localisation to the plasma membrane at the caveolae using confocal imaging [145].

The sequence identity of cavin-2 with cavin-1 is 66%, 68% with cavin-3 and 57% with cavin-4 [106]. It was found that excessive expression of cavin-2 led to caveolae deformity as well as tubular membrane structures as seen by immunofluorescence and electron microscopy [145].

On the other hand, knockdown of cavin-2 was associated with loss of caveolae and a significant reduction of cavin-1 and CAV-1 expression [145]. Overall, these reports demonstrate an essential role of cavin-2 in the formation of caveolae.

A clear relationship between cavin-2 and cholesterol has been shown when 3T3-L1 adipocytes exposed to the cholesterol-depleting agent methyl- $\beta$ -cyclodextrin, which led to cavin-2 degradation by the proteasome. Interestingly, cholesterol repletion fully reversed the effect of methyl  $\beta$ - cyclodextrin and restored cavin-2 levels, which allowed reformation of the caveolae [139].

cavin-2 is highly expressed in the heart with considerable expression also detected in the lung and adipose tissue [146]. The role of cavin-2 in cardioprotection is still debated although it has been suggested that cavin-2 might act as a negative regulator of Akt and extracellular signal-regulated kinase (ERK1/2) signalling. This is because inadequate cavin-2 expression in the heart results in hypertrophy and resistance to apoptosis caused by H<sub>2</sub>O<sub>2</sub> stimulation and hypoxia [147]. Moreover, Higuchi et al. [148] reported that cavin-2 may be considered an important mediator in the progression of heart failure, as it modulated phosphatase and tensin homolog (PTEN)/Akt signalling and enhanced cardiac cell death in response to pressure overload. The authors suggested that this protein might be a promising therapeutic target for heart disease [148]. Another recent report by Boopathy et al. [149] showed a critical role of cavin-2 in regulation of nitric oxide production in endothelial cells through an adequate control of the activity and stability of nitric-oxide synthase. Indeed, this might reveal an important impact of cavin-2 on endothelial cell maintenance and function. It is noteworthy that immunofluorescence and immunoblotting analyses have shown that cavin-2 expression was higher with the progressive differentiation status of liposarcoma tumour cell lines rather than their proliferation, suggesting cavin-2 as a potential marker for liposarcoma differentiation [150].

In terms of disease association, the location of cavin-2 on the 2q32-q33 locus suggests a potential role in cancer. This might be attributable to the previous evidence of a genomewide linkage screen, which showed a possible correlation between the 2q32-q33 locus and familial serrated neoplasia (Jass syndrome), a rarely reported form of colorectal cancer [151]. Moreover, the cavin-2 gene locus is involved in the pathogenesis of the eponymous chromosome 2q32-q33 deletion syndrome, which is characterised by marked mental retardation, craniofacial dysmorphism and microcephaly [152, 153]. Recently, Unozawa et al. [154] found that cavin-2 expression was down-regulated in oral squamous cell carcinoma using immunoblot analyses and the clinical data of immunohistochemistry revealed an increase in tumour progression in patients deficient in cavin-2 [154]. However, these cancer phenotypes were not

observed in the knockout studies in mice, which might highlight the need to conduct future investigations concerned with malignancies.

#### **1.2.2.4 Cavin-3**

Cavin-3 was first identified as a protein that interacted with PKC delta ( $\delta$ ), which was later found to be directly associated with caveolins and localised in the caveolae fraction [155]. Co-immunoprecipitation experiments suggest that cavin-3 interacts with cavin-1 and cavin-2 [106]. Cavin-3 is expressed a variety of cells, including brain cells and adipocytes [106]. However, cavin-3 is more widely distributed in the tissue, which may suggest other physiological functions outside the caveolae [109, 155]. Further, cavin-3 cardiac expression is comparable to that of caveolins [146].

Bastiani et al. [106] stated that the general similarity of cavin-3 to other cavins has been estimated to be 59% to cavin-1, 68% to cavin-2, and 51% to cavin-4. Five variants of cavin-3 protein can be generated as a result of alternative splicing of cavin-3 mRNA resulting in a considerable variation in the molecular weight (14 to 31-kDa) [155].

Multiple functions of cavin-3 have been reported, including intracellular transport and endocytosis [155]. The importance of cavin-3 is more apparent in cell signalling since it can mediate AAKt, ERK1/2, and EGFR signalling pathways. It may act also as a coupling agent to these signals to the transport machinery within the cells [155, 156]. McMahon et al. [155] suggested that caveolae signalling could be mediated by cavin-3 by budding of distinct vesicles called “cavicles” by microtubules. The authors supported their findings by the fact that cavicle trafficking was reduced in absence of cavin-3 [155].

Cavin-3 deficiency in lung tissue is associated with an increase in phospho-Akt levels and a reduction in phospho-Erk levels when compared to wild-type counterparts. Moreover, it has been shown that cavin-3 deficiency was associated with a pleiotropic phenotype, where a late cachexia with shortened life span occurred [156]. Heart tissue deficient in cavin-3 did not show changes in the expression of cavin-1 and CAV-1 and cavin-3 was found dispensable for

formation of endothelial caveolae [146]. Nonetheless, recent evidence has shown that loss of cavin-3 in mice produces a 40% reduction in the expression of cavin-1 in the smooth muscles of the urinary bladder and blood vessels [157]. Although this was also associated with a reduction in caveolae number, the physiological consequences were mild, with the main effect being marginal elevation of soluble guanylyl cyclase expression [158].

#### **1.2.2.5 Cavin-4**

Cavin 4, is the most recently identified member of the cavin family. Cavin-4 is encoded by two conserved exons and has no splice variants, yielding a single 362 amino acids long polypeptide [106]. This protein is also named muscle-restricted coiled-coil protein (MURC) since it is exclusively expressed in cardiomyocytes, skeletal myocytes, and smooth muscle cells [159]. Based on its sequence homology with cavin-1 as well as its caveolae localisation, MURC was re-named cavin-4 [106, 145]. It seems that the role of cavin-4 is modest in the process of caveolae formation despite its apparently important impact on the disrupted caveolar shape. The latter function was demonstrated by the observed increase in caveolae size by cavin-4 overexpression [160]. Maturation of cardiac muscle cells and cultured muscle cells would entail cavin-4 upregulation. On the other hand, expression levels of cavin-4 and CAV-3 are impaired in cases of severe myopathy and both proteins may together cooperate for proper functioning of skeletal muscle tissue [106, 159].

Cavin-4 has the ability to form complexes with CAV-3, cavin-1, and cavin-2. The localisation of cavin-4 to caveolae and T-tubules in cardiac muscle cells was reported although cavin-4 is dispensable for caveola formation [161]. The coiled-coil domain of cavin-4 is thought to be responsible for protein oligomerisation, and other proteins that contain this domain (including the cartilage oligomeric matrix protein,  $\alpha$ -keratin, and vimentin) are involved in a number of important cellular functions, such as cell division, membrane extrusion, gene regulation, and drug extrusion [162, 163]. Naito et al. [161] showed that deletion of the coiled-coil domain impaired cavin-4 localisation in cardiomyocytes, caused a significant reduction in CAV-3 levels in the plasma membrane, and eventually led to cardiac dysfunction.

Overexpression of cavin-4 results in induction of fibrosis, atrial arrhythmia, ventricular hypertrophy, and alterations in gene expression [159]. Moreover, six non-synonymous cavin-4 mutations have been identified in patients with hypertrophic cardiomyopathy [164]. Cavin-4 overexpression in rat cardiac muscle cells has been induced by hypoxia, which could be a result of induction of cavin-4 by serum response factor [165]. Conversely, cavin-4 deficiency might lead to attenuation of phenylephrine-induced cardiac hypertrophy following  $\alpha$ 1-adrenergic receptor stimulation [160]. Further, cavin-4 knockdown prevented myocardial ischemia-reperfusion injury via reduction of oxidative damage and is thought to be associated with reactive oxygen species (ROS)-p38 mitogen-activated protein kinase (MAPK) signalling pathway [166]. In addition to cardiac pathology, cavin-4 might be involved in modulating the progression of abdominal aortic aneurysm through activation of matrix metalloproteinase-9 (MMP-9) and JNK [167]. Actually, the aforementioned studies indicate that cavin-4 might be a novel therapeutic target for ischemic heart disease as well as abdominal aortic aneurysm progression. Finally, cavin-4 was found to be disrupted along with CAV-3 in human suffering from rippling muscle disease [60]. Collectively, future studies should importantly consider targeting cavin-4 to investigate its potential therapeutic benefits for inhibiting the exacerbation of cardiac, vascular, and muscular disease.

### **1.2.3 Caveolae biogenesis**

Caveolae biogenesis is a stepwise process that involves trafficking of proteins and vesicles from the endoplasmic reticulum (ER) to the plasma membrane [48]. The Caveolins are synthesized in the rough ER and co-translationally inserted in the ER membrane. After the insertion, CAV monomers aggregate to give rise to 8S-Cav oligomers (150-200kDa). 8S- CAV oligomers translocate to ER exit sites (ERES) from where they traffic to the Golgi apparatus through coat protein 2 (COPII) vesicle-dependent transport (reviewed in [48]). At the cis-media Golgi, 8S- CAV oligomers further oligomerize into more complex structures that contain roughly 160 CAV monomers and are referred to as 70S-Cav oligomers. Simultaneously, CAV molecules associate to cholesterol-rich

membranes, perhaps via the CRAC (cholesterol recognition amino acid consensus) domain (reviewed in [48]). At this point the cholesterol associated 70S-CAV oligomers exit the Golgi network in phosphate adapter protein 1 and 2 (FAPP1-2) and phosphatidylinositol-4- phosphate (PI4P) dependent transport and head to the PM (Figure 1–5) [48]. When 70S-CAV-cholesterol vesicles approach the PM, members of the cavin protein family are recruited. The exact mechanism of Cavin recruitment at 70S-CAV-cholesterol vesicles sites remains unclear, but some hypotheses have been made. 1) low affinity interaction of cavins with phosphatidylserine and CAV-1 simultaneously, is the trigger for recruitment or 2) changes in the PM curvature could already trigger the recruitment of cavins without further molecular interactions [112]. Once at the PM, CAV oligomers and cavin oligomers interact to form hetero-oligomeric complexes [73].

The interaction of CAV, cavins and cholesterol generate the membrane curvature necessary to form caveolae [48]. Caveolins and cavins together produce the membrane invagination by forming an extended tubular structure along the PM. In addition, EHD2 is another protein that may be involved in producing the fully-invaginated caveolae as well as controlling their stabilisation and association to cell surfaces [168, 169]. Furthermore, Hansen et al. [170] have reported that pacsin 2, that contains a membrane curvature-associated F-BAR domain, has also an important role in sculpting caveolae. The end result is a mature caveola, composed of three layers: a cholesterol-enriched membrane (negatively charged), a 70S-CAV oligomers coat, and a layered 60S-Cavin complex that runs outside the 70S-CAV oligomers coat (Figure 1–5) [48].

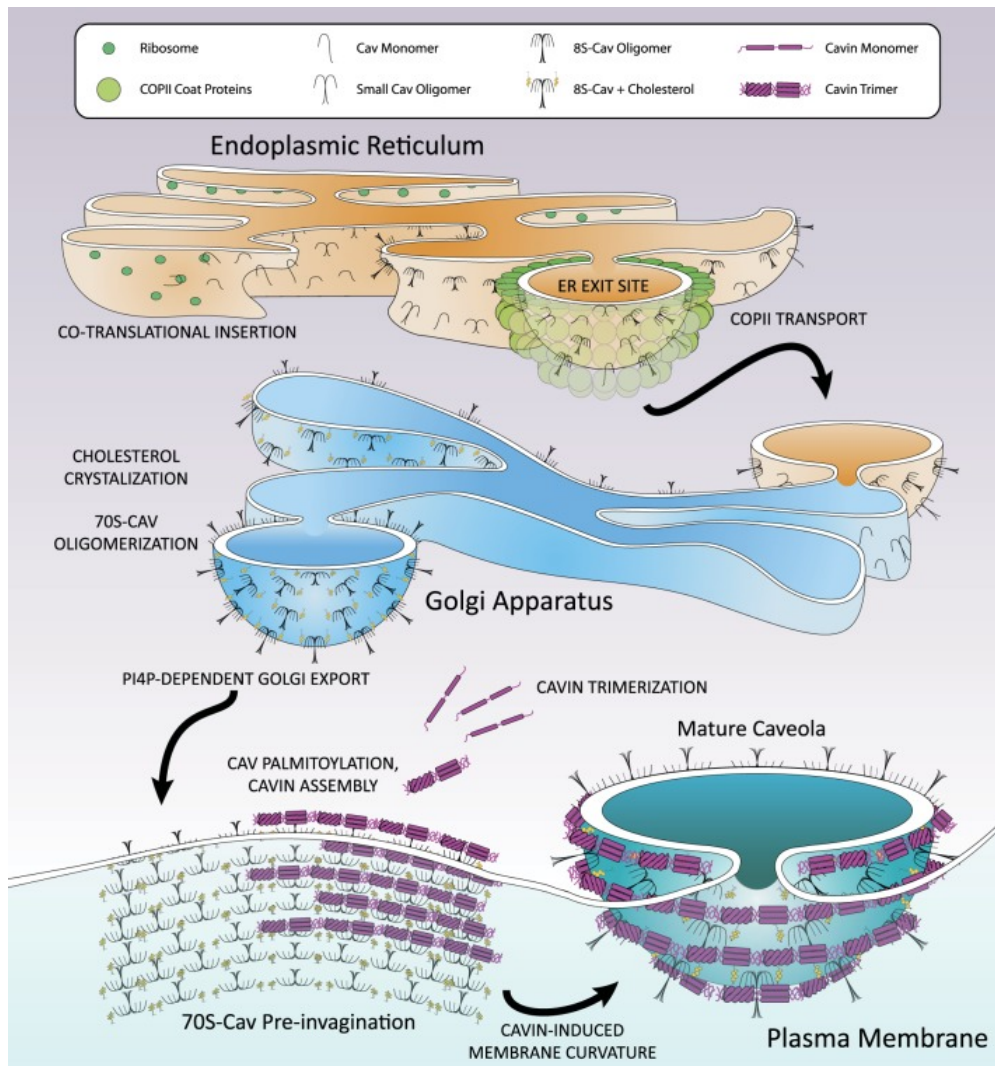


**Figure 1–5: Caveolae biogenesis.**

CAV-1 and CAV-2 enters the endoplasmic reticulum, where they are oligomerised into 8S-CAV oligomers. After their exit through the endoplasmic reticulum exit sites, these oligomers are transported to the Golgi apparatus, where the 70S-CAV complexes are formed by the help of cholesterol crystallisation. The complexes are then transported to the plasma membrane. At or near this site, the oligomers are palmitoylated by palmitoyl acyltransferases and the trimerised cavins are aggregated on the 70S-Cav membrane, where they assist in the membrane curvature to eventually form mature caveolae. Adapted from Busija et al. [48]

## 1.2.4 Functions of caveolae

A growing body of evidence suggested that the lack of caveolae impairs multiple functions of endothelial cells, adipocytes, and myocytes [112, 129]. This is because caveolae are involved in a variety of functions, including lipid homeostasis, endocytosis, mechanoprotection and signal transduction cascades [112]. The best evidence of caveolar functions comes from phenotypes of mice and patients lacking genes relevant to caveolae formation.

### 1.2.4.1 Mechanoprotection

In general, the morphology of caveolae buffer against rapid changes in membrane tension [59]. This property was first shown by Dulhunty and Franzini-Armstrong [171] when they suggested that caveolae could function as “safety valves” by flattening during increased membrane tension as a result of mechanical stretch as observed in the stretched frog muscles. In such circumstances, caveolae flatten due to detachment of the associated coats of cavin-1 from the membrane, leading to an increase in the surface area [129]. This would, in turn, prevent rupture of cell membrane and subsequent cell lysis. In addition to skeletal muscle tissue, caveolae have a mechanoprotective role in endothelial tissue and cardiac muscle cells, providing protection against hypo-osmotic swelling and increased mechanical force [172-174]. It has been shown that caveolae are essential elements for signalling cascades induced by mechanical stress on the PM, such as Akt phosphorylation and  $\text{Ca}^{2+}$  fluxes [175, 176].

Another mechanoprotective role of caveolae is apparent following membrane damage, during which caveolae modulate membrane repair through the formation of clusters at the site of damage [177]. Corrotte et al. [178] showed that caveolae repair membrane damage that can be induced by the pore-forming toxin streptolysin O. They emphasized also the role of CAV-1 in the resistance against membrane damage caused by mechanical insults and toxins [178]. The importance of caveolae can be best demonstrated in the reported phenotypes of muscular and pulmonary dysfunction in human and mice that have been associated with loss of caveolae [99, 127, 179-181]. Overall, this

model of caveolar functions reveals a potential paradox. While lateral forces implied on the PM causing a mechanical stress would lead to disassembly of caveolae, these forces might result in disruption of the membrane, where caveolae can act by removing the membrane lesion. As such, the complex mechanoprotective role of caveolae needs to be further clarified, including the actual stimuli that trigger caveolar budding, the molecular components involved in stimuli detection, and finally the signalling pathways induced by mechanical stress.

#### **1.2.4.2 Endocytosis**

Several research studies have been conducted to investigate the role of caveolae in endocytosis. For example, it has been shown that SV40 virus and cholera toxin could be endocytosed by caveolae (Figure 1–6) [182-184]. However, linking caveolae to endocytosis has been controversial. Recent studies revealed that overexpression of CAV-1-green fluorescent protein (GFP) resulted in its degradation in the late endosomal compartments, and this supports the possibility of involvement of classical endocytosis processes in cargoes uptake rather than via caveolae [185]. In addition, the investigations based on quantitative analysis and microscopy demonstrated a minimal contribution of caveolae in the endocytic flux that might reach to only 5% of the total caveolar population at high lipid induced levels [186]. Although the results of recent studies did suggest a possible role of caveolae in the regulation of clathrin-independent endocytic processes [52], the cellular functions of caveolar endocytosis remain incompletely defined [129].

Similarly, the impact of dynamin on caveolar budding is still doubtful. While reports have shown the localisation of dynamin at the neck of caveolae [187, 188], it seems that it is not essentially involved in caveolar endocytosis of damaged membrane [178]. Conversely, caveolar dynamics are controlled by the ATPase EHD2 during uptake of the affected membrane via co-localisation with caveolae [178].

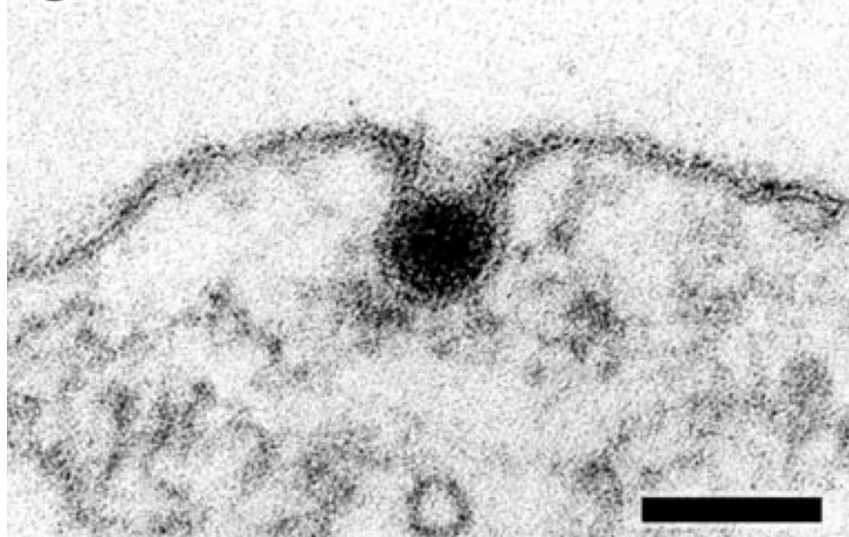


**Figure 1–6: Caveola-Mediated Endocytosis.**

An electron micrograph of a CV-1 monkey kidney cell showing Simian virus binding to gangliosides in the plasma membrane and entry via caveolae. Scale bar = 100 nm. Adapted from Marsh and Helenius [189].

### 1.2.4.3 Transcytosis

A specialised form of endocytosis has been shown in the endothelial cells, namely transcytosis, which involves the transport of lipids and proteins through the apical surface of vascular endothelial cells. Multiple reports proposed that caveolae could mediate transcytosis and transport of albumin, insulin, and low-density lipoproteins [190-192]. Caveolae-based transcytosis might take place via fusion-fission model that facilitate vesicular transport and/or the formation of temporary trans-endothelial pores [193, 194]. However, these data were in contrast with studies based on CAV-1-deficient mice, showing that transvascular protein transport has been accomplished in such animals [195, 196]. Therefore, there are still outstanding questions about whether caveolae are required for vesicular transcytosis in endothelial cells, if not, another set of cellular machinery for this process has to be addressed [129].

### 1.2.4.4 Lipid homeostasis

In general, the most frequently-reported phenotypes in caveolae-deficient mice are loss of subcutaneous fat, lipodystrophy, and dysfunctions of adipocytes [44, 197]. The functions of CAV-1 in lipid trafficking were first reported in *Caenorhabditis elegans* [198, 199]. CAV-1 has the ability to bind to fatty acids and cholesterol and it may have an important function in cholesterol trafficking [200]. Studies have shown that glycosphingolipids trafficking was altered and glycosphingolipids were accumulated in lysosomes present in CAV-1<sup>-/-</sup> cells [186, 201]. In addition, the expression of lipid biosynthetic enzymes is decreased with loss of CAV-1, leading to a significant reduction of specific lipids such as the glycosphingolipid GM3 and phosphatidylcholine [202]. Such evidence corroborates the importance of caveolae in the regulation of lipid composition in the plasma membrane. Moreover, alteration of lipid composition would have deleterious effects on the membrane nanoclusters, which contain distinct sets of proteins specialised for signal transduction. Therefore, this may represent an indirect mechanism by which caveolae disruption could alter signal transduction through disorganisation of particular lipids at the plasma membrane rather than through a direct interaction with membrane proteins [203].

#### 1.2.4.5 Caveolae-localised signalling

Reports have shown that caveolae are involved in cellular response to a diverse set of mechanical and chemical stimuli [204]. Caveolae have the ability to act as molecular switches for several cellular processes, in which they may be responsible for activation, inhibition, and modulation of multiple functions according to the self-interactions between signalling molecules. Such molecules include endothelial nitric oxide synthase (eNOS), insulin receptors, MAPK, and EGFR [205-209]. Ariotti et al. [202] have shown that agonist-stimulated MAPK activation might become unaffected by cholesterol depletion in CAV-1<sup>-/-</sup> MEFs, which could be mediated by a switch to K-RAS signalling. CAV-2 has been also shown to be an inhibitor of TGF- $\beta$  signalling and antiproliferative action in lung endothelial cells and, on the other hand, this function is switched to a pro-proliferative effect in the presence of TGF- $\beta$  [210].

The involvement of caveolae in cell signalling became clear following the discovery of caveolin gene family. For example, it has been reported that a single knockout of caveolin genes would have no effect on the vitality and fertility in mice, while cardiomyopathy and inflammation would be the consequences of double deletion of CAV-1 and CAV-3 [128]. These observations sparked considerable interest in understanding the pathological implications of dysfunctional caveolae with impairments in cell signalling.

Involvement of caveolae in signal transduction came from studies conducted on CAV-1, focusing on capability of such protein to bind and sequester a number of signalling adapters and the role of such binding in the essential regulation of downstream pathways. It has been shown that the CAV-1 binds to signalling molecules through its CSD domain and these molecules might be activated or inactivated within the caveolae.

The scaffolding property of CAV-1 led to the development of the “caveolae signalling hypothesis” [72, 211] which proposed a potential interaction between the 20-amino acid segment in CSD and a particular caveolin binding motif on

specific protein targets as a mechanism for caveola-mediated regulation of signal transduction. Actually, binding to CSD can cause inhibition of G-proteins, eNOS, EGFR, and H-Ras [208, 212, 213]. Nonetheless, such hypothesis has been refuted via a structure-based study of Collins et al. [214], whereby the most of conserved caveolin-binding motifs in signalling molecules are buried and inaccessible to the CSD domain.

Another observation which raised the interest regarding the role of caveolae in signal transduction is that caveolins might have the ability to modulate signalling regardless of their structural actions exerted during caveolae formation [215]. Within the endothelial cell models, it has been found that a variety of signal transduction receptors, such as GPCR and receptor tyrosine kinase (RTK), are either localised in caveolae or in a continuous interaction with caveolins [216]. There is also an evidence of caveolar contribution during GPCR internalisation. For instance, Escriche et al. [217] used cholera toxin to label the ganglioside GM1 in smooth muscle cell lines to study the involvement of caveolae in A1 adenosine receptor internalisation. The authors found that caveolae and CAV-1 contributed significantly during the receptor-mediated endocytic process. Indeed, caveolae might be an important therapeutic target for repairing the damaged endothelial tissue [204] relying on the critical roles of adenosine in inflammation and ischemia as well as the expression of adenosine receptors in endothelial cells [218]. In addition, RTKs represent a large family of molecules and their deregulation is involved in several diseases. Studies revealed that members of RTK family including angiopoietin, vascular endothelial growth factor (VEGF), and Platelet-derived growth factor (PDGF), have an essential role during angiogenesis and endothelial caveolin-1 specifically regulates VEGF-induced angiogenesis suggesting that localisation of VEGF to caveolae microdomains is crucial for VEGF-mediated signalling [219]. Overall, although the idea that supports the role of caveolar proteins in intracellular signalling has been confirmed elsewhere in the literature, many signalling-related aspects of caveolae are still unclear. It is imperative to reveal the effect of multiple caveolar isoforms on signalling in a given cell type. Given the post-translational modifications of caveolins [220], the putative impact of modified caveolins on cell signalling should be investigated.

### 1.2.5 Potential caveolae-targeting therapeutics

Caveolae provide a distinct environment where multiple receptor signalling components are sequestered, clustered and compartmentalized for efficient signal transduction. As such, considerable attention has been focused on the biology of lipid rafts generally and caveolae specifically as important sites of cell signalling. Indeed, a pivotal role of caveolae in the regulation of vascular contractility through binding to eNOS has been well-characterised [221]. In essence, eNOS was found to be inactive while it is linked to the scaffolding domain of CAV-1. Such linkage is disrupted when  $\text{Ca}^{2+}$  concentration is increased in the cytosol due to activation of calmodulin. As a result, nitric oxide is increasingly generated with a subsequent vasodilatation. This could be supported by blocking the interaction between CAV-1 and eNOS by a cell-permeable peptide that contains the CAV-1 scaffolding domain, namely cavnoxin, leading to sustained production of nitric oxide and a marker reduction in the blood pressure of wild-type but not eNOS knockout mice [221].

Indeed, caveolae can occupy up to 40% of the area of the plasma membrane in mammalian cell types such as adipocytes and muscle cells [185]. Moreover, the PM also contains a vital class of proteins that play central roles in cellular processes such as regulation of signal transduction, trafficking as well as the recently discovered scaffolding and shaping of the PM itself [14, 39]. Because of these diverse roles, the PM proteome accounts for 50% of the mass across biological membranes [222] and current estimates suggest that 15-39% of the genes in most sequenced genomes encode membrane proteins [223].

The study of PM proteins holds a great potential to yield many therapeutic targets across disease types. Mutations or improper folding of these proteins are implicated in a wide range of human diseases such as heart disease, obesity, cancer, cystic fibrosis, depression and many others. Currently, approximately 60% of commercially produced drugs target membrane proteins, mainly GPCRs [224, 225]. Thus, characterisation of PM proteins and their functions are critical for providing the molecular framework for understanding signalling and the effects of stimulation with various signal molecules [226]. Defining membrane proteomes is crucial to understanding the role of

membranes in the fundamental biological processes and for finding new targets for action in drug development.

### **1.3 Cytokine Signalling**

Cytokines are a complex of soluble extracellularly-secreted proteins that act as regulators of most aspects of the immune function, such as inflammation, as well as multiple facets of physiological processes, such as the wound healing [227, 228]. The main actions of cytokines generally include paracrine, autocrine, juxtacrine, and endocrine cellular communications which are exerted in a synergistic and pleiotropic manner. Notably, the expression of cytokines is transient and may last for hours to days to induce anti- or pro-inflammatory responses. Such action is essentially specific to cells in order to activate the effects of particular leukocytic compartments [229]. While the effects of cytokines are primarily targeted for the clearance of infection, other negative sequelae might emerge, such as lethargy, fever, allergy, sleepiness, and loss of appetite. Furthermore, multiple chronic inflammatory conditions, such as cardiovascular disease (Figure 1–7) and chronic rheumatoid arthritis, can be associated with persistent cytokine production [230, 231].

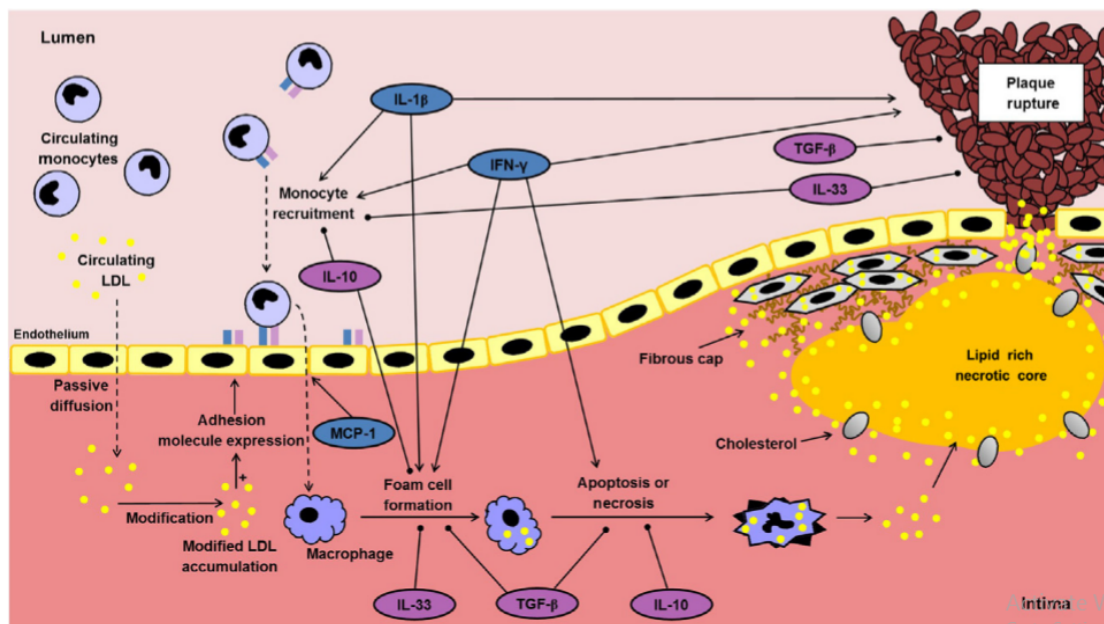


**Figure 1–7: The role of cytokines during atherosclerosis development.**

The expression of adhesion molecules on the activated endothelial cells recruits the circulating monocytes, which would differentiate into macrophages in the arterial wall. Such macrophages express scavenger receptors to take up modified low-density lipoproteins (LDL). A fibrous cap is formed due to an increase in the lipid content that released from the dead foam cells. In addition, an atherosclerotic plaque forms due to persistent formation of foam cells along with profound inflammatory responses. Several anti-inflammatory (purple) and pro-inflammatory (blue) cytokines are involved in plaque development. IL, interleukin; IFN, interferon; MCP, monocyte chemoattractant protein; and TGF, transforming growth factor. Adapted from Moss and Ramji [232].

There are over 50 cytokines and many exist in families that share receptor components and signal transduction pathways [229]. Cytokines include interleukins (IL), interferons (IFN), tumour necrosis factors (TNF), transforming growth factors (TGF), and colony stimulating factors (CSF). Additionally, researchers have identified about 70 potential candidates by using sequence comparisons [233]. The structure of the target receptors, that include hematopoietin/type 1, interferon/type 2, IL1/toll-like receptor, and TNF is considered an important determinant of the affecting cytokine. For instance, the effects of IL-6 can be exerted on the haematopoietin/type 1 receptors, where glycoprotein (gp)-130 is the commonest signalling unit [234].

The biological effects of cytokines involve dimerisation of cell receptors into assemblies [235, 236]. In the canonical model of cytokine signalling, this would in turn result in activation of Janus Kinases (JAKs) and non-receptor tyrosine kinase (TYK2) [237]. At this stage, both TYK2 and JAKs are constitutively bound to cell receptors. JAKs then cause phosphorylation and activation of signal transducer and activator of transcription (STAT) proteins, which subsequently mediate gene expression modulation and eventually the fate of the cell [238-240]. Additionally, some cytokines may have a role in the activation of the ERK1,2 and Akt signalling and other signalling pathways [241, 242].

In general, pleiotropy and redundancy represent the main features of cytokines, in which their degenerate nature is responsible for such properties [243]. Pleiotropy is defined as the ability of a given cytokine to induce a variety of responses. The impact of a single cytokine might be exerted on more than one receptor complex leading to activation of specific JAK/STAT signalling pathways and subsequently a number of functional responses [244]. In addition, the capacity of a group of cytokines to induce their actions in overlapping activities is another remarkable feature of cytokines, that is their redundancy. Indeed, multiple cytokines might share the receptor subunits to form certain cytokine complexes which, due to the presence of four JAKs and seven STAT proteins, would activate a set of JAK/STAT combinations [245, 246]. Despite utilising a limited number of signalling proteins in these combinations, cytokines still have the capacity to perform a variety of activities

and they can be involved in highly complicated immune functional responses [247]. Nonetheless, the current understanding is still incomplete regarding multifarious determinants of cytokine receptor signalling that integrate into a broad range of biological actions and it seems that researchers in this field have to elucidate more details about the ways by which such specificity could be attained, considering the redundant and pleiotropic nature of cytokines.

It is noteworthy that most recent knowledge emphasises complex relationship between a given activated signalling molecule and the resultant biological activity. For example, although STAT3 could be activated by both the IL-6 and IL-10, the exact roles of such cytokines are typically contrasted, in which the former induces a pro-inflammatory and the latter elicits an anti-inflammatory response [248, 249]. Moreover, another clear example is that there are more than 16 subtypes in the type I IFN system that could share a corresponding receptor complex, inducing a set of distinct biological activities [250, 251]. Given the importance of lipid rafts-mediated cytokines receptors signalling that has been demonstrated by several lines of evidence [252-254], knowledge about the effects of caveolin expression or function on the JAK/STAT signalling pathways is still insufficient. In the following sections, I explain the JAK/STAT signalling pathway and its potential interaction with cavin-1.

### **1.3.1 The JAK/STAT pathway and its regulation**

Four proteins constitute the JAK family, namely JAK1, JAK2, JAK3, and TYK2 [255]. On the other hand, the STAT family in mammals is composed of seven proteins, STAT1, STAT2, STAT3, STAT4, STAT5A, STAT5B and STAT6 [256]. All STATs are highly homologous in multiple regions, such as the SRC homology 2 (SH2) domain, which is involved in the process of STAT activation and dimerisation [257]. The JAK/STAT pathway is utilised by multiple cytokines, hormones and growth factors. Following cytokine receptor activation by its ligand, the kinase function is activated and this would be accompanied with auto-phosphorylation as well as cross-phosphorylation of a distinct JAK molecule that is bound to the heterodimer domain of the cytokine receptor [258]. In addition, the intracellular tail of the receptor (tyrosine residues) is phosphorylated, creating suitable docking sites and allowing binding of the

cytoplasmic STATs to these regions through the SH2 domain (Figure 1–8). After their phosphorylation, conformational changes would occur in the STATs leading to their separation from the receptor followed by dimerisation (or binding of two homologous STATs). STATs are then translocated to the nucleus, where they promote the expression of their specific genes [238]. Given the high functional specificity of the resultant complexes of different JAK/STAT proteins in various aspects of the immune response as revealed by the genetic knockout studies [259, 260], it is thought that such specificity can be attributed to the activation patterns of individual cytokines and, to some extent, specific regulation of gene expression [261].

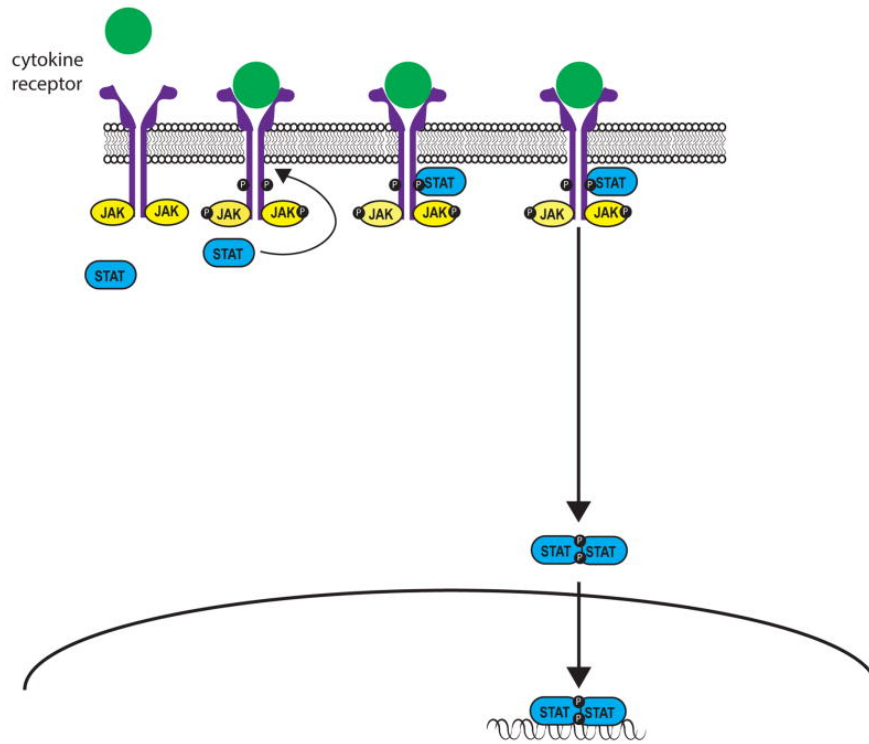


**Figure 1–8: A schematic representation of the JAK/STAT pathway.**

Cytokine-induced JAK activation leads to phosphorylation of STATs with subsequent dimerisation and translocation to the nucleus. Adapted from O'Shea et al. [262].

The JAK/STAT pathway is tightly regulated by distinct mechanisms at several steps. The mechanisms of the post-translational regulation include the protein inhibitor of activated STAT (PIAS), protein tyrosine phosphatases (PTPs), and suppressor of cytokine signalling (SOCS) proteins. In addition, other levels of regulations might involve the typical cross-talks between the various JAK/STAT pathways as well as other cell signalling pathways [263].

Multiple PTPs have been implicated in the regulation of JAKs, such as SH2-containing PTP (SHP)-1, SHP-2, T-cell PTP, and PTP1B [264]. An additional role of SHP-2 in case of IL-6 has been emphasised as it is required for ERK1/2 and PI3K pathways [265, 266]. Furthermore, studies have shown that SHP1 might be responsible for dephosphorylation of JAK1 and JAK2 [267, 268], while JAK2 and TYK2 can act as potential substrates of PTP1B [269]. In addition, JAK1 and JAK3 are dephosphorylated by T-cell PTP [270]. Indeed, PTPs have important physiological and pathophysiological consequences [271].

The role of PIAS is targeted for the regulation of several transcription factors, including STATs [272]. The family of PIAS proteins includes PIAS1, PIAS3, PIASX, and PISAY. The interaction of PIAS proteins with STAT members have been identified in the mammalian cultured cells, in which PIAS1 interacts with STAT1 in macrophages [273], PIAS3 with STAT3, and PIASX with STAT4 [272, 274, 275]. Moreover, PIAS1-STAT1 interaction has been reported [276]. It has been shown that STAT regulation via PIAS proteins is cytokine-dependent and this interaction is not demonstrated in the unstimulated cells. This can be supported by the interaction of PIAS1 with the dimeric, rather than the monomeric, form of STAT1 [277]. All PIAS family members have the ability to inhibit STAT-induced gene activation through inhibition of their DNA binding or recruitment of histone deacetylases [278].

### **1.3.2 Suppressor of cytokine signalling proteins**

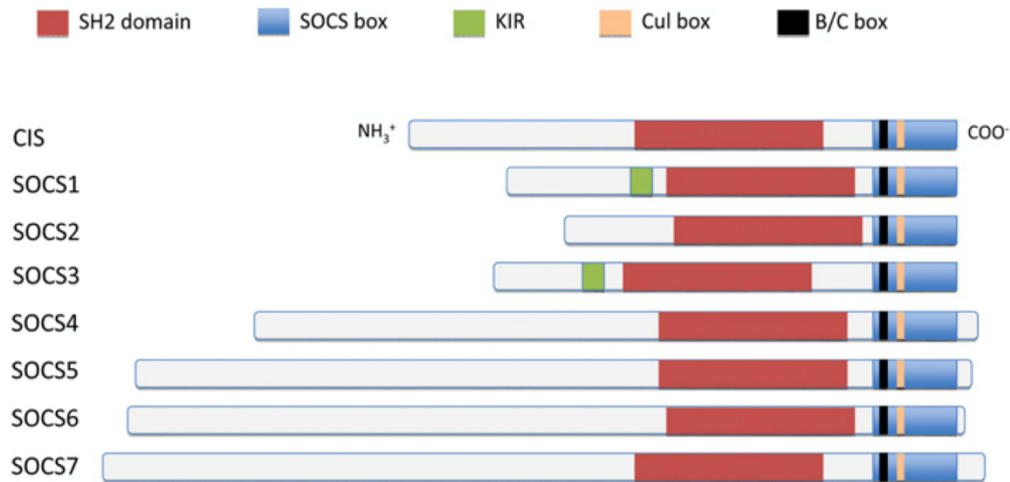
#### **1.3.2.1 Structure and functions of SOCS**

CIS was the first identified member of the SOCS family in 1995 [279]. This was followed by an evidence of the inhibitory effects of SOCS1 on STAT1 signalling

[280, 281] along with the prediction of existence of other homologous SOCS proteins. Currently, there are eight identified members, SOCS1-7 and CIS. Each member of the SOCS family contains a central SH2 domain, which is flanked by a short C-terminal domain (the SOCS box) and a variable N-terminal domain (Figure 1–9a) [282].

Some of the inhibitory effects of the SOCS are performed by ubiquitination and proteasome-induced degradation. The SOCS box binds to a complex that contains elongin B and C and cullin-5 [283, 284]. Having a central SH2 domain, SOCS proteins can function as substrate adapters for phosphorylated JAKs, phosphorylated STATs, and phosphorylated receptors (Figure 1–9b). Therefore, the SH2 domains would mediate the degradation of kinase-activated proteins [284].

A



B

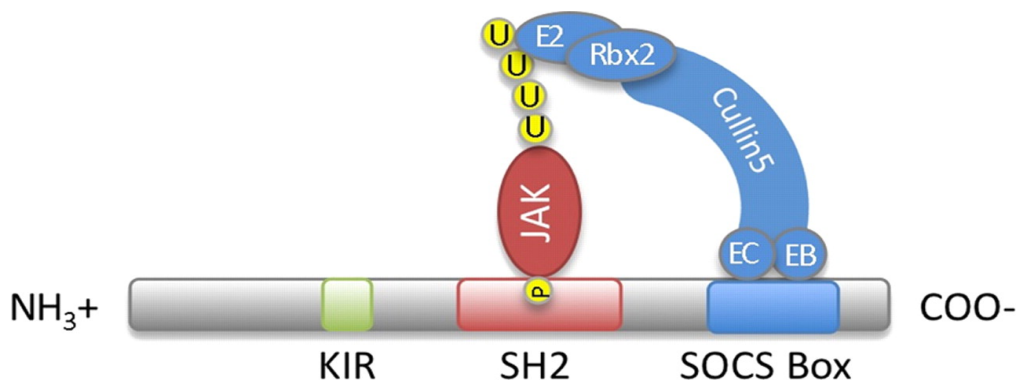


**Figure 1–9: The structural domains of the SOCS family proteins and their perceived interaction in cellular signalling.**

(A) Different structural domains of SOCS 1-7 and CIS; (B) The functional interaction of the SOCS domains. The SH2 domain binds to specific phosphorylated tyrosine residues located on its substrates, mostly JAK proteins, while the SOCS box facilitates ubiquitination of target proteins through the interaction with Elongin B (EB), Elongin C (EC), Cullin5, RING-box-2 (Rbx2), and an E2 ubiquitin-conjugating enzyme. The kinase inhibitory region (KIR) is located in some SOCS proteins and it might act as a pseudosubstrate to inhibit the kinase activity of bounded proteins. Adapted from Galic et al. [285] and Akhtar and Benveniste [286]

Nonetheless, it has been reported that both SOCS1 and SOCS3 exhibit inhibitory activity even in the absence of their SOCS box domains [287]. These SOCS box domains can be also bound to the E3 ubiquitin ligase in a lower level than that of other SOCS proteins [284]. In particular, SOCS1 and SOCS3 can bind directly to the JAKs causing inhibition of their catalytic activity. While the inhibition of tyrosine phosphorylated JAKs by SOCS1 depends on the direct binding to its SH2 domains, the inhibition of JAKs by SOCS3 requires the interaction, or binding, between SOCS3 and the activated receptor [280, 281, 288, 289].

Experimental studies revealed an important role of SOCS proteins on the physiological and pathological levels. For example, early lethality occurs within 3 weeks in mice deficient for the SOCS1 molecule as a result of severe generalised inflammation and excessive interferon signalling [290]. Further, SOCS2 knockout led to the development of gigantism in mice, possibly due to hyper-responsiveness to growth hormone [291]. Finally, defective placental formation was the most apparent reason of perinatal death that has been reported resulting from homozygous deletion of the SOCS3 gene [292, 293].

#### **1.3.2.2 Regulation of cytokine signalling by the SOCS proteins**

SOCS represent one of the major regulatory mechanisms of cytokine signalling [294]. They can generally act as negative feedback circuits, where each SOCS molecule is transcriptionally induced by its corresponding, or target, STAT protein. It is necessary to note that the SOCS proteins are scarcely detectable in unstimulated cells, while cytokines induce rapid expression of SOCS genes.

Given the essential control exerted by the SOCS on JAK activity in terms of intensity and duration, SOCSs have the potential to regulate both the quantitative and qualitative patterns of cytokine signalling. For example, the transcriptional signature of IL-6 is transitioned from a STAT3-mediated to a STAT1-mediated process in the absence of SOCS3, demonstrating the qualitative side of cytokine signalling [295, 296]. As a consequence, studies have shown that SOCS proteins have remarkable effects on immune cell function, which is supported by the inflammation-induced death in mice

lacking SOCS1 protein as well as the role of the latter protein in T cell development and pro-allergic T cell responses [294, 297, 298].

In addition, the roles of SOCS2 and SOCS3 has been emphasised in macrophage differentiation [299], which is related to the control of SOCS3 ubiquitination and turnover by SOCS2 [300]. Moreover, SOCS3 plays a key role in the regulation of macrophage functions as demonstrated by the IL-6-mediated suppression of LPS-induced TNF- $\alpha$  production in SOCS3<sup>-/-</sup> macrophages [301].

## 1.4 SOCS3

The induction of SOCS3 proteins is mediated by several cytokines, such as those affecting the gp130 receptors (IL-6), IL-2, IL-3, IL-4, IL-10, type I and type II IFNs, and leptin. Moreover, agonists of the toll-like receptors, including lipopolysaccharide (LPS) and CpG-DNA, cyclic AMP-mobilising hormones, prolactin, and growth hormone might also mediate SOCS3 induction [294, 302-304]. At this step, SOCS3 proteins have an important role in the regulation of the magnitude, quality, and the different kinetics of JAK/STAT signalling. A key factor is the binding of the SH2 domain of SOCS3 proteins to particular phosphorylated tyrosine (PTyr) residues on their targets (Figure 1–10). Given the primary action of SHP2 in the activation of the ERK1/2 pathway which might also drive the Gab1-dependent phosphatidylinositol-3-kinase (PI3K)-Akt signalling [305] and, on the other hand, the ability of SOCS3 to bind to the SHP2 binding site on gp130, it is expected for the SOCS3 proteins to inhibit ERK1/2 and PI3K activation through a direct competing mechanism on the SHP binding site. However, this competition has not been demonstrated since Lehmann et al. [306] found that both SOCS3 and SHP2 can act independently to inhibit IL-6 signalling.

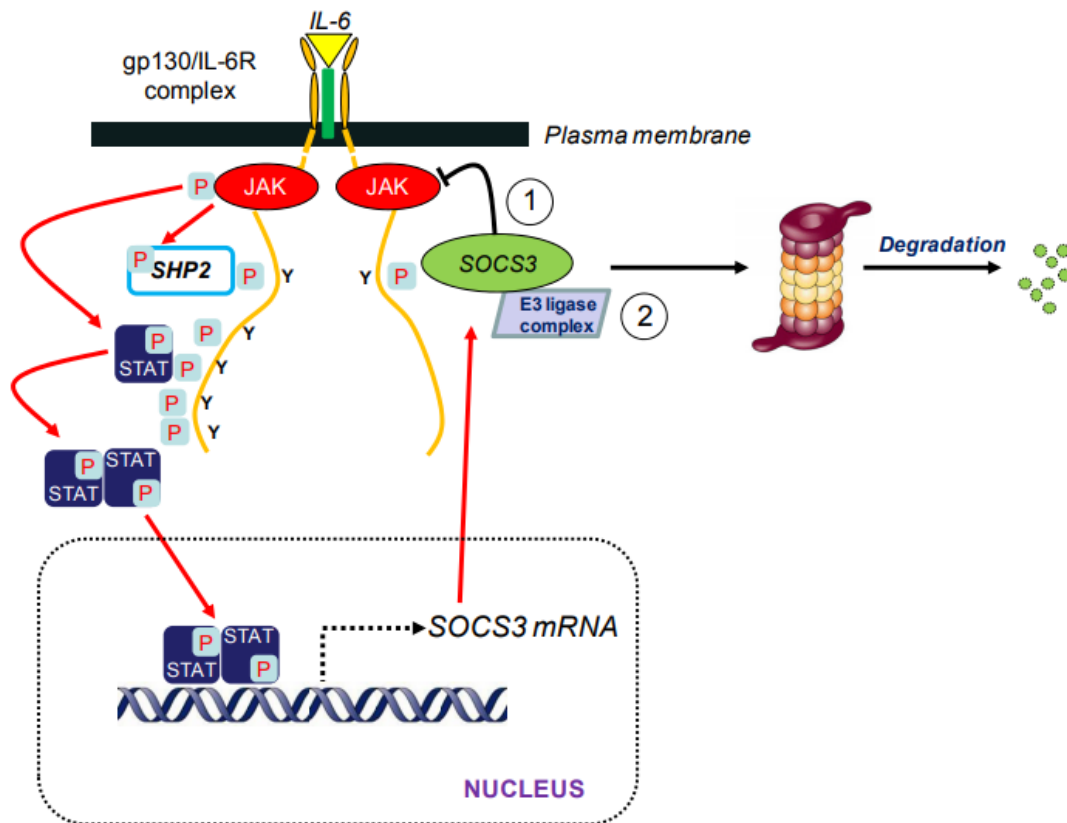


**Figure 1–10: Inhibition of IL-6 signalling via SOCS3.**

Following activation of gp130-bound JAKs via IL-6 interaction, gp130 tyrosine residues are phosphorylated and act as docking sites for STAT proteins (predominantly STAT3). Following their phosphorylation, STATs dimerise and translocate to the nucleus to induce gene expression. Then SOCS3 proteins are encoded by one of the induced genes to interact with the phosphorylated gp130. Such interaction is exerted via two distinct mechanisms: 1) inhibition of the receptor-bound JAKs via the KIR domain and 2) integration in an E3 ubiquitin complex that mediates the proteasomal degradation of target proteins. Adapted from Williams et al. [307].

### 1.4.1 SOCS3 structure

In general, three domains have been identified in SOCS3 proteins: the N-terminal domain (which includes the kinase inhibitory region “KIR”, containing residues from 1 to 29), the SH2 domain (residues from 30 to 185), and the SOCS box domain (residues from 186 to 225, Figure 1–11A).

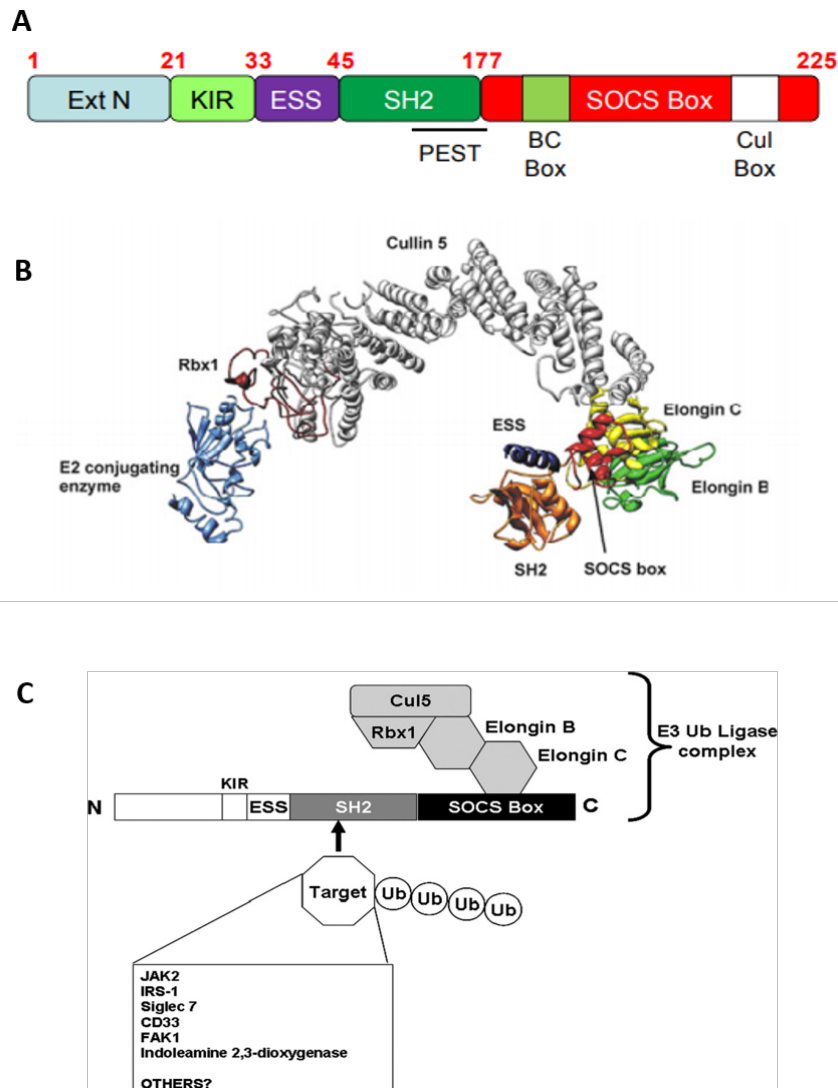


**Figure 1–11: Structural organisation of the SOCS3 domains**

(A), structural homology modelling of the ECS-E3 ubiquitin ligase complex in a graphical illustration (B) and a schematic diagram (C). Adapted from Piessevaux et al. [308] and Williams and Palmer [309].

#### 1.4.1.1 The KIR domain

It has been shown that both SOCS1 and SOCS3 have a pseudosubstrate domain, namely the KIR, at the N-terminal domain (a 12-residue motif) which is able to interact with the receptor-associated JAKs via their JH1 domain (Figure 1–11). This interaction is thought to have an inhibitory effect on substrate phosphorylation [310]. Since the first eight residues of KIR are not structured and the remaining residues represent the first part of the  $\alpha$ -helix [311, 312], KIR has been reclassified as residues 21-32, with the 33-44 residues forming the extended SH2 domain (ESS) [313].

Studies have shown that the KIR might act as a pseudosubstrate for JAK1 and JAK2 causing inhibition of their activity [314]. This might be attributable to the similarity of sequence between KIR and the activation loop that is located on all JAKs. While unphosphorylated, such loop blocks substrate/ATP binding through acting as a potential pseudosubstrate. Therefore, the process of binding of the SH2 domain of SOCS3 to the phosphorylated activation loop would entail a significant inhibition of its action. Nonetheless, Babon et al. [315] postulated that SOCS3 might act as a non-competitive inhibitor of JAKs by binding to a specific glycine-glutamine-methionine (GQM) motif in distinct JAK proteins rather than the competitive inhibition of the activation loop. More details about SOCS3-GQM interaction would be discussed in section 1.4.3.

#### 1.4.1.2 The SH2 domain

The activity of SH2 domains is linked to their ability to bind to the phosphotyrosine residues on some proteins, such as the pY1007 residue on JAK2 [310] and pY757 on the gp130 co-receptor. In fact, the affinity of binding of the gp130 co-receptor to the SH2 domain of SOCS3 is more than 1000-fold greater than the binding to pY1007 on JAK2 [316, 317]. Moreover, other SH2-binding cytokine receptors include leptin [318], granulocyte colony-stimulating factor receptor [319], erythropoietin receptor [317, 319], growth hormone receptor [320], insulin receptor [321], and IL-12R $\beta$ 2 [322]. The high affinity of the SH2 domain for binding with such distinct cytokine receptors might be the major player in the specificity of SOCS3 in the process of signalling

suppression. It is important to note that the predominant targets of SOCS3 for signalling inhibition are IL-6, IL-11, ciliary neurotrophic factor, granulocyte-colony stimulating factor, and leptin as per results based on genetic knockout studies in mice.

The crystal structure of the SOCS3/JAK2/gp130 complex revealed whether SOCS3 can bind to gp130 and JAK in a sequential or simultaneous manner [323]. In fact, SOCS3 is able to bind to both the cytokine receptor and JAK2 at the same time and it can also exert its action targeting the specific JAK/gp130 complexes. Such structure showed that the gp130 receptor was bound to the SH2 domain via its phosphotyrosine binding pocket. On the other hand, the JAK2 kinase was bound to the other side of the SH2 domain as well as the KIR and the ESS helix in a phospho-independent fashion. The ability of SOCS3 to exclusively inhibit a distinct set of cytokines that signal via JAK1, JAK2, and TYK2 might be explained by the SOCS3 requirements to simultaneously bind to the receptor-JAK complex [324].

Another remarkable feature of the SH2 domain is that it contains an unstructured loop of 35 residues in which its sequence mimics that of the Pro-Glu-Ser-Thr-rich (PEST) motif [311, 325]. It is thought that the PEST motif mediates the proteasome degradation of proteins. In fact, the role of the PEST motif in SOCS3 degradation is as the half-life of SOCS was increased without altering SOCS3 functionality when the PEST motif was deleted [324].

#### **1.4.1.3 The SOCS box domain**

The SOCS box domain was initially-identified as a characteristic motif in the C-terminal domain of SOCS3 proteins, but it is now known to be shared by more than 80 other proteins in humans [326]. In general, two interaction sites have been identified in the SOCS box: the Cul5-box and the BC-box. The former is known for its ability to bind to cullin 5, the scaffold proteins, while the latter is responsible for elongin B and C recruitment [281, 327]. Elongin B and C as well as SOCS3, cullin 5 and the Rbx2 Really Interesting New Gene (RING) protein form the E3 ubiquitin ligase complex [284], for subsequent proteasomal

degradation. More details about the elongin-cullin-SOCS (ECS)-E3 ubiquitin ligase complex can be found in section 1.4.4.

### **1.4.2 SOCS3 expression and regulation**

Both the mRNA and protein expression of SOCS3 are tightly regulated. Transcription of SOCS3 is rapidly induced by several type I and type II cytokines. Induction of SOCS3 expression by IL-6 is dependent on the specificity protein 3 [328], while LPS induces SOCS3 expression via the c-Jun N-terminal kinase (JNK) and MAPK-ERK1/2 pathways [329]. In addition, TNF $\alpha$ -induced expression occurs by activation of the MAP kinase kinase (MKK)/MAPK pathway [330], whereas Epac-1 (exchange protein directly activated by cAMP 1) is utilised to induce expression of SOCS3 by cyclic adenosine monophosphate (cAMP) [304]. IL-1, IL-9, IL-10, and leptin are considered other contributors in inducing SOCS3 expression [331-334]. On other hand, proto-oncoprotein growth factor independence-1B and hepatocyte nuclear factor-1 $\beta$  might suppress SOCS3 transcription [335, 336], while TGF- $\beta$  inhibits SOCS3 induction [337].

Proteasomal and non-proteasomal degradation pathways are involved in controlling SOCS3 proteins. This could be demonstrated in several in vitro studies via modification or knockout of the SOCS box, PEST motif, or mutation of ubiquitination site Lys<sup>6</sup> to Gln [283, 311, 338] although their significance in vivo has not been fully discerned. Experimental evidence in cell lines have shown that the increased expression of SOCS2 proteins might contribute to enhanced SOCS3 degradation [300, 339]. It has been suggested that the formation of an E3 ubiquitin ligase comprised of SOCS2, SOCS3, and elongin B/C might promote SOCS3 ubiquitination and thereby mediate SOCS3 degradation. In contrast, SOCS3 regulation has been shown to be independent of SOCS2 in SOCS2-deficient primary mice cell lines, suggesting some redundancy in this process [340].

### **1.4.3 SOCS3 as an inhibitory protein through KIR-JAK2 interaction**

Babon et al. [315] have shown that the ability of SOCS3 to selectively bind to JAK1 and JAK2 as well as TYK2 rather than JAK3 may be attributable to the lack of hydrophobic amino acid sequences (GQM sequences) in the latter. In general, the GQM sequence is located at the JH1 kinase domain at its  $\alpha$ -helical region that is exclusively present in the JAK proteins [341]. More specifically, the location of GQM sequence at positions 1071-1073 on JAK2 enables the binding of SOCS3 protein through the KIR, SH2, and ESS (Figure 1–11). Although the structural changes of JAK2 implied by binding of the GQM sequence to SOCS3 might be minimal [323], the inhibitory functions of SOCS3 are lost when mutations take place in specific key residues (Phe25Ala) at the KIR domain of SOCS3, indicating the importance of such domain [323]. Further, it has been suggested that SOCS3 might inhibit JAK2 by prevention of cognate substrate binding and thereby can be a JAK2 pseudosubstrate [315]. Additional confirmatory evidence of KIR importance is demonstrated by a ten-fold increase in the half maximal inhibitory concentration ( $IC_{50}$ ) of the inhibitory effect of SOCS3 exerted on JAK2 when the first 3 residues in the KIR are deleted. Additionally, studies of the crystalline construct of the SOCS3-JAK2-gp130 complex demonstrated that Arg21, which flanks the KIR, might act as a true pseudosubstrate residue as it interacts with the substrate binding domain of JAK2 [323]. Indeed, SOCS3 phosphorylation would occur upon mutation of the first 3 residues in the KIR [323].

### **1.4.4 SOCS3 and E3 Ubiquitin Ligase activity**

The SOCS box domain in all SOCS family members is able to form a complex called ECS-E3 ubiquitin ligase complex, which would target its substrates for subsequent ubiquitylation and proteasome-mediated degradation (Figure 1–11). E3 ligase is one of three sequential enzymes that catalyse the conjugation of ubiquitin to lysine residues of the target proteins [342]. The Leu<sup>210</sup>ProGlyPro domain of the SOCS box of SOCS3 has the ability to directly bind the cullin 5 protein [343]. In addition, SOCS3-cullin5 binding could be attained indirectly via the interaction between SOCS3 and elongin B/C heterodimer which is bound to

the N-terminal domain of cullin 5. Cullin 5 is bound also to the Rbx2 protein via its RING domain in the C-terminus, leading to facilitation of the interaction with the E2 conjugation protein (Figure 1–11B) [324, 344].

Nonetheless, the short half-life and slow on-rate properties of SOCS3 caused a significant reduction of its affinity for the E3 scaffold proteins (ten-fold lower when compared to other SOCS members) [284, 307]. Such low affinity might be related to the variations in the binding sequences, where LeuProGlyPro binds to SOCS3 while LeuProLeuPro binds to other SOCS proteins except SOCS1 [284]. Hence, SOCS proteins can be divided into two subclasses according to their affinity to cullin 5 binding. While SOCS1 and SOCS3 act in a dual pattern, other SOCS proteins can only exert their inhibitory actions through ubiquitin-dependent pathways [284]. Nonetheless, in light of the reported E3 ligase functionality with SOCS1 and SOCS3 proteins, E3 actions should be investigated for other SOCS proteins [284]. The knowledge concerning SOCS1/3 substrates which are regulated by ubiquitin is incomplete. The immunological defects that have been reported in mice deficient in the SOCS box of SOCS1 or SOCS3 might raise the interest in understanding the regulatory roles of both SOCS family members in such proteasome-dependent processes [345, 346].

The dual inhibitory mechanisms of SOCS3 proteins is supported by the central SH2 domain that allows binding of SOCS proteins to the phosphorylated targets (Figure 1–11B). It is worthy to note that the formation of an E3 ligase complex, which is of a large size, might sterically hinder the binding of SOCS3 proteins to their targets. It seems that the availability or the abundance of E3 ligase is the essential determinant of assembly and functionality [307]. However, the inhibition or ubiquitylation of SOCS3 substrates might be performed in a sequential manner, which means that, in certain events, it is not possible to perform these roles independently [307].

Currently, several targets of the elongin-cullin-SOCS (ECS)-E3 ubiquitin ligase complex have been identified. These include JAK1 [347], Siglec7 [348], and G-CSFR [349]. In the case of G-CSFR, SOCS3 exerts a direct inhibitory effect,

via binding to the pY729 motif of the receptor and inhibiting receptor-bound JAK via the KIR domain, as well as indirectly inhibiting signalling through forming a ligase complex to ubiquitinate Lys632 of the G-CSFR leading to signal attenuation and sorting of lysosomal proteins [350].

Experimental studies on mouse myeloid progenitor cells have revealed a SOCS box-dependent inhibition of colony formation via the G-CSF [351]. Furthermore, a significant reduction of SOCS3 mRNA and protein expression as well as an enhanced activation ratio of STAT5/STAT3 in response to G-CSF were observed in mice with a truncated form of G-CSFR lacking the SOCS3 recruitment site (Tyr729) [352]. In addition to G-CSFR, the proteolytic role of the ECS-E3 ubiquitin ligase complex has been demonstrated on the insulin receptor substrate (IRS)-1/2 [353].

#### **1.4.5 Identifying cavin-1 as an interactor SOCS-3**

Protein ubiquitylation is a post-translational modification that regulates cell signalling. It might be associated with several outcomes, such as endocytosis, DNA repair, endocytosis and protein degradation. E3 ligases are considered a vital element of the ubiquitin proteasome system (UPS) that outline the specificity of substrate via the covalent binding to ubiquitin. Although there are more than 600 E3 ligases that have been identified, several aspects relevant to their characterisation are still not completely elucidated, particularly those pertinent to the specific protein substrates [354]. Target identification by using novel methods, models, and tools might represent a major approach for enhancing the understanding of various aspects of UPS function as well as improving knowledge about a variety of disease processes in which it is involved [354].

Currently, ubiquitylation and proteasomal degradation in a SOCS3 SOCS box-dependent manner have been observed in a limited number of SOCS3 substrates (Table 1–1). Nonetheless, such observations are based on cellular overexpression models, and this ultimately entails validation via cell-free-ubiquitylation studies that utilise purified components [307]. The identified SOCS3 substrates perform unique functions in the cells, and these substrates

shared two properties which are: (1) their interaction with the SH2 domain of SOCS3 occurs in a Tyr phosphorylation-dependent manner, and (2) the process of substrate ubiquitylation requires an intact SOCS box [307, 309].

<b>Substrate</b>	
1	Janus kinase 1 (JAK1)
2	Focal adhesion kinase 1 (FAK1)
3	Insulin receptor substrate 1/2 (IRS1/2)
4	Sialic acid-binding Ig-like lectin (SIGLEC) 3/CD33
5	Sialic acid-binding Ig-like lectin (SIGLEC) 7
6	Indoleamine 2,3-dioxygenase (IDO)
7	Granulocyte colony-stimulating factor receptor (G-CSFR)

**Table 1–1: Known SOCS3 substrates**

An updated list of the identified SOCS3 substrates that can be ubiquitylated and proteasomally-degraded. Adapted from Williams and Munro [307].

Novel physiological functions of SOCS3 are likely to be revealed by the discovery of additional substrates of the SOCS3 E3 ubiquitin ligase. This will provide adequate knowledge about the down regulation of the inflammatory response as well as the protein degradation pathways relying on ubiquitin. This would possibly lead to further identification of novel therapeutic targets which might be applicable to cytokine-driven conditions such as atherosclerosis, arthritis, viral or bacterial infection, or cancer [307, 324]. However, false-positive outcomes could be attained as a result of some limitations in the currently-utilised methodologies. In addition, protein-protein interaction can be employed for validation purposes. This might include co-immunoprecipitation, fluorescence resonance energy transfer, protein-microarray, peptide array, and glutathione-S-transferase-pull-down assays [354].

Williams et al. [309] used an unbiased identification approach to experimentally identify the proteins that might be targeted by SOCS3 for ubiquitylation. To this end, (His)<sub>6</sub>-biotin-tagged Ub (HB-Ub)-expressing WT and SOCS3<sup>-/-</sup> mouse embryonic fibroblasts (MEFs) were produced via retrovirus-mediated gene transfer. These cell lines were tested by immunoblotting for stably expressing equivalent levels of a tandem-affinity-tagged ubiquitin transgene as previously described by Meierhofer et al. [355]. This enabled a tandem affinity purification of ubiquitin, maintaining the ubiquitylation status by the denaturing conditions and reducing the possibility of co-purification of proteins that are bound to ubiquitin. Using a targeted analysis of the purified ubiquitin comprised of stable isotopic labelling of amino acids in cell culture (SILAC) and liquid chromatography (LC), multiple ubiquitylated proteins have been identified by Williams and Palmer [309] in wild type MEFs but not their SOCS3<sup>-/-</sup> counterparts, indicating that these proteins could be newly identified potential targets for the ECS<sup>SOCS3</sup> complex. Notably, the detection of FAK1, which was formerly described as a substrate for SOCS3-dependent ubiquitylation, provided supportive evidence for the validity of this approach [309].

Experimental procedures and data analyses:

Intracellular cAMP was elevated along with forskolin (50  $\mu$ M) as an adenylyl cyclase activator to induce SOCS3 (Figure 1–12) [356]. To enhance the possibility of identifying SOCS3-dependent ubiquitylating proteins, a combination composed of sodium orthovanadate and H<sub>2</sub>O<sub>2</sub> was used to inhibit protein tyrosine phosphatases and to maximise binding to the SH2 domain of SOCS3. In addition, the proteasome inhibitor MG132 was used to preserve the cellular ubiquitinome. An Orbitrap Velos fourier transform mass spectrometer (FTMS) was utilised to analyse the tandem affinity-purified ubiquitinomes from the WT and SOCS3-deficient MEFs. Data processing was performed using the MaxQuant quantitative proteomics software package [356].

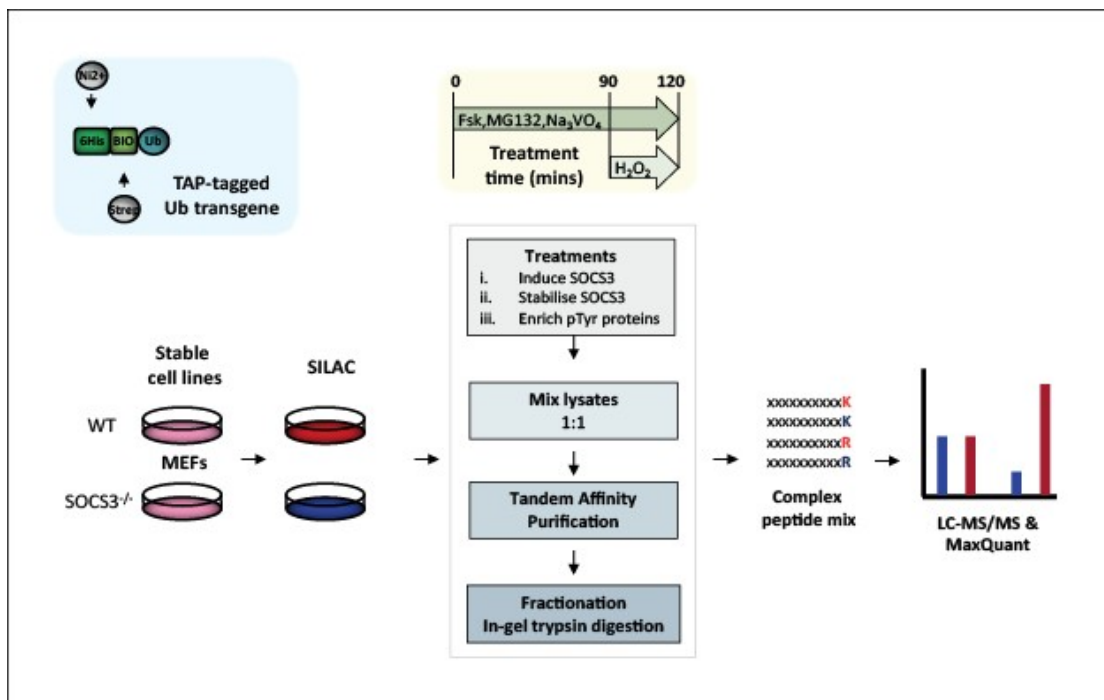


**Figure 1–12: WT and SOCS3<sup>-/-</sup> MEFs proteomics screen.**

A comparison between tandem-affinity purified, SILAC-labelled ubiquitinomes isolated from WT MEFs and SOCS3<sup>-/-</sup> MEFs. After SOCS3 induction via forskolin (50  $\mu$ M) and MG132 for 2 hrs (blue box). Adapted from Williams et al. [356].

Results revealed a significant elevation of cavin-1 protein in WT MEFs (5 unique peptides, count ratio of 6, and  $\log_2(H/L) = 1.37$ ), indicating the ubiquitylation of cavin-1 specifically via a SOCS3-dependent pathway. It could be also suggested that such interaction was independent on tyrosine phosphorylation. However, the exact regulatory mechanism of that implied by SOCS3 on cavin-1 ubiquitylation and its functional consequences have not been fully identified. As such, further investigations are warranted to reveal the mechanism of such interaction, referring to cavin-1 expression, caveolar stability and effective inhibition of JAK/STAT signalling.

## 1.5 Hypothesis

Caveolae represent a distinct membrane microenvironment that are involved in regulating multiple signalling pathways. Several diseases in human, such as heart failure, degenerative muscular illness, and vascular diseases, might result due to the disruption of caveolar integrity. The main caveolar structural membrane protein is cavin-1 and it has been shown to play a major role in caveolae assembly as shown by caveolae destabilisation due to cavin-1 deletion. However, the exact cellular process that regulate the functionality of cavin-1 has not been fully elucidated. One of the signalling pathways that have been found localised and distributed within caveolae is the JAK/STAT signalling, which is downregulated via the suppressor of cytokine signalling-3 (SOCS3). Studies based on proteomic screening and biochemical analysis have revealed an interaction between cavin-1 and SOCS3. As such, we hypothesised that SOCS3/cavin-1 interaction is an important controlling element in caveolae stability and/or the pro-inflammatory signalling pathway mediated by IL-6 in the endothelial cells.

## 1.6 Aims

1. To generate human vascular endothelial cell lines lacking SOCS3 via CRISPR/Cas9-mediated gene knockout which will form the basis for further examination of the working hypothesis.

2. To characterise the cavin-1/SOCS3 interaction and to assess the stability of cavin-1 at the basal level or following SOCS-3 induction by intracellular cAMP elevation in WT and SOCS3<sup>-/-</sup> cells.
3. To assess whether cavin-1 controls SOCS3 recruitment to caveolae.
4. To examine the impact of SOCS3 deletion on cavin-1 stability, cavin-1 expression and plasma membrane levels of caveolae in human vascular endothelial cells.
5. To investigate regulation of cytokine signalling pathways due to altered caveolae stability in SOCS3-deficient cells.

## 2 Materials and Methods

### 2.1 Materials

Table 2–1 List of general materials and reagents

Supplier	Description	Cat. No.
Agar Scientific Ltd UK	Sodium cacodylate	AGR1104
	Osmium tetroxide	AGR1015
Agilent Technologies, UK	XL1-Blue Competent Cells	200249
Bio-Rad Laboratories Ltd, UK	Precision Plus Protein® Kaleidoscope® Standards	161-0375
	Precision Plus Protein Kaleidoscope Standards	161-0375
Biolog Life Sciences	8-pCPT-2'-O-Me-cAMP-AM	C 051
Carestream Health, UK	Medical X-ray Blue/MXBE Film	7710783
GE Healthcare Life Sciences, UK	Amersham® Protran® 0.2 µm pore Nitrocellulose Membrane	10600001
Invitrogen Ltd, Paisley, UK	SuperScript™ II Reverse Transcriptase	18064022
Melford Laboratories	Dithiothreitol	M1505
Merck Biosciences, UK	Forskolin	344270
	MG-132	474790
Millipore	H-89 dihydrochloride	371963

Perkin-Elmer Life Sciences, UK	Enhanced chemiluminescence (ECL) reagents	NEL 104
	Wizard® Plus SV minipreps	A1330
	6 x Blue/Orange Loading Dye	G1881
	1kb DNA ladder	G5711
	100bp DNA ladder	G2101
Premier International Foods	“Marvel” milk powder	
Qiagen, UK	Polyfect Transfection reagent	301105
	SuperFect transfection reagent	301305
Roche Applied Science, UK	Complete, EDTA-free protease inhibitor cocktail tablets	11836170001
Sigma-Aldrich, UK	Paraformaldehyde	158127
	Emetine	E2375
	Tween – 20	P5927
	30% (w/v) acrylamide/0.8% (w/v) bis-acrylamide	A3699
	Soybean trypsin inhibitor	T9003
	Benzamidine	12072
	Bovine serum albumin	A7030

Sigma-Aldrich, UK	N, N, N',N'-tetramethylethylenediamine (TEMED)	T9281
	Phenylmethanesulphonyl fluoride (PMSF)	P7626
	Donkey serum	D9663
	Ponceau S dye	P3504
	Glutaraldehyde (25% aqua Pure, EM Grade)	G5882
	Triton® X-100	T8787
SMITH SCIENTIFIC	13mm glass coverslips	NPS13/2222
Thermo Fisher Scientific	Solaris Mouse qPCR Gene Expression Assay (PTRF)	AX-040777-00-0200
	Solaris Mouse qPCR Gene Expression Assay (Gapdh)	AX-040917-00-0100
	ProLong® Gold antifade reagent with DAPI	P36935
ThermoScientific	Thermanox coverslips	150067

**Table 2–2 Reagents and materials used in cell culture applications**

Supplier	Description	Cat. No.
Fischer Scientific	Opti-MEM® Reduced Serum Media	11058021
Lonza	EGM-2 Endothelial Medium	CC-3162
Sarstedt	Tissue culture cell scraper 25cm	83.183
Sigma-Aldrich, UK	Greiner CELLSTAR® white flat bottom 96 well plate	655083
	Dulbecco's Modified Eagle's Medium	D6046

Sigma-Aldrich, UK	Foetal bovine serum	F9665
	L-glutamine	G7513
	Penicillin-Streptomycin solution	P0781
	Endotoxin-free phosphate buffered saline (PBS)	14140-094
	1x Trypsin-EDTA solution	T3924
	Sterile filtered cell culture water	W3500
	Puromycin	P8833
	Medium 199	M7528
VWR International Ltd, UK	Corning® 6 well flat bottomed cell culture plate	734-1599
	Corning® 60mm cell culture dish	734-1699
	Corning® 100mm cell culture dish	734-1815

Cell lines	
Wild-type (SOCS3 <sup>+/+</sup> ) murine embryonic fibroblasts (MEFs)	Generously provided by Prof. Akihiko Yoshimura (Kyushu University, Japan) [353]
SOCS3 <sup>-/-</sup> MEFs	
Wild-type (cavin-1 <sup>+/+</sup> ) MEFs	Generously provided by Prof. Paul F. Pilch (Boston University, USA) [102]
Cavin-1 <sup>-/-</sup> MEFs	
Human endothelial angiosarcoma (AS-M.5)	Generously provided by Dr Vera Krump-Konvalinkova V (Johannes Gutenberg University, Germany) [357]

**Table 2–3 Plasmid constructs**

Construct Name	Vectors	Donor/Supplier
cavin-1	pEGFP-N1 (Clontech)	a kind gift from Prof. Paul Pilch (Boston University, USA) [102]
SOCS3	pEGFP-N1 (Clontech)	In-house
$\Delta$ PEST SOCS3	pEGFP-N1 (Clontech)	In-house ( $\Delta$ PEST SOCS3 was generously provided by Dr Jeff Babon, Walter and Eliza Hall Institute of Medical Research, Australia) (Nicholson, Willson [288])
Human SOCS3 CRISPR/Cas9 KO	CRISPR/Cas9 KO Plasmid	Santa Cruz Biotechnology
human SOCS3 HDR	Cre Vector	Santa Cruz Biotechnology
cavin-1	pmCherry-N1 (Clontech)	a kind gift from Dr Ben Nichols (MRC Laboratory of Molecular Biology, Cambridge, UK) [145]

**Table 2–4 Primary antibodies used for western blotting**

Target Protein	Predicted molecular weight of the protein	Host species	Suppliers/ Cat. No.	Working Dilution/ Diluent*
SOCS3	24.7 kDa	Rabbit	In house	1:000 (5% (w/v) dried milk)
SOCS3	24.7 kDa	Rabbit	Abcam #ab16030	1:1000 (5% (w/v) dried milk)
SOCS3	24.7 kDa	Goat	Santa Cruz Biotechnology #sc-7009	1:500 (5% (w/v) dried milk)
$\alpha$ -phospho CREB (Ser133)	43 kDa	Mouse	New England Biolabs #9196	1:1000 (5% (w/v) BSA)
Phospho- STAT3 (Tyr705)	79 kDa-86 kDa	Rabbit	Cell Signaling #9131	1:1000 (5% (w/v) BSA)
STAT3	79 kDa-86 kDa	Mouse	Cell Signaling #9132	1:1000 (5% (w/v) dried milk)

GAPDH	36 kDa	Mouse	Abcam #ab8245	1:20,000 (5% (w/v) dried milk)
Cavin-1	50 kDa	Rabbit	Abcam #ab48824	1:1000 (5% (w/v) dried milk)
Caveolin-1	22 kDa	Rabbit	BD Biosciences #610059	1:1000 (5% (w/v) dried milk)
Nurr1/Nur77	Nurr1: 66 kDa Nur77: 64 kDa	Rabbit	Santa Cruz Biotechnology # sc-990	1:2000 (5% (w/v) dried milk)
GFP	27 kDa	Sheep	In house	1:2000 (5% (w/v) dried milk)
$\beta$ -Actin	45 kDa	Rabbit	New England Biolabs #4970S	1:1000 (5% (w/v) dried milk)

**Table 2–5 Secondary detection agents for western blotting**

Linked molecule	Epitope	Species	Suppliers/ Cat. No.	Working Dilution/ Diluent*
HRP	Mouse IgG	Goat	Sigma-Aldrich A4416	1:1000 (5% (w/v) dried milk)
HRP	Rabbit IgG	Goat	Sigma-Aldrich A9169	1:1000 (5% (w/v) dried milk)
HRP	Goat IgG	Rabbit	Sigma-Aldrich A5420	1:2000 (5% (w/v) dried milk)

\*Diluent solution: TBS-Tween (50mM Tris pH 7.5, 150mM NaCl, 0.05% (v/v) Tween-20)

## **2.2 Methods**

### **2.2.1 Cell culture**

All cell types were cultured at 37°C in a humidified atmosphere regulated at 5% (v/v) CO<sub>2</sub>.

#### **2.2.1.1 Cell culture growth media for MEFs**

The cell culture medium for murine embryonic fibroblasts (MEFs) was Dulbecco's modified Eagle's medium (DMEM) supplemented with 10% (v/v) inactivated foetal bovine serum (FBS), 100U/ml penicillin, 100µM streptomycin, and 1mM L-glutamine. The cell monolayers were grown in Corning® 150cm<sup>2</sup> flasks until ~80% confluence. Passaging (sub-culturing) of MEF monolayers was performed by removal of the cell culture medium, followed by rinsing with 4 ml tissue culture grade PBS. Cells were incubated in 2 ml pre-warmed sterile trypsin (0.05% (v/v) in diaminethanetetra-acetic acid, disodium salt [EDTA]) for 2-3 minutes at room temperature to detach the cells from the flask. The trypsin was then neutralised with 8 ml fresh medium. Cells were finally resuspended via gentle pipetting before transferring to 10-12ml of fresh media. Cells were split 1 in 20 into fresh T150cm flasks at each passage.

#### **2.2.1.2 Culture of endothelial AS-M.5 cell lines**

Human endothelial angiosarcoma (AS-M.5) cells were maintained as monolayers in endothelial growth medium (EGM, Lonza) consisting of endothelial basal medium supplemented with 2% (v/v) foetal bovine serum (FBS), 0.04% (v/v) hydrocortisone, 0.4% (v/v) human fibroblast growth factor-B (hFGF-B), 0.1 % (v/v) vascular endothelial growth factor (VEGF), 0.1% (v/v) insulin-like growth factor-I (IGF-I), 0.1% (v/v) ascorbic acid, 0.1% (v/v) human epidermal growth factor (hEGF), 0.1% (v/v) gentamicin sulphate and amphotericin-B (GA-1000) and 0.1% (v/v) heparin, as recommended by the supplier (Lonza). Cells were cultured in Corning® 150cm<sup>2</sup> flasks and sub-cultured by washing the cells twice with tissue culture grade PBS and adding 2ml of sterile endothelial grade trypsin-EDTA solution (5 U/ml porcine trypsin, 1.8 % (w/v) EDTA) to each flask. Cells were left for a few minutes at 37°C to

allow detachment from the flask surface. Once adherent cells detached, fresh EGM was added to neutralise the action of the trypsin. The cell mixture was transferred to a Falcon centrifuge tube and spun down at 1200 x g for 5 minutes. The cell pellet was then resuspended in fresh medium and seeded into plates or dishes at an appropriate level according to the experiment performed. Cells were split 1 in 20 into fresh T150cm flasks at each passage.

### **2.2.1.3 Preparation of protein lysates from cultured cells**

Confluent cells cultured on appropriately sized dishes were placed on ice and washed twice with ice-cold 1 x PBS to remove any residual media components. Cell lysates were obtained by harvesting the cells with 100µl ice-cold radioimmuno-precipitation assay (RIPA) buffer (50 mM sodium HEPES [pH 7.5], 150 mM sodium chloride, 5 mM EDTA, 10 mM sodium fluoride, 10 mM sodium phosphate, 1% (v/v) Triton X-100, 0.5% (w/v) sodium deoxycholate, 0.1% (w/v) sodium dodecyl sulphate (SDS), 0.1 mM phenylmethylsulphonyl fluoride, 10 µg/ml soybean trypsin inhibitor, 10 µg/ml benzamidine, and EDTA-free complete protease inhibitor mix).

The cells were scraped off using a cell lifter and transferred into pre-cooled 1.5 ml microcentrifuge tubes. To facilitate cell lysis and protein solubilisation, the extracts were incubated for one hour at 4°C with rotation. Cell extracts were then centrifuged (15 minutes at 21000 x g, 4°C) to remove detergent-insoluble cellular fractions. The supernatants were subsequently collected and frozen in aliquots for storage at -20°C.

### **2.2.2 Protein concentration determination**

The protein concentration in cell lysates was determined using a bicinchoninic acid assay (BCA). This colorimetric assay [358] is based on measuring purple  $\text{Cu}^{+1}$  generated by proteins in the sample. The intensity of the purple complex is directly proportional to the amount of protein present in the solution and it can be estimated by comparison to a protein standard, such as bovine serum albumin (BSA) (0.0-2.0 mg/ml). Protein lysates were diluted 1 in 5 in the same

lysis buffer (2µl sample + 8µl buffer). Both standards and samples were added to a clear 96-well plate in duplicate (total volume 10 µl/well).

The BCA working solution was prepared in a 20ml universal at a ratio of 1:50 dilution of copper sulphate (4% (v/v) to BCA reagent (1% (w/v) 4,4 dicarboxy-2,2 biquinoline, disodium salt, 2% (w/v) sodium carbonate anhydrous, 0.16%(w/v) sodium potassium tartate, 0.4% (w/v) sodium hydroxide, 0.95% (w/v) sodium bicarbonate, pH 11.25). 200µl were then added to each well before incubating at 37°C for 10 minutes. Spectrophotometric analysis was performed using a POLARstar OPTIMA (BMG LabTech) microplate reader. The plate was read at 495nm and the mean absorbance for each sample duplicate. Measuring the absorbance of the BSA standards allowed plotting a best fit straight line from which the concentrations of the protein samples were quantified. Protein concentrations were determined using POLARstar OPTIMA MARS data analysis package v.1.20 and GraphPad Prism v.4.

### **2.2.3 SDS-Polyacrylamide Gel Electrophoresis**

Following protein determination by BCA assay, detergent-soluble whole cells lysates were equalised for protein content (15-30 µg/sample) and volume. Samples were prepared for SDS-PAGE to total volume of 30µl by addition of equal volume of SDS-loading buffer (50 mM Tris pH 6.8, 10% (v/v) glycerol, 12% (w/v) SDS, 1 mM dithiothreitol (DTT), 0.02 % (w/v) bromophenol blue). Using the BioRad Mini-PROTEAN® cell system, proteins were resolved via SDS-PAGE on 1.5 mm thick vertical slab gels containing between 10-12% (w/v) poly-acrylamide gels. Size estimation of immunoreactive protein bands was consequently determined by running a Bio-Rad Rainbow marker alongside the samples. Electrophoresis was performed in 1% (w/v) SDS running buffer (0.1% (w/v) SDS, 192 mM glycine, 25 mM Tris, pH 8.3) at a constant voltage of 150 V for approximately 1.5 hours until the blue dye had reached the bottom of the resolving gel and good separation of the molecular weight markers had been obtained.

**Table 2–6 Resolving gel components**

Component	10%	12%
	Volume required	
dH <sub>2</sub> O	3.4ml	2.74ml
Buffer 1 (1.5M Tris, pH 8.8, 0.4% (w/v) SDS)	2.5ml	2.5ml
50% (v/v) glycerol	0.65ml	0.65ml
Ammonium persulphate (APS, 0.3mg/ml)	32µl	32µl
TEMED	8µl	8µl
30% (w/v) acrylamide/0.8 (w/v) bis-acrylamide	3.3ml	3.96ml

**Table 2–7 Stacking gel components**

Component	Volume required
dH <sub>2</sub> O	3.4ml
Buffer 2 (0.5M Tris-HCl, pH 6.8, 0.4% (w/v) SDS)	1.34ml
Ammonium persulphate (APS, 0.3mg/ml)	54µl
TEMED	7µl
30% (w/v) acrylamide/ 0.8 (w/v) bis-acrylamide	0.63ml

## 2.2.4 Immunoblotting for proteins

### 2.2.4.1 Electrophoretic transfer of fractionated proteins onto nitrocellulose

Following gel electrophoresis, the gels were removed from the glass casing and placed on top of an equal-sized sheet of nitrocellulose membrane (0.2 µm pore size). Transfer cassettes were assembled with sponges, filter paper (Whatman 3MM blotting paper), SDS gel and nitrocellulose membrane, all pre-wetted in transfer buffer (24.7 mM Tris, 0.19 M glycine in 20% (v/v) methanol).

The proteins were electrophoretically transferred to the nitrocellulose membrane using the Mini PROTEAN® Tetra Cell (Bio-Rad) transfer system at a constant current of 400 mA for 45 minutes. Ponceau stain (0.1% [w/v] Ponceau S acid red diazo dye in 1% [v/v] acetic acid) was used to confirm the transfer of protein from the gel to the membrane.

#### **2.2.4.2 Blocking of membranes and probing with primary antibodies**

To reduce non-specific antibody binding the membrane was incubated with 5% (w/v) skimmed milk powder in TBST (10 mM Tris-HCl PH 7.5, 150 mM NaCl, 0.05% (v/v) Tween 20) for 1hr at room temperature. Following blocking, the appropriate primary antibody (Table 2–1) diluted in 5% (w/v) milk-TBST or 5% (w/v) BSA-TBST for phospho-specific antibodies was applied to the blot and incubated, with shaking, overnight at 4°C.

#### **2.2.4.3 Secondary antibodies and chemiluminescence western blot detection**

Following incubation with primary antibody, membranes were washed three times for 10 min in TBS/T at room temperature with rotation on a shaker (150rpm). Membranes were subsequently incubated with the appropriate horseradish peroxidase (HRP)-conjugated secondary antibody for 1 hour at RT in 5% (w/v) dried milk powder in TBS/T, followed by three washes for 10 min in TBS/T to remove unbound antibodies. Equal volumes of enhanced chemiluminescence (ECL) reagent 1 and 2 (Perkin-Elmer Life Sciences, UK) were mixed and membranes were immersed in the combined ECL substrate for 1 min. After removal of the detection reagents, membranes were placed between plastic film in autoradiography cassette with Kodak film, and developed using a X-OMAT 2000 processor (Kodak).

#### **2.2.4.4 Stripping of nitrocellulose membranes**

Stripping buffer (0.15M NaCl, 0.1M Glycine, pH 2.6) was prepared to remove primary and secondary antibodies bound to a western blot membrane. Membranes were incubated in stripping buffer for 30 mins at room temperature

with shaking. The membranes were then washed in TBS/T (3 x 5 min) and blocked in 5% (w/v) dried milk before incubation with another primary antibody.

#### **2.2.4.5 Densitometric quantification of protein bands**

Immunoreactive proteins on the developed film were scanned on HP Scanjet G3110 scanner using Adobe Photoshop software. The optical density of the immune-detected protein was measured using Totallab v2.0 imaging software (Phoretix).

### 2.2.5 Cell Transfection

MEFs were seeded and allowed to grow to 50-60% confluency on 6 cm<sup>2</sup> dishes. Transient transfection of DNA constructs was then carried out using PolyFect transfection reagent (Qiagen, 301105) according to manufacturer's instructions. Briefly, 4 µg of plasmid DNA was mixed with 150 µl Opti-MEM (Life Technologies) followed by addition of 40µl PolyFect transfection reagent and mixed thoroughly via gentle pipetting. The DNA/PolyFect mixture was incubated for 10 minutes at room temperature to allow formation of transfection complexes. In the meantime, 3 ml fresh DMEM growth medium was added to the 6 cm<sup>2</sup> dish. The DNA/PolyFect solution was then mixed with 1 ml DMEM growth medium prior to being added drop-wise to the target cells. Cells were incubated in a humidified incubator (5% CO<sub>2</sub>, 37°C) for 24 hrs to allow transfer of DNA into cells. Transfection efficiency of DNA constructs was assessed using the Axiovert 40 CFL (Zeiss Microscopy,) fluorescent microscope and Zeiss Vision AxioVision Viewer 4.0 software. Cells were subsequently split onto 6 well plates and treated as described in the figure legends.

## **2.2.6 RNA Extraction, Purification and Quantification**

### **2.2.6.1 Extraction of RNA from MEFs**

RNA from MEFs was extracted using a miRNeasy mini kit (including on-column DNase treatment) according to manufacturer's instructions (Qiagen, Hilden, Germany). Briefly, the media was removed and the cells were washed with ice-cold PBS. Cells were then lysed directly with 700  $\mu$ l QIAzol lysis reagent and homogenised through a sterile 23-gauge needle and syringe 10 times. Cell homogenates were placed into pre-cooled 1.5ml eppendorf tubes and stored at -80°C until required.

Cell lysates were thawed on ice and mixed with 140  $\mu$ L chloroform by shaking the tube vigorously for 15 sec. Lysates were incubated at room temperature for 2 min, prior to centrifugation at 12,000 x g (15 min, 4°C). After centrifugation, the upper aqueous phase containing total RNA was carefully collected and transferred to a new 1.5 ml tube and mixed thoroughly with 550  $\mu$ L 100% ethanol. Lysates were transferred to RNeasy mini spin columns and centrifuged at 8,000 x g for 1 min and the flow-through discarded. The columns were washed with 350  $\mu$ L RWT buffer and two times with 500  $\mu$ L RPE buffer. Each wash was followed by centrifugation at 8,000 x g for 1 min at room temperature. miRNeasy spin columns were then transferred to new 2 mL collect tubes and centrifuged at 14,000 x g for 2 min at room temperature to remove any buffer contaminants. Total RNA was then eluted by adding 30  $\mu$ L of nuclease-free water through the spin column for 1 min at 8,000 x g. To obtain an optimal RNA yield, the RNA eluates were collected and re-eluted through the column.

The RNA concentration were quantified by measuring the absorbance of the sample at 260nm using a NanoDrop ND-1000 spectrophotometer (Thermo Scientific, Paisley, UK) and samples stored at -80°C until required.

### **2.2.6.2 cDNA synthesis by reverse transcription**

For messenger RNA (mRNA) expression analysis, cDNA was generated from total RNA using Super-Script™ II Reverse Transcriptase (Invitrogen) according to manufacturer's instructions.

Per reaction, 1 µg of DNase-free RNA were reverse transcribed. Each reaction contained 100 ng random hexamers, 2.5 mM of each deoxyribonucleotide triphosphates (dNTPs), 40 U RNaseOUT (Invitrogen) and 200 U Super-Script™ II Reverse Transcriptase. RNase-free water was used to make up the reaction volume to 20 µl.

Samples were incubated as follows:

Temperature °C	Cycle time (Min)	Function
25	10	annealing of random primers
42	50	reverse transcription
70	15	inactivate the reverse transcriptase

cDNA samples were stored at -20°C.

### 2.2.6.3 Quantitative Real-Time PCR (qRT-PCR) analysis for expression of cavin-1 gene transcripts

qRT-PCR) analysis was performed using Power SYBR® Green PCR Master Mix (Applied Biosystems). The final volume per reaction was 10 µl, containing 1 µl of cDNA, 1 x Power SYBR Green master mix and 0.5 mM of each primer. Non-template controls in which cDNA was substituted with water were included in each reaction. Samples were loaded in triplicate in real-time PCR 96-well plates (primerdesign, UK) which was covered with optical cover and centrifuged at 1000 RPM for 1 minute.

Real-time quantitative PCRs were performed on a MX3000P® QPCR system (Stratagene). The gene amplification began with an initial denaturation at 95°C for 10 minutes, 40 cycles of 95°C for 5 seconds and 60°C for 20 seconds, followed by a final extension at 72°C for 5 minutes.

Glyceraldehyde-3-phosphatase dehydrogenase (GAPDH) was used as a reference gene.

Primers in Table 2–8 were used to amplify genes of interest.

**Table 2–8 List of primer sequences used for qRT-PCR analysis in this study**

Gene	Species	forward primer	reverse primer
cavin-1	Mouse	5'-GCAAGGTCAGCGTCAAC-3'	5'-CCGGCAGCTTGACTTCA-3'
GAPDH	Mouse	5'-GGCTGGCATTGCTCTCAA-3'	5'-GCTGTAGCCGTATTCATTGTC-3'

Data obtained were analysed using the comparative threshold cycle(Ct) method. The formula  $2^{-\Delta\Delta Ct}$  [359] was employed to compare the Ct value of the target gene to the Ct value of the control gene. Data was calculated in Microsoft Excel 2007 and expressed as the fold change of the gene of interest compared to the control condition.

## 2.2.7 Ultrastructural analysis

### 2.2.7.1 Preparation and Fixation of AS-M.5 cells

WT and SOCS3-null AS-M.5 cells were seeded at a density of  $1 \times 10^6$  cells per ml into 6-well plates and onto Thermanox coverslips (13 mm diameter) for culturing to confluency. The cells were then fixed in 1.5% (w/v) glutaraldehyde in 0.1 M sodium cacodylate buffer at 4°C for 1 h.

### 2.2.7.2 Post-fixation

Cells were washed 3 times in 0.1M sodium cacodylate buffer in 2% (w/v) sucrose prior to incubation with 1% (w/v) osmium tetroxide/0.1 M sodium cacodylate for 1 h. The cells were then washed 3 times in distilled water and incubated in 0.5% (w/v) uranyl acetate in the dark for 1 hour followed by 2 rinses in distilled water.

### 2.2.7.3 Dehydration, embedding and microscopy

Dehydration was carried out with a graded alcohol series (30–100% (v/v)), followed by overnight incubation in a 1:1 mix of propylene oxide/TAAB araldite Epon 812 resin. The propylene oxide was allowed to evaporate to leave pure

resin, which was changed twice before the sample was embedded flat in fresh resin polymerised overnight at 60 °C. Ultrathin sections were cut using a Leica Ultracut UCT and a Diatome diamond knife, contrast stained with aqueous 2% (w/v) methanolic uranyl acetate and Reynolds lead citrate, and viewed using a LEO 912AB TEM (Carl Zeiss) at an accelerating voltage of 120 kV. TIF images were captured using an Olympus Soft Imaging System and image contrast modified using Adobe Photoshop CS.

## **2.2.8 Immunofluorescent Confocal Microscopy**

### **2.2.8.1 Cells preparation and fixation**

For immunofluorescent analysis of endogenous cavin-1 and transfected SOCS3-GFP, WT, and cavin-1<sup>-/-</sup> MEFs, cells were allowed to grow at appropriate density in 10 cm dishes and transiently transfected with or without SOCS3-GFP expression constructs using the method described previously in section 2.2.5. After 24 h, cells were split on ethanol-sterilised 13 mm glass coverslips and allowed to adhere overnight. On the following day, cells were washed with PBS and fixed with 4% (w/v) paraformaldehyde (PFA) in PBS for 25 min.

### **2.2.8.2 Permeabilisation and staining**

After washing with PBS and quenching residual PFA with 20 mM glycine in PBS, cells were permeabilised with 0.1% (v/v) Triton X-100 for 10 mins, and non-specific binding sites blocked by a 30 min of incubation at room temperature in PBS containing 3% (w/v) BSA and 10% (v/v) donkey serum. Cells were then incubated with rabbit anti-cavin-1 antibody (Abcam ab48824, 1 in 100 dilution) for 90 min at room temperature.

Cells were washed with PBS containing 0.1% (v/v) Triton X-100, 1% (w/v) BSA, and 10% (v/v) donkey serum prior to incubation with Alexa Fluor 594-conjugated donkey anti-rabbit IgG (Life Technologies A21207, 1 in 200 dilution) for 1 hour at room temperature. The cells were washed with PBS and the coverslips were mounted onto glass slides using ProLong<sup>®</sup> Gold anti-fade reagent containing nuclear stain 4',6-diamidino-2-phenylindole (DAPI).

### **2.2.8.3 Visualisation by confocal microscopy**

Cells were visualised using a 63x oil-immersion Plan Fluor Apochromat objective lens, on a Zeiss LSM510 laser scanning confocal microscope (Carl Zeiss GmbH, Oberkochen, Germany) equipped with a Zeiss LSM5 Pascal instrument and AOTF Laser module.

GFP fusion proteins were excited with an argon laser at 488 whereas Alexa Fluor 594 were excited with a helium neon laser. Images were analysed using MetaMorph® imaging software to generate Pearson's correlation coefficients.

### **2.2.9 Production of SOCS3 Knockout AS-M.5 via CRISPR**

$2 \times 10^5$  AS-M.5 cells were seeded into 6 cm<sup>2</sup> dishes and grown in endothelial growth medium (EGM) until reaching approximately 80% confluency. Cells were then co-transfected with human SOCS3 CRISPR/Cas9 KO and human SOCS3 HDR plasmids using SuperFect transfection reagent (Qiagen) according to the manufacturer's protocol. Briefly, 30 µL of Superfect reagent was mixed with 3 µg of each DNA construct and made up to 300 µL with cell growth medium. Following 10 minutes incubation at room temperature, the DNA-Superfect complexes were then added directly to the cells and allowed to incubate for 3 hours at 37°C. DNA complexes were then removed and complete EGM was added to dishes.

48 hours after transfection, the cells were split into 6-well plates at 1:10-1:15 ratio and allowed to proliferate for another 48 hrs prior to selection in medium supplemented with puromycin ( $2 \mu\text{g ml}^{-1}$ ). Cultures were maintained for up to 14 days and the media was replaced every 2-3 days. Following dilution and re-plating, individual clones were identified for the successful elimination of SOCS3 gene production (as described in Chapter 3) and a single knockout clone was compared with an unselected control cell population.

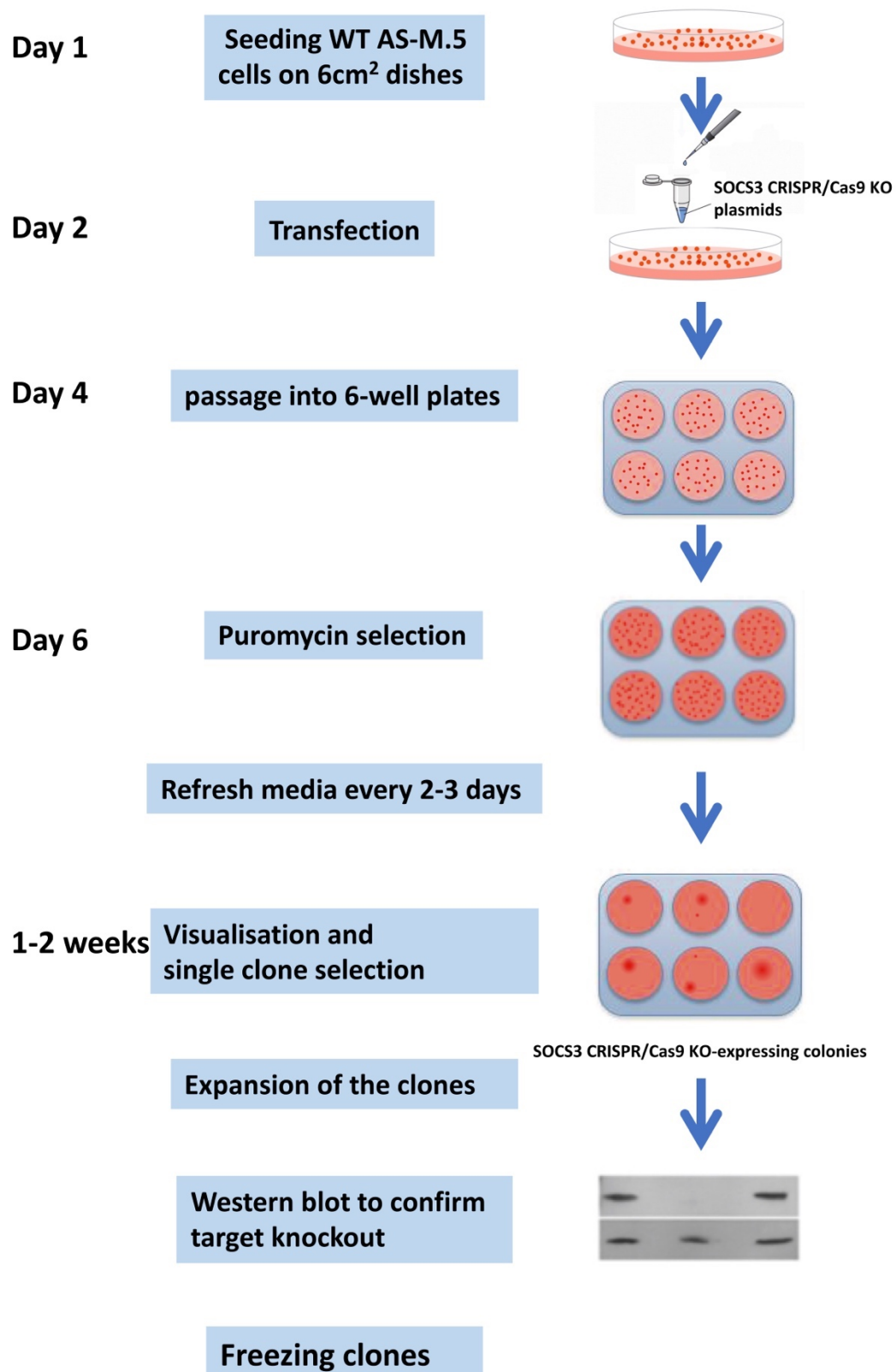


Figure 2–1 Flowchart outlining the experimental procedures to generate SOCS3 KO AS-M.5 cell lines.

### **2.2.10 Statistical analysis**

Results were expressed as the mean  $\pm$  standard error of the mean (SEM). Statistically analysis included unpaired, two-tail t-test or a one-way analysis of variance (ANOVA) followed by the Bonferroni multiple comparisons test when comparing the means of multiple treatment groups. P value  $<0.05$  was deemed statistically significant.

### **3 Generation and characterisation of endothelial SOCS3KO cells for the further examination of the working hypothesis**

#### **3.1 Perturbation of Target Gene Expression**

The basic functionality and relationships of proteins could be elucidated via understanding of their levels and activities in the cell. Several methods have been utilised to transiently and specifically perturb target protein expression, including knockdown by RNA interference, chemical inhibition or overexpression by non-integrating vectors. For more stable perturbations, editing of the endogenous gene locus encoding the protein of interest can also be employed [360].

Two early forms of customised nucleases have been utilised for this purpose; zinc-finger nucleases (ZFNs) and Transcription activator-like effector nucleases (TALENs) [361]. The ZFNs system is composed of DNA-binding domains and zinc finger proteins (ZFPs) as well as a DNA-cleavage domain (FokI) (Figure 3-1a). Different combinations of ZFPs can be produced to target a distinct DNA sequence since the ZFP region has the ability to interact with nucleotide (nt) triplets. The specificity of ZFNs systems is apparently demonstrated in creating double-stranded breaks (DSBs), FokI dimerisation, and DNA cleavage [361]. TALENs proteins originate from repeated domains of bacterial (prokaryotic) transcription activator-like effector that interact with a single nt and is bound to a FokI nuclease (Figure 3-1b). Pairs of TALENs are constructed to position the FokI nuclease domains to adjacent genomic target sites, where they induce DSBs that stimulate error-prone nonhomologous end-joining (NHEJ) or homology-directed repair (HDR) [362]. Although ZFN and TALEN platforms enable site-specific gene mutagenesis and editing, the need of extensive labour efforts and prolonged time may represent major limitations, in addition to having low efficiency, suboptimal precision, and poor scalability [363].

Recently, clustered regularly interspaced short palindromic repeat/associated 9 (CRISPR/Cas9) (Figure 3-1c) has provided a more straightforward approach for genome editing and has been efficiently utilised to produce model organisms

in multiple species [364]. Despite its initial presentation as unknown sequences of unidentified biological significance, a considerable progress has been made in the CRISPR system suggesting it as the method of choice for genome editing [363].

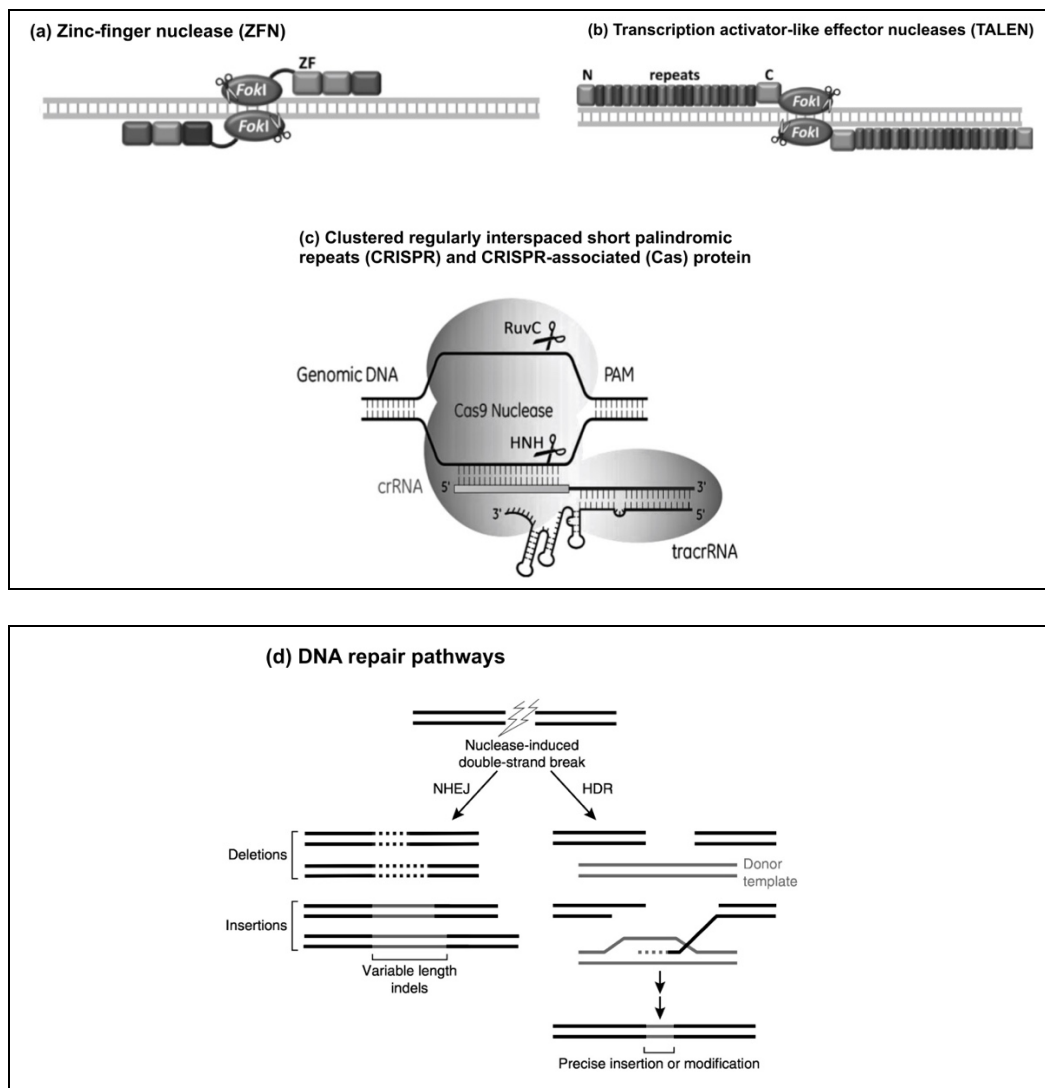


**Figure 3–1 Nuclease-induced genome editing**

(a) Two monomers of zinc-finger nuclease containing three zinc fingers and a FokI cleavage domain in each. (b) The FokI cleavage domain is coupled to two TALEN monomers that entail a repeat region and C- and N-terminal extensions. (c) tracrRNA:crRNA recruits Cas9 to the target site of the DNA sequence. The complementary PAM sequence binds to crRNA and the DSBs are generated by Cas9 HNH and RuvC domains. (d) the process of DNA repair can be performed in two different pathways. A small number of bases can be removed and this might be associated with inducing a frameshift mutation via a NHEJ process. NHEJ typically inactivate gene function. Additionally, HDR may be followed if the donor template is transfected with Cas9 mRNA and the guide RNA. In this pathway, single base alterations could be inserted into the repaired strand, resulting in gene knockout. HDR: homology-directed repair; PAM: protospacer-adjacent motif; NHEJ: Non-homologous end joining; tracrRNA: trans-activating crRNA; ZF: Zinc finger (Adapted from [365, 366]).

### 3.1.1 Advances in the development of the CRISPR/Cas9 system

The history of CRISPR discovery extends back to 1987, when a set of 29 nt repeats in *Escherichia coli* were found to be divided by short non-repetitive sequences [367]. Later, Mojica et al. [368] reported similar repeats in other bacterial species and in some prokaryotic Archaea. In 2002, the acronym “CRISPR” was created to replace the short regularly spaced repeats (SRSR) [369]. A conserved gene sequence that can interact with CRISPR repeats has been subsequently discovered and named CRISPR-associated (Cas) genes. Such genes encode various important proteins, such as the Cas3 gene which encodes a single-stranded DNA nuclease and ATP-dependent helicase, and Cas4 which encodes exonuclease [363]. Additionally, a large protein with nuclease activity has been found to be encoded by Cas9 gene as revealed by Bolotin et al. [370]. Furthermore, the protospacer adjacent motif (PAM), another component of the CRISPR system, has been discovered and contributed to revealing several technical details pertinent to the novel gene editing tool [370]. A more recent remarkable discovery is that certain complexes of *Streptococcus thermophilus* and *Streptococcus pyogenes* (Cas9–CRISPR (cr)RNA complexes) might exert an *in vitro* RNA-guided endonuclease action [369]. As a consequence, these complexes might be utilised in genome editing thereby expanding horizons for use of CRISPR technology in new applications.

Of the three CRISPR systems, the CRISPR type II system has been well characterised. It is composed of pre-crRNA, trans-activating (tra)crRNA, and Cas9 proteins [363]. In Cas9, the HNH domain and RuvC-like domain are known for their prominent nuclease activity (Figure 3-1c). Pre-crRNA is cut into crRNA by a coordinating action of tracrRNA and RNaseIII. Then, an interaction between crRNAs and tracrRNAs occurs, helping the appropriate recognition of Cas9 to the specific DNA sites. The random identification of DNA sequences starts by the Cas9–RNA complexes and it requires a PAM motif to match its sequence. Once identified, the HNH nuclease domain on Cas9 cleaves the DNA strand at its specific cleavage site that is bound to crRNA. Additionally, the other DNA strand is cut by the RuvC-like domain to generate the relevant DSBs. Following creating the break sites, the repair mechanism is directed in

either two different ways depending on the stage of cell cycle or the existence of a donor template. These repair mechanisms include NHEJ or HDR. The NHEJ pathway entails conjoining the broken strands through multiple insertions or deletions (indels) leading to a frame shift and inducing premature stop codons in the reading sequence. On the other hand, when a donor template is available, distinct insertions, deletions, or mutations are generated in the HDR repair mechanism [363].

### **3.1.2 Experimental cell lines**

Vascular endothelium of an adult human is composed of  $1-6 \times 10^{13}$  endothelial cells lining a total surface of 4000-7000 m<sup>2</sup> of blood and lymph vessels [371]. Endothelial cells play a key role in diverse physiological and pathological process such as inflammation, thrombosis, wound healing, angiogenesis, and tumour metastasis. Thus, systematic identification of the specific molecular features of the endothelial cells is essential for the development of new approaches for both the prevention and therapy of cardiovascular diseases [372].

Utilising human endothelial cells has been an essential element in experimental culture systems to investigate drug interactions, vascular remodelling and inflammation as well as blood haemostasis [373]. In the present thesis, the use of AS-M.5 cell line was considered. This cell line is derived from a rare malignancy in scalp endothelium, namely cutaneous angiosarcoma [374]. Immunohistochemical analyses and RT-PCR analyses have shown they display several characteristics of primary vascular endothelial cells: these include inducible expression of cell surface adhesion molecules (intercellular adhesion molecule-1 (ICAM-1), vascular endothelial cell adhesion molecule 1 (VCAM-1), and E-selectin) when exposed to LPS, TNF, and IL-1 $\beta$ ) and the expression of endothelium markers von Willebrand factor (vWF) and CD31 [357]. Confirmation of the endothelial origin of this cell line was originally based on their increased uptake of acetylated-low density lipoprotein (acLDL), which is considered a defining function of endothelial cells [357, 375]. These characteristics are all comparable to those of primary isolated human umbilical endothelial cells (HUVECs) which have been widely used to study the

endothelial physiology and pathology. Unlike HUVECs that exhibit a limited proliferative capacity in culture [376], AS-M.5 cells can undergo more than 100 population doublings (PDs) while remaining morphologically stable [357] and thus maintained many of endothelial characteristics. Additionally, AS-M.5 culture systems are a cheaper and more tractable alternative for stable knock-in or knockout experiments. Therefore, WT and SOCS3-null AS-M.5 cells could potentially be useful cell models for further examination of the specific roles of cavin-1/SOCS3 interaction in JAK-STAT signalling and caveolae stability in endothelial cells..

### **3.1.3 Aims**

In this Chapter, Generation of an immortalized human endothelial cell line that lacks SOCS3 protein expression is documented. This was achieved by:

- 1) Obtaining commercially CRISPR/Cas9 KO Plasmids that have a suitable gRNA for SOCS3 gene editing.
- 2) Determining the optimal Plasmid DNA: transfection reagent ratio to minimize cell toxicity followed by co-transfection the appropriate amount of CRISPR/Cas9 KO Plasmid with HDR Plasmid aiming at the highest level of transfection efficiency in WT AS-M.5 cell lines.
- 3) Examining successful transfection of CRISPR/Cas9 KO Plasmid and HDR Plasmid by detection of the green fluorescent protein (GFP) and the red fluorescent protein (RFP) via visual confirmation using fluorescent microscopy.
- 4) Selection SOCS3 KO cells with media containing puromycin antibiotic, followed by phenotypic analysis of SOCS3 KO in selected clones using fluorescent microscopy and western blotting.

## **3.2 Results and discussion**

Caveolae and their major protein components, particularly cavin-1, are abundantly located in the endothelial cells [121]. Generation of endothelial

SOCS3 knockout cells is instrumental to define specific roles of cavin-1/SOCS3 interaction and caveola abundance in endothelial cells.

### 3.2.1 CRISPR/Cas9 Constructs

SOCS-3 CRISPR/Cas9 KO Plasmid (h2) (sc-400455-KO-2) and SOCS-3 HDR Plasmid (h2)(sc-400455-HDR-2) were utilised (Santa Cruz Biotechnology, Inc., Texas, U.S). In the SOCS-3 CRISPR/Cas9 KO Plasmid (h2) product, a 3-plasmid-containing pool is used to create a DSB in a 5' constitutive exon causing disruption of the genomic expression of the SOCS3 gene. DSBs could be made by the CRISPR plasmids via cloning of three 20 nt target sites into the gRNA scaffold. The pool of the SOCS3 CRISPR/Cas9 plasmids consists of 3 sgRNA sequences developed from the Genome-Scale CRISPR Knock-Out library (GeCKO v1 and v2 lentiviral sgRNA libraries) as formerly described by Zhang Lab (Broad Institute, Massachusetts, U.S) [377, 378] where further off-site modifications were prohibited or minimised by the selection of each specific target site. As such, three gRNAs (20 nt each) would target SOCS3 (Table 3–1) and then the respective SOCS-3 CRISPR/Cas9 KO Plasmids (h2) were cloned, encoding the Cas9 nuclease along with an enhanced green fluorescent protein (EGFP) to enhance the visualisation of positive clones [379]. The gRNAs, which are located immediately adjacent to a PAM sequence, target a specific DNA sequence by Cas9. Subsequently, either the high-fidelity HDR or the error-prone NHEJ mechanisms are employed to repair the target sequence [380]. At this end, the role of the SOCS-3 HDR Plasmid (h2)(sc-400455-HDR-2) could be apparent. Such repair template would render the edited cells containing a puromycin resistance gene, which could be further utilised for selection purposes. Figure 3–2 depicts a scheme for both plasmids used for transfection.

**Table 3–1 Guide RNA sequences used for constructing knockout cells.**

gRNA	gRNA sequence
sgRNA1	Sense: CTTAAAGCGGGGCATCGTAC
sgRNA2	Sense: CACAGCAAGTTTCCCGCCGC
sgRNA3	Sense: GCTTGAGCACGCAGTCGAAG

Data were adapted with permission from Santa Cruz Biotechnology, Inc.[381]

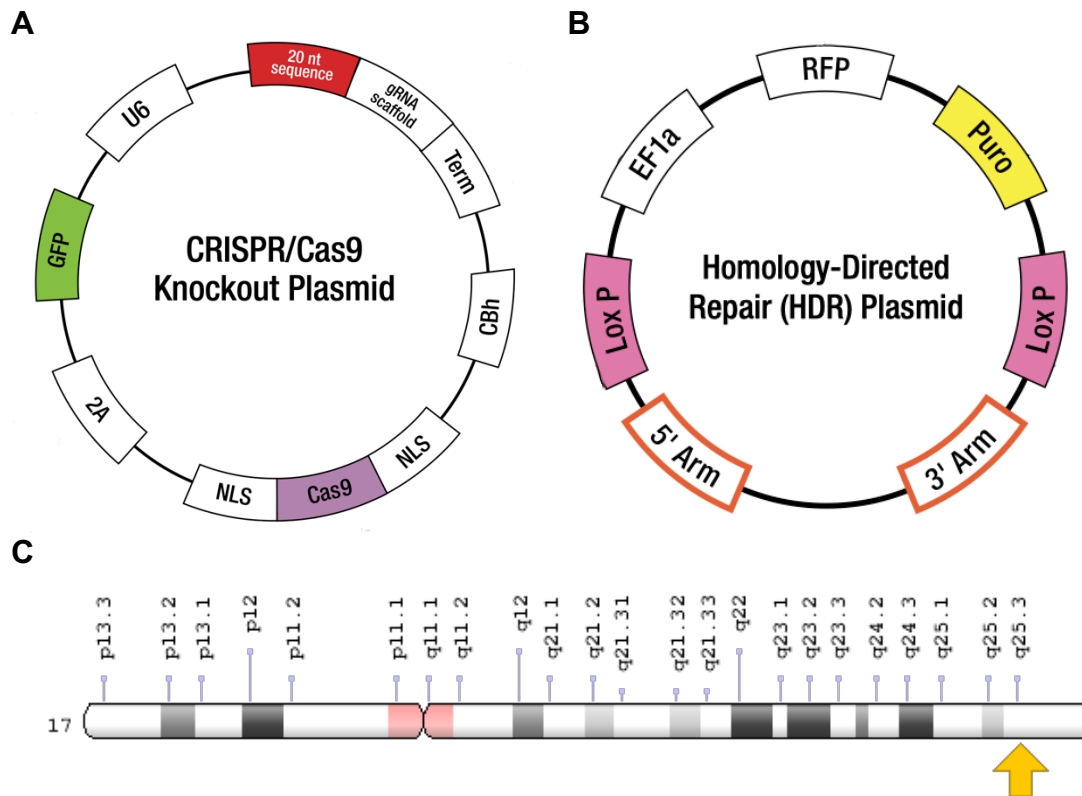


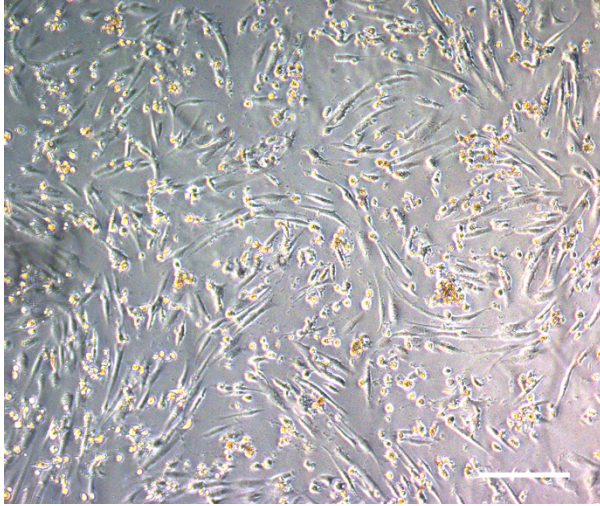
**Figure 3–2: Design of the CRISPR/CAS9 system for SOCS3 gene deletion.**

(A) A scheme of the SOCS-3 CRISPR/Cas9 KO Plasmid (h2) which includes the following sites: 1) 20 nt RNA sequence that act as a guide to target Cas9 to a specific sequence in the genomic DNA. 2) gRNA scaffold which facilitates Cas9 binding to the target DNA. 3) termination signal. 4) chicken  $\beta$ -Actin hybrid (CBh) promoter which drives Cas9 expression 5) Nuclear localization signal 6) SpCas9 ribonuclease 7) nuclear localisation signal 8) 2A peptide that enables producing both GFP and Cas9 from the same CBh promoter 9) Green Fluorescent Protein to facilitate the visualisation of transfection. 10) U6 promoter: drives expression of gRNA. (B) A scheme of the SOCS-3 HDR Plasmid (h2) containing the following sites: 1) EF1a promoter which initiates expression of the Puromycin resistance gene. 2) Red Fluorescent Protein to enable accurate visualisation of transfection. 3) Puromycin resistance gene enables selection of cells in which DSBs have been induced by Cas9. 4) a Cre recombinase-recognisable Lox P (34 bp) recombination site. (C) The human SOCS3 gene is located on the 17q25.3 locus, which constitutes the long arm of the chromosome. The molecular location on chromosome 17 from the base pair 78,356,777 to 78,360,079. Adapted from the Genetics Home Reference [382].

### 3.2.2 Transfection of CRISPR/Cas9 Constructs

In the current experimental work, liposomal transfection was initially employed using the PolyFect® Transfection Reagent (QIAGEN, Venlo, The Netherlands) but it was of a very low efficiency (data not shown). Therefore, it has been replaced with another commercially poly(amidoamine) (PAMAM) dendrimers-based gene delivery system, SuperFect® Transfection Reagent (QIAGEN, Venlo, The Netherlands) (Figure 3–3). Seemingly, PAMAM dendrimers-mediated transfection depends on both the charge of the complexes (where a net positive charge is more preferable and is inversely correlated with the hydrophobicity of the complexes) and dendrimer generation (higher efficiency is prospected with larger sized-dendrimers) [383].

Bright-field



Fluorescent field

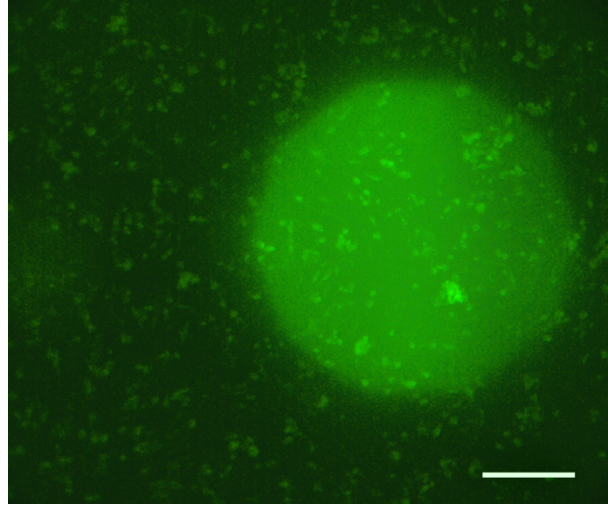


**Figure 3–3: Fluorescence expression in AS-M.5 cells transfected with a CRISPR/Cas9 plasmid that expresses enhanced GFP.**

AS-M.5 cells were co-transfected with CRISPR/Cas9 KO Plasmid and HDR Plasmid (Santa Cruz Biotechnology, Inc.) using SuperFect® Transfection Reagent (QIAGEN). 24 hours post transfection, cells were visualized under a Zeiss Axiovert fluorescence microscope (Carl Zeiss, Germany). Representative bright field image of transfected cells and fluorescence image of the same field of cells. Scale bars: 100  $\mu\text{m}$

### 3.2.3 Puromycin selection

AS-M.5 cells were co-transfected with CRISPR/Cas9 KO Plasmid and HDR Plasmid using the SuperFect® Transfection Reagent according to the manufacturer's instruction. Five days post transfection, puromycin selection was used to select cells that had taken up the CRISPR/Cas9 KO Plasmid with HDR Plasmid. Titration of puromycin on the AS-M.5 cell line was previously performed and the optimal concentration 2 µg/ml was found sufficient to kill parental cells within 2 days (Kirsten Munro, University of Glasgow, personal communication). Selection was continued for 10 days (Figure 3–4), which resulted in large cell death. Dilution plating was performed for puromycin-resistant cells using 10 cm cell culture dishes. Dilution would facilitate formation of separate discrete colonies with large gaps in-between for better characterisation.

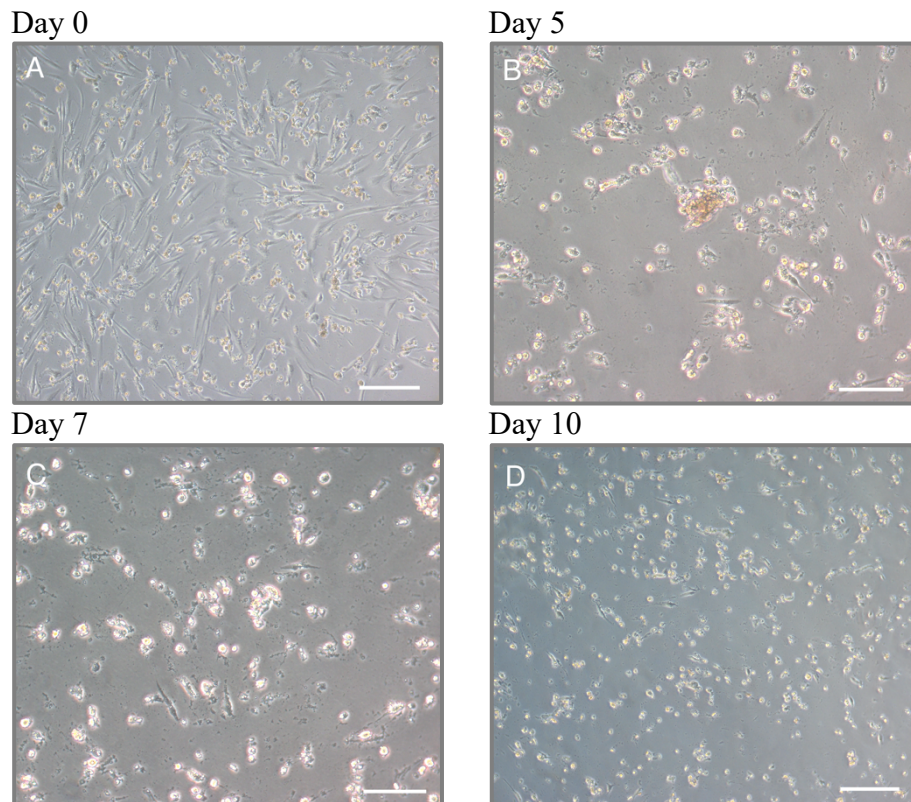


**Figure 3–4: The effect of puromycin treatment on CRISPR/Cas9-transfected AS-M.5 cells.**

Representative phase contrast micrographs AS-M.5 cell after 5, 7, 10 days of exposure to puromycin treatment (2 $\mu$ g/ml) as indicated (panels A-D). The number of dead cells increased significantly which aided the enrichment of targeted cells (puromycin-resistant cells). Images were taken using a Zeiss Axiovert microscope (Carl Zeiss, Germany), Scale bars: 100  $\mu$ m. n=1.

### 3.2.4 Cell assay to confirm complete allelic knockouts

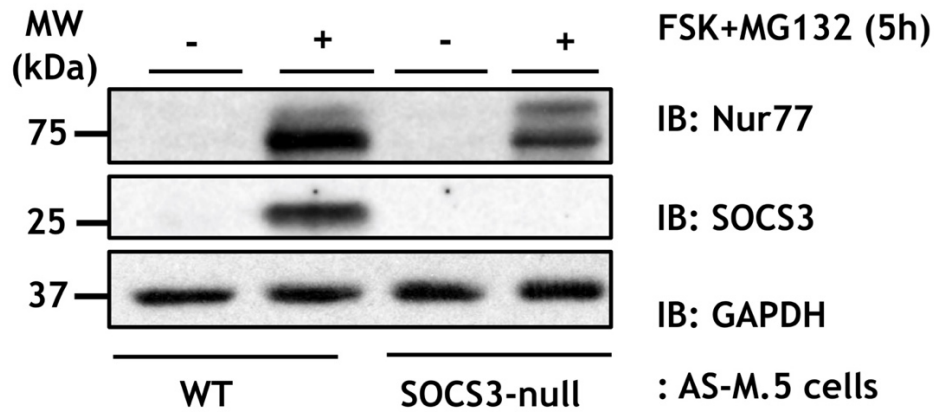
The small-sized colonies (enough to be physically recognisable) were collected using trypsin-immersed cloning disks (Sigma-Aldrich). Single foci were picked from 10 cm dishes and seeded into separate wells of non-coated 48-well tissue culture plates. Following the expansion phase, characterisation of Cas9-mediated SOCS3 genome editing was performed via western blotting. As shown in Figure 3–5, cells grown from one clone were treated with the adenylyl cyclase activator forskolin (Fsk) at a concentration of 50 $\mu$ M for 5 hours, in the presence of the proteasome inhibitor, MG132 at a concentration of 6 $\mu$ M. Polyclonal rabbit anti-SOCS3 antibodies (Abcam; Ab16030) were utilised to analyse SOCS3 expression. cAMP-elevation by Fsk induced endogenous SOCS3 expression and MG132 inhibited proteasome mediated degradation in the WT AS-M.5 cells whereas SOCS3 protein levels in the single-cell clone was null (Figure 3–5). Interestingly, Nur77, a well-characterised immediate early response gene whose expression is rapidly induced by cAMP elevation [384], was detectable in both WT and SOCS3-null AS-M.5 cells. Thus, the lack of response to the Fsk stimuli provided an evidence that such cells are SOCS3 knockouts. Likewise, SOCS3 was detected (~27KDa) in the WT AS-M.5 cells treated with Fsk + MG132 but not in the six single cell clones which were expanded as potential SOCS3 knockouts (Figure 3–6). Notably, one single clone appeared to have a single allele (heterozygous) deletion as it exhibited incomplete knockout. Overall, deletion of SOCS3 via the CRISPR/Cas9 system was efficiently performed and occurred in six clonal cell lines in the current experiment.

### 3.2.5 Phenotypic Differences in SOCS3<sup>-/-</sup> Endothelial Cells

To determine whether SOCS3 deletion affected the quality of AS-M cells, the morphology of the endothelial clones was observed and digital images were taken using a microscope (Zeiss AxioVert, Germany). Phase contrast images showed that SOCS3-null endothelial cell clones grew in loose arrangements and at a slower rate when compared to the parental cells. Additionally, in contrast to the WT spindle-shaped AS-M.5 cells that grew in swirling patterns,

the endothelial clones exhibited a polygonal morphology with a growth pattern resembling a cobblestone (**Figure 3–7**).

A



B

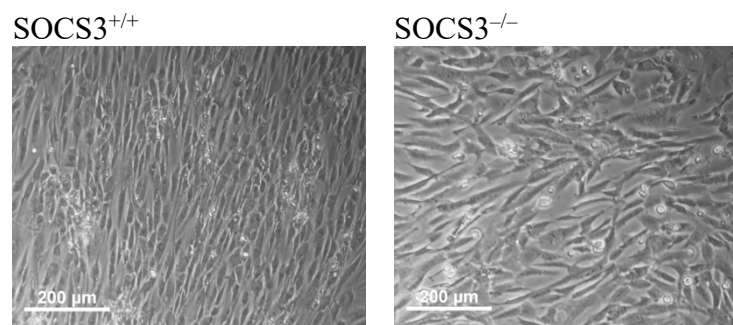


**Figure 3–5 CRISPR/Cas9 mediated disruption of SOCS3 locus generated complete gene knockouts.**

**(A)** Detergent-soluble whole cell lysates from WT and SOCS3-null AS-M.5 human angiosarcoma-derived ECs treated with either vehicle or Fsk (50 μM) plus MG132 (6 μM) for 5 hr were equalised for protein content for SDS-PAGE for immunoblotting with the indicated antibodies. N=3.

**(B)** Representative phase-contrast micrographs showing the morphology of WT AS-M.5 cells and one clonal cell lines lacking SOCS3 protein. Images were taken using a Nikon Eclipse Ti-S inverted microscope (Nikon, Tokyo, Japan). Scale bar, 200 μm.

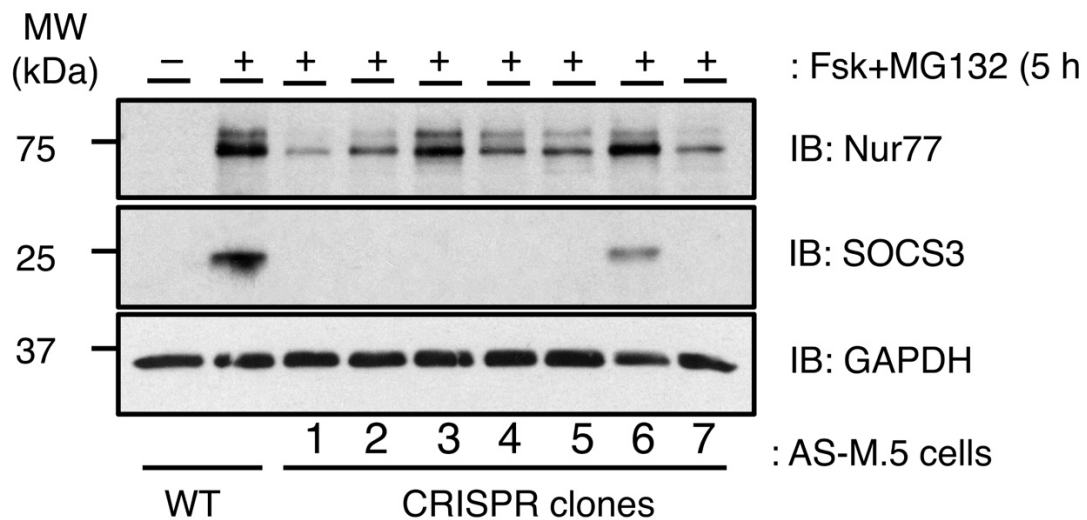


**Figure 3–6 Immunoblot screening of CRISPR/Cas9-mediated SOCS3 gene knockout in AS-M.5 cells**

WT human angiosarcoma-derived ECs and clonal cell lines were treated with Fsk (50  $\mu$ M) in the presence of MG132 (6 $\mu$ M) for 5 hr. Detergent-soluble whole cell lysates were equalised for protein content and then resolved by SDS-PAGE for immunoblotting with the indicated antibodies. Data shown are representative of three separate experiments.

## CRISPR CLONE

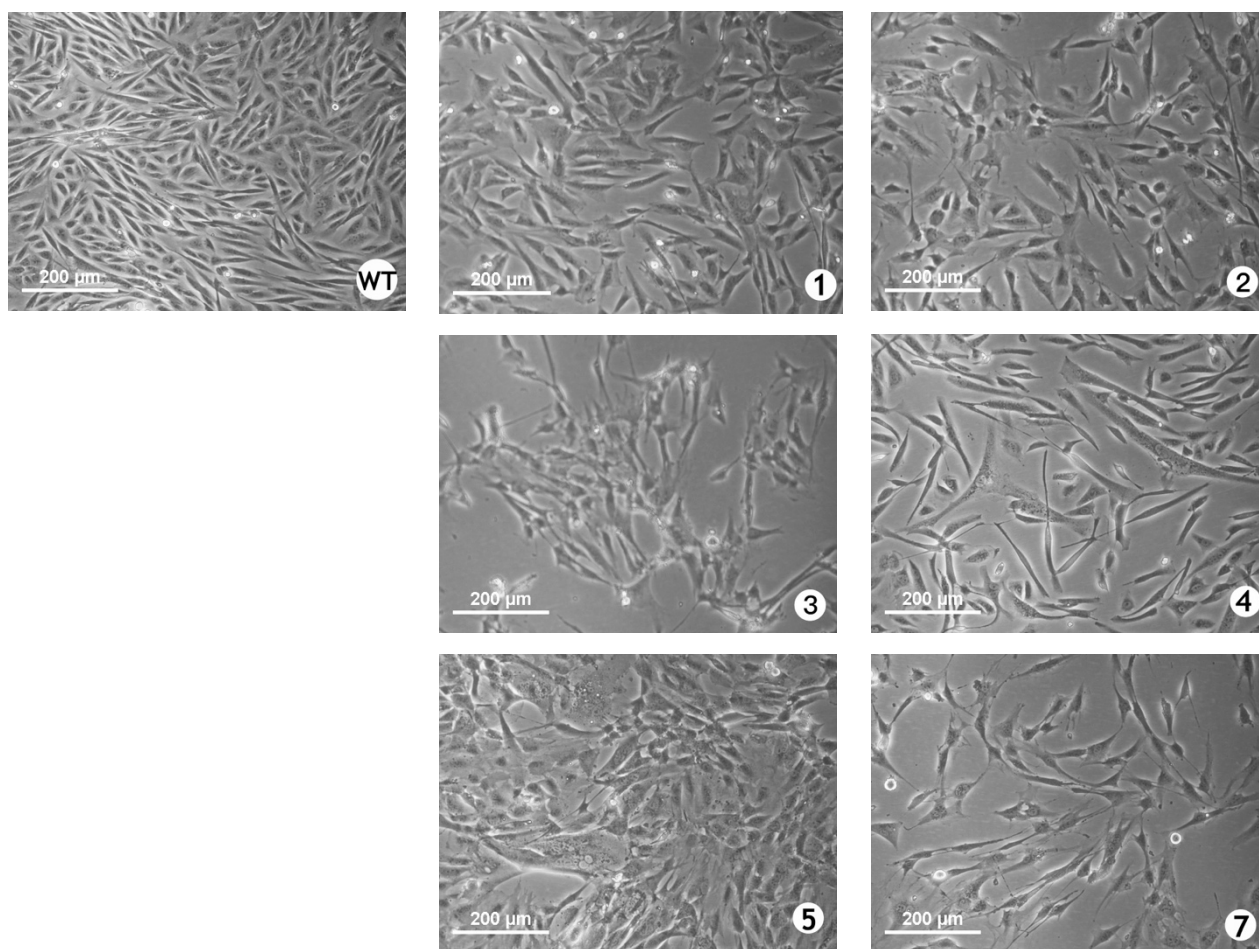


**Figure 3–7 Phase contrast photomicrographs of the parental AS-M.5 human angiosarcoma-derived ECs and clonal cell lines in culture.**

WT AS-M.5 and the immortalized CRISPR/Cas9-mediated SOCS3 knockout cell monolayers exhibit the typical cobblestone cell morphology that is characteristic of endothelial cells. While AS-M.5 cells were spindle-shaped, clonal cell lines exhibited a polygonal-shape. Brightfield cell images were visualized under a Nikon Eclipse Ti-S inverted microscope (Nikon, Tokyo, Japan) equipped with a Nikon Digital Sight DS-Fi2 camera.

### 3.3 Conclusion

In the present study, CRISPR/Cas9 gene editing was utilised to knockout SOCS3 gene expression. Three gRNAs were used to successfully generate six clonal cell lines with a complete absence of SOCS3 protein expression as detected by the Western blot analysis compared to unedited controls. SOCS3 knockout cell lines could be created within a 7-week-period that extends from the day of transfection to cryopreservation of clonal production cell lines.

SOCS3 has a significant regulatory role in inflammatory-mediated pathways. Functional studies of SOCS3 are critical to elucidate the pathological mechanisms underlying complex human diseases, such as insulin resistance, cardiovascular diseases, rheumatoid arthritis and specific cancers [324]. Other SOCS3-related diseases include anaemia [385], viral infection [386], and psoriasis, where psoriasis-like inflammation is induced by SOCS3 deletion [387]. Focusing on the heart, the interaction between SOCS3 proteins and gp130-JAK1 complexes yields a remarkable regulatory role of three major downstream pathways, including the Ras/MEK/ERK, JAK/STAT, and PI3K/AKT [388, 389]. These multifaceted aspects of SOCS3 in different diseases highlight the importance of conducting future relevant studies to reveal the potential pathophysiological and therapeutic implications. Transitional research relies on mutant cell lines with a specific knocked-out protein to investigate the sequelae of allelic dysfunctionality in a given experimental study. The microbial CRISPR/Cas9 systems offered unprecedented ways of genomic manipulation induce gene knockouts in diploid cells and hence the biological significance of generating SOCS3-deficient endothelial cell lines as novel tools for the current experimental project and beyond. To the best of our knowledge, this study is the first to create endothelial SOCS3-deficient clonal cell lines using CRISPR/Cas9.

## 4 Characterisation of cavin-1/SOCS3 interaction

### 4.1 Introduction

SOCS3 proteins have a vital role in regulating specific cytokine-mediated signalling and thus can be regarded as key players in various processes in the hematopoietic and immune systems, such as negative regulation of granulopoiesis, regulation of a number of cytokine receptors, and other regulatory roles in T cell development and functions [315, 390]. The inhibitory actions of SOCS3 are exerted on the catalytic activity of JAKs which have been implicated in initiating cytokine signalling [323]. Such actions are attributable to the central SH2 domain which binds to distinct phosphorylated tyrosine residues on target proteins [307]. Following the recognition of these residues by SH2 domains, downstream signalling pathways are regulated either via enhancing a distinct enzymatic activity or undergoing SH2-mediated protein-protein interactions (Section 1.4.3 and 1.4.4). As such, the interest in investigating phosphotyrosine-dependent SOCS3 substrates has been substantially-increased. The characteristics of the identified substrates so far include a specific Tyr phosphorylation-dependent interaction with the SOCS3 SH2 domain as well as the presence of an intact SOCS box required for ubiquitylation of the bound targets [307]. Subsequently, proteasome-mediated degradation of some targets, such as FAK1, would follow substrate ubiquitylation [307]. However, the exact regulatory mechanisms of SOCS3 functions by other cellular proteins and the knowledge about ubiquitylated SOCS3 substrates remain unclear.

Comparison of tandem affinity purified ubiquitinomes have shown that SOCS3-expressing fibroblasts have a significant enhancement of cavin-1 ubiquitylation when compared to SOCS3-null cells [356]. Cavin-1 protein contributes to caveolae coupling to the microtubule network to inhibit caveolin-1 degradation and thus prevent caveolar disassembly [121]. A direct interaction between SOCS3 and two specific regions on cavin-1 independent of tyrosine phosphorylation has been demonstrated in studies employing co-

immunoprecipitations and overlapping peptide array overlays [356]. Since elevated JAK/STAT signalling is involved in the pathophysiology of chronic inflammatory disorders, it is plausible that the SOCS3 might have a therapeutic role as an E3 ligase [307]. A novel therapeutic potential may emerge through the adequate identification of cAMP/Epac1-regulated ECS<sup>SOCS-3</sup> E3 ubiquitin ligase targets and investigation of their impact on the cell.

#### **4.1.1 Aims**

This chapter aims to demonstrate whether SOCS3 could play a role in cavin-1 and caveolin-1 regulation through assessment of their endogenous protein expression in wild type and SOCS3-null AS-M.5 cells and MEFs. This was further examined at the gene expression of cavin-1 in MEFs. In addition, the impact of cAMP-mediated elevation of SOCS3 expression was investigated to elucidate the effects of changes in endogenous SOCS3 expression on cavin-1.

## **4.2 The effect of SOCS3 on cavin-1 stability in fibroblasts and endothelial cells**

The most significant non-lysosomal proteolytic pathway in the cell is mediated by the regulatory protein ubiquitin. In this pathway, protein degradation takes place via sequential catalytic reactions by three enzymes: ubiquitin activating enzyme (E1), ubiquitin-conjugating enzyme (E2), and ubiquitin ligase (E3). Subsequently, the 26S proteasome hydrolyses the target protein. Indeed, E3 ligases are highly specific to their substrates and the control of such proteolytic pathway relies basically on the ubiquitin-substrate interaction [391]. The latter is not only important in protein turnover control in physiological and pathological conditions but also may contribute in the endeavour of developing novel therapeutic approaches (Section 1.4.1 and 1.4.4).

Studies concerned with investigating the protein-protein interaction are designed not only to reveal the specific binders, but also to measure the resultant dynamic changes that might follow any disruptions. Gene knockout may be induced temporarily via siRNA or shRNA or more preferably through a

CRISPR/Cas9 KO control which would yield a permanent and stable negative control [392].

The potential regulatory effects of SOCS3 on endogenous cavin-1 levels were assessed by investigating the impact of homozygous SOCS3 gene deletion on cavin-1 expression in AS-M.5 cells. Results have shown that cavin-1 expression was significantly reduced in SOCS3<sup>-/-</sup> AS-M.5 cells when compared to WT cells as revealed by immunoblotting of whole-cell extracts. This was also associated with a decrease in CAV-1 protein expression levels, which has been similarly reported by other studies in normal and pathological conditions [121] (Figure 4–1). Furthermore, SOCS3<sup>-/-</sup> MEFs showed a significant reduction of cavin-1 levels as compared to WT MEFs (Figure 4–2). Thus, loss of SOCS3 in two distinct cellular systems (embryonic fibroblasts and endothelial cells) using two different methods (homologous recombination and CRISPR/Cas9 gene editing) results in reduced cavin-1 expression.

Other regulatory mechanisms, including splicing and post-translational modifications, might exist and they may increase proteome complexity. In the present thesis, the observed reduction of cavin-1 levels in SOCS3<sup>-/-</sup> cells might be caused by post-translational modifications of the existing proteins rather than a de-novo synthesis of proteins, providing a novel mechanism of SOCS3 protein involvement. To test whether the observed reduction in cavin-1 protein was accompanied by a corresponding decrease in mRNA levels, cavin-1 mRNA levels in WT and SOCS3-null MEFs, total RNA was extracted and quantitative real time-PCR measurements of cavin-1 mRNA abundance were performed as described previously (Section 2.2.6.1). There was a significant increase in the abundance of cavin-1 gene transcripts in SOCS3<sup>-/-</sup> cells versus WT MEFs (Figure 4–2). These results suggest that the steady state of cavin-1 proteins in SOCS3-deficient cells cannot be explained by a parallel reduction in the relative abundance of cavin-1 mRNA and suggests instead that the presence of SOCS3 may enhance cavin-1 stability in WT MEFs.

Cycloheximide is usually used in the kinetic experiments to inhibit protein synthesis. However, emetine was alternatively utilised in the present thesis as

it does not activate stress-activated MAP kinases such as p38 [393]. Emetine acts by preventing the enzymatic translocation of peptidyl-tRNA from the acceptor site to the donor site [394]. To quantify cavin-1 protein turnover in WT and SOCS3 deficient AS-M.5 cells, changes in the expression of cavin-1 was monitored following emetine-induced protein synthesis inhibition. Consistent with emetine chase experiments using MEFs [356], the lack of SOCS3 in AS-M.5 cells caused a significant reduction of the half-life of cavin-1 from >8 hours in WT cells to 3 hours in SOCS3-null AS-M.5 cells (Figure 4–4). Therefore, these data indicate that the presence of SOCS3 enhances cavin-1 stabilisation in AS-M.5 cells. Interestingly, these results contrast the well-established role of SOCS3 in substrate-destabilisation via ubiquitylation and proteasomal degradation [307].

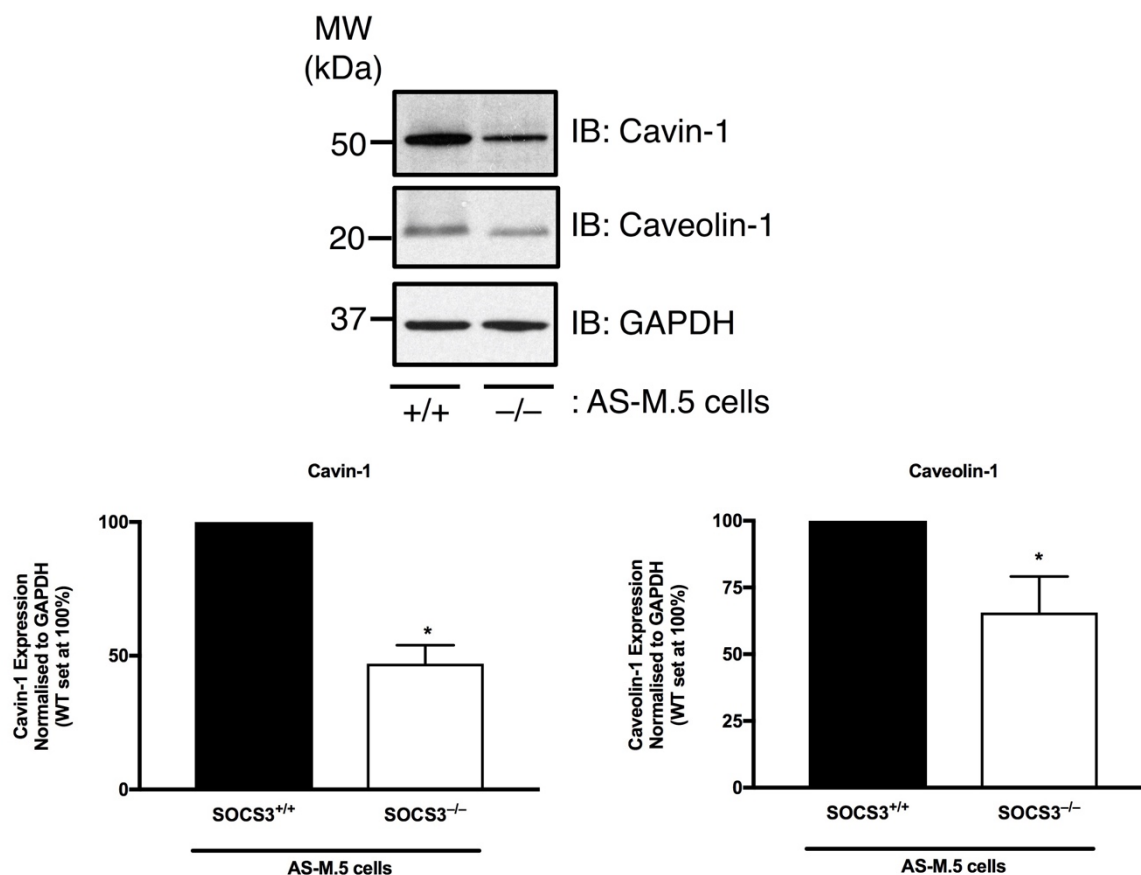


**Figure 4–1 SOCS3 deletion significantly reduces endogenous protein levels of cavin-1 and caveolin-1 in AS-M.5 cells.**

WT and SOCS3<sup>-/-</sup> AS-M.5 cells were grown to confluency in 6-well plates and harvested in RIPA lysis buffer. Soluble protein lysates were equalised for protein content before fractionation by SDS-PAGE on 10 % (w/v) polyacrylamide gels for immunoblotting with antibodies as indicated. Densitometry analysis of three independent experiments were performed using Image Studio Lite Software Version 5.2.5. Values are means  $\pm$  SEM. The statistical significance was assessed using an unpaired, two-tail t-test (GraphPadPrism, \* $p < 0.05$ ).

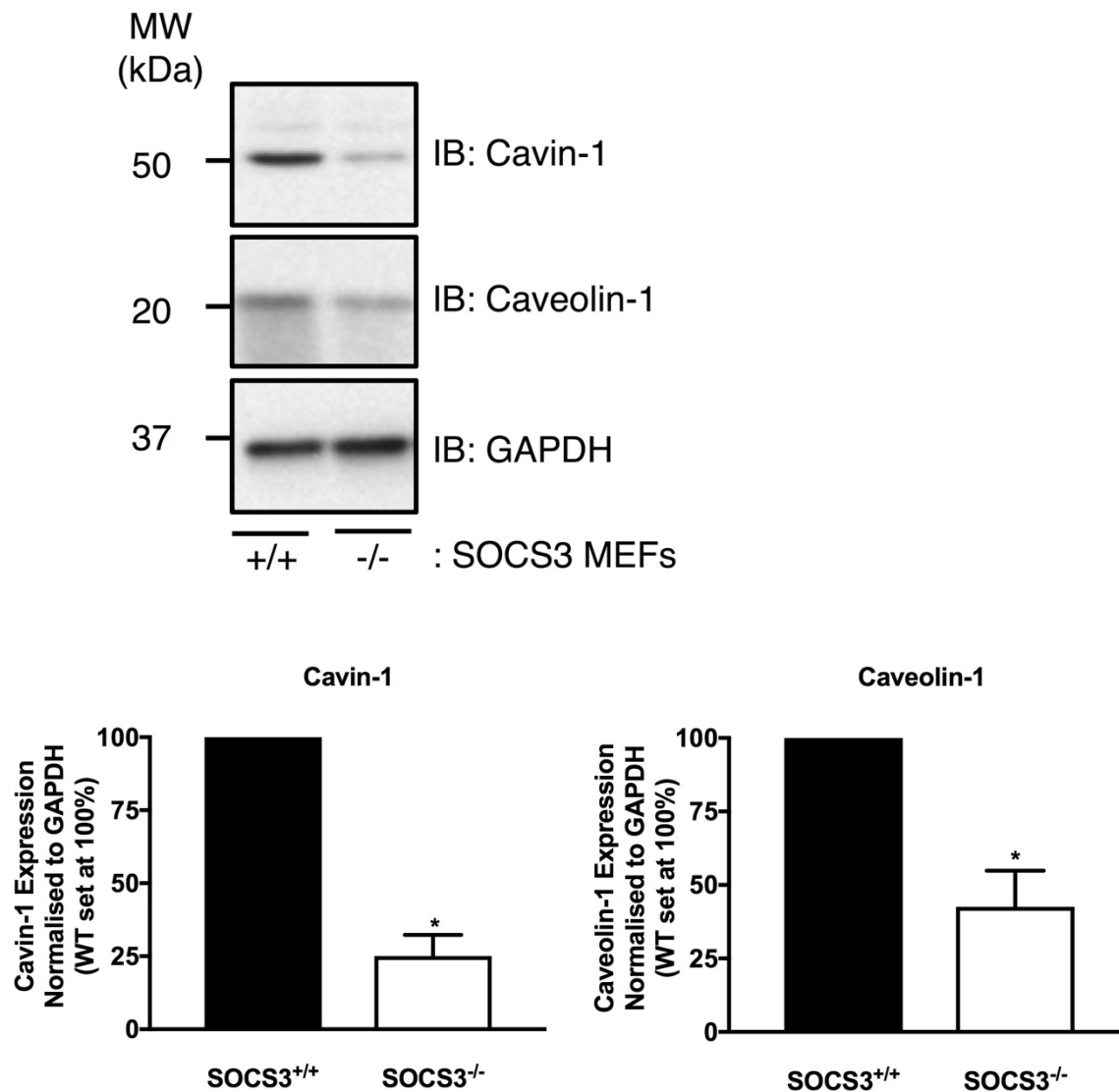


**Figure 4–2 SOCS3 deletion significantly reduces endogenous protein levels of cavin-1 and caveolin-1 in MEFs.**

WT and SOCS3<sup>-/-</sup> MEFs were grown to confluency in 6-well plates and harvested in RIPA lysis buffer. Soluble protein lysates were equalised for protein content before fractionation by SDS-PAGE on 10 % (w/v) polyacrylamide gels for immunoblotting with antibodies as indicated. Densitometry analysis of the immunoreactive bands was performed using Image Studio Lite Software Version 5.2.5. Values are means  $\pm$ SEM of three different experiments. The statistical significance was assessed using an unpaired, two-tail t-test (GraphPadPrism, \*p < 0.05).

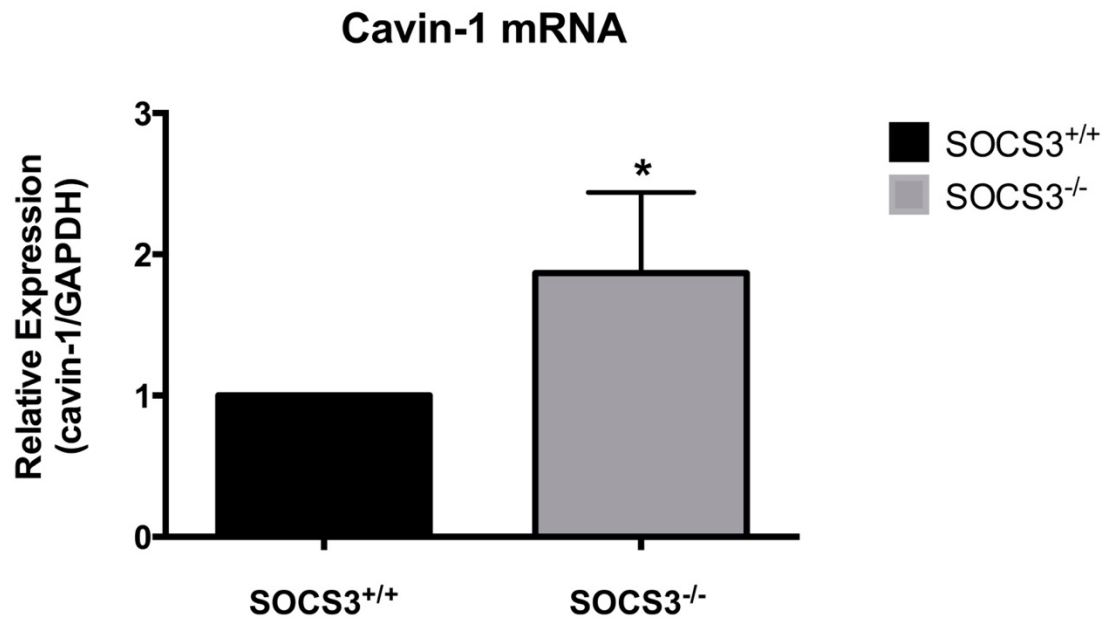


**Figure 4–3 Real-time qPCR revealed that the mRNA expression level of cavin-1 is significantly increased in SOCS3<sup>-/-</sup> MEFs as compared to WT (SOCS3<sup>+/+</sup>) controls.**

Total RNA samples were obtained, and cavin-1 mRNA levels were quantified by reverse transcription followed by qPCR analysis. GAPDH mRNA was used as an endogenous control. Real-time qPCR was performed to measure cavin-1 mRNA levels using the primers as shown in Table 2-8. The data were analysed using the  $2^{-\Delta\Delta C_t}$  method. Results representative of n=3 experiments. Statistical analysis was performed with the Student t test and are presented as the mean  $\pm$  SEM. Significant differences are marked by asterisk (\* = p < 0.05).

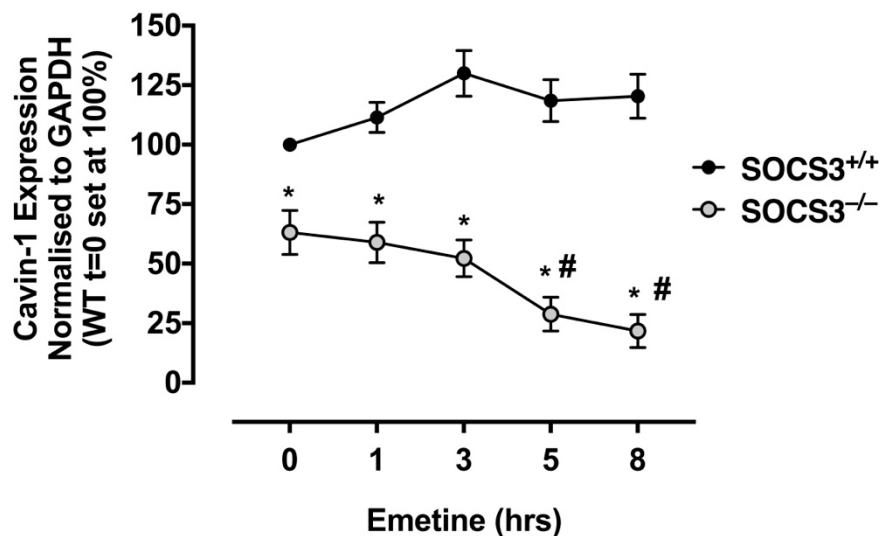


**Figure 4–4 Destabilisation of cavin-1 in SOCS3- deficient endothelial cells.**

WT and SOCS3<sup>-/-</sup> AS-M.5 cells were seeded into 6cm diameter dishes and grown until confluent. Cells were then treated with emetine, a protein synthesis inhibitor, at a concentration of 100 $\mu$ M for 1, 2, 3, 5 and 8 hours in serum-free medium. Following treatment, soluble cell extracts equalised for protein concentration were fractionated by SDS-PAGE for immunoblotting with cavin-1 and GAPDH antibodies. Quantitative analysis of cavin-1 protein levels in WT and SOCS3-null AS-M.5 cells from three experiments is presented as mean values  $\pm$  SEM (\* $p$ <0.05 versus cavin-1 levels in SOCS3<sup>+/+</sup> AS-M.5 cells, #  $p$ <0.05 vs.  $t=0$ ).

### **4.3 The effect of SOCS3 induction by cAMP elevation on cavin-1**

cAMP plays a major role in the regulation of multiple functions in the innate and adaptive immune response. Such regulatory function is clearly demonstrated when cAMP-elevating drugs enhance the production of anti-inflammatory mediators and reduce the pro-inflammatory factors produced by multiple immune cells [395]. cAMP homeostasis is maintained through the expression of adenylate cyclases (ACs), which catalyse its formation from ATP. Furthermore, phosphodiesterases (PDEs) comprise a family of more than 100 enzyme variants that contribute to degradation of intracellular cyclic nucleotides. Indeed, these variants are allocated into 11 families [396] according to their structure and the interaction and specificity for cyclic nucleotides.

cAMP triggers several downstream pathways in the cell via activation of protein kinase A (PKA) [397], which dissociates into its regulatory and catalytic subunits upon binding of cAMP. These catalytic units phosphorylate specific Ser and Thr residues on several target proteins [398]. Furthermore, multiple cAMP-responsive transcription factors, including activating transcription factor-1 (ATF-1), cAMP-response element binding protein (CREB), and distinct members of the cAMP-responsive element modulator (CREM) family [399], are also phosphorylated by PKA. Importantly, nuclear-localised PKA can phosphorylate CREB at serine-133[400] and this promotes translocation to the nucleus where it binds to target promoters and, following binding to CRE promoter sites and recruitment of transcriptional activators such as p300 and CBP, promotes gene transcription. Generally, the phosphorylated transcription factors bind to cAMP-response elements (CREs) in the target genes with a significant interaction with CREB-binding protein (CBP) and p300, which coactivate the transcription process [401]. Phosphorylation of CREM, CREB, and ATF-1 could be also established by other kinases while distinct protein phosphatases can counterbalance PKA effects [398]. In addition to activation of PKA, cAMP can also act by modulation of cyclic nucleotide-gated channels (CNGs), the

exchange protein directly activated by cAMP (Epac) and guanine-nucleotide-exchange factor (GEF) [402, 403].

#### **4.3.1 SOCS3 induction by cAMP stabilises cavin-1**

Although proteasomal degradation maintains low SOCS3 levels in the cell, several routes are implicated in SOCS3 induction, including Toll-like receptors [344], the JAK/STAT pathway and cAMP elevation through activation of EPAC and PKA-independent ERK activation [304, 404]. As a result of the abundance of SOCS3-inducing routes, several ubiquitinated targets exist. Actually, the abundance of SOCS3-inducing routes renders a variable pool of ubiquitinated targets. SOCS3 has been recognised as one of two ubiquitin ligases induced by cAMP [405]. The latter has been identified as a potent inhibitor of the pro-inflammatory signalling pathways [395]. Therefore, multiple anti-inflammatory therapeutic approaches could be elucidated by revealing novel cAMP/EPAC1 targets.

Williams et al. [356] attempted to identify novel ubiquitinated SOCS3 substrates following cAMP activation to further elucidate the involvement of cAMP in inflammation. The proteomic screening experiments have shown an interaction between cavin-1 and SOCS3 proteins. As presented in Section 4.2, SOCS3 can contribute to cavin-1 stability. Thus, it is important to investigate the impact of cAMP-induced SOCS3 accumulation on the levels of cavin-1 and the resultant functional consequences. A time-dependent accumulation of SOCS3 was observed following exposure to the cAMP-elevating agent forskolin (Fsk, 50  $\mu$ M). Such accumulating pattern, which peaked after 4 h, was associated with transient increase in SOCS-3 mRNA, which could be detectable at 1, 3 and 5 h (data not shown). Following treatment of WT and SOCS3<sup>-/-</sup> MEFs with Fsk for 6 hours, cavin-1 expression was decreased in SOCS3-deficient MEFs at t=6 hrs vs t=0, whereas SOCS3 accumulation in response to Fsk-stabilised cavin-1 levels in the WT counterparts after 6 hrs of Fsk exposure (Figure 4–5).

cAMP causes CREB phosphorylation via protein kinase A induction. CREB then binds to the cAMP-regulated enhancer, which is located in many target genes. Of those genes, Nur77 is one of those genes and it can be induced by cAMP [356, 384]. Therefore, Nur77 expression was utilised in the present thesis to aid as a positive control to monitor cAMP elevation.

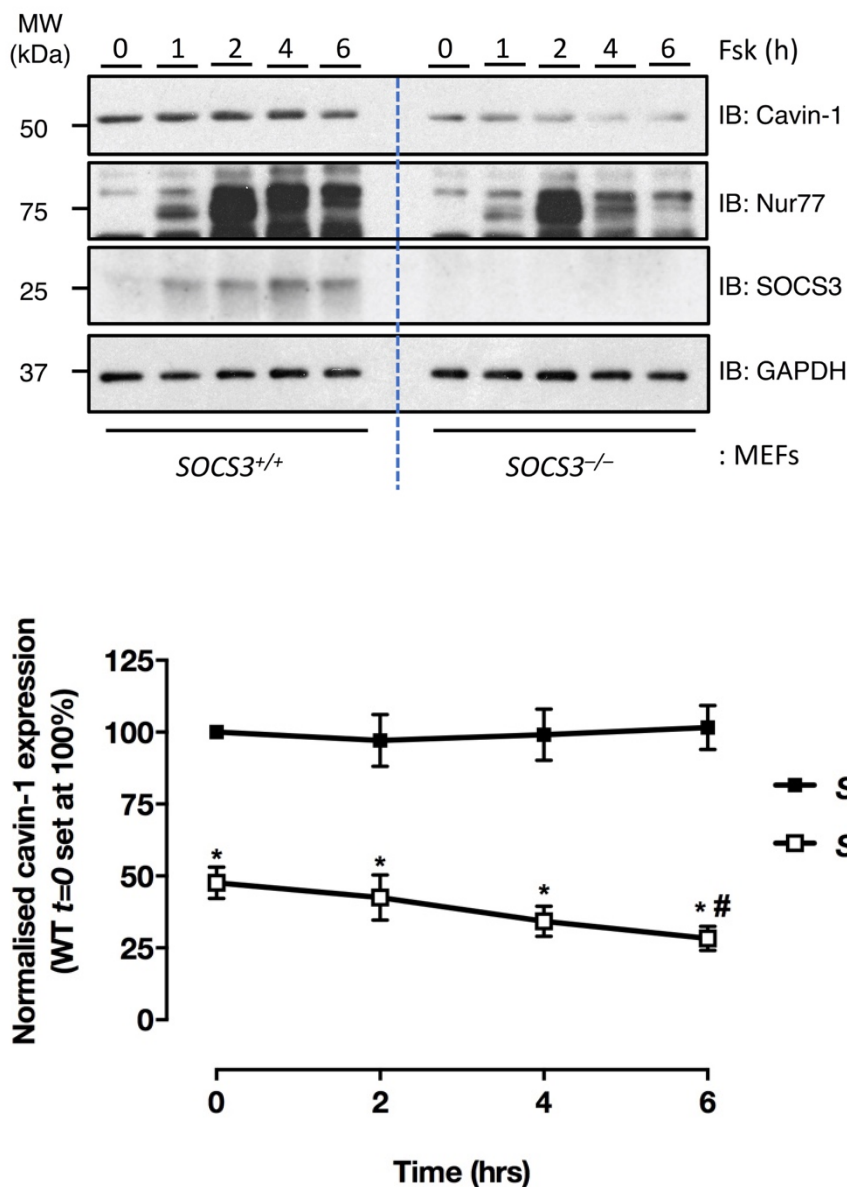


**Figure 4–5 The effect of SOCS3 deletion on Fsk-mediated regulation of cavin-1 and Nur77 expression levels in MEFs.**

WT and *SOCS3*<sup>-/-</sup> MEFs were seeded in 6 well plates and grown until confluent. Cells were then treated with Fsk (50 $\mu$ M) for 1, 2, 4 and 6 hours. Following treatment, soluble cell extracts equalised for protein concentration prior to fractionation by SDS-PAGE for immunoblotting with indicated antibodies. Quantitative analysis of cavin-1 protein levels in WT and *SOCS3*-null MEFs is presented as mean values  $\pm$  SEM (\* $p$ <0.05 versus cavin-1 levels in *SOCS3*<sup>+/+</sup> MEFs, #  $p$ <0.05 vs.  $t=0$ ). One of seven experiments.

### 4.3.2 Examining cAMP-dependent regulation of cavin-1

Previous studies suggested that cavin-1 migrates at a high molecular weight (10-15 kDa) upon separation by polyacrylamide gel electrophoresis, which is probably due to posttranslational modifications [114]. Cavin-1 acetylation takes place at the N-terminal methionine residue [406] and it can be also SUMOylated and ubiquitinated [307]. In addition, the involvement of cavin-1 in cell signalling is supported by its phosphorylation at multiple sites [118, 407]. Cavin-1 fractionation into active and inactive forms for transcription is possible and such phosphorylation sites may potentially change the capacity of cavin-1 to dissociate ternary transcription complexes [408]. Aboulaich et al. [406] found that cavin-1 has four phosphorylation sites as demonstrated by immobilized-metal affinity chromatography. Ser-36 and Ser-40 are sites for phosphorylation by glycogen synthase kinase-3, whereas protein kinase A and casein kinase 2 phosphorylate Ser-365 and Ser366 sites, respectively [406].

Hormone-stimulated lipolysis in the adipocytes is one of the important intracellular processes that has been linked to cavin-1 [409]. Glucagon and epinephrine cause activation of cAMP/PKA signalling after binding to their receptors (glucagon and  $\beta$ -adrenergic receptors, respectively) [406]. Hormone-sensitive lipase (HSL) is an intracellular lipase that regulates lipolysis. It contains PKA phosphorylation sites [410, 411] and it can co-immunoprecipitate with cavin-1 proteins. Interestingly, insulin can cause translocation of both HSL and cavin-1 from the plasma membrane to the cytosol [409].

The results of the present thesis indicated that cavin-1 was detected as an approximately 50-kDa band in the positive-control WT cells. However, cavin-1 immunoreactivity was observed in preliminary time course experiments following Fsk treatment (data not shown). The involvement of immunoreactive cavin-1 proteins in cAMP/PKA signalling was investigated by conducting time course experiments in which WT MEFs were stimulated with Fsk in the presence or absence of a PKA inhibitor (H89). Although H89 treatment inhibited the ability of Fsk to induce cAMP-responsive gene Nur77, cavin-1 levels evidenced no change (Figure 4–7). Therefore, cavin-1 immunoreactivity is supposedly regulated independent of cAMP/PKA signalling.

To further attain a confirmatory evidence, molecular cAMP induction requirements were assessed. Given that such induction entails new protein synthesis (Nur77 is translation-dependent), the assumption of requiring new protein synthesis with the changes in cavin-1 immunoreactivity was investigated. Thus, WT MEFs were incubated with protein synthesis inhibitor emetine (100  $\mu$ M) or a vehicle 30 min prior to treating with Fsk. Although this treatment was sufficient to inhibit Nur77 accumulation in response to Fsk treatment, emetine had no effect on cavin-1 immunoreactivity as compared to the vehicle control groups (Figure 4–7). Thus, a cavin-1 activity, which seems to be translation-independent, is not regulated via a cAMP/PKA Pathway.

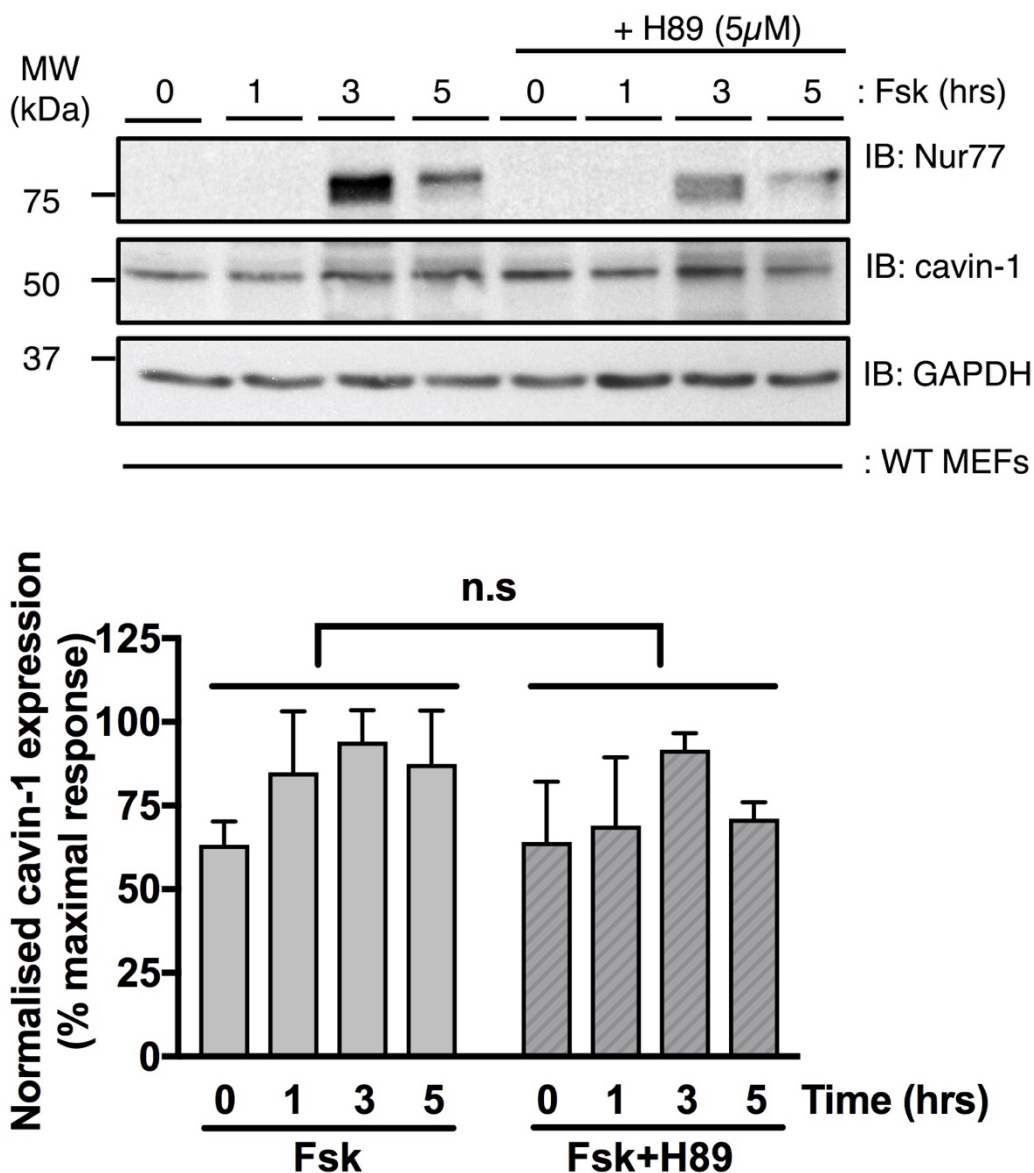


**Figure 4–6 Stabilisation of cavin-1 following cAMP elevation is PKA-independent.**

WT MEFs were seeded in 6 well plates and grown until confluent. Cells were then treated with H89 (5 μM) 30 min prior Fsk (50 μM) stimulation for 1, 3, and 5 hours as indicated. Following treatment, soluble cell extracts equalised for protein concentration and then separated by SDS-PAGE for immunoblotting with indicated antibodies. Quantitative analysis of cavin-1 protein levels in WT MEFs is presented as mean values ± SEM. All samples were analysed in three independent experiments. n.s. indicates statistically non-significant difference between H89-treated and untreated groups.

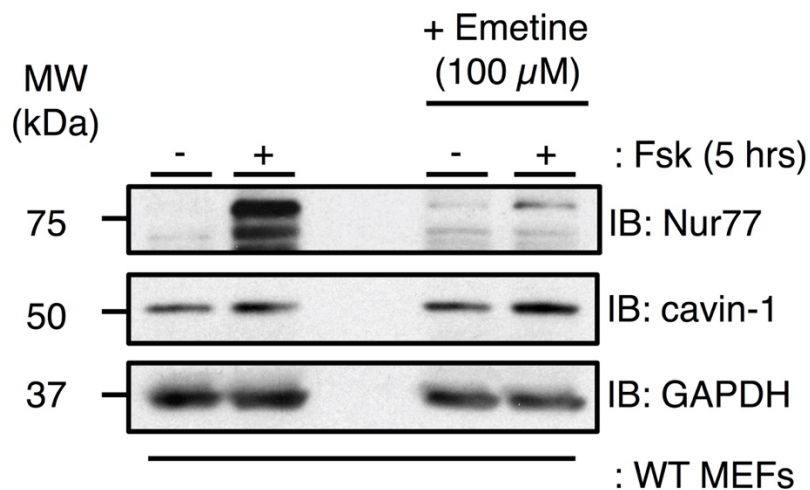


**Figure 4-7 Effect of protein synthesis inhibitor emetine on Fsk-mediated changes in cavin-1 immunoreactivity.**

WT MEFs were grown to confluency in 6-well plates and then treated with Fsk (50 μM) in the presence or absence of emetine (100 μM) for 5 hours prior to harvesting. Protein extracts were prepared and equalised for protein content before fractionation by SDS-PAGE on 10 % (w/v) polyacrylamide gels for immunoblotting with the indicated antibodies. Results representative of n=3 experiments.

### 4.3.3 Examining phosphorylation status of cavin-1 following cAMP elevation

Protein phosphorylation is one of the important regulatory processes in all cells. Two major classes of enzymes, protein kinases and protein phosphatases, can control such reversible events. The important biological processes of relevance that could be activated or inactivated by phosphorylation include protein synthesis, signal transduction and DNA transcription as well as other cellular actions, such as motility and division [412].

The experiments in the present section used treatment with a non-selective phosphatase to determine whether phosphorylation altered cavin-1 protein immunoreactivity [413]. To this end, WT MEFs were lysed in a lysis buffer without phosphatase inhibitors and divided into two aliquots; one received calf intestinal phosphatase (CIP) and the other received buffer alone. Following incubation for 2 hrs at 37°C, samples were resolved by SDS-PAGE and immunoblotted for cavin-1. Given that phosphorylation has been suggested to be the primary mechanism by which CREB was controlled [414], anti-Ser-133 pCREB antibody was used as a positive control to assess CIP activity.

As shown in Figure 4–8, CREB phosphorylation on Ser-133 was detected 2h following Fsk stimulation and this modification was abolished by phosphatase treatment. In contrast, no changes in cavin-1 immunoreactivity were detectable, suggesting that any cAMP-mediated phosphorylation of cavin1 had no effect on immunoreactivity.

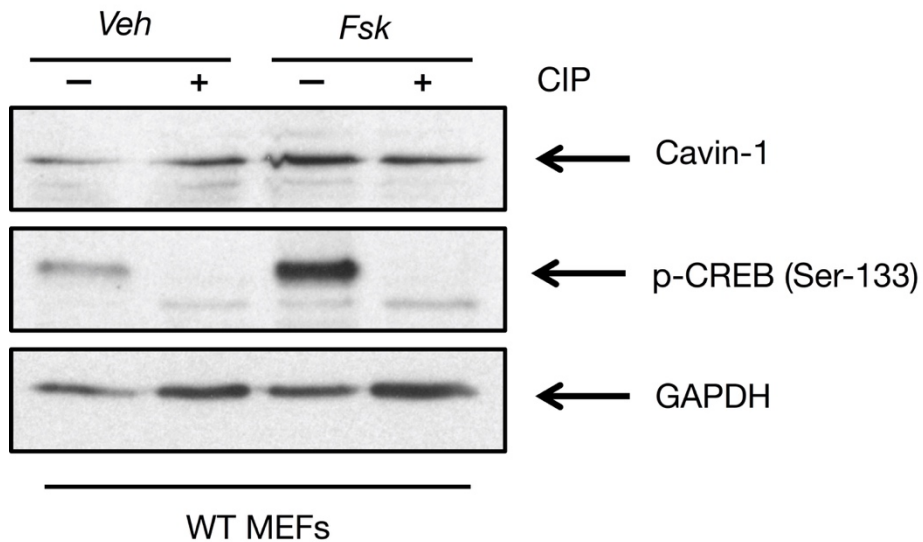


**Figure 4–8 Effect of phosphatase treatment on cavin-1 immunoreactivity.**

WT MEFs were grown to confluency in 6cm diameter dishes after which the media was refreshed before treating with Fsk (50  $\mu$ M) for 2h prior to harvesting. Cells were lysed in the absence of phosphatase inhibitors. Protein-equalised soluble cell extracts were divided into aliquots and then incubated at 37°C for 2 h in the presence (+) or absence (-) of calf intestinal alkaline phosphatase (1 unit/1 $\mu$ g protein). Following phosphatase treatment, samples were resolved by 12% SDS-PAGE for immunoblotting with the indicated antibodies. Results representative of n=3 experiments.

## **4.4 Discussion**

### **4.4.1 Role of SOCS3 in stabilising cavin-1**

Cavin-1 is a novel SOCS3-interacting protein. Williams et al. [356] confirmed such interaction via co-immunoprecipitation experiments, showing a co-expression of myc-tagged cavin-1 proteins exclusively with Flag-SOCS3, and also the interaction was confirmed between HA-SOCS3 and Flag-cavin-1 to exclude the effect of tag-mediated combination. An overexpression approach was exploited in the early experiments aimed to characterise cavin-1/SOCS3 interaction. Here, I sought to define this interaction in cell systems expressing the endogenous protein.

The results of this chapter have shown that SOCS3 knockout in the whole-cell extracts of AS-M.5 and MEFs resulted in a significant reduction of cavin-1 and CAV-1. Interestingly, this reduction was found in the absence of any changes in cavin-1 mRNA suggesting that the presence of SOCS3 stabilises cavin-1 through an unknown mechanism. In addition, SOCS3 knockout in endothelial AS-M.5 cells caused a significant shortening of the half-life of cavin-1 as compared to WT MEFs. SOCS3 does not ubiquitinate cavin-1 but instead supports cavin-1. This indicates a potent SOCS3-mediated stabilisation of cavin-1, which contrasts the well-established destabilising effect of SOCS3 on its target proteins. So far, only Eps15 homology domain-containing protein 2 (EHD2) has been shown to be a cavin-1 interacting protein despite the lack of a direct effect on cavin-1 turnover [168]. Therefore, it is possible that cavin-1 becomes less susceptible to proteolysis when bound to SOCS3 which limits further proteolysis. Stabilising cavin-1 might potentially be critical for controlling inflammatory pathways involved in diabetes and cardiovascular disease.

### **4.4.2 Role of cAMP elevation in cavin-1 stabilisation**

cAMP elevation has been linked with SOCS3 induction in multiple cell lines, including primary endothelial cells from multiple vascular beds [304], MEFs [404], and AS-M.5 cells [356]. Fsk-mediated cAMP elevation maintained cavin-1 levels in SOCS3<sup>+/+</sup> MEFs over a time period of 6 hrs and this effect was

diminished in SOCS3<sup>-/-</sup> MEFs (Figure 4–5), suggesting a role of SOCS3 induction in cavin-1 stabilisation.

Moreover, there is no evidence to suggest that cavin-1 is directly regulated by the cAMP/PKA pathway. Likewise, cAMP-mediated CREB ser-133 phosphorylation may not be involved in cavin-1 phosphorylation. To the best of my knowledge, the role of caveolar proteins in cAMP/PKA pathway has only been recently reported by Kuo et al. [415] where loss of caveolae led to increased cAMP/PKA signalling in EC and CAV-1 was found negatively regulated cAMP/PKA signalling at the level or upstream of G proteins. In addition, the authors have revealed that CAV-1-deficient EC enhanced Fsk-stimulated PKA CREB phosphorylation at Ser-133 and they suggested a unique mechanism of CAV-1-dependent regulation of cAMP/PKA signalling-mediated lipolysis in endothelium versus adipocytes [415]. This is consistent with the observed effect of cAMP elevation on CAV-1 upregulation in EC (data not shown). However, it seems that cavin-1 regulation is independent of the cAMP/PKA pathway. In sum, there may be a potential unidentified relationship of CAV-1 with cavin-1 following Fsk-induced cAMP/PKA signalling.

## **5 Functional investigation of cavin-1/SOCS3 interaction**

### **5.1 Introduction**

The knowledge regarding the basic molecular components that contribute to caveolar generation is increasing remarkably. One of these components is a group of biomechanical integral membrane proteins, namely caveolins, that form distinct oligomers in the inner leaflet of the plasma membrane [114, 214, 416]. In addition, cavin proteins that contain assembled trimeric coiled coils, show higher levels of solubility than caveolins [102, 145, 417]. The size and shape of caveolae are determined by a large 80S complex that comprises caveolins and cavins [122, 418], while both cavin-1 and CAV-1 are crucial for caveolae formation [121, 181]. Other caveolar components include Eps15 Homology Domain (EHD) proteins, which functions at the caveolar neck [419-421], and pacsin 2 (Syndapin 2), which is located less frequently at the neck of caveolae as compared to EHD [422].

Both cavin-1 and CAV-1 have integral roles in a variety of diseases resulting from loss-of-function mutations as revealed in knockout mice and human patients. Indeed, this suggests caveolae-mediated effects on the maintenance and functionality of a number of cell types, including cells of the endothelium, muscles, and adipose tissue [112, 114, 214]. However, the mechanisms by which the resulting diseases take place remain fairly understood. Moreover, caveolae are presumably involved in the modulation of a wide variety of signalling pathways, including signalling to regulate the activities of insulin receptors and eNOS [41, 423, 424].

Given the complicated functional aspects of caveolae in the cell (detailed in chapter 1 section 1.2.4), cellular response to the absence of such structures seems to be a plausible matter of further investigations. This would be of a particular importance for those cells that are mostly caveolae-dependent, such as endothelial cells.

### 5.1.1 Aims

According to data presented in chapter 4, MEFs and AS-M.5 cells lacking SOCS3 had reduced protein expression of CAV-1 and cavin-1. As such, the first aim of this chapter was to investigate the potential effect of SOCS3 deletion on caveolae abundance in both cell lines. Moreover, to determine whether cavin-1 is a functionally significant SOCS3-interacting protein, we aimed to (1) assess subcellular localisation of SOCS3 in cavin-1-deficient MEFs and their wild counterparts using immunofluorescence microscopy and (2) to define the integrative role of cavin-1 in SOCS3 -dependent IL-6 inhibition.

## 5.2 Results

### 5.2.1 Effect of SOCS3 deletion on caveolae abundance

In section 4-2, the regulatory role of SOCS3 on CAV-1 abundance was demonstrated via promoting cavin-1 stabilisation. SOCS3-deficient MEFs had reduced cavin-1 levels by  $47 \pm 4\%$  and Cav-1 levels by  $65 \pm 7\%$  in MEFs while cavin-1 and Cav-1 levels decreased by  $25 \pm 4\%$  and  $42 \pm 7\%$ , respectively, in SOCS3-null AS-M.5 cells (section 4-2). Therefore, the effect of reduced cavin-1 and CAV-1 expression on the abundance of caveolae was investigated using transmission electron microscopy (TEM), which allows the assessment of caveolae morphology and dynamic biogenesis in SOCS3-deficient cells and their wild counterparts.

TEM is utilised to directly visualise the organisation of different cellular components on a nanometre scale. The significant role of TEM is augmented when used in combination with molecular detection techniques given the enhanced resolution of TEM is sufficient to detect intracellular proteins in the respective compartments and small membrane proteins. This could be attained by electron-dense markers, including gold particles, which are conjugated to secondary antibodies. Therefore, labelling of the ultrastructural antigens in this technique is called immunogold EM [425]. Given that CAV-1 is a major structural protein (22 kDa) that can act as a biomechanical marker of caveolae [114] (Section 1.2.1.1), our preliminary experiments were designed to identify

caveolae via detection of the intracellular localisation of CAV-1 through immunogold staining in WT MEFs.

As such, following their growth on 6 cm cell culture dishes, confluent cells were scraped off, centrifuged at 1,500g for 5 min and subsequently prepared for electron microscopy (section 2.2.7). The pellets were then incubated with polyclonal Rabbit antibodies designated to target multiple unique CAV-1 peptides (BD Biosciences 610059) followed by incubation with gold-nanoparticle-associated secondary antibodies directed against the primary antibodies. Results showed that CAV-1 proteins distributed on the cellular surface and other regions in WT MEFs (Figure 5–1). Despite the substantial visualisation of cellular content and biomolecules by immunogold EM, it may be regarded an extremely laborious technique that entails multiple technical challenges. As a result of these technical challenges, gold labelling was not pursued in the present work. Instead, caveolar morphology was directly detected on the cell surface. Morphologically, caveolae are identified as spherical or flask-shaped plasma membrane invaginations of notably consistent shape and size (~70 nm average outer diameter). The unique omega-shaped  $\Omega$  morphology of caveolae as well as their arrangement as single structures or in chains or grape-like clusters [426, 427] can be visualised under electron microscopy (Figure 5-1B).

Immortalised SOCS3<sup>-/-</sup> and cavin-1<sup>-/-</sup> MEFs and the corresponding WT cell lines grown until confluency on Thermanox<sup>®</sup> coverslips were fixed and embedded in Epon (section 2.2.7). Ultrathin sections were viewed on a LEO 912AB TEM and images were captured. The length of plasma membrane was calculated and the number of caveolae/ $\mu\text{m}$  was counted including caveolae that opened to the outside of the plasma membrane. Caveolae abundance was significantly increased in WT MEFs as compared to SOCS3-deficient cells ( $p < 0.01$ ). Interestingly, caveolae were not detectable in cavin-1 KO MEFs (Figure 5–2) and this was consistent with a previous evidence in the literature [121].

Caveolae are well-known for their abundance in all cell types of the cardiovascular system, including cardiac myocytes, vascular smooth muscle cells, macrophages, and endothelial cells [428]. Therefore, the effects of SOCS3 deletion on caveolae abundance in the endothelial AS-M.5 cells were investigated in the present project. In addition, caveolae were morphologically characterised using TEM techniques. Results revealed that caveolae were detectable and abundant in WT AS-M.5 cells but, on the other hand, they were significantly reduced in SOCS3-deficient cells (Figure 5-3). As such, it can be concluded that the abundance of plasma membrane caveolae was markedly affected by CAV-1 and cavin-1 reduction in SOCS3-deficient cells.

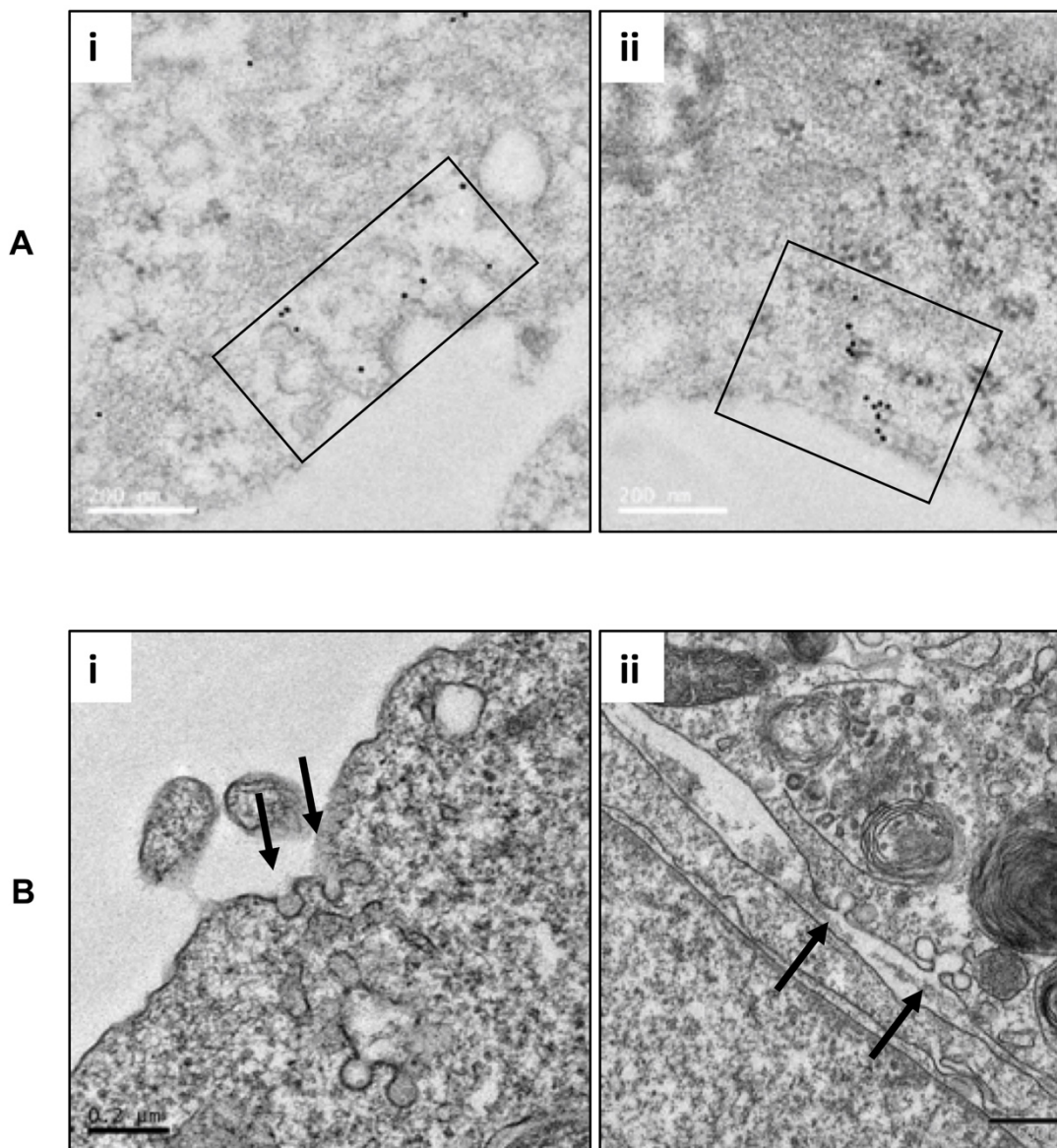


**Figure 5–1 Detection of caveolae**

(A) Immunogold labelling of caveolin-1-rich fraction examined by electron microscopy. WT MEFs were prepared for electron microscopy as described in section 2.2.7. Ultrathin sections were cut and incubated with anti-caveolin-1 antibody (BD Biosciences 610059) followed by incubation with gold-conjugated secondary antibody. Samples were imaged using a transmission electron microscope. (i-ii) Electron micrographs of WT MEFs depicting localisation of caveolin-1. The insets show the distribution of gold particles near the plasma membrane. Data shown were N=1. *Scale bar* =0.2μm

(B) Caveolae are readily visualized via electron microscopy. Electron micrographs show typical membrane invaginations (single caveolae and clustered caveolae) found on the surface of (i) WT MEF and (ii) WT AS-M.5 endothelial cell. Arrows indicate caveolae. *Scale bars* are (i) 0.2 μm and (ii) 0.5 μm.



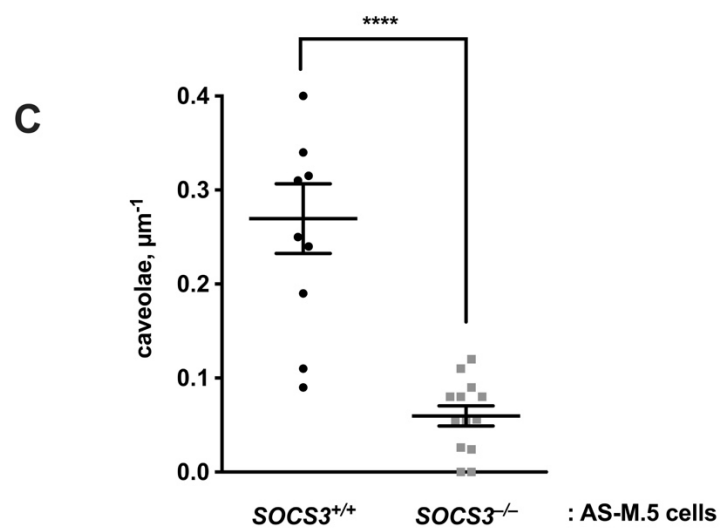
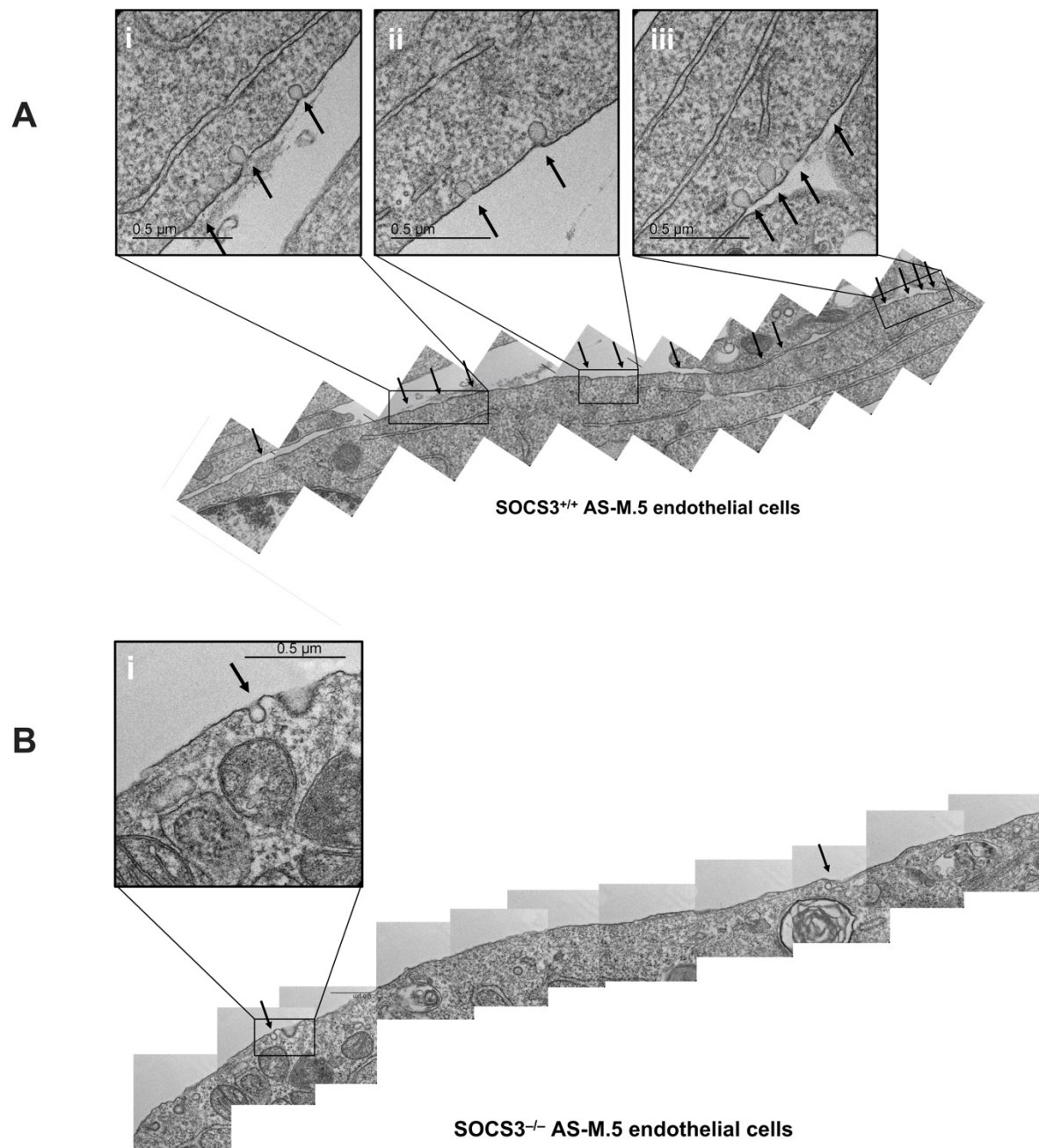


**Figure 5–3 Ultrastructural analysis of caveolae on the WT and SOCS3-null AS-M.5 endothelial cell surface.**

Confluent immortalised SOCS3-null and WT AS-M.5 cells were fixed, dehydrated and Epon-embedded as described in Methods (2.2.7). Ultrathin sections were processed and then viewed under a LEO 912AB TEM at an accelerating voltage of 120kv. (A) Representative electron micrographs of WT AS-M.5 cells showing caveolae around the perimeter (i-iii). (B) A representative electron micrograph of caveolae on the SOCS3<sup>-/-</sup> AS-M.5 cell surface (i). Arrows: caveolae. *Scale bar*=0.5  $\mu$ m. In the presence of SOCS3, 13 caveolae were identified on the surface of a single WT AS-M.5 cell, for a total length of 14 $\mu$ m (0.93 cav/ $\mu$ m) after the reconstruction of image stacks as depicted in (A). In contrast, only 2 caveolae were identified from a similar length (0.14 cav/ $\mu$ m) on a SOCS3<sup>-/-</sup> AS-M.5 cell surface as depicted in (B). (C) Quantitation of these invaginations from three independent experiments indicated that this phenomenon is significant (unpaired, one-tailed Student's t-test, \*\*P < 0.02). Data represent caveolae per  $\mu$ m  $\pm$  SEM.

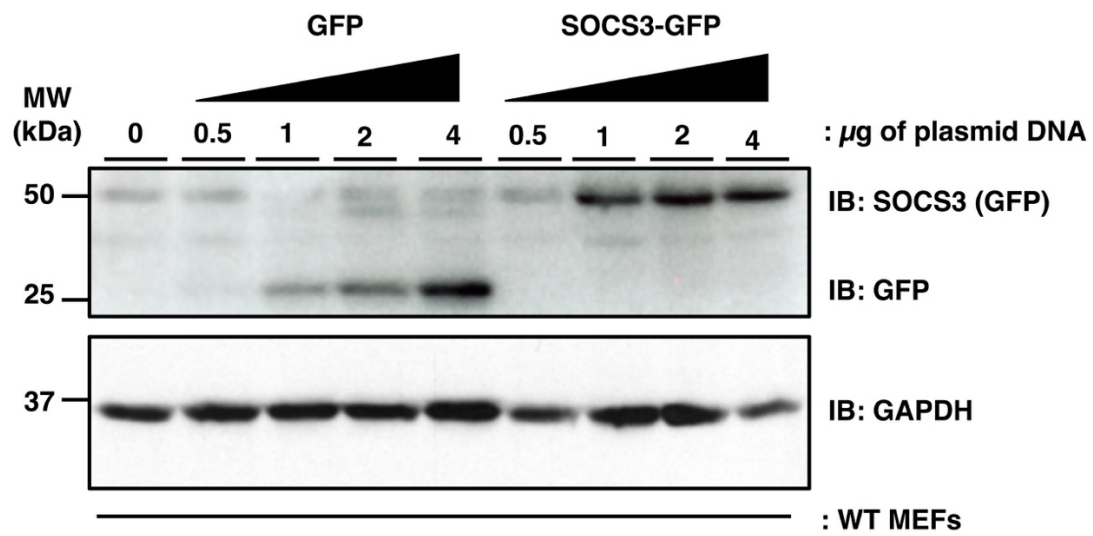
## **5.2.2 Using confocal microscopy to characterise SOCS3/cavin-1 interaction**

Protein-protein interaction could be identified using multiple techniques yet the best methods are those which distil and refine such interactions. Of them, confocal microscopy has been established as an essential confirmatory technique to elucidate protein-protein interaction [429]. Hence, confocal microscopy was utilised to visualise SOCS3 and cavin-1 localisation in the cell as well as their potential co-existence.

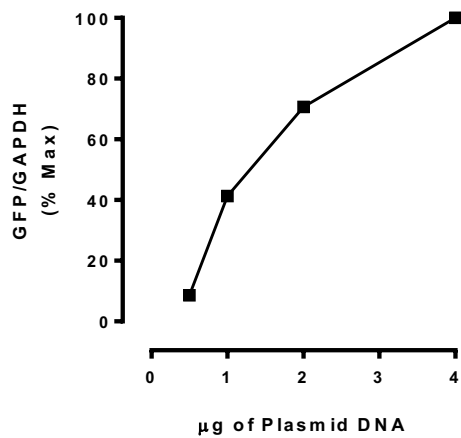
### **5.2.2.1 Optimisation of green fluorescent protein (GFP)-tagged SOCS3**

To investigate protein-protein interactions using fluorescence microscopy, fluorophores can be utilised either directly (by using green fluorescent protein [GFP] or as a tag on a primary antibody) or as a tag on a secondary antibody (indirect) [429]. For SOCS3 localisation, three commercial anti-SOCS3 antibodies were validated for use in a preliminary confocal-microscopy-dependent experiment in the present thesis (data not shown). Nonetheless, the endogenous staining of SOCS3 in WT MEFs could not be detected over and above background staining in SOCS3-null MEFs. As such, a transfected SOCS3-GFP model was alternatively utilised. Furthermore, a titration assay was employed to identify the amount of SOCS3-GFP plasmid required for optimal expression (Figure 5–4). The Immunoblotting technique was able to detect SOCS3-GFP expression using anti-GFP antibodies. The amount of the plasmid sufficient to transiently transfect WT and cavin-1-deficient MEFs was estimated to be 2 $\mu$ g and thus SOCS3 distribution was examined by confocal microscopy accordingly.

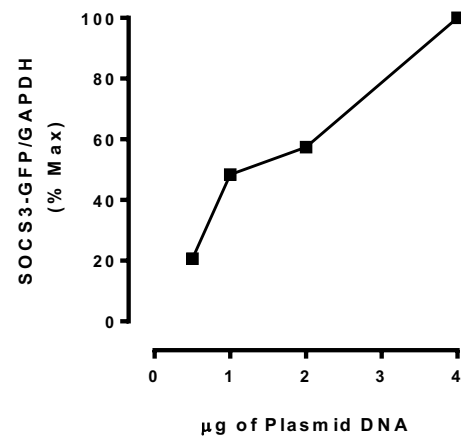
A



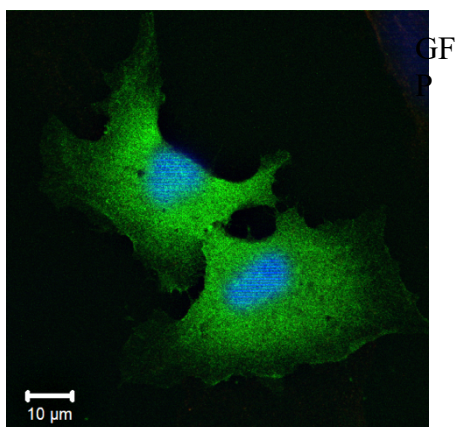
B



C



D



E

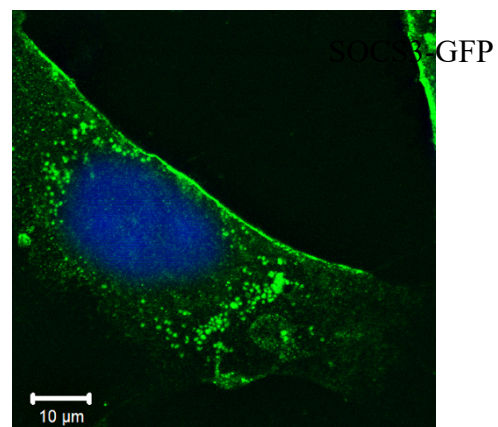


**Figure 5–4 Evaluation of the expression of GFP and SOCS3-GFP in WT MEFs.**

(A) WT MEFs grown on 6 cm dishes were transiently transfected with GFP or GFP-SOCS3 plasmids. These plasmids were titrated to detect and optimise GFP or GFP-SOCS3 expression for upcoming confocal microscopy experiments. Whole cell lysates were resolved via SDS - PAGE and immunoblot analysis performed with anti-GFP and anti-GAPDH. The experiment was performed to N=1. (B) Densitometric intensity of GFP bands normalised to GAPDH were calculated. (C) Densitometric intensity of SOCS3-GFP bands normalised to GAPDH were calculated.

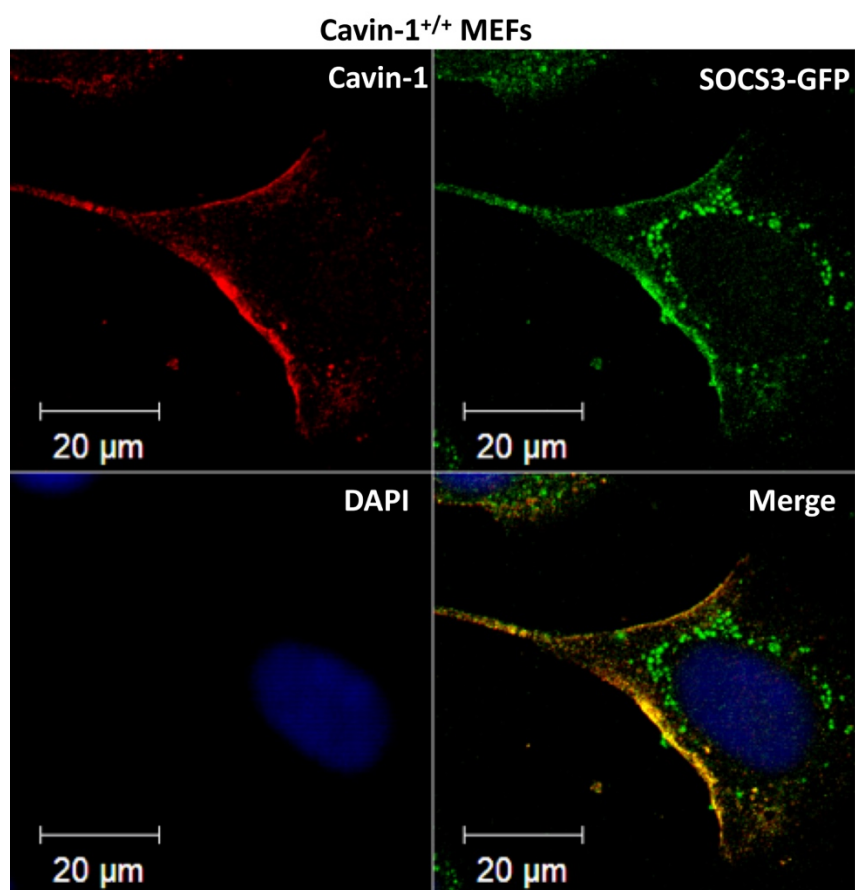
WT MEFs plated at low density on coverslips were transiently transfected with 2µg GFP or SOCS3-GFP and then prepared for immunofluorescence (section 2.2.2). Representative confocal microscopy images show (D) a cell expressing GFP fluorescence (green) and (E) a cell expressing SOCS3-GFP (green). *Scale bars: 10 µm.*

### 5.2.2.2 SOCS3 localisation to plasma membrane is cavin-1-dependent

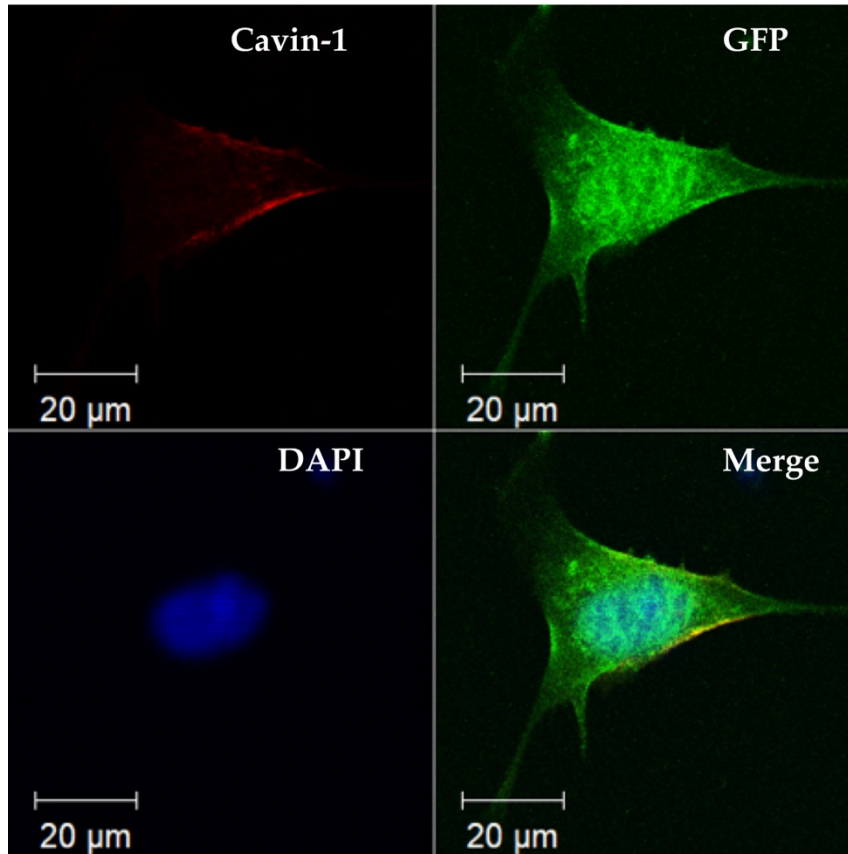
Confocal microscopy was utilised to assess the subcellular localisation of endogenous cavin-1 as well as GFP and SOCS3-GFP in transiently transfected cavin-1<sup>+/+</sup> and cavin-1<sup>-/-</sup> MEFs. In cavin-1<sup>+/+</sup> MEFs. Our data revealed that SOCS3-GFP was distributed in two subcellular pools, in the cytoplasm and in the plasma membrane (Figure 5–5A). Immunofluorescent staining with specific antibody for cavin-1 (Abcam ab48824) showed cavin-1 signal was predominantly localised at the rear or trailing edge of the cells as previously reported [430]. Interestingly, we observed co-localisation of cavin-1 and SOCS3-GFP exclusively at the plasma membrane and such co-localisation was found to be statistically significant on staining analysis by Pearson correlation coefficient ( $r^2 \geq 0.90$ ). In contrast, in cavin-1-deficient cells, SOCS3-GFP was localised in an intracellular pool but not at the plasma membrane (Figure 5–5C). Expression of GFP solely showed a similar distribution in both WT and cavin-1<sup>-/-</sup> MEFs while it was not co-localised with cavin-1 in WT cells (Figure 5–5D).

Subsequently, to obtain a confirmatory evidence linking distinct localisation of SOCS3 at the plasma membrane to cavin-1, rescue experiments were performed using cavin-1-mCherry. On an immunoblot, as shown in (Figure 5-6A), cavin-1 expression was restored in transiently transfected cavin-1<sup>-/-</sup> MEFs overexpressing cavin-1-mCherry cDNAs. In addition, confocal images of the transiently transfected cavin-1-deficient cells showed that the co-expression of cavin-1-mCherry and SOCS3-GFP was also restored at the plasma membrane (Figure 5-6B). Collectively, the results indicate that, in addition to the notable SOCS3/cavin-1 co-localisation, cavin-1 can be regarded a crucial determinant of SOCS3 localisation at the plasma membrane of intact cells.

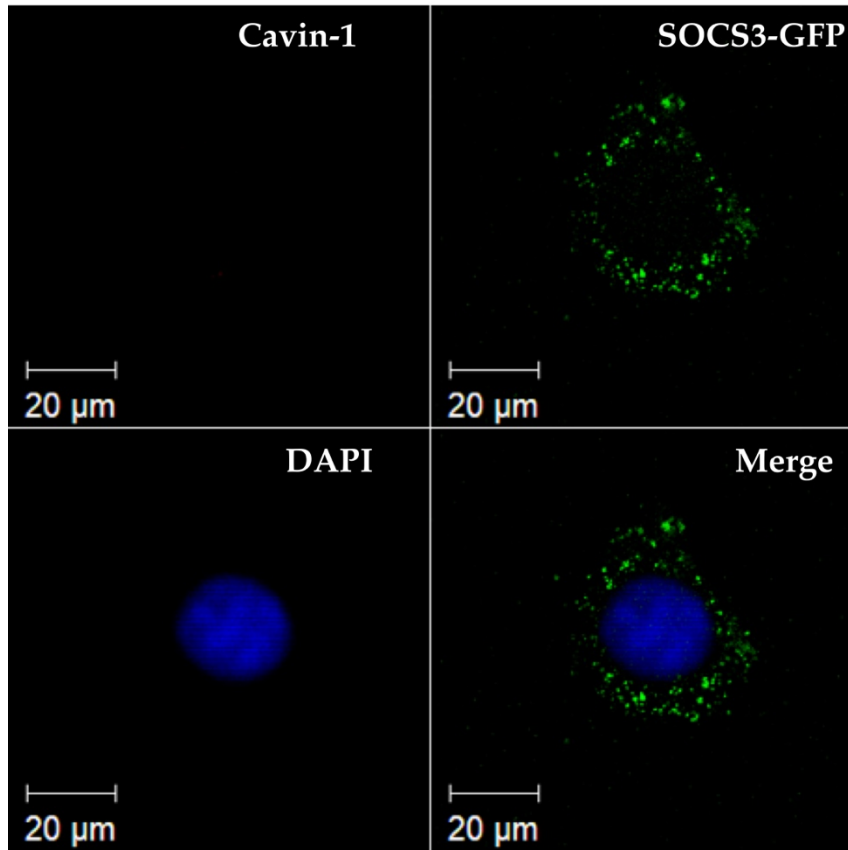
A



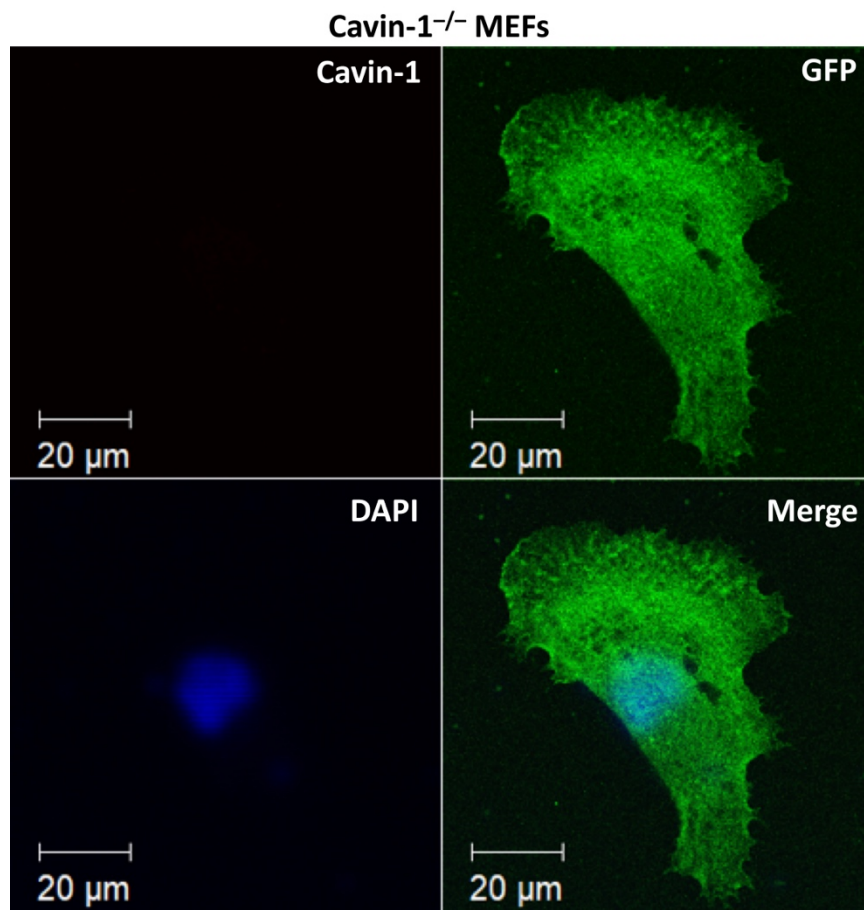
B

Cavin-1<sup>+/+</sup> MEFs

C

Cavin-1<sup>-/-</sup> MEFs

D



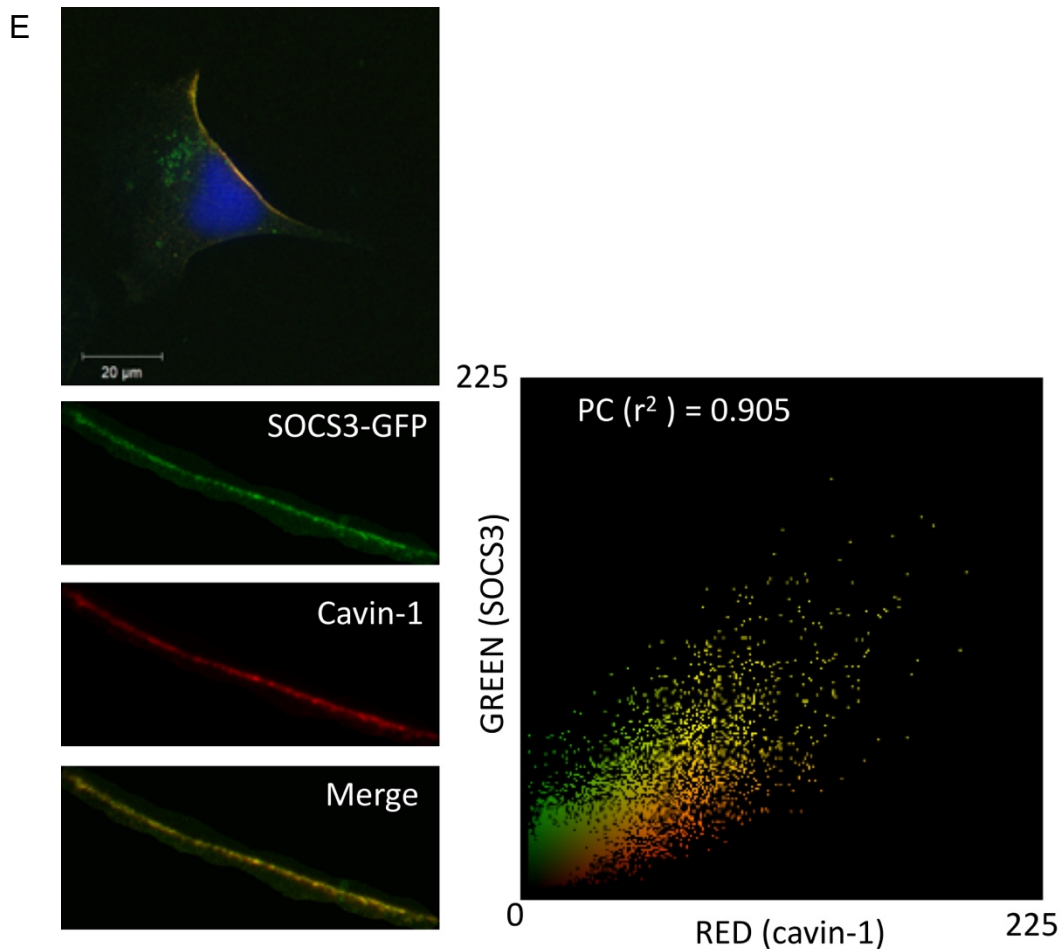
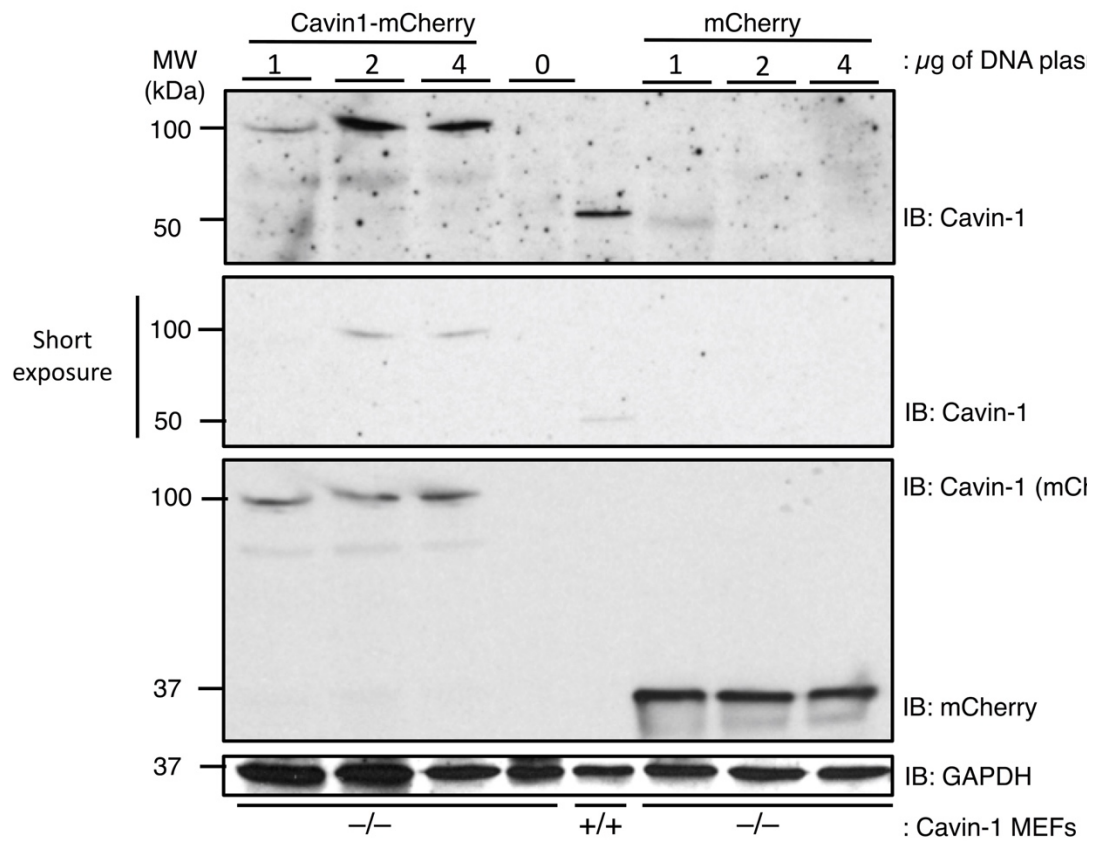


**Figure 5–5 Subcellular localisation of SOCS3-GFP and cavin-1 in WT and cavin-1-null MEFs.**

WT and *cavin-1*<sup>-/-</sup> MEFs differentiated on coverslips were transiently transfected with either SOCS3-GFP or GFP (2  $\mu$ g). One day post-transfection, cells were fixed with paraformaldehyde, permeabilised, and labelled with anti-cavin-1 antibody (red) as described in Methods (2.2.8). Confocal images showing WT MEFs expressing (A) SOCS3-GFP, (B) GFP (green). Confocal images showing *cavin-1*<sup>-/-</sup> MEFs expressing (C) SOCS3-GFP, (D) GFP (green). The nucleus has been stained with DAPI (blue). *Scale bar* = 10  $\mu$ m. (E) Pearson correlation coefficient ( $r^2$ ) were calculated from the intensity of expression of cavin-1/SOCS3-GFP at the plasma membrane in WT MEFs using Fiji/ImageJ software.

A



B

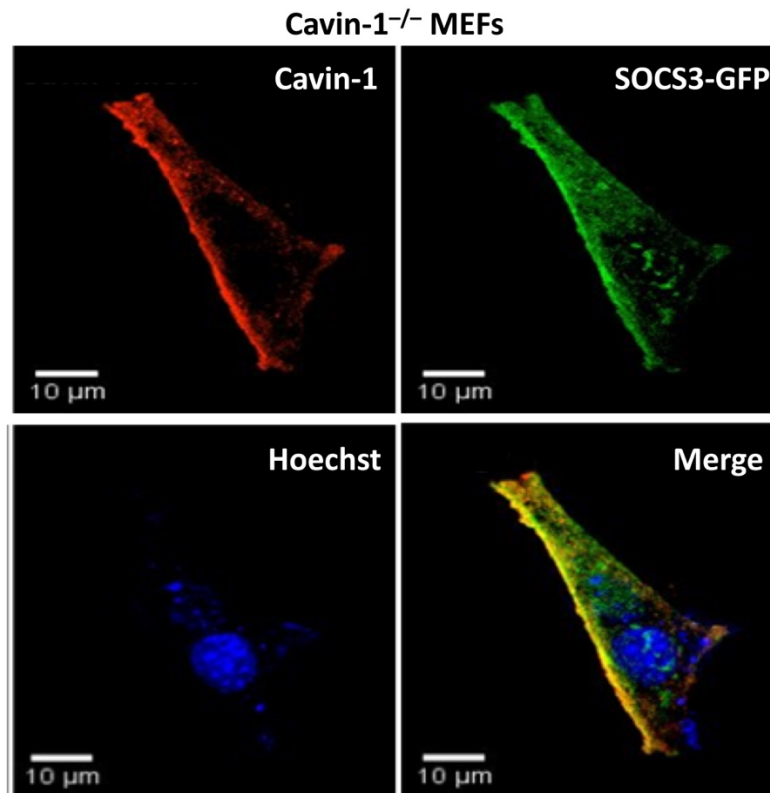


**Figure 5–6 Distribution of GFP in WT and *cavin-1*<sup>-/-</sup> MEFs.**

(A) Lysates from *cavin-1*<sup>-/-</sup> MEFs transiently transfected with mCherry or *cavin-1*-mCherry (amounts are indicated) were separated by SDS-PAGE and subjected to immunoblot analysis using anti-*cavin-1*, anti-mCherry and GAPDH antibodies. Experiment was performed to N=1. (B) *Cavin-1*<sup>-/-</sup> MEFs were transiently transfected with *cavin-1*-mCh for imaging by confocal microscopy. Data revealed colocalisation of SOCS3-GFP and *cavin-1*-mCh at the plasma membrane. *Scale bars* =10  $\mu$ m (Data presented in (B) were generated by Dr Jamie Williams, University of Glasgow).

### 5.2.3 Examining SOCS3 and cavin-1 in lipid rafts Isolated from WT and Cavin-1 KO MEFs

To further examine whether SOCS3 recruitment to membrane fractions is dependent on the presence of cavin-1, a previously-utilised protocol was employed in the present work [115, 431]. It relies on the separation of caveolae-containing fractions from bulk cellular proteins exploiting the low buoyant density and detergent resistance properties in of lipid rafts.

cavin-1<sup>+/+</sup> and cavin-1<sup>-/-</sup> MEFs were solubilised and centrifuged in 1% (v/v) Triton X-100 and a discontinuous sucrose gradient, respectively. Fsk was used to elevate SOCS3 levels in the cell lines. Results showed differences in the accumulation patterns of drug-resistant lipid rafts, including their marker flotillin-1, where such accumulation was more apparent at the interface of the 5 and 30% (w/v) sucrose layers than the 40% sucrose layer (Figure 5–7). In vehicle-treated WT cell lines, higher densities showed low levels of immunoreactive reactions of SOCS3 and non-raft fractions were low in unstimulated cells. In both raft and non-raft fractions, SOCS3 levels were increased with the addition of Fsk (Figure 5–7A). For cavin-1, its distribution included both non-raft and raft fractions of low density sucrose and positive for flotillin-1 and caveolin-1. Notable, such distribution patterns were not affected by Fsk treatment (Figure 5–7A). In cavin-1-deficient MEFs, Fsk treatment was also associated with increased SOCS3 accumulation yet, in contrast to WT cells, SOCS3 localisation was greater in higher density fractions and rarely observed in lipid rafts (Figure 5–7B).

Hence, these findings indicate SOCS3 accumulation in lipid rafts is mainly dependent on cavin-1 in agreement with the aforementioned confocal imaging results that revealed a remarkable SOCS3-GFP/cavin-1 co-localisation.

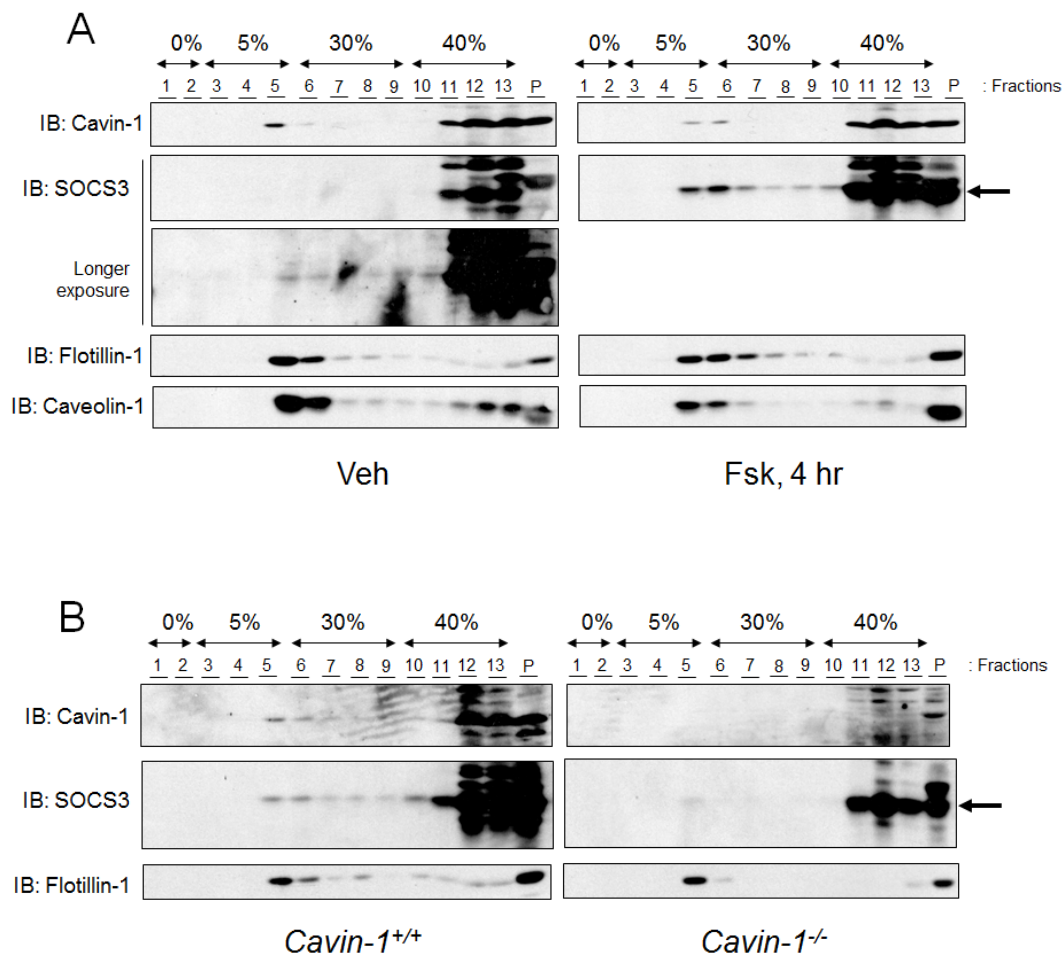


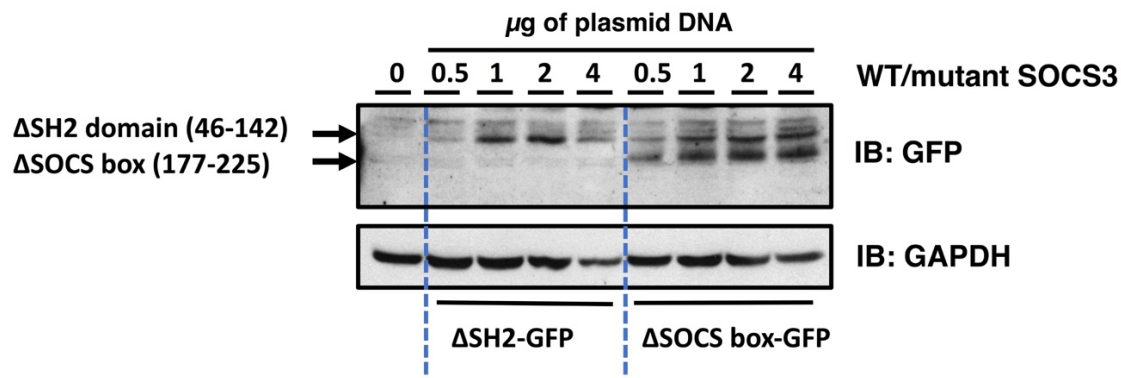
**Figure 5–7 Localisation and expression of SOCS3 and cavin-1 in lipid rafts.**

(A) Fsk (50  $\mu$ M) or vehicle (Veh) were added to WT MEFs for 4 hours followed by solubilisation in 1% (v/v) Triton X-100 for 30 mins and a subsequent centrifugation in a discontinuous gradient including the recommended (w/v) sucrose concentrations. SDS-PAGE was then used on equal fractions for immunoblotting with specific antibodies. P=pellet. (B) Fsk (50  $\mu$ M, for 4 hrs) was added to *cavin-1*<sup>+/+</sup> and *cavin-1*<sup>-/-</sup> MEFs followed by processing and analysis as described in (A). (Data generated by Dr Jamie Williams, University of Glasgow)

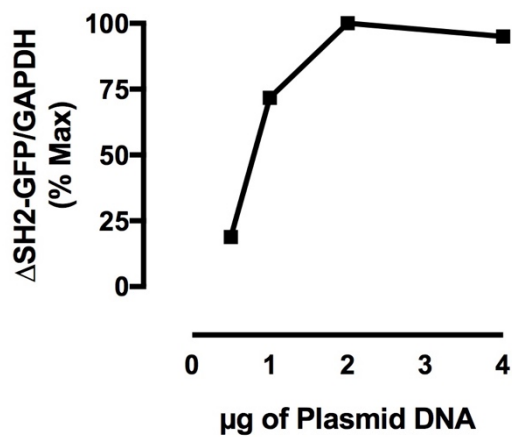
### 5.2.4 Characterisation the regions within SOCS3 that interact with cavin-1

As previously reported (Figure 5–5), the full-length SOCS3 proteins (residues 1-225) showed a significant interaction and co-localisation with cavin-1 at the plasma membrane. Subsequently, immunofluorescence imaging was used in this section to investigate the interactive regions in SOCS3 proteins with cavin-1, including SH2 residues (residues 46-142) and SOCS box domains (residues 177-225). As such, GFP-fused SOCS3 constructs, including  $\Delta$ SH2 domains ( $\Delta$ SH2) and  $\Delta$ SOCS box domains ( $\Delta$ SB), were utilised in this experiment. Either constructs were transiently transfected to WT MEFs and titrated with different amounts (0.5, 1, 2 and 4 $\mu$ g). Western blot analysis was used to quantify the expression of  $\Delta$ SH2-GFP or  $\Delta$ SB-GFP (Figure 5-8A). In transfected WT cells, fluorescent  $\Delta$ SH2-GFP and  $\Delta$ SB-GFP constructs were identified at the plasma membrane and intracellularly (Figure 5-8E). Furthermore, endogenous cavin-1 was detectable at the plasma membrane of the trailing edge. Merged images showed a remarkable co-localisation of SOCS3 $\Delta$ SH2-GFP and SOCS3 $\Delta$ SB-GFP constructs with endogenous cavin-1 particularly at the plasma membrane.

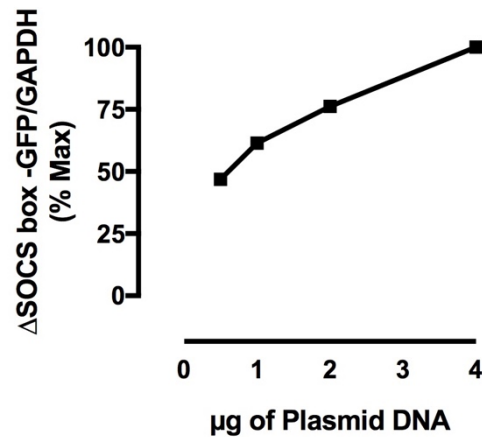
A



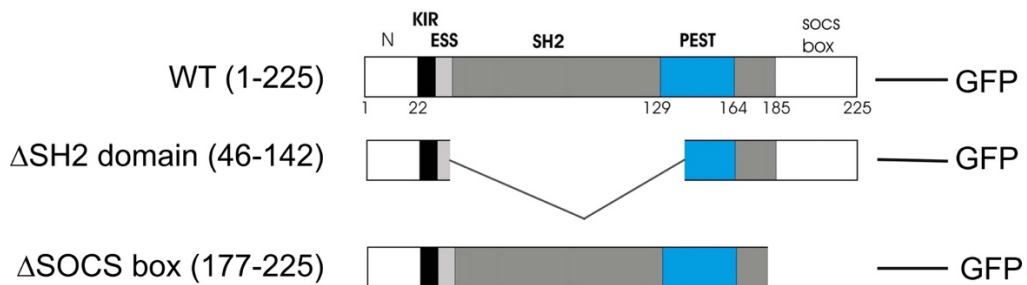
B



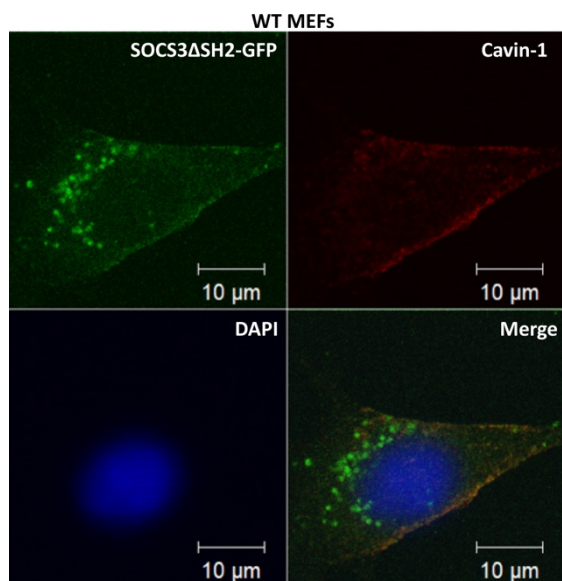
C



D



E



F

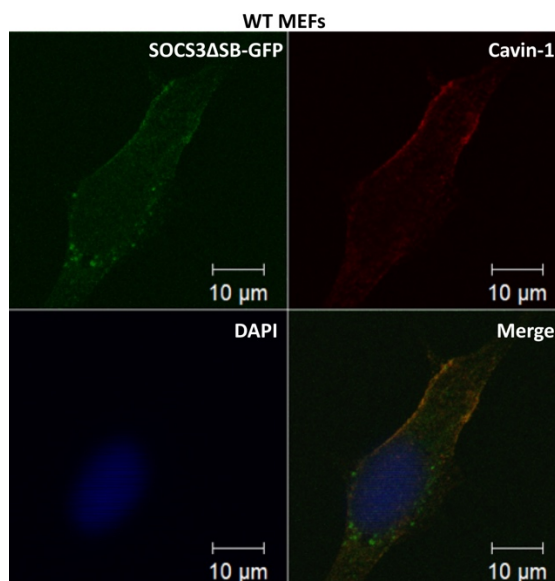


**Figure 5–8 Localisation of SOCS3 mutants in WT MEFs.**

(A) WT MEFs were transiently transfected with increasing amounts of SOCS3 $\Delta$ SH2-GFP or SOCS3 $\Delta$ SB-GFP cDNAs. Cell lysates were analysed for SOCS3 and GAPDH expression by SDS-PAGE and immunoblotting. Data shown were N=1. Densitometric intensity of bands normalised to GAPDH were calculated for (B) SOCS3 $\Delta$ SH2-GFP and (C) SOCS3 $\Delta$ SB-GFP. (D) A schematic diagram of SOCS3 $\Delta$ SH2-GFP and SOCS3 $\Delta$ SB-GFP constructs used in this experiment as well as full-length SOCS3-GFP. Different domains of SOCS3 were depicted, including a C-terminal SOCS box (white), SH2 domain (dark gray), extended SH2 subdomain (light gray), kinase inhibitory domain (black), small N-terminal domain (white). Residue 44-185 comprise the extended SH2 domain, which is interrupted by a 35 amino acid PEST motif (blue). Adapted with modifications from [311].

WT MEFs transiently transfected with either SOCS3 $\Delta$ SH2-GFP or SOCS3 $\Delta$ SB-GFP (2  $\mu$ g) were fixed with paraformaldehyde, permeabilised, and labelled with anti-cavin-1 antibody (red) as described in Methods (2.2.8). Confocal images showing WT MEFs expressing (E) SOCS3 $\Delta$ SH2-GFP, (F) SOCS3 $\Delta$ SB-GFP (green). The nucleus has been stained with DAPI (blue). *Scale bar* = 10  $\mu$ m.

### 5.3 Investigating roles for cavin-1 in regulating pro-inflammatory IL-6 signalling

As previously detailed (sections 1.3, 1.4), the JAK/STAT and MAPK pathways are activated by most cytokines, including IL-6. Such cytokine family causes STAT3 activation predominantly and, to a less extent, STAT1 [432]. The pathways that aim to negatively regulate the JAK/STAT pathway, such as SOCS proteins, phosphatases, and protein inhibitors of activated STAT (PIAS), can thus prevent chronic inflammation [432].

Several types of cells can secrete IL-6, including endothelial cells, keratocytes bone marrow cells, fibroblasts, and white blood cells [433]. This 22-28 kDa protein acts via a trans-signalling mechanism to regulate gp130 receptor-mediated signalling. IL-6 and IL-6R have a high affinity to bind to gp130 receptors via the IL-6R subunit. While gp130 is constantly expressed, IL-6R expression is limited to lymphocytes, hepatocytes, and leukocytes. Therefore, IL-R availability is crucial for IL-6 signalling. Shedding or alternate splicing could lead to the formation of soluble IL-6R (sIL-6R) and subsequently mediate inflammatory signalling pathways (Borish and Steinke [433]).

Confocal imaging revealed a direct interaction between SOCS3 and endogenous cavin-1 and their co-localisation at the plasma membrane (Figure 5–5), while in the absence of cavin-1, SOCS3 localisation was limited to the cytosol. Key Tyr residues are phosphorylated by cytokine-activated JAKs leading to the generation of a SOCS3 interaction motif and hence SOCS3 recruitment to activated cytokine receptors takes place [323].

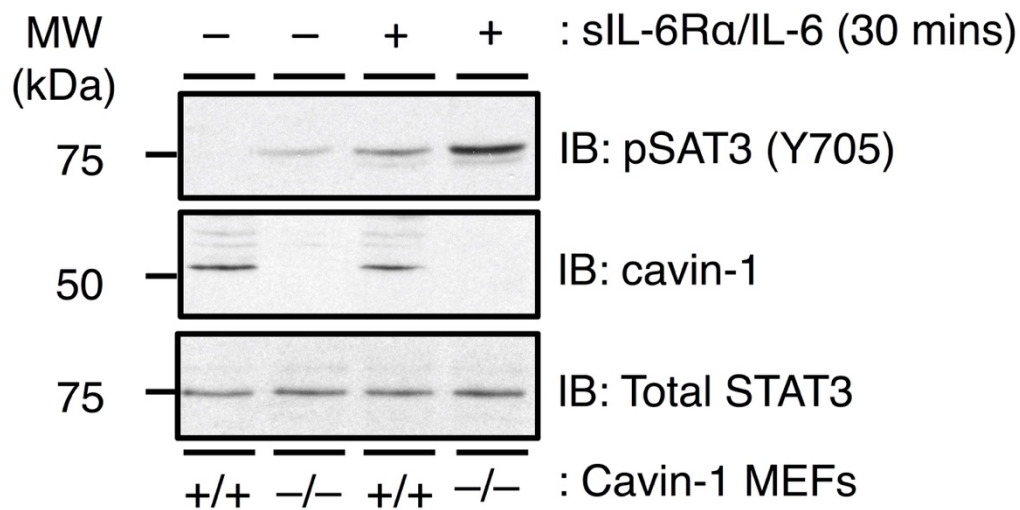
In the current experiment, the impact of cavin-1 deletion on STAT3 activation mediated by IL-6 was investigated in MEFs. This was performed by identifying Tyr705 phosphorylation which is crucial for the formation of transcriptionally-active STAT3-derived complexes [434].

sIL-6R $\alpha$  (25ng/ml), IL-6 (sIL-6R $\alpha$ /IL-6, 5ng/ml), or a vehicle (25ng/ml) were added to the confluent MEFs cultures for 30 minutes and then the western blot showed a strong variation STAT3 phosphorylation on Tyr705 between WT and

cavin-1<sup>-/-</sup> MEFs (Figure 5–9A). The densitometric analysis revealed a ~3-fold increase of IL-6-mediated STAT3 phosphorylation on Tyr705 in cavin-1-deficient cells as compared to WT MEFs (Figure 5–9B).

So as to ascertain the typical role of cavin-1 in reducing such IL-6-mediated phosphorylation, cavin-1<sup>-/-</sup> cell lines that constitutively expressed GFP or cavin-1-GFP were established by growing these MEFs in 6 cm dishes followed by transfection with a GFP plasmid or a cavin-1 plasmid tagged with GFP and then selected in G418. Microscopic techniques were used to visualise positive clones while isolation was performed by limiting dilution. Western blot was used to analyse the expression of cavin-1-GFP and GFP in cavin-1<sup>-/-</sup> MEFs (Figure 5–10). The immunoblot showed that cavin-1 expression was restored in cavin-1<sup>-/-</sup> MEFs constitutively expressing cavin-1-GFP. This cell line was successfully generated which could be utilised for functional investigation of the novel roles for cavin-1-SOCS3 interaction in regulating pro-inflammatory IL-6 signalling. To do this, WT and cavin-1<sup>-/-</sup> MEFs stably expressing GFP and cavin-1-GFP were treated with sIL-6R $\alpha$ /IL-6 trans-signalling complex. Results showed that STAT3 phosphorylation on Tyr705 was significantly enhanced in cavin-1<sup>-/-</sup> MEFs expressing GFP (\*\**p* < 0.001). Interestingly, this response was significantly reduced by rescuing cavin-1 expression in cavin-1<sup>-/-</sup> MEFs (\*\**p* < 0.001) although it was not to the same level of WT (cavin-1<sup>+/+</sup>) MEFs (Figure 5-11).

A



B

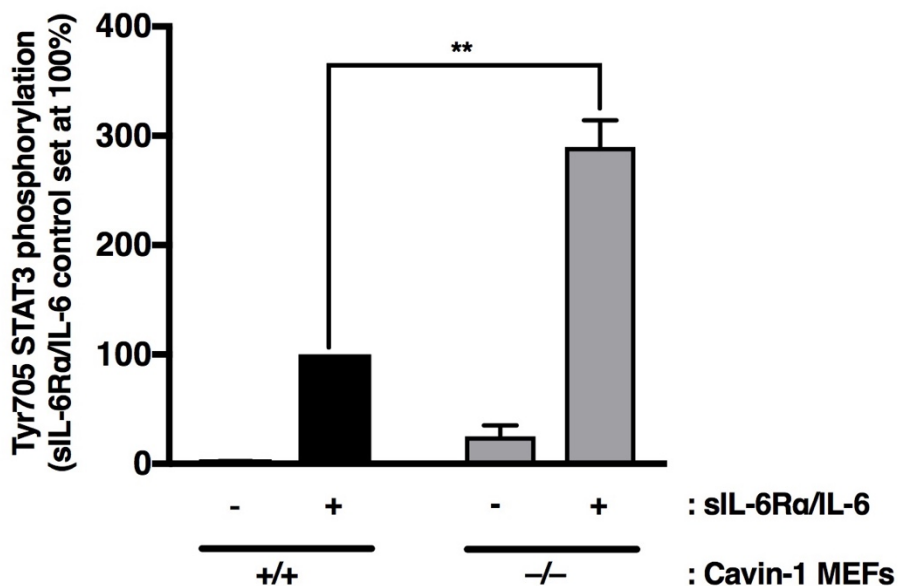
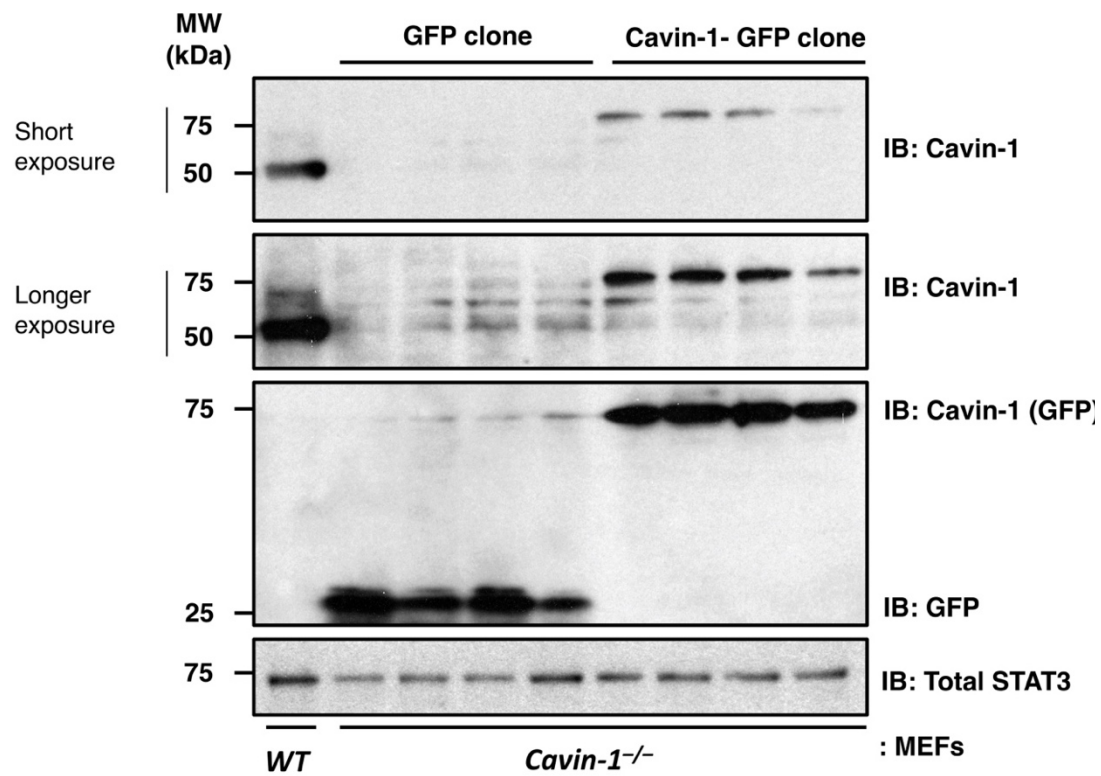


**Figure 5–9 Cavin-1 deletion enhances Tyr705 STAT3 phosphorylation.**

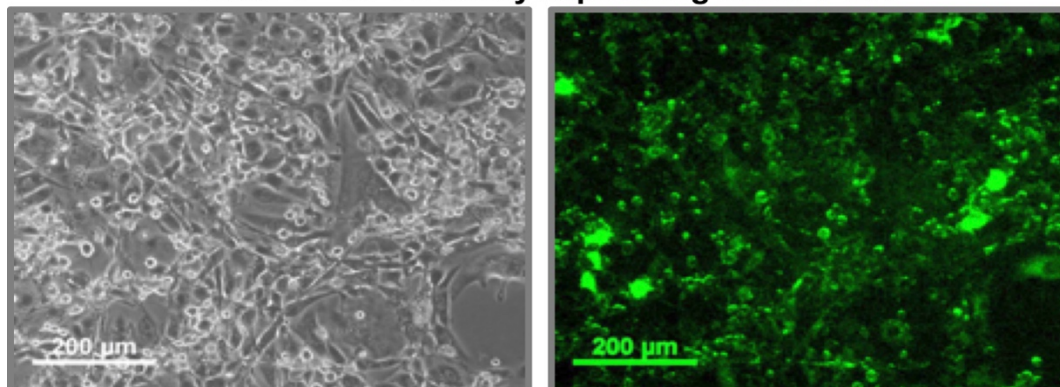
WT (cavin-1<sup>+/+</sup>) and cavin-1<sup>-/-</sup> MEFs grown on 6 well plates were incubated with sIL-6R $\alpha$ /IL-6 (25 ng/ml, 5 ng/ml) for 30 min. Protein-equalized cell lysates were then analysed by SDS-PAGE and immunoblotting with the indicated antibodies. Densitometric analysis for Tyr705 phospho-STAT3 normalized to respective total levels is presented as mean  $\pm$ SEM for n=3 independent experiments. \*\*P < 0.01

A



B

### *Cavin-1*<sup>-/-</sup> MEFs stably expressing cavin-1-GFP



C

### *Cavin-1*<sup>-/-</sup> MEFs stably expressing GFP

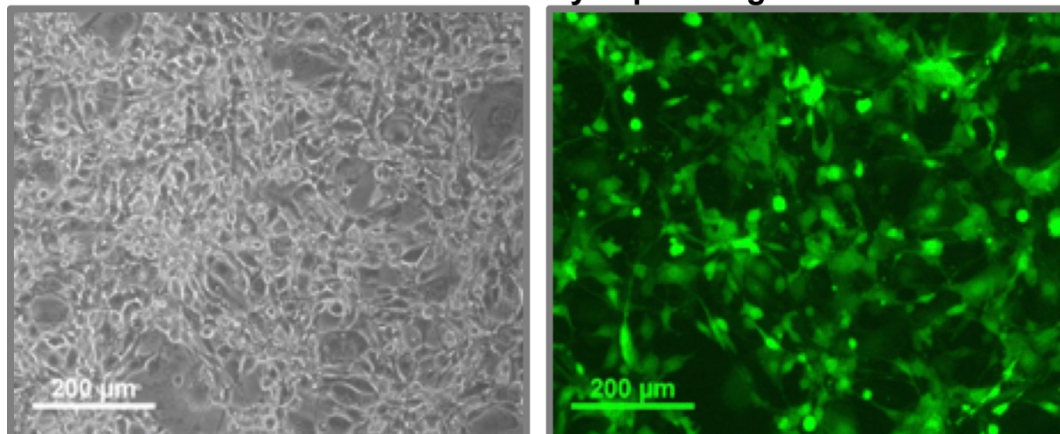


**Figure 5–10 Cavin-1<sup>-/-</sup> MEFs stably expression GFP and cavin-1-GFP.**

Cavin-1<sup>-/-</sup> MEFs seeded in 6 cm dishes were transfected with 4µg of either a cavin-1-GFP construct or a GFP control construct using PolyFect transfection reagent (Qiagen) as per manufacturer's instructions. Following dilution and re-plating, cells stably expressing the constructs were selected by supplementing growth media with 0.5 mg/ml G418. (A) Detergent-soluble whole cell lysates from WT MEFs and cavin-1<sup>-/-</sup> MEF clones stably expressing GFP or cavin-1-GFP were separated by SDS-PAGE and subjected to immunoblot analysis with the indicated antibodies. N=3. Representative images showing WT MEFs stably expressing (B) cavin-1-GFP or (C) GFP. Images on the left shows phase contrast of the same field. *Scale bar* = 200 µm.

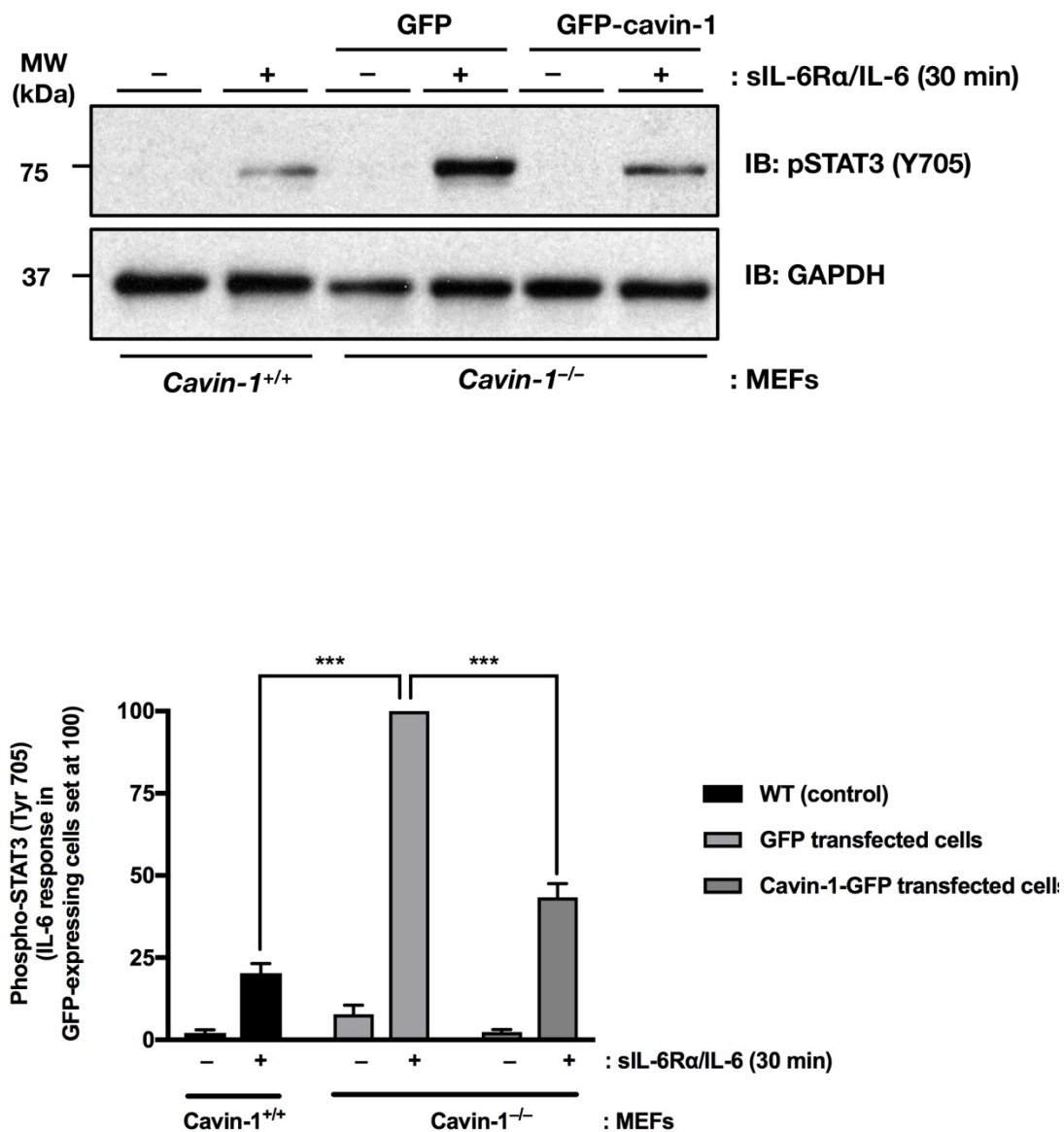


**Figure 5–11 Tyr705 phosphorylation of STAT3 is limited by cavin-1**

WT (cavin-1<sup>+/+</sup>) and cavin-1<sup>-/-</sup> MEFs stably expressing GFP or cavin-1-GFP were treated with sIL-6Rα/IL-6 (25 ng/ml, 5 ng/ml) for 30 min. Protein-equalized cell lysates were then fractionated by SDS-PAGE prior to immunoblotting with the indicated antibodies. Densitometric analysis for Tyr705 phospho-STAT3 normalized to a loading control (GAPDH). The mean data with SEM error bars were plotted and statistical significance tested using a Student's t-test (2-tailed, un-paired) (GraphPadPrism, \*\*\* p < 0.001). N=3.

## 5.4 Discussion

SOCS3 has been well-recognised for its great relevance in suppressing downstream signalling mediated by cytokine receptors that employ the leptin receptor ObRb, the G-CSFR, and more importantly gp130 receptors [356]. However, the interaction of SOCS3 with other proteins within the cell might alter such inhibitory effect yet the relevant knowledge is scarce. The target proteins of SOCS3 for ubiquitination have been recently investigated in a study relying on a global proteomics approach [356]. Intriguingly, SOCS3 has been found to interact with cavin-1 and regulate its ubiquitination. In this chapter, the functional outcome of SOCS3-cavin-1 interaction was evaluated. In line with the significant role of direct and indirect immunofluorescence approaches in characterising protein-protein interactions, the microscopy techniques were utilised to define the mode of SOCS3/cavin-1 interaction. This chapter identified novel roles for SOCS3 in caveolae integrity as well as for cavin-1 in SOCS3 recruitment to the plasma membrane. Additionally, a novel mechanism relying on SOCS3/cavin-1 interaction has been demonstrated to have a significant modulatory effect on IL-6-mediated proinflammatory signalling. Together, these data highlighted numerous important aspects of interaction between SOCS3 and cavin-1 responsible for reciprocal regulation of their respective functions.

The results in this chapter, as visualized by TEM, revealed that caveolae abundance has been significantly reduced in SOCS3-null MEFs and endothelial AS-M.5 as compared to WT cells. As such, a novel mechanism of SOCS3 regulation has been identified in which SOCS3 can exert a regulatory role on cavin-1 function and stability and consequently maintain CAV-1 expression and caveolae. These findings were further confirmed by imaging and biochemical approaches. A similar caveolae-stabilising effect has been previously demonstrated by the Eps15 homology domain-containing protein 2 (EHD2) [168], which is known to function at the caveolar neck and being integrated in caveolae dynamics [419].

Additionally, the present chapter showed that SOCS3/cavin-1 binding is directly exhibited and this plays a role in the efficient recruitment of SOCS3 to the

plasma membrane. In agreement with another study [430], results showed that cavin-1 localisation in the plasma membrane in WT MEFs was not uniformly-distributed but rather cavin-1 is localised to the trailing edge of migrating cells and, notably, the same compartment of the plasma membrane was co-localised by a significant number of SOCS3-GFP. On the other hand, in the absence of cavin-1, confocal imaging showed that the distribution of SOCS3-GFP was chiefly intracellular while it was not detected in the plasma membrane. Nonetheless, SOCS3-GFP localisation at the plasma membrane was regained after transfection of cavin-1-deficient MEFs with cavin-1-mCherry and, again, both SOCS3-GFP and cavin-1-mCherry were co-localised consistently. Furthermore, given that cavin-1 localisation was essentially detected in membrane and cytoplasmic fractions as revealed by subcellular fractionation experiments [356], it is plausible that SOCS3 followed the same pattern of localisation in WT MEFs following induction by Fsk treatment for 5 h. Intriguingly, in the absence of cavin-1, SOCS3 distributed chiefly to the cytoplasm, indicating the importance of cavin-1 for the efficient localisation of endogenous SOCS3 to the membrane fraction. Moreover, SOCS3 deletion yielded a significant reduction of CAV-1 expression at the plasma membrane as shown by subcellular fractionation experiments. Indeed, the latter observation implies an indirect cavin-1-mediated role of SOCS3 in maintaining the expression of CAV-1. Such CAV-1 changes mediated by SOCS3 or cavin-1 deletion were exclusive since flotillin levels were not affected by their deletion. Collectively, these data showed an intact co-localisation of cavin-1 and SOCS3 at the plasma membrane, while cavin-1 is an important determinant of SOCS3 at this site.

SOCS3 contains a central SH2 domain flanked by a distinct N-terminal region and a C-terminal SOCS box. The SOCS box is a 40-residue-region that is involved in the degradation of target proteins [313]. The ability of the SOCS box region to bind elongin B and C (adaptor proteins) would subsequently lead to the formation of a ligase complex that involve Cul5 and Rbx2 and mediate the process of substrate ubiquitylation via the SH2 domain of SOCS3. Interestingly, SOCS3 could be associated with multiple membrane-bound receptors via the

SH2 domain and might have role in the regulation of their downstream signalling pathways [315] (detailed in section 1.4).

In order to reveal the distinct regions in SOCS3 proteins that could be crucial for their interaction with cavin-1, a number of N- and C-terminal truncation mutants of SOCS3 has been investigated to get an insight into the important residues that have the ability to coimmunoprecipitate GFP-cavin-1 [356]. Importantly, all tested mutants showed a similar pattern of GFP-cavin-1 coimmunoprecipitation to that of the full-length SOCS3 in WT cells. This indicates that SOCS3/cavin-1 binding is mediated by a specific region within the SH2 domain in these mutants. For further confirmation, confocal microscopy was used to investigate the important regions in SOCS3 proteins which are necessary for cavin-1/SOCS3 interaction. Results showed that the GFP-SOCS3 $\Delta$ SH2 and GFP-SOCS3  $\Delta$ SB mutants were localised within the cytoplasm and plasma membrane with a similar pattern of distribution to that of full-length SOCS3.

It has been found that the SH2 domain of SOCS3 formed a complex with cavin-1 at a non-pTyr location [356]. Structurally, residues 46-127 and residues 128-142 comprise the main components of the SH2 domain of SOCS3 [311]. The PTyr-binding pocket located in all SH2 domains is formed partly of the  $\beta$ -sheet and  $\alpha$ -helical regions within residues 46-127. On the other hand, residues 128–142 comprise a part of an unstructured PEST motif which links the helix B of the SH2 domain with residues 166-185 (forming the BG loop and  $\beta$ G strand motifs) [311]. PEST motifs are involved in multiple functions, including protein turnover and protein-protein interactions [311]. To investigate the role of the PEST insert of the SOCS3 SH2 domain in cavin-1 interaction, coimmunoprecipitation experiments in transfected HEK293 cells using SOCS3  $\Delta$ PEST mutants have been conducted, where (Gly-Ser) $\times$ 4 peptides were used to replace the PEST motif (Pro129-Arg163). No coimmunoprecipitation could be observed, indicating a loss of the ability of SOCS3  $\Delta$ PEST to bind cavin-1 [356]. Furthermore, in contrast to early overexpression experiments that tested the effect of the PEST sequence on SOCS3 functionality [311], the recent functional experiments which investigated endogenous SOCS3 signalling

revealed that the PEST motif of SOCS3 has an important role in cavin-1 interaction via mediating a regulatory role on the JAK-STAT signalling pathway [356].

Much data in the scientific literature demonstrate a fundamental involvement of caveolae in concentrating various signalling components, such as Ras, Src family kinases,  $\beta$ -arrestins, GPCRs, G proteins and downstream enzymes such as adenylyl cyclases (ACs) and eNOS, NOS3 [435]. Hence, caveolae are regarded as platforms that coordinate signalling transduction by compartmentalising receptors and their downstream effectors. This concept has been extensively validated in early experiments, in which the disruption of such domains via treatment of the plasma membrane with sphingomyelinases or changing membrane cholesterol levels could eventually lead to either enhancing or reducing distinct signalling events, including phospholipase D (PLD) activity and ERK activation, respectively [436].

Experiments relying on biochemical fractionation of cell extracts revealed that gp130 and JAK2 (specific JAK-STAT signalling components) were localised to lipid rafts. Nonetheless, the functional consequences seem to be dependent on the context given the varied effects of raft disruption (either inhibitory or activating) via treatment with  $\beta$ -cyclodextrin (a cholesterol-depleting agent) or homozygous deletion of caveolin-1 [356]. Other reports have exclusively tested the significance of caveolae for gp130 function, showing the ability of a large proportion of gp130 molecules, which are located in detergent-resistant lipid rafts, to coimmunoprecipitate with CAV-1 [437]. Additionally, gp130 could be redistributed to non-raft fraction on treatment with the cholesterol depleting agent  $\beta$ -cyclodextrin and this would also preclude STAT3 Tyr705 phosphorylation by IL-6 [437]. Conversely, other reports have shown that both STAT3 and gp130 are localised to lipid rafts [252] and that both CAV-1 expression and STAT3 activation are negatively correlated [438]. Hence, although membrane microdomains and the components of JAK-STAT signalling are weakly associated, the exact molecular mechanisms that drive such interaction still unclear.

The current study emphasises the significant role of cavin-1 in the SOCS3-mediated inhibition of JAK-STAT signalling via direct binding to specific cytokine receptors, such as gp130 causing their inhibition. Additionally, loss of cavin-1 altered the inhibitory pathways that suppress Tyr phosphorylation of STAT3 mediated by IL-6. The effect of cavin-1 deletion on the inhibitory role of cAMP, which has been shown to be dependent on SOCS3, was investigated in a recent report [356]. The authors found that treatment of WT MEFs with Fsk (a cAMP-elevating drug) led to a significant inhibition of IL-6-mediated STAT3 Tyr705 phosphorylation. Moreover, cavin-1-deficient cells exhibited loss of such effect despite the production of equivalent SOCS3 levels in both cell lines by the effect of a combination of Fsk and IL-6. Therefore, it can be concluded that cavin-1 was indispensable for SOCS3-mediated inhibition of IL-6 signalling by cAMP.

From another perspective, experimental studies in mice shown that CAV-1 knockout resulted in a marked increase of the inflammatory cytokine (TNF- $\alpha$ , IL-6 and IL-12a) levels, elevation of superoxide dismutase in the lung, kidney, and liver, and a significant reduction of the phagocytic activity of macrophages [439]. In the same study, STAT3 was significantly activated. Importantly, despite the marked increase of SOCS3, which inversely correlates with STAT3, both STAT3 activation and its associated inflammatory response were not well-controlled. Therefore, data in the present chapter provide an important explanatory evidence of the reasons of compromised SOCS3-mediated negative regulation on the inflammatory response in CAV-1 KO mice. Given the previously-demonstrated relevance of CAV-1 to mediating cavin-1 recruitment to the plasma membrane [102, 121], the present chapter showed a novel important mechanism by which SOCS3-mediated suppression of cytokine signalling is linked to plasma membrane localisation through the interaction with and stabilisation of cavin-1.

## 6. Final Discussion

The pathophysiological outcomes of dysregulated gp130-mediated signalling on haematopoiesis, cell metabolism, inflammation and immune responses have been widely documented [440-442]. Thus, limiting the magnitude and duration of IL-6-dependent gp130/JAK/STAT signalling remains of paramount importance. In this regard, different mechanisms of negative regulation have evolved to restrict gp130-dependent intracellular signalling. Notably, SOCS3 plays a prominent negative regulatory role by inhibiting JAK–STAT3 activation and targeting cytokine receptor complexes for proteasomal degradation via SOCS3 E3 ligase activity [443].

To date, several substrates, such as CD33, FAK1, Siglec7, IRS1/2, G-CSFR and JAK1, of the SOCS3 E3 ubiquitin ligase were identified (Section 1.4.5). Yet, the full spectrum of ubiquitin-regulated SOCS3 substrates remains unknown. Utilising an unbiased quantitative proteomics screen to identify SOCS3-regulated proteins, Williams et al, 2018 revealed a novel and direct interaction between SOCS3 and the essential component of caveolae cavin-1 [356]. Consequently, we hypothesised that SOCS3-cavin-1 interaction is an important controlling element in caveolae stability and/or the pro-inflammatory signalling pathway mediated by IL-6 in the endothelial cells. In this study, one of the aims was to establish endothelial cell lines lacking SOCS3 expression via the CRISPR/Cas9 system. This system enabled us to investigate the effects of SOCS3 deletion on endogenous cavin-1 levels. The findings from this study demonstrated that the absence of SOCS3 increases cavin-1 turnover and significantly reduces both cellular levels of CAV-1 and cell surface caveolae in MEFs and endothelial AS-M.5 cells. Consequently, via cavin-1 stabilisation, this study revealed a novel role for SOCS3 in regulating the assembly of caveolae. Additionally, results obtained using confocal microscopy highlighted the important role of cavin-1 in the recruitment of SOCS3 to the plasma membrane. Collectively, our data would uncover a novel mechanism by which the essential component of caveolae cavin-1 negatively regulates gp130-mediated signalling through recruiting SOCS3 (Figure 6-1).

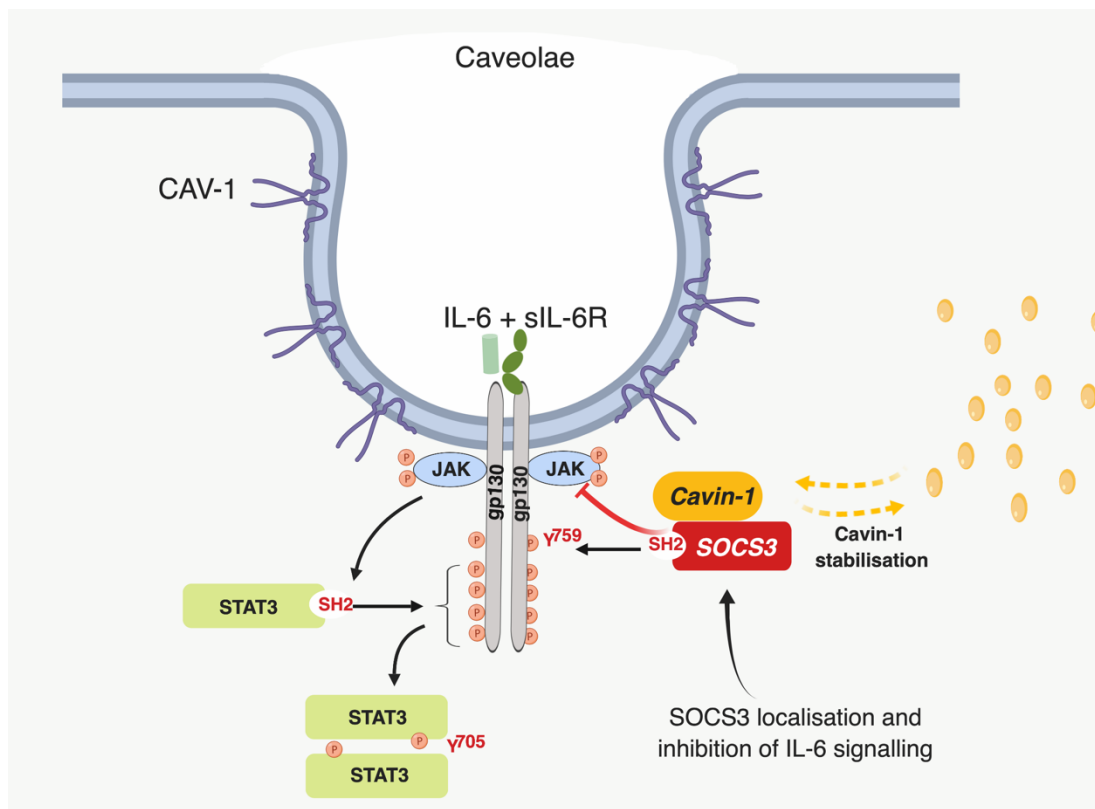


**Figure 6–1 The proposed interaction between cavin-1 and SOCS3 to inhibit cytokine signalling.**

The complex of IL-6 and soluble IL-6 receptor (sIL-6R) can bind to gp130 on endothelial cells, which subsequently induces pro-inflammatory cytokine trans-signalling. The signal is transmitted from the extracellular space into the cytoplasm. The gp130-associated JAKs are then activated, leading to phosphorylation of tyrosine motifs within the cytoplasmic domains of gp130, which recruit STAT3. Consequently, STAT proteins are phosphorylated, dimerised, and translocated to the nucleus. This would eventually induce the expression of proinflammatory and prosurvival genes. Additionally, SOCS3 expression is induced as a negative feedback loop to suppress the signalling pathway. Intriguingly, SOCS3 is integrated as an essential component of the E3 ubiquitin ligase complex, which ubiquitinate JAK. Ultimately, the signalling cascade is terminated by proteasomal degradation [307]. The findings of the present thesis proposed a model of a direct SOCS3-cavin-1 interaction, which contributes to effective SOCS3 recruitment to the plasma membrane and its efficient binding to cytokine receptors, such as gp130 causing their inhibition. Reproduced with modifications from Williams et al 2018 [356].

## 6.1 Therapeutic possibilities

### 6.1.1 Modulation of caveolae

Body-fat distribution is a known risk factor for unfavourable cardiovascular consequences [444]. Studies have shown that the lack of cavin-1 expression in animal models led to loss of caveolae and the development of a lipodystrophic phenotype, which is characterised by glucose intolerance, hyperlipidaemia, and overall adiposity. Although the hyperlipidaemic phenotype was apparent in both cavin-1-null and CAV-1-null animals, the onset of dyslipidaemia was earlier and its severity was more pronounced in cavin-1-deficient models as they showed a complete absence of caveolae arguably in all tissues, including cardiac and skeletal muscles [445].

In human, alterations in cavin-1 protein, which result from distinct frameshift mutations within the exon 2 of the expressing gene, have been identified and were associated with muscular dystrophy, insulin resistance, and general lipodystrophy [44, 127, 130]. In these patients, all caveolin subtypes were downregulated in skeletal muscles, while surface caveolae were lacking in skeletal muscles [127] and patient-derived fibroblasts [44]. Since the interaction of cavin-1 and SOCS3 requires multiple functional regions on cavin-1 for optimal binding [356], it would be expected that patients with congenital generalised lipodystrophy, and subsequently cavin-1 mutations, would have impaired SOCS3-cavin-1 interactions and hence exaggerated IL-6 responses. In this context, cardiac-specific SOCS3 knockout in murine models has been associated with contractile dysfunctions along with ventricular arrhythmias [389]. Intriguingly, patients with dysfunctional cavin-1 proteins exhibit a wide variety of ventricular arrhythmias. Therefore, future investigations are needed to reveal the mechanism by which SOCS3 and/or cavin-1 mutations could contribute to specific defective regulatory pathways and hence to the incidence of these pathologies [356].

Furthermore, atherosclerosis is basically a condition that involves large conduit arteries and is instigated by a number of chemical, immunological, or mechanical risk factors which lead to endothelial activation [446]. Patients with

atherosclerosis usually experience a chronic damage to the endothelial lining associated with proliferation of smooth muscles in the vessel wall as well as lipid deposits formation [447]. Despite the major progress accomplished in understanding the pathogenesis of atherosclerosis and its relation to cardiovascular disease, the exact process by which an atherosclerotic plaque is initiated and developed remains relatively unclear [448]. For such a purpose, the associated risk factors have been investigated, revealing that patients with smoking, diabetes, obesity, hypertension, and increased plasma lipids are more likely to develop atherosclerosis [449]. Interestingly, the pathogenic changes during plaque formation are regulated by caveolae as evidenced from studies based on genetically-modified mice. For instance, when CAV-1<sup>-/-</sup> mice were cross bred with apoE<sup>-/-</sup> mice, loss of CAV-1 was associated with a significant downregulation of specific proatherogenic molecules and hence yielded a protective role against atherosclerosis [450]. The authors attributed the reduction in plaque formation to the significant reduction of oxidised lipids transcytosis, which is originally mediated by caveolae. Later on, these results were confirmed by Sessa's group, where a specific endothelial re-expression model of CAV-1/caveolae was developed relying on the re-establishment of atherosclerotic lesions, validating the relevance of caveolae in atherosclerosis [451]. In a follow-up study, the authors evaluated CAV-1 overexpression in endothelial cells in transgenic mice and they found a profound atherosclerotic formation and progression, supporting the role of CAV-1 in the regulation of atheroma development [452].

Based on these findings, it would be expected that the reduction of caveolae abundance would be of clinical potential. However, there is a remarkable challenging cut-off, where the plaque-limiting levels of caveolae should, on the other hand, maintain the normal physiologic functions of the endothelium. Importantly, reduction the levels of caveolae for therapeutic purposes might be considered based on the following observations. First, it has been shown previously that a 40–50% reduction of CAV-1 expression could be performed using HMG-CoA reductase inhibitors in endothelial cells [453], which signifies an additional atheroprotective role of statins rather than the well-established lipid-lowering actions. Second, it seems that caveolae position within the

endothelium and its relation to the prevailing hemodynamic patterns could be impactful. That is, exercise training in individuals with a high risk of atherosclerosis development would change flow profiles, alter caveolae levels, and ultimately lower the atherogenic liability in endothelial cells [446]. Therefore, several atherosclerosis-ameliorating approaches could be further uncovered and targeted accordingly. In this respect, novel drugs could be developed to target the newly-identified SOCS3-cavin-1 interaction to reduce the risk of cardiovascular disease in patients at risk as well as to maintain the vascular health in specific populations, such as diabetic patients. The current era of small-molecule immunomodulators provides promising targets for drug development in the future. Besides, targeted disruption of the cavin-1/SOCS3 complex would not only refine our therapeutics, particularly with improved understanding of inflammation, but also would help discovering novel drugs.

### **6.1.2 Regulation of JAK–STAT signalling pathway**

Aberrant catalytic activities of JAK proteins can lead to either an increase or reduction of kinase activity and subsequently the development of hematological defects, inflammatory diseases, immunodeficiencies, autoimmune diseases, myeloproliferative disorders and increased susceptibility to infection. Therefore, in light of the plethora of studies concerning JAK-STAT signalling and its relevance to health and disease, it is expected that this pathway could be a promising drug target. Multiple mechanisms have been implicated in JAK dysregulation, such as somatic or inherited point mutations, gene translocations, receptor mutations, and changes in the activity of SOCS proteins or phosphatases, which are considered important JAK regulators [454].

Multiple exon12 mutations in the JAK2 genes have been identified in patients with V617F-negative idiopathic erythrocytosis (IE) or polycythaemia vera (PV) [455]. The most prominent findings in these patients are low serum erythropoietin (EPO) levels, erythrocytosis and ligand-independent cell growth. In addition, the amino acids 542–543 (N542-E543del) of JAK2 are predominantly deleted. In the instance of JAK2V617F positivity, SOCS3-

mediated downregulation of EPO signalling and proliferation of V617F-expressing cells are not established.

Furthermore, Suessmuth et al. (2009) reported a PV patient with a SOCS3<sup>F136L</sup> mutation (within the SH2 domain) and an additional heterozygous mutation in JAK2<sup>N542-E543del</sup>. In such a patient, EPO-induced proliferation was markedly elevated by SOCS3<sup>F136L</sup>-expressing cells, leading to a persistent phosphorylation of JAK2 mediated by EPO. Indeed, these results indicate that SOCS3 function is disrupted by the SOCS3<sup>F136L</sup> mutation, which has a robust clinical potential in PV [455]. Given that F136 is located within the cavin-1-interacting domain, the PEST insert [356], such a mutation might change the patterns of SOCS3-cavin-1 interaction and subsequently alter SOCS3-mediated inhibition of JAK-STAT signalling. As such, future studies are warranted to investigate the way by which SOCS3 and/or cavin-1 mutations can affect or dysregulate signalling pathways to trigger diseases.

Moreover, SOCS3 inhibits JAK kinase activity by preventing both substrate and ATP binding and hence preclude IL-6-induced JAK/STAT activation [456]. The clinical potential of SOCS3 is increasingly appreciated given its induction by a number of routes as well as its direct involvement in cancer, diabetes, inflammation and both viral and bacterial infections [457]. In addition, it has been shown that the *in vivo* regulatory role of SOCS3 proteins is exerted on distinct subsets of cytokines, such as IL-6, IL-11, LIF and CNTF, as well as leptin, G-CSF, and IL-12 as revealed by the recently developed conditional deletion models and biochemical analyses methodologies (Fig. 6-2). Such selectivity is potentially attributable to the high affinity of SOCS3 for its receptors, including gp130, leptinR, IL-12R $\beta$ , and G-CSFR [324]. Although several cytokines, including EPO, GM-CSF, or thrombopoietin (TPO) are able to utilise the JAK-STAT pathway and to induce SOCS3 expression, there is no evidence so far for their dysregulation in SOCS3 conditional knockout mice. Actually, this signifies the redundant nature of the SOCS family [324]. Thus, the discovery of novel proteins which have the ability to interact with SOCS3 would presumably reveal new biological implications of SOCS3. It is possible that additional proteins should be integrated as interactors to maximise the

regulatory roles of SOCS3. In this respect, the CUE domain-containing 2 (CUEDC2) protein was found using a yeast two-hybrid screening to specifically interact with SOCS3 and this interaction is required for effective inhibition of JAK1/STAT3 signalling [458]. In conclusion, SOCS3 has been implicated in the regulation of a variety of signalling pathways. Based on the previously-established evidence over the past 20 years, SOCS3 regulation seems to be a promising therapeutic solution to treat pathogenic infections, diabetes, rheumatoid arthritis, and cancer. Therefore, SOCS3-cavin-1 interaction opens a new horizon to cytokine response and immune responses.

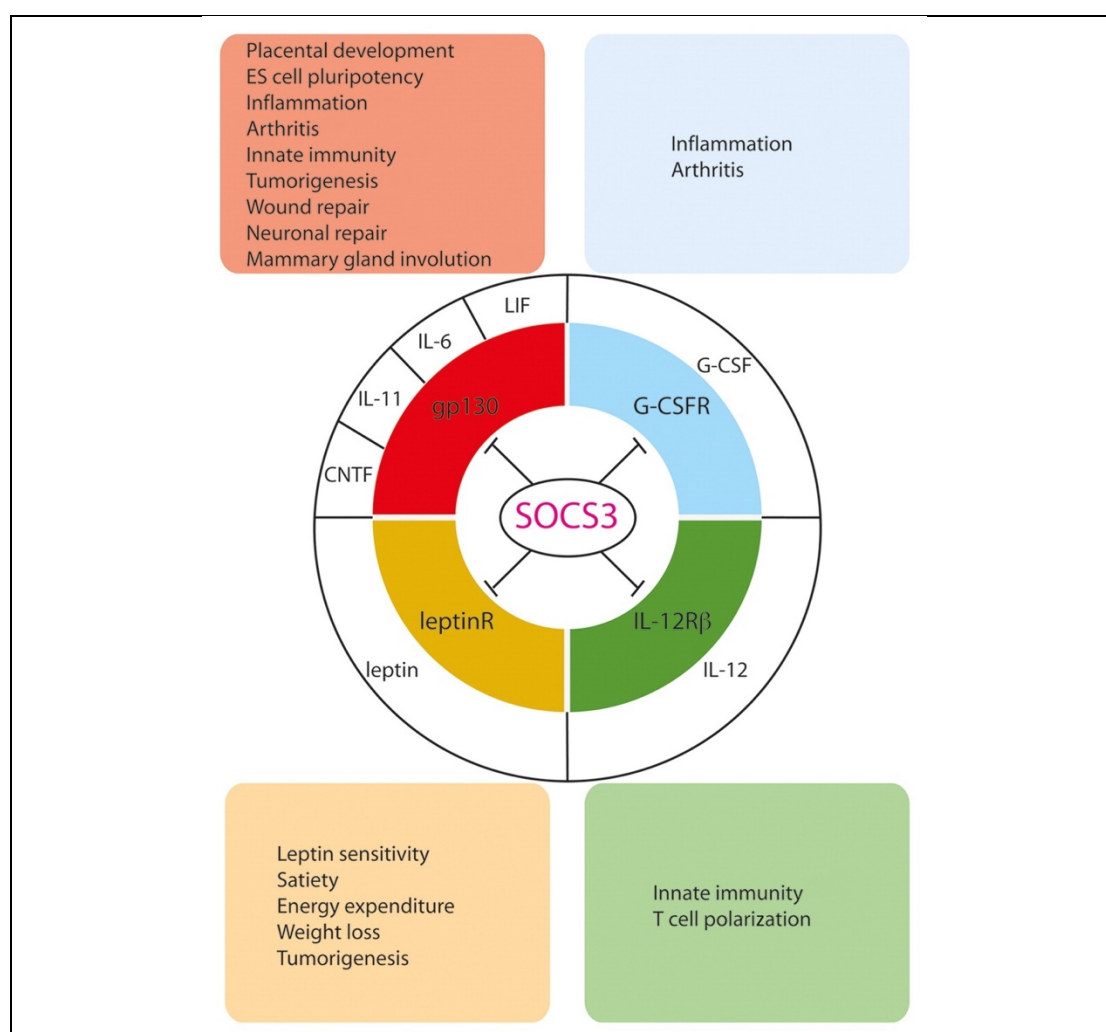


**Figure 6–2: The physiological functions of SOCS3**

SOCS3 role is mediated by direct binding to specific receptors, including gp130, G-CSFR, IL-12R $\beta$ , and leptinR. The inhibitory effects of SOCS3 on signalling pathways regulate several biological processes. Figure adapted from [324].

## 6.2 Limitations of the study

The current study has some limitations worth noting. First, although SOCS3 knockout clones were effectively produced in AS-M.5 cells as described (Section 2.2.9) and subsequently six knockout clones were confirmed by immunoblots (Figure 3-6), some variations between clones were observed following the induction of Nur77 in response to cAMP. Thus, PCR genotyping and Sanger sequencing are needed to verify efficient allelic knockout in clonal cell lines by identifying the CRISPR-induced alterations at the DNA level.

Second, antibody-based detection of endogenous SOCS3 in our preliminary immunofluorescence experiments was challenging due to the lack of specificity and the immunoreactivity demonstrated in SOCS3<sup>-/-</sup> cells. Therefore, the expression of fluorescent protein fusions was used to investigate the subcellular distribution of SOCS3.

Finally, cavin-1<sup>-/-</sup> MEFs stably expressing GFP-cavin-1 were established and characterised as described in (Figure 5-10). However, it is recommended to utilise a fluorescence-activated cell sorter (FACS) to enrich and sort the expressing cells in an accurate and quantitative manner for optimal clonal purity.

## 6.3 Future work

Targeting SOCS3-cavin-1 interaction may be exploited for desired functional outcomes in a diverse array of biological pathways, including IL-6, insulin, and eNOS. This could be approached using a combination of immunoblotting cell lysates with or without peptide inhibitors, which interfere with such interaction. In addition, experiments involving SOCS3 and cavin-1 null mice are likely to shed some light into pathophysiological significance of the present PhD study.

## Appendices

APPENDIX A: Interaction of suppressor of cytokine signalling 3 with cavin-1 links SOCS3 function and cavin-1 stability

### A.1 CONTRIBUTION TO WORK

The following appendix is a reprint of Williams et al. “Interaction of suppressor of cytokine signalling 3 with cavin-1 links SOCS3 function and cavin-1 stability”, published in *Nature Communications* volume 9, Article number: 168 (2018). Nasser Alotaiq is second author on this publication. His contribution to the work including (1) a novel tool: Establishing stable endothelial cell lines completely lacking SOCS3 expression via CRISPR/Cas system, (2) novel data generated by confocal microscopy and transmission electron microscopy.

A.2 REPRINT OF “Interaction of suppressor of cytokine signalling 3 with cavin-1 links SOCS3 function and cavin-1 stability”

## References

1. Singer, S.J. and G.L. Nicolson, *The fluid mosaic model of the structure of cell membranes*. Science, 1972. **175**(4023): p. 720-31.
2. Goñi, F.M., *The basic structure and dynamics of cell membranes: An update of the Singer–Nicolson model*. Biochimica et Biophysica Acta (BBA) - Biomembranes, 2014. **1838**(6): p. 1467-1476.
3. Sezgin, E., et al., *The mystery of membrane organization: composition, regulation and roles of lipid rafts*. Nature Reviews Molecular Cell Biology, 2017. **18**(6): p. 361-374.
4. Pike, L.J., *Rafts defined: a report on the Keystone symposium on lipid rafts and cell function*. Journal of Lipid Research, 2006. **47**(7): p. 1597-1598.
5. Simons, K., *Cell membranes: A subjective perspective*. Biochimica et Biophysica Acta (BBA) - Biomembranes, 2016. **1858**(10): p. 2569-2572.
6. Harder, T. and K. Simons, *Clusters of glycolipid and glycosylphosphatidylinositol-anchored proteins in lymphoid cells: accumulation of actin regulated by local tyrosine phosphorylation*. European Journal of Immunology, 1999. **29**(2): p. 556-562.
7. Edidin, M., *The State of Lipid Rafts: From Model Membranes to Cells*. Annual Review of Biophysics and Biomolecular Structure, 2003. **32**(1): p. 257-283.
8. Das, M. and D. Das, *Lipid Raft in Cardiac Health and Disease*. Current Cardiology Reviews, 2009. **5**(2): p. 105-111.
9. McDonald, G., et al., *Normalizing glycosphingolipids restores function in CD4+ T cells from lupus patients*. Journal of Clinical Investigation, 2014. **124**(2): p. 712-724.
10. Lingwood, D. and K. Simons, *Lipid Rafts As a Membrane-Organizing Principle*. Science, 2009. **327**(5961): p. 46-50.
11. Stan, R.-V., *Structure and function of endothelial caveolae*. Microscopy Research and Technique, 2002. **57**(5): p. 350-364.
12. Browman, D.T., M.B. Hoegg, and S.M. Robbins, *The SPFH domain-containing proteins: more than lipid raft markers*. Trends in Cell Biology, 2007. **17**(8): p. 394-402.
13. Simons, K. and D. Toomre, *Lipid rafts and signal transduction*. Nature Reviews Molecular Cell Biology, 2000. **1**(1): p. 31-39.
14. Sonnino, S. and A. Prinetti, *Membrane Domains and the Lipid Raft Concept*. Current Medicinal Chemistry, 2012. **20**(1): p. 4-21.
15. Reeves, V.L., C.M. Thomas, and E.J. Smart, *Lipid Rafts, Caveolae and GPI-Linked Proteins*, in *Advances in Experimental Medicine and Biology*. 2012, Springer US. p. 3-13.
16. Field, K.A., D. Holowka, and B. Baird, *Fc epsilon RI-mediated recruitment of p53/56lyn to detergent-resistant membrane domains accompanies cellular signaling*. Proceedings of the National Academy of Sciences, 1995. **92**(20): p. 9201-9205.
17. Hooper, N.M., *Detergent-insoluble glycosphingolipid/cholesterol-rich membrane domains, lipid rafts and caveolae*. Molecular membrane biology, 1999. **16**(2): p. 145-156.

18. Waugh, M.G., D. Lawson, and J.J. Hsuan, *Epidermal growth factor receptor activation is localized within low-buoyant density, non-caveolar membrane domains*. *Biochemical Journal*, 1999. **337**(Pt 3): p. 591-597.
19. Janes, P.W., S.C. Ley, and A.I. Magee, *Aggregation of lipid rafts accompanies signaling via the T cell antigen receptor*. *The Journal of cell biology*, 1999. **147**(2): p. 447-461.
20. Harder, T., et al., *Lipid domain structure of the plasma membrane revealed by patching of membrane components*. *The Journal of cell biology*, 1998. **141**(4): p. 929-942.
21. Mayor, S. and F.R. Maxfield, *Insolubility and redistribution of GPI-anchored proteins at the cell surface after detergent treatment*. *Molecular biology of the cell*, 1995. **6**(7): p. 929-944.
22. Fujimoto, T., *GPI-anchored proteins, glycosphingolipids, and sphingomyelin are sequestered to caveolae only after crosslinking*. *J Histochem Cytochem*, 1996. **44**(8): p. 929-41.
23. Varma, R. and S. Mayor, *GPI-anchored proteins are organized in submicron domains at the cell surface*. *Nature*, 1998. **394**(6695): p. 798-801.
24. Friedrichson, T. and T.V. Kurzchalia, *Microdomains of GPI-anchored proteins in living cells revealed by crosslinking*. *Nature*, 1998. **394**(6695): p. 802-5.
25. Harder, T. and K. Simons, *Caveolae, DIGs, and the dynamics of sphingolipid-cholesterol microdomains*. *Curr Opin Cell Biol*, 1997. **9**(4): p. 534-42.
26. Janes, P.W., et al., *The role of lipid rafts in T cell antigen receptor (TCR) signalling*. *Seminars in Immunology*, 2000. **12**(1): p. 23-34.
27. Gupta, N. and A.L. DeFranco, *Visualizing Lipid Raft Dynamics and Early Signaling Events during Antigen Receptor-mediated B-Lymphocyte Activation*. *Molecular Biology of the Cell*, 2003. **14**(2): p. 432-444.
28. Buk, D.M., *Polarity and lipid raft association of the components of the ciliary neurotrophic factor receptor complex in Madin-Darby canine kidney cells*. *Journal of Cell Science*, 2004. **117**(10): p. 2063-2075.
29. Ohtsuka, H., et al., *SDF-1 $\alpha$ /CXCR4 Signaling in Lipid Rafts Induces Platelet Aggregation via PI3 Kinase-Dependent Akt Phosphorylation*. *PLOS ONE*, 2017. **12**(1): p. e0169609.
30. Jahn, T., et al., *Lipid rafts are required for Kit survival and proliferation signals*. *Blood*, 2007. **110**(6): p. 1739-1747.
31. Wysoczynski, M., *Incorporation of CXCR4 into membrane lipid rafts primes homing-related responses of hematopoietic stem/progenitor cells to an SDF-1 gradient*. *Blood*, 2005. **105**(1): p. 40-48.
32. Dessauer, C.W., et al., *International Union of Basic and Clinical Pharmacology. Cl. Structures and Small Molecule Modulators of Mammalian Adenylyl Cyclases*. *Pharmacological Reviews*, 2017. **69**(2): p. 93-139.
33. Palade, G., *Fine structure of blood capillaries*. *J Appl Physics*, 1953. **24**(11): p. 1424-1424.
34. Yamada, E., *THE FINE STRUCTURE OF THE GALL BLADDER EPITHELIUM OF THE MOUSE*. *The Journal of Cell Biology*, 1955. **1**(5): p. 445-458.

35. Laude, A.J. and I.A. Prior, *Plasma membrane microdomains: Organization, function and trafficking (Review)*. Molecular Membrane Biology, 2004. **21**(3): p. 193-205.
36. Gorodinsky, A., *Glycolipid-anchored proteins in neuroblastoma cells form detergent-resistant complexes without caveolin*. The Journal of Cell Biology, 1995. **129**(3): p. 619-627.
37. Fra, A.M., et al., *Detergent-insoluble glycolipid microdomains in lymphocytes in the absence of caveolae*. Journal of Biological Chemistry, 1994. **269**(49): p. 30745-30748.
38. Tan, S., H.T. Tan, and M.C.M. Chung, *Membrane proteins and membrane proteomics*. PROTEOMICS, 2008. **8**(19): p. 3924-3932.
39. Shibata, Y., et al., *Mechanisms Shaping the Membranes of Cellular Organelles*. Annual Review of Cell and Developmental Biology, 2009. **25**(1): p. 329-354.
40. Branza-Nichita, N., A. Macovei, and C. Lazar, *Caveolae-dependent endocytosis in viral infection*, in *Molecular Regulation of Endocytosis*. 2012, InTech.
41. Chidlow Jr, J.H. and W.C. Sessa, *Caveolae, caveolins, and cavins: complex control of cellular signalling and inflammation*. Cardiovascular research, 2010. **86**(2): p. 219-225.
42. Sotgia, F., et al., *Caveolin-1 and cancer metabolism in the tumor microenvironment: markers, models, and mechanisms*. Annual Review of Pathology: Mechanisms of Disease, 2012. **7**: p. 423-467.
43. Shastry, S., et al., *Congenital generalized lipodystrophy, type 4 (CGL4) associated with myopathy due to novel PTRF mutations*. American journal of medical genetics Part A, 2010. **152**(9): p. 2245-2253.
44. Rajab, A., et al., *Fatal cardiac arrhythmia and long-QT syndrome in a new form of congenital generalized lipodystrophy with muscle rippling (CGL4) due to PTRF-CAVIN mutations*. PLoS genetics, 2010. **6**(3): p. e1000874.
45. Bai, L., et al., *Down-regulation of the cavin family proteins in breast cancer*. Journal of cellular biochemistry, 2012. **113**(1): p. 322-328.
46. Zöchbauer-Müller, S., et al., *Expression of the candidate tumor suppressor gene hSRBC is frequently lost in primary lung cancers with and without DNA methylation*. Oncogene, 2005. **24**(41): p. 6249.
47. Pilch, P., et al., *Caveolae and lipid trafficking in adipocytes*. Clinical lipidology, 2011. **6**(1): p. 49-58.
48. Busija, A.R., H.H. Patel, and P.A. Insel, *Caveolins and cavins in the trafficking, maturation, and degradation of caveolae: implications for cell physiology*. American Journal of Physiology-Cell Physiology, 2017. **312**(4): p. C459-C477.
49. Kwon, H., et al., *A novel domain of caveolin-2 that controls nuclear targeting: regulation of insulin-specific ERK activation and nuclear translocation by caveolin-2*. Journal of cellular and molecular medicine, 2011. **15**(4): p. 888-908.
50. Fuhs, S.R. and P.A. Insel, *Caveolin-3 Undergoes SUMOylation by the SUMO E3 Ligase PIASy SUMOYLATION AFFECTS G-PROTEIN-COUPLED RECEPTOR DESENSITIZATION*. Journal of Biological Chemistry, 2011. **286**(17): p. 14830-14841.
51. Venema, V.J., et al., *Interaction of neuronal nitric-oxide synthase with caveolin-3 in skeletal muscle Identification of a novel caveolin*

- scaffolding/inhibitory domain*. Journal of Biological Chemistry, 1997. **272**(45): p. 28187-28190.
52. Chaudhary, N., et al., *Endocytic crosstalk: caveins, caveolins, and caveolae regulate clathrin-independent endocytosis*. PLoS biology, 2014. **12**(4): p. e1001832.
  53. Shaul, P.W. and R.G. Anderson, *Role of plasmalemmal caveolae in signal transduction*. American Journal of Physiology-Lung Cellular and Molecular Physiology, 1998. **275**(5): p. L843-L851.
  54. Cohen, A.W., et al., *Role of caveolae and caveolins in health and disease*. Physiol Rev, 2004. **84**(4): p. 1341-79.
  55. Williams, T.M. and M.P. Lisanti, *The caveolin proteins*. Genome biology, 2004. **5**(3): p. 214.
  56. Razani, B. and M.P. Lisanti, *Caveolin-deficient mice: insights into caveolar function human disease*. The Journal of clinical investigation, 2001. **108**(11): p. 1553-1561.
  57. Roy, S., et al., *Dominant-negative caveolin inhibits H-Ras function by disrupting cholesterol-rich plasma membrane domains*. Nature cell biology, 1999. **1**(2): p. 98.
  58. Yu, J., et al., *Direct evidence for the role of caveolin-1 and caveolae in mechanotransduction and remodeling of blood vessels*. The Journal of clinical investigation, 2006. **116**(5): p. 1284-1291.
  59. Sinha, B., et al., *Cells respond to mechanical stress by rapid disassembly of caveolae*. Cell, 2011. **144**(3): p. 402-413.
  60. Mercier, I., et al., *Clinical and translational implications of the caveolin gene family: lessons from mouse models and human genetic disorders*. Lab Invest, 2009. **89**(6): p. 614-23.
  61. Sverdlov, M., A.N. Shajahan, and R.D. Minshall, *Tyrosine phosphorylation-dependence of caveolae-mediated endocytosis*. Journal of cellular and molecular medicine, 2007. **11**(6): p. 1239-1250.
  62. Scherer, P.E., et al., *Caveolin isoforms differ in their N-terminal protein sequence and subcellular distribution. Identification and epitope mapping of an isoform-specific monoclonal antibody probe*. Journal of Biological Chemistry, 1995. **270**(27): p. 16395-16401.
  63. Kogo, H. and T. Fujimoto, *Caveolin-1 isoforms are encoded by distinct mRNAs. Identification Of mouse caveolin-1 mRNA variants caused by alternative transcription initiation and splicing*. FEBS Lett, 2000. **465**(2-3): p. 119-23.
  64. Fujimoto, T., et al., *Isoforms of caveolin-1 and caveolar structure*. Journal of cell science, 2000. **113**(19): p. 3509-3517.
  65. Ramirez, M.I., et al., *The  $\alpha$ -isoform of caveolin-1 Is a marker of vasculogenesis in early lung development*. Journal of Histochemistry & Cytochemistry, 2002. **50**(1): p. 33-42.
  66. Nohe, A., et al., *Dynamics and interaction of caveolin-1 isoforms with BMP-receptors*. Journal of cell science, 2005. **118**(3): p. 643-650.
  67. Li, S., R. Seitz, and M.P. Lisanti, *Phosphorylation of caveolin by src tyrosine kinases. The alpha-isoform of caveolin is selectively phosphorylated by v-Src in vivo*. J Biol Chem, 1996. **271**(7): p. 3863-8.
  68. Nomura, R. and T. Fujimoto, *Tyrosine-phosphorylated caveolin-1: immunolocalization and molecular characterization*. Molecular biology of the cell, 1999. **10**(4): p. 975-986.

69. Gottlieb-Abraham, E., et al., *Src-mediated caveolin-1 phosphorylation affects the targeting of active Src to specific membrane sites*. *Molecular biology of the cell*, 2013. **24**(24): p. 3881-3895.
70. Sargiacomo, M., et al., *Oligomeric structure of caveolin: implications for caveolae membrane organization*. *Proceedings of the National Academy of Sciences*, 1995. **92**(20): p. 9407-9411.
71. Li, S., J. Couet, and M.P. Lisanti, *Src Tyrosine Kinases, Gα Subunits, and H-Ras Share a Common Membrane-anchored Scaffolding Protein, Caveolin* CAVEOLIN BINDING NEGATIVELY REGULATES THE AUTO-ACTIVATION OF Src TYROSINE KINASES. *Journal of Biological Chemistry*, 1996. **271**(46): p. 29182-29190.
72. Couet, J., et al., *Identification of peptide and protein ligands for the caveolin-scaffolding domain Implications for the interaction of caveolin with caveolae-associated proteins*. *Journal of Biological Chemistry*, 1997. **272**(10): p. 6525-6533.
73. Root, K.T., S.M. Plucinsky, and K.J. Glover, *Recent progress in the topology, structure, and oligomerization of caveolin: a building block of caveolae*. *Curr Top Membr*, 2015. **75**: p. 305-36.
74. Das, K., et al., *The membrane-spanning domains of caveolins-1 and -2 mediate the formation of caveolin hetero-oligomers. Implications for the assembly of caveolae membranes in vivo*. *J Biol Chem*, 1999. **274**(26): p. 18721-8.
75. Aoki, S., et al., *The Role of Proline in the Membrane Re-entrant Helix of Caveolin-1*. *The Journal of Biological Chemistry*, 2010. **285**(43): p. 33371-33380.
76. Rui, H., et al., *Probing the U-shaped conformation of caveolin-1 in a bilayer*. *Biophys J*, 2014. **106**(6): p. 1371-80.
77. Monier, S., et al., *Oligomerization of VIP21-caveolin in vitro is stabilized by long chain fatty acylation or cholesterol*. *FEBS Lett*, 1996. **388**(2-3): p. 143-9.
78. Fujimoto, T., et al., *Caveolin-2 Is Targeted to Lipid Droplets, a New "Membrane Domain" in the Cell*. *The Journal of Cell Biology*, 2001. **152**(5): p. 1079-1086.
79. Scherer, P.E., et al., *Cell-type and tissue-specific expression of caveolin-2. Caveolins 1 and 2 co-localize and form a stable hetero-oligomeric complex in vivo*. *J Biol Chem*, 1997. **272**(46): p. 29337-46.
80. Sowa, G., *Novel Insights into the Role of Caveolin-2 in Cell- and Tissue-Specific Signaling and Function*. *Biochemistry Research International*, 2011. **2011**: p. 809259.
81. Razani, B., et al., *Caveolin-2-deficient mice show evidence of severe pulmonary dysfunction without disruption of caveolae*. *Molecular and cellular biology*, 2002. **22**(7): p. 2329-2344.
82. Sowa, G., et al., *The phosphorylation of caveolin-2 on serines 23 and 36 modulates caveolin-1-dependent caveolae formation*. *Proceedings of the National Academy of Sciences of the United States of America*, 2003. **100**(11): p. 6511-6516.
83. de Almeida, C.J.G., et al., *Genetic ablation of caveolin-2 sensitizes mice to bleomycin-induced injury*. *Cell Cycle*, 2013. **12**(14): p. 2248-2254.
84. Xie, L., et al., *Endothelial cells isolated from caveolin-2 knockout mice display higher proliferation rate and cell cycle progression relative to their*

- wild-type counterparts*. Am J Physiol Cell Physiol, 2010. **298**(3): p. C693-701.
85. Lee, S., et al., *Regulation of cancer cell proliferation by caveolin-2 down-regulation and re-expression*. Int J Oncol, 2011. **38**(5): p. 1395-402.
  86. Liu, Y., et al., *Host deficiency in caveolin-2 inhibits lung carcinoma tumor growth by impairing tumor angiogenesis*. Cancer research, 2014. **74**(22): p. 6452-6462.
  87. de Almeida, C.J., et al., *Caveolin-2-deficient mice show increased sensitivity to endotoxemia*. Cell Cycle, 2011. **10**(13): p. 2151-2161.
  88. Way, M. and R.G. Parton, *M-caveolin, a muscle-specific caveolin-related protein*. FEBS Lett, 1996. **378**(1): p. 108-12.
  89. Song, K.S., et al., *Expression of caveolin-3 in skeletal, cardiac, and smooth muscle cells. Caveolin-3 is a component of the sarcolemma and co-fractionates with dystrophin and dystrophin-associated glycoproteins*. J Biol Chem, 1996. **271**(25): p. 15160-5.
  90. Parton, R.G., et al., *Caveolin-3 associates with developing T-tubules during muscle differentiation*. J Cell Biol, 1997. **136**(1): p. 137-54.
  91. Ralston, E. and T. Ploug, *Caveolin-3 Is Associated with the T-Tubules of Mature Skeletal Muscle Fibers*. Experimental Cell Research, 1999. **246**(2): p. 510-515.
  92. Galbiati, F., B. Razani, and M.P. Lisanti, *Caveolae and caveolin-3 in muscular dystrophy*. Trends Mol Med, 2001. **7**(10): p. 435-41.
  93. Oshikawa, J., et al., *Insulin resistance in skeletal muscles of caveolin-3-null mice*. Proc Natl Acad Sci U S A, 2004. **101**(34): p. 12670-5.
  94. Woodman, S.E., et al., *Caveolin-3 knock-out mice develop a progressive cardiomyopathy and show hyperactivation of the p42/44 MAPK cascade*. J Biol Chem, 2002. **277**(41): p. 38988-97.
  95. Gutierrez-Pajares, J.L., et al., *Caveolin-3 promotes a vascular smooth muscle contractile phenotype*. Frontiers in cardiovascular medicine, 2015. **2**: p. 27.
  96. Talukder, M.A.H., et al., *Heterozygous caveolin-3 mice show increased susceptibility to palmitate-induced insulin resistance*. Physiological Reports, 2016. **4**(6): p. e12736.
  97. Minetti, C., et al., *Mutations in the caveolin-3 gene cause autosomal dominant limb-girdle muscular dystrophy*. Nat Genet, 1998. **18**(4): p. 365-8.
  98. Galbiati, F., et al., *Limb-girdle muscular dystrophy (LGMD-1C) mutants of caveolin-3 undergo ubiquitination and proteasomal degradation. Treatment with proteasomal inhibitors blocks the dominant negative effect of LGMD-1C mutant and rescues wild-type caveolin-3*. J Biol Chem, 2000. **275**(48): p. 37702-11.
  99. Woodman, S.E., et al., *Caveolinopathies: Mutations in caveolin-3 cause four distinct autosomal dominant muscle diseases*. Neurology, 2004. **62**(4): p. 538-543.
  100. Galbiati, F., et al., *Caveolin-3 null mice show a loss of caveolae, changes in the microdomain distribution of the dystrophin-glycoprotein complex, and t-tubule abnormalities*. Journal of Biological Chemistry, 2001. **276**(24): p. 21425-21433.
  101. Capozza, F., et al., *Caveolin-3 knockout mice show increased adiposity and whole body insulin resistance, with ligand-induced insulin receptor*

- instability in skeletal muscle*. American Journal of Physiology-Cell Physiology, 2005. **288**(6): p. C1317-C1331.
102. Hill, M.M., et al., *PTRF-Cavin, a conserved cytoplasmic protein required for caveola formation and function*. Cell, 2008. **132**(1): p. 113-124.
  103. Mason, S.W., E.E. Sander, and I. Grummt, *Identification of a transcript release activity acting on ternary transcription complexes containing murine RNA polymerase I*. The EMBO journal, 1997. **16**(1): p. 163-172.
  104. Gustincich, S. and C. Schneider, *Serum deprivation response gene is induced by serum starvation but not by contact inhibition*. Cell growth and differentiation, 1993. **4**: p. 753-753.
  105. Izumi, Y., et al., *A protein kinase C $\delta$ -binding protein SRBC whose expression is induced by serum starvation*. Journal of Biological Chemistry, 1997. **272**(11): p. 7381-7389.
  106. Bastiani, M., et al., *MURC/Cavin-4 and cavin family members form tissue-specific caveolar complexes*. The Journal of cell biology, 2009. **185**(7): p. 1259-1273.
  107. Kovtun, O., et al., *Structural insights into the organization of the cavin membrane coat complex*. Developmental cell, 2014. **31**(4): p. 405-419.
  108. Nassar, Z.D. and M.-O. Parat, *Cavin family: new players in the biology of caveolae*, in *International review of cell and molecular biology*. 2015, Elsevier. p. 235-305.
  109. Briand, N., I. Dugail, and S. Le Lay, *Cavin proteins: New players in the caveolae field*. Biochimie, 2011. **93**(1): p. 71-77.
  110. Reverte, C.G., M.D. Ahearn, and L.E. Hake, *CPEB degradation during Xenopus oocyte maturation requires a PEST domain and the 26S proteasome*. Developmental biology, 2001. **231**(2): p. 447-458.
  111. Shumway, S.D., M. Maki, and S. Miyamoto, *The PEST Domain of I $\kappa$ B $\alpha$  Is Necessary and Sufficient for In Vitro Degradation by  $\mu$ -Calpain*. Journal of Biological Chemistry, 1999. **274**(43): p. 30874-30881.
  112. Parton, R.G. and M.A. Del Pozo, *Caveolae as plasma membrane sensors, protectors and organizers*. Nature reviews Molecular cell biology, 2013. **14**(2): p. 98.
  113. Liu, L. and P.F. Pilch, *PTRF/Cavin-1 promotes efficient ribosomal RNA transcription in response to metabolic challenges*. Elife, 2016. **5**: p. e17508.
  114. Hansen, C.G. and B.J. Nichols, *Exploring the caves: cavins, caveolins and caveolae*. Trends in cell biology, 2010. **20**(4): p. 177-186.
  115. Liu, L. and P.F. Pilch, *A critical role of cavin (polymerase I and transcript release factor) in caveolae formation and organization*. J Biol Chem, 2008. **283**(7): p. 4314-22.
  116. Williams, J.J. and T.M. Palmer, *Cavin-1: caveolae-dependent signalling and cardiovascular disease*. 2014, Portland Press Limited.
  117. Breen, M.R., et al., *Cholesterol depletion in adipocytes causes caveolae collapse concomitant with proteosomal degradation of cavin-2 in a switch-like fashion*. PLoS One, 2012. **7**(4): p. e34516.
  118. Aboulaich, N., et al., *Polymerase I and transcript release factor regulates lipolysis via a phosphorylation-dependent mechanism*. Diabetes, 2011. **60**(3): p. 757-765.
  119. Humphrey, S.J., et al., *Dynamic adipocyte phosphoproteome reveals that Akt directly regulates mTORC2*. Cell Metab, 2013. **17**(6): p. 1009-20.

120. Kruger, M., et al., *Dissection of the insulin signaling pathway via quantitative phosphoproteomics*. Proc Natl Acad Sci U S A, 2008. **105**(7): p. 2451-6.
121. Liu, L., et al., *Deletion of Cavin/PTRF causes global loss of caveolae, dyslipidemia, and glucose intolerance*. Cell metabolism, 2008. **8**(4): p. 310-317.
122. Ludwig, A., et al., *Molecular composition and ultrastructure of the caveolar coat complex*. PLoS biology, 2013. **11**(8): p. e1001640.
123. Gambin, Y., et al., *Single-molecule analysis reveals self assembly and nanoscale segregation of two distinct cavin subcomplexes on caveolae*. Elife, 2014. **3**.
124. Jansa, P., et al., *Cloning and functional characterization of PTRF, a novel protein which induces dissociation of paused ternary transcription complexes*. The EMBO journal, 1998. **17**(10): p. 2855-2864.
125. Vinten, J., et al., *Identification of a major protein on the cytosolic face of caveolae*. Biochimica et Biophysica Acta (BBA)-Biomembranes, 2005. **1717**(1): p. 34-40.
126. Kasahara, T., et al., *PTRF/Cavin-1 Knock-out Mice Develop a Progressive Cardiomyopathy with ERK1/2 Hyperactivation and Caveolin-3 Reduction*. 2014, Am Heart Assoc.
127. Hayashi, Y.K., et al., *Human PTRF mutations cause secondary deficiency of caveolins resulting in muscular dystrophy with generalized lipodystrophy*. The Journal of clinical investigation, 2009. **119**(9): p. 2623-2633.
128. Park, D.S., et al., *Caveolin-1/3 double-knockout mice are viable, but lack both muscle and non-muscle caveolae, and develop a severe cardiomyopathic phenotype*. The American journal of pathology, 2002. **160**(6): p. 2207-2217.
129. Cheng, J.P. and B.J. Nichols, *Caveolae: one function or many?* Trends in cell biology, 2016. **26**(3): p. 177-189.
130. Dwianingsih, E.K., et al., *A Japanese child with asymptomatic elevation of serum creatine kinase shows PTRF-CAVIN mutation matching with congenital generalized lipodystrophy type 4*. Molecular genetics and metabolism, 2010. **101**(2): p. 233-237.
131. Barrett, J.C., et al., *Genome-wide association study and meta-analysis find that over 40 loci affect risk of type 1 diabetes*. Nature genetics, 2009. **41**(6): p. 703.
132. Ikram, M.A., et al., *Common variants at 6q22 and 17q21 are associated with intracranial volume*. Nature genetics, 2012. **44**(5): p. 539.
133. Konishi, H., et al., *Mutation of a single allele of the cancer susceptibility gene BRCA1 leads to genomic instability in human breast epithelial cells*. Proceedings of the National Academy of Sciences, 2011. **108**(43): p. 17773-17778.
134. Wang, F., et al., *PTRF suppresses the progression of colorectal cancers*. Oncotarget, 2017. **8**(30): p. 48650.
135. Aung, C.S., et al., *PTRF-cavin-1 expression decreases the migration of PC3 prostate cancer cells: Role of matrix metalloprotease 9*. European journal of cell biology, 2011. **90**(2-3): p. 136-142.
136. Gámez-Pozo, A., et al., *PTRF/cavin-1 and MIF proteins are identified as non-small cell lung cancer biomarkers by label-free proteomics*. PloS one, 2012. **7**(3): p. e33752.

137. Huang, K., et al., *The role of PTRF/Cavin1 as a biomarker in both glioma and serum exosomes*. *Theranostics*, 2018. **8**(6): p. 1540.
138. Echarri, A. and M.A. Del Pozo, *Caveolae—mechanosensitive membrane invaginations linked to actin filaments*. *J Cell Sci*, 2015: p. jcs. 153940.
139. Breen, M.R., *Cavin-2 is a cholesterol sensor linking caveolae to the adipocyte cortical cytoskeleton*. 2012, Boston University.
140. Verma, P., A.G. Ostermeyer-Fay, and D.A. Brown, *Caveolin-1 induces formation of membrane tubules that sense actomyosin tension and are inhibited by polymerase I and transcript release factor/cavin-1*. *Mol Biol Cell*, 2010. **21**(13): p. 2226-40.
141. Volonte, D. and F. Galbiati, *Polymerase I and transcript release factor (PTRF)/cavin-1 is a novel regulator of stress-induced premature senescence*. *Journal of Biological Chemistry*, 2011. **286**(33): p. 28657-28661.
142. Uyy, E., et al., *High-fat diet alters protein composition of detergent-resistant membrane microdomains*. *Cell and tissue research*, 2013. **354**(3): p. 771-781.
143. Hayer, A., et al., *Caveolin-1 is ubiquitinated and targeted to intraluminal vesicles in endolysosomes for degradation*. *J Cell Biol*, 2010. **191**(3): p. 615-29.
144. Mineo, C., et al., *Targeting of protein kinase Ca to caveolae*. *The Journal of cell biology*, 1998. **141**(3): p. 601-610.
145. Hansen, C.G., et al., *SDPR induces membrane curvature and functions in the formation of caveolae*. *Nature cell biology*, 2009. **11**(7): p. 807.
146. Hansen, C.G., et al., *Deletion of cavin genes reveals tissue-specific mechanisms for morphogenesis of endothelial caveolae*. *Nature communications*, 2013. **4**: p. 1831.
147. Maruyama, N., et al., *SDPR/Cavin-2 Modulates Akt Signaling Involved in Regulation of Hypertrophy and Apoptosis in Cardiomyocytes*. 2014, Am Heart Assoc.
148. Higuchi, Y., et al., *SDPR/Cavin-2 Modulates Apoptosis via PTEN/Akt Signaling Pathway and Deteriorates Cardiac Function in Pressure Overload-Induced Heart Failure*. 2017, Am Heart Assoc.
149. Boopathy, G.T., et al., *Cavin-2 regulates the activity and stability of endothelial nitric-oxide synthase (eNOS) in angiogenesis*. *Journal of Biological Chemistry*, 2017. **292**(43): p. 17760-17776.
150. Codenotti, S., et al., *Cavin-2 is a specific marker for detection of well-differentiated liposarcoma*. *Biochemical and biophysical research communications*, 2017. **493**(1): p. 660-665.
151. Roberts, A., et al., *Linkage to chromosome 2q32. 2-q33. 3 in familial serrated neoplasia (Jass syndrome)*. *Familial cancer*, 2011. **10**(2): p. 245-254.
152. Glass, I., et al., *Interstitial deletion of the long arm of chromosome 2 with normal levels of isocitrate dehydrogenase*. *Journal of medical genetics*, 1989. **26**(2): p. 127-130.
153. Van Buggenhout, G., et al., *The del (2)(q32. 2q33) deletion syndrome defined by clinical and molecular characterization of four patients*. *European journal of medical genetics*, 2005. **48**(3): p. 276-289.
154. Unozawa, M., et al., *Cavin-2 in oral cancer: A potential predictor for tumor progression*. *Mol Carcinog*, 2016. **55**(6): p. 1037-47.

155. McMahon, K.A., et al., *SRBC/cavin-3 is a caveolin adapter protein that regulates caveolae function*. The EMBO journal, 2009. **28**(8): p. 1001-1015.
156. Hernandez, V.J., et al., *Cavin-3 dictates the balance between ERK and Akt signaling*. Elife, 2013. **2**.
157. Zhu, B., et al., *Cavin-3 deficiency reduces caveolae abundance in vascular and urinary bladder smooth muscle cells*. The FASEB Journal, 2017. **31**(1 Supplement): p. 1015.23-1015.23.
158. Zhu, B., et al., *Cavin-3 (PRKCDBP) deficiency reduces the density of caveolae in smooth muscle*. Cell and tissue research, 2017. **368**(3): p. 591-602.
159. Ogata, T., et al., *MURC, a muscle-restricted coiled-coil protein that modulates the Rho/ROCK pathway, induces cardiac dysfunction and conduction disturbance*. Molecular and cellular biology, 2008. **28**(10): p. 3424-3436.
160. Ogata, T., et al., *MURC/Cavin-4 facilitates recruitment of ERK to caveolae and concentric cardiac hypertrophy induced by  $\alpha$ 1-adrenergic receptors*. Proceedings of the National Academy of Sciences, 2014. **111**(10): p. 3811-3816.
161. Naito, D., et al., *The coiled-coil domain of MURC/cavin-4 is involved in membrane trafficking of caveolin-3 in cardiomyocytes*. American Journal of Physiology-Heart and Circulatory Physiology, 2015. **309**(12): p. H2127-H2136.
162. McFarlane, A.A., G.L. Orriss, and J. Stetefeld, *The use of coiled-coil proteins in drug delivery systems*. European journal of pharmacology, 2009. **625**(1-3): p. 101-107.
163. Burkhard, P., J. Stetefeld, and S.V. Strelkov, *Coiled coils: a highly versatile protein folding motif*. Trends in cell biology, 2001. **11**(2): p. 82-88.
164. Rodriguez, G., et al., *Molecular genetic and functional characterization implicate muscle-restricted coiled-coil gene (MURC) as a causal gene for familial dilated cardiomyopathy*. Circulation: Genomic and Precision Medicine, 2011: p. CIRCGENETICS. 111.959866.
165. Shyu, K.-G., et al., *Hypoxia activates muscle-restricted coiled-coil protein (MURC) expression via transforming growth factor- $\beta$  in cardiac myocytes*. Clinical Science, 2014. **126**(5): p. 367-375.
166. Nishi, M., et al., *P1094Myocardial ischemia-reperfusion injury is reduced in MURC/Cavin-4-deficient mice*. European Heart Journal, 2017. **38**(suppl\_1).
167. Miyagawa, K., et al., *Loss of MURC/Cavin-4 induces JNK and MMP-9 activity enhancement in vascular smooth muscle cells and exacerbates abdominal aortic aneurysm*. Biochemical and biophysical research communications, 2017. **487**(3): p. 587-593.
168. Morén, B., et al., *EHD2 regulates caveolar dynamics via ATP-driven targeting and oligomerization*. Molecular biology of the cell, 2012. **23**(7): p. 1316-1329.
169. Hoernke, M., et al., *EHD2 restrains dynamics of caveolae by an ATP-dependent, membrane-bound, open conformation*. Proceedings of the National Academy of Sciences, 2017: p. 201614066.

170. Hansen, C.G., G. Howard, and B.J. Nichols, *Pacsin 2 is recruited to caveolae and functions in caveolar biogenesis*. J Cell Sci, 2011. **124**(16): p. 2777-2785.
171. Dulhunty, A.F. and C. Franzini-Armstrong, *The relative contributions of the folds and caveolae to the surface membrane of frog skeletal muscle fibres at different sarcomere lengths*. The Journal of physiology, 1975. **250**(3): p. 513-539.
172. Lo, H.P., et al., *The caveolin–cavin system plays a conserved and critical role in mechanoprotection of skeletal muscle*. J Cell Biol, 2015. **210**(5): p. 833-849.
173. Cheng, J.P., et al., *Caveolae protect endothelial cells from membrane rupture during increased cardiac output*. J Cell Biol, 2015. **211**(1): p. 53-61.
174. Rizzo, V., et al., *Recruitment of endothelial caveolae into mechanotransduction pathways by flow conditioning in vitro*. American Journal of Physiology-Heart and Circulatory Physiology, 2003. **285**(4): p. H1720-H1729.
175. Albinsson, S., et al., *Differential dependence of stretch and shear stress signaling on caveolin-1 in the vascular wall*. American Journal of Physiology-Cell Physiology, 2008. **294**(1): p. C271-C279.
176. Yamamoto, K., et al., *Visualization of flow-induced ATP release and triggering of Ca<sup>2+</sup> waves at caveolae in vascular endothelial cells*. J Cell Sci, 2011. **124**(20): p. 3477-3483.
177. Goetz, J.G., et al., *Biomechanical remodeling of the microenvironment by stromal caveolin-1 favors tumor invasion and metastasis*. Cell, 2011. **146**(1): p. 148-163.
178. Corrotte, M., et al., *Caveolae internalization repairs wounded cells and muscle fibers*. Elife, 2013. **2**: p. e00926.
179. Austin, E.D., et al., *Whole exome sequencing to identify a novel gene (caveolin-1) associated with human pulmonary arterial hypertension*. Circulation: Genomic and Precision Medicine, 2012: p. CIRCGENETICS. 111.961888.
180. Zhao, Y.-Y., et al., *Defects in caveolin-1 cause dilated cardiomyopathy and pulmonary hypertension in knockout mice*. Proceedings of the National Academy of Sciences, 2002. **99**(17): p. 11375-11380.
181. Drab, M., et al., *Loss of caveolae, vascular dysfunction, and pulmonary defects in caveolin-1 gene-disrupted mice*. Science, 2001. **293**(5539): p. 2449-2452.
182. Pelkmans, L., D. Püntener, and A. Helenius, *Local actin polymerization and dynamin recruitment in SV40-induced internalization of caveolae*. Science, 2002. **296**(5567): p. 535-539.
183. Orlandi, P.A. and P.H. Fishman, *Filipin-dependent inhibition of cholera toxin: evidence for toxin internalization and activation through caveolae-like domains*. The Journal of cell biology, 1998. **141**(4): p. 905-915.
184. Pelkmans, L., J. Kartenbeck, and A. Helenius, *Caveolar endocytosis of simian virus 40 reveals a new two-step vesicular-transport pathway to the ER*. Nat Cell Biol, 2001. **3**(5): p. 473-83.
185. Parton, R.G. and M.T. Howes, *Revisiting caveolin trafficking: the end of the caveosome*. J Cell Biol, 2010. **191**(3): p. 439-41.

186. Shvets, E., et al., *Dynamic caveolae exclude bulk membrane proteins and are required for sorting of excess glycosphingolipids*. Nature communications, 2015. **6**: p. 6867.
187. Oh, P., D.P. McIntosh, and J.E. Schnitzer, *Dynamin at the neck of caveolae mediates their budding to form transport vesicles by GTP-driven fission from the plasma membrane of endothelium*. The Journal of cell biology, 1998. **141**(1): p. 101-114.
188. Fagerholm, S., et al., *Rapid insulin-dependent endocytosis of the insulin receptor by caveolae in primary adipocytes*. PloS one, 2009. **4**(6): p. e5985.
189. Marsh, M. and A. Helenius, *Virus entry: open sesame*. Cell, 2006. **124**(4): p. 729-740.
190. Vasile, E., M. Simionescu, and N. Simionescu, *Visualization of the binding, endocytosis, and transcytosis of low-density lipoprotein in the arterial endothelium in situ*. The Journal of cell biology, 1983. **96**(6): p. 1677-1689.
191. Bendayan, M. and E.A. Rasio, *Transport of insulin and albumin by the microvascular endothelium of the rete mirabile*. Journal of Cell Science, 1996. **109**(7): p. 1857-1864.
192. Ghitescu, L., et al., *Specific binding sites for albumin restricted to plasmalemmal vesicles of continuous capillary endothelium: receptor-mediated transcytosis*. The Journal of cell biology, 1986. **102**(4): p. 1304-1311.
193. Milici, A., et al., *Transcytosis of albumin in capillary endothelium*. The Journal of Cell Biology, 1987. **105**(6): p. 2603-2612.
194. Peters, K.-R., W.W. Carley, and G.E. Palade, *Endothelial plasmalemmal vesicles have a characteristic striped bipolar surface structure*. The Journal of Cell Biology, 1985. **101**(6): p. 2233-2238.
195. Rosengren, B.-I., et al., *Transvascular protein transport in mice lacking endothelial caveolae*. American Journal of Physiology-Heart and Circulatory Physiology, 2006. **291**(3): p. H1371-H1377.
196. Rippe, B., et al., *Transendothelial transport: the vesicle controversy*. Journal of vascular research, 2002. **39**(5): p. 375-390.
197. Kim, C.A., et al., *Association of a homozygous nonsense caveolin-1 mutation with Berardinelli-Seip congenital lipodystrophy*. The Journal of Clinical Endocrinology & Metabolism, 2008. **93**(4): p. 1129-1134.
198. Kirkham, M., et al., *Evolutionary analysis and molecular dissection of caveola biogenesis*. Journal of cell science, 2008. **121**(12): p. 2075-2086.
199. Parker, S., et al., *Caveolin-2 is required for apical lipid trafficking and suppresses basolateral recycling defects in the intestine of Caenorhabditis elegans*. Molecular biology of the cell, 2009. **20**(6): p. 1763-1771.
200. Meshulam, T., et al., *Role of caveolin-1 and cholesterol in transmembrane fatty acid movement*. Biochemistry, 2006. **45**(9): p. 2882-2893.
201. Le Lay, S. and T.V. Kurzchalia, *Getting rid of caveolins: phenotypes of caveolin-deficient animals*. Biochimica et Biophysica Acta (BBA)-Molecular Cell Research, 2005. **1746**(3): p. 322-333.

202. Ariotti, N., et al., *Caveolae regulate the nanoscale organization of the plasma membrane to remotely control Ras signaling*. J Cell Biol, 2014: p. jcb. 201307055.
203. Prior, I.A., et al., *Direct visualization of Ras proteins in spatially distinct cell surface microdomains*. The Journal of cell biology, 2003. **160**(2): p. 165-170.
204. Filippini, A., G. Sica, and A. D'Alessio, *The caveolar membrane system in endothelium: From cell signaling to vascular pathology*. Journal of cellular biochemistry, 2018. **119**(7): p. 5060-5071.
205. Repetto, S., et al., *Insulin and IGF-I phosphorylate eNOS in HUVECs by a caveolin-1 dependent mechanism*. Biochemical and biophysical research communications, 2005. **337**(3): p. 849-852.
206. Yamamoto, H., H. Komekado, and A. Kikuchi, *Caveolin is necessary for Wnt-3a-dependent internalization of LRP6 and accumulation of  $\beta$ -catenin*. Developmental cell, 2006. **11**(2): p. 213-223.
207. Lin, D., et al., *Protein Kinase C $\gamma$  Regulation of Gap Junction Activity through Caveolin-1-Containing Lipid Rafts*. Investigative ophthalmology & visual science, 2003. **44**(12): p. 5259-5268.
208. Couet, J., M. Sargiacomo, and M.P. Lisanti, *Interaction of a receptor tyrosine kinase, EGF-R, with caveolins Caveolin binding negatively regulates tyrosine and serine/threonine kinase activities*. Journal of Biological Chemistry, 1997. **272**(48): p. 30429-30438.
209. Shaul, P.W., et al., *Acylation targets endothelial nitric-oxide synthase to plasmalemmal caveolae*. Journal of Biological Chemistry, 1996. **271**(11): p. 6518-6522.
210. Xie, L., et al., *Caveolin-2 is a negative regulator of anti-proliferative function and signaling of transforming growth factor-beta in endothelial cells*. Am J Physiol Cell Physiol, 2011. **301**(5): p. C1161-74.
211. Lisanti, M.P., et al., *Caveolae, caveolin and caveolin-rich membrane domains: a signalling hypothesis*. Trends in cell biology, 1994. **4**(7): p. 231-235.
212. García-Cardena, G., et al., *Endothelial nitric oxide synthase is regulated by tyrosine phosphorylation and interacts with caveolin-1*. Journal of Biological Chemistry, 1996. **271**(44): p. 27237-27240.
213. Engelman, J.A., et al., *Caveolin-mediated regulation of signaling along the p42/44 MAP kinase cascade in vivo*. FEBS letters, 1998. **428**(3): p. 205-211.
214. Collins, B.M., et al., *Structure-based reassessment of the caveolin signaling model: do caveolae regulate signaling through caveolin-protein interactions?* Developmental cell, 2012. **23**(1): p. 11-20.
215. Bauer, P.M., et al., *Endothelial-specific expression of caveolin-1 impairs microvascular permeability and angiogenesis*. Proceedings of the National Academy of Sciences of the United States of America, 2005. **102**(1): p. 204-209.
216. Patel, H., F. Murray, and P. Insel, *G-protein-coupled receptor-signaling components in membrane raft and caveolae microdomains*, in *Protein-Protein Interactions as New Drug Targets*. 2008, Springer. p. 167-184.
217. Escriche, M., et al., *Ligand-induced caveolae-mediated internalization of A1 adenosine receptors: morphological evidence of endosomal sorting and receptor recycling*. Experimental cell research, 2003. **285**(1): p. 72-90.

218. Sands, W.A. and T.M. Palmer, *Adenosine receptors and the control of endothelial cell function in inflammatory disease*. Immunology letters, 2005. **101**(1): p. 1-11.
219. Jeltsch, M., et al., *Receptor tyrosine kinase-mediated angiogenesis*. Cold Spring Harbor perspectives in biology, 2013. **5**(9): p. a009183.
220. Dietzen, D.J., W.R. Hastings, and D.M. Lublin, *Caveolin is palmitoylated on multiple cysteine residues. Palmitoylation is not necessary for localization of caveolin to caveolae*. J Biol Chem, 1995. **270**(12): p. 6838-42.
221. Bernatchez, P., et al., *A noninhibitory mutant of the caveolin-1 scaffolding domain enhances eNOS-derived NO synthesis and vasodilation in mice*. The Journal of clinical investigation, 2011. **121**(9).
222. Guidotti, G., *Membrane Proteins*. Annual Review of Biochemistry, 1972. **41**(1): p. 731-752.
223. Ahram, M., et al., *Estimation of membrane proteins in the human proteome*. In Silico Biol, 2006. **6**(5): p. 379-86.
224. Overington, J.P., B. Al-Lazikani, and A.L. Hopkins, *How many drug targets are there?* Nat Rev Drug Discov, 2006. **5**(12): p. 993-6.
225. Moraes, I., et al., *Membrane protein structure determination — The next generation*. Biochimica et Biophysica Acta (BBA) - Biomembranes, 2014. **1838**(1): p. 78-87.
226. Rawlings, A.E., *Membrane proteins: always an insoluble problem?* Biochemical Society Transactions, 2016. **44**(3): p. 790-795.
227. Bazan, J.F., *A novel family of growth factor receptors: a common binding domain in the growth hormone, prolactin, erythropoietin and IL-6 receptors, and the p75 IL-2 receptor  $\beta$ -chain*. Biochemical and biophysical research communications, 1989. **164**(2): p. 788-795.
228. Bazan, J.F., *Haemopoietic receptors and helical cytokines*. Immunology today, 1990. **11**: p. 350-354.
229. Tedgui, A. and Z. Mallat, *Cytokines in atherosclerosis: pathogenic and regulatory pathways*. Physiological reviews, 2006. **86**(2): p. 515-581.
230. Steiner, G., et al., *Cytokine production by synovial T cells in rheumatoid arthritis*. Rheumatology (Oxford, England), 1999. **38**(3): p. 202-213.
231. Lovato, P., et al., *Constitutive STAT3 activation in intestinal T cells from patients with Crohn's disease*. Journal of Biological Chemistry, 2003. **278**(19): p. 16777-16781.
232. Moss, J.W.E. and D.P. Ramji, *Chapter 6 - Cytokines in Atherosclerosis*, in *Cytokine Effector Functions in Tissues*, M. Foti and M. Locati, Editors. 2017, Academic Press. p. 109-118.
233. Steinke, J.W. and L. Borish, *3. Cytokines and chemokines*. Journal of Allergy and Clinical Immunology, 2006. **117**(2): p. S441-S445.
234. Fitzgerald, K.A., et al., *The cytokine factsbook and webfacts*. 2001: Elsevier.
235. Stroud, R.M. and J.A. Wells, *Mechanistic diversity of cytokine receptor signaling across cell membranes*. Sci. STKE, 2004. **2004**(231): p. re7-re7.
236. Wang, X., et al., *Structural biology of shared cytokine receptors*. Annual review of immunology, 2009. **27**: p. 29-60.
237. Ihle, J.N., et al., *Signaling through the hematopoietic cytokine receptors*. Annual review of immunology, 1995. **13**(1): p. 369-398.

238. Levy, D.E. and J. Darnell Jr, *Signalling: Stats: transcriptional control and biological impact*. Nature reviews Molecular cell biology, 2002. **3**(9): p. 651.
239. Schindler, U., T. Hoey, and S.L. McKnight, *Differentiation of T-helper lymphocytes: selective regulation by members of the STAT family of transcription factors*. Genes to Cells, 1996. **1**(6): p. 507-515.
240. Murray, P.J., *The JAK-STAT signaling pathway: input and output integration*. The Journal of Immunology, 2007. **178**(5): p. 2623-2629.
241. Plataniias, L.C., *Mechanisms of type-I-and type-II-interferon-mediated signalling*. Nature Reviews Immunology, 2005. **5**(5): p. 375.
242. Gough, D.J., et al., *IFN $\gamma$  signaling—Does it mean JAK–STAT?* Cytokine & growth factor reviews, 2008. **19**(5-6): p. 383-394.
243. Ozaki, K. and W.J. Leonard, *Cytokine and cytokine receptor pleiotropy and redundancy*. Journal of Biological Chemistry, 2002. **277**(33): p. 29355-29358.
244. Zurawski, S.M., et al., *Receptors for interleukin-13 and interleukin-4 are complex and share a novel component that functions in signal transduction*. The EMBO journal, 1993. **12**(7): p. 2663-2670.
245. Pestka, S., et al., *Interleukin-10 and related cytokines and receptors*. Annu. Rev. Immunol., 2004. **22**: p. 929-979.
246. Pestka, S., C.D. Krause, and M.R. Walter, *Interferons, interferon-like cytokines, and their receptors*. Immunological reviews, 2004. **202**(1): p. 8-32.
247. Delgoffe, G.M., P.J. Murray, and D.A. Vignali, *Interpreting mixed signals: the cell's cytokine conundrum*. Current opinion in immunology, 2011. **23**(5): p. 632-638.
248. Hunter, C.A. and R. Kastelein, *New paradigms in inflammation: where to next?* Immunological reviews, 2008. **226**(1): p. 6-9.
249. Mosser, D.M. and X. Zhang, *Interleukin-10: new perspectives on an old cytokine*. Immunological reviews, 2008. **226**(1): p. 205-218.
250. Borden, E.C., et al., *Interferons at age 50: past, current and future impact on biomedicine*. Nature reviews Drug discovery, 2007. **6**(12): p. 975.
251. Piehler, J., et al., *Structural and dynamic determinants of type I interferon receptor assembly and their functional interpretation*. Immunological reviews, 2012. **250**(1): p. 317-334.
252. Sehgal, P.B., et al., *Cytokine signaling: STATS in plasma membrane rafts*. Journal of Biological Chemistry, 2002.
253. Tai, Y.-T., et al., *Insulin-like growth factor-1 induces adhesion and migration in human multiple myeloma cells via activation of  $\beta$ 1-integrin and phosphatidylinositol 3'-kinase/AKT signaling*. Cancer research, 2003. **63**(18): p. 5850-5858.
254. Elsasser, T.H., et al., *Caveolae nitration of Janus kinase-2 at the 1007Y-1008Y site: coordinating inflammatory response and metabolic hormone readjustment within the somatotrophic axis*. Endocrinology, 2007. **148**(8): p. 3803-3813.
255. Stark, G.R., et al., *How cells respond to interferons*. 1998, Annual Reviews 4139 El Camino Way, PO Box 10139, Palo Alto, CA 94303-0139, USA.
256. Darnell, J.E., *STATs and gene regulation*. Science, 1997. **277**(5332): p. 1630-1635.

257. Fu, X.-Y. and J.-J. Zhang, *Transcription factor p91 interacts with the epidermal growth factor receptor and mediates activation of the c-fos gene promoter*. *Cell*, 1993. **74**(6): p. 1135-1145.
258. Darnell, J.E., I.M. Kerr, and G.R. Stark, *Jak-STAT pathways and transcriptional activation in response to IFNs and other extracellular signaling proteins*. *Science*, 1994. **264**(5164): p. 1415-1421.
259. Igaz, P., S. Toth, and A. Falus, *Biological and clinical significance of the JAK-STAT pathway; lessons from knockout mice*. *Inflammation Research*, 2001. **50**(9): p. 435-441.
260. O'Shea, J.J., *Jaks, STATs, cytokine signal transduction, and immunoregulation: are we there yet?* *Immunity*, 1997. **7**(1): p. 1-11.
261. Levy, D.E. and I.J. Marié, *STATus report on tetramers*. *Immunity*, 2012. **36**(4): p. 553-555.
262. O'Shea, J.J., et al., *The JAK-STAT pathway: impact on human disease and therapeutic intervention*. *Annual review of medicine*, 2015. **66**: p. 311-328.
263. Shuai, K. and B. Liu, *Regulation of JAK–STAT signalling in the immune system*. *Nature Reviews Immunology*, 2003. **3**(11): p. 900.
264. Neel, B.G. *Structure and function of SH2-domain containing tyrosine phosphatases*. in *Seminars in cell biology*. 1993. Elsevier.
265. Selimoglu-Buet, D., et al., *Oncogenic kit triggers Shp2/Erk1/2 pathway to down-regulate the pro-apoptotic protein Bim and to promote apoptosis resistance in leukemic cells*. *PLoS one*, 2012. **7**(11): p. e49052.
266. Zhang, S.Q., et al., *Receptor-specific regulation of phosphatidylinositol 3'-kinase activation by the protein tyrosine phosphatase Shp2*. *Mol Cell Biol*, 2002. **22**(12): p. 4062-72.
267. Klingmüller, U., et al., *Specific recruitment of SH-PTP1 to the erythropoietin receptor causes inactivation of JAK2 and termination of proliferative signals*. *Cell*, 1995. **80**(5): p. 729-738.
268. David, M., et al., *Differential regulation of the alpha/beta interferon-stimulated Jak/Stat pathway by the SH2 domain-containing tyrosine phosphatase SHPTP1*. *Molecular and cellular biology*, 1995. **15**(12): p. 7050-7058.
269. Myers, M.P., et al., *TYK2 and JAK2 are substrates of protein-tyrosine phosphatase 1B*. *Journal of Biological Chemistry*, 2001. **276**(51): p. 47771-47774.
270. Simoncic, P.D., et al., *The T cell protein tyrosine phosphatase is a negative regulator of janus family kinases 1 and 3*. *Current biology*, 2002. **12**(6): p. 446-453.
271. Xu, D. and C.-K. Qu, *Protein tyrosine phosphatases in the JAK/STAT pathway*. *Frontiers in bioscience: a journal and virtual library*, 2008. **13**: p. 4925.
272. Liu, B., et al., *Inhibition of Stat1-mediated gene activation by PIAS1*. *Proceedings of the National Academy of Sciences*, 1998. **95**(18): p. 10626-10631.
273. Liu, B., et al., *PIAS1 selectively inhibits interferon-inducible genes and is important in innate immunity*. *Nature immunology*, 2004. **5**(9): p. 891.
274. Chung, C.D., et al., *Specific inhibition of Stat3 signal transduction by PIAS3*. *Science*, 1997. **278**(5344): p. 1803-1805.

275. Arora, T., et al., *PIASx is a transcriptional co-repressor of signal transducer and activator of transcription 4*. Journal of Biological Chemistry, 2003. **278**(24): p. 21327-21330.
276. Liu, B., et al., *A transcriptional corepressor of Stat1 with an essential LXXLL signature motif*. Proceedings of the National Academy of Sciences, 2001. **98**(6): p. 3203-3207.
277. Liao, J., Y. Fu, and K. Shuai, *Distinct roles of the NH<sub>2</sub>-and COOH-terminal domains of the protein inhibitor of activated signal transducer and activator of transcription (STAT) 1 (PIAS1) in cytokine-induced PIAS1-Stat1 interaction*. Proceedings of the National Academy of Sciences, 2000. **97**(10): p. 5267-5272.
278. Shuai, K. and B. Liu, *Regulation of gene-activation pathways by PIAS proteins in the immune system*. Nature Reviews Immunology, 2005. **5**(8): p. 593.
279. Yoshimura, A., et al., *A novel cytokine-inducible gene CIS encodes an SH2-containing protein that binds to tyrosine-phosphorylated interleukin 3 and erythropoietin receptors*. The EMBO journal, 1995. **14**(12): p. 2816-2826.
280. Endo, T.A., et al., *A new protein containing an SH2 domain that inhibits JAK kinases*. Nature, 1997. **387**(6636): p. 921.
281. Naka, T., et al., *Structure and function of a new STAT-induced STAT inhibitor*. Nature, 1997. **387**(6636): p. 924.
282. Kile, B.T., et al., *The SOCS box: a tale of destruction and degradation*. Trends in biochemical sciences, 2002. **27**(5): p. 235-241.
283. Zhang, J.-G., et al., *The conserved SOCS box motif in suppressors of cytokine signaling binds to elongins B and C and may couple bound proteins to proteasomal degradation*. Proceedings of the National Academy of Sciences, 1999. **96**(5): p. 2071-2076.
284. Babon, J.J., et al., *The SOCS box encodes a hierarchy of affinities for Cullin5: implications for ubiquitin ligase formation and cytokine signalling suppression*. Journal of molecular biology, 2009. **387**(1): p. 162-174.
285. Galic, S., et al., *Suppressor of cytokine signalling (SOCS) proteins as guardians of inflammatory responses critical for regulating insulin sensitivity*. Biochemical Journal, 2014. **461**(2): p. 177-188.
286. Akhtar, L.N. and E.N. Benveniste, *Viral exploitation of host SOCS protein functions*. Journal of Virology, 2011. **85**(5): p. 1912-1921.
287. Fletcher, T.C., A. DiGiandomenico, and J. Hawiger, *Extended anti-inflammatory action of a degradation-resistant mutant of cell-penetrating suppressor of cytokine signaling 3*. Journal of Biological Chemistry, 2010. **285**(24): p. 18727-18736.
288. Nicholson, S.E., et al., *Mutational analyses of the SOCS proteins suggest a dual domain requirement but distinct mechanisms for inhibition of LIF and IL-6 signal transduction*. The EMBO journal, 1999. **18**(2): p. 375-385.
289. Sasaki, A., et al., *CIS3/SOCS-3 suppresses erythropoietin (EPO) signaling by binding the EPO receptor and JAK2*. Journal of Biological Chemistry, 2000. **275**(38): p. 29338-29347.
290. Starr, R., et al., *Liver degeneration and lymphoid deficiencies in mice lacking suppressor of cytokine signaling-1*. Proceedings of the National Academy of Sciences, 1998. **95**(24): p. 14395-14399.

291. Metcalf, D., et al., *Gigantism in mice lacking suppressor of cytokine signalling-2*. *Nature*, 2000. **405**(6790): p. 1069.
292. Marine, J.-C., et al., *SOCS3 is essential in the regulation of fetal liver erythropoiesis*. *Cell*, 1999. **98**(5): p. 617-627.
293. Roberts, A.W., et al., *Placental defects and embryonic lethality in mice lacking suppressor of cytokine signaling 3*. *Proceedings of the national academy of sciences*, 2001. **98**(16): p. 9324-9329.
294. Yoshimura, A., T. Naka, and M. Kubo, *SOCS proteins, cytokine signalling and immune regulation*. *Nature Reviews Immunology*, 2007. **7**(6): p. 454.
295. Lang, R., et al., *SOCS3 regulates the plasticity of gp130 signaling*. *Nature immunology*, 2003. **4**(6): p. 546.
296. Croker, B.A., et al., *SOCS3 negatively regulates IL-6 signaling in vivo*. *Nature immunology*, 2003. **4**(6): p. 540.
297. Takahashi, R., et al., *SOCS1 is essential for regulatory T cell functions by preventing loss of Foxp3 expression as well as IFN- $\gamma$  and IL-17A production*. *Journal of Experimental Medicine*, 2011: p. jem. 20110428.
298. Luckey, M.A., et al., *The transcription factor ThPOK suppresses Runx3 and imposes CD4+ lineage fate by inducing the SOCS suppressors of cytokine signaling*. *Nature immunology*, 2014. **15**(7): p. 638.
299. Spence, S., et al., *Suppressors of cytokine signaling 2 and 3 diametrically control macrophage polarisation*. *Immunology*, 2012. **137**: p. 282-283.
300. Tannahill, G.M., et al., *SOCS2 can enhance interleukin-2 (IL-2) and IL-3 signaling by accelerating SOCS3 degradation*. *Molecular and cellular biology*, 2005. **25**(20): p. 9115-9126.
301. Yasukawa, H., et al., *IL-6 induces an anti-inflammatory response in the absence of SOCS3 in macrophages*. *Nat Immunol*, 2003. **4**(6): p. 551-6.
302. Naka, T., et al., *Negative regulation of cytokine and TLR signalings by SOCS and others*. *Advances in immunology*, 2005. **87**: p. 61-122.
303. Flores-Morales, A., et al., *Negative regulation of growth hormone receptor signaling*. *Molecular endocrinology*, 2006. **20**(2): p. 241-253.
304. Sands, W.A., et al., *Exchange protein activated by cyclic AMP (Epac)-mediated induction of suppressor of cytokine signaling 3 (SOCS-3) in vascular endothelial cells*. *Molecular and cellular biology*, 2006. **26**(17): p. 6333-6346.
305. Eulendorf, R., et al., *Interleukin-6 signalling: more than Jaks and STATs*. *European journal of cell biology*, 2012. **91**(6-7): p. 486-495.
306. Lehmann, U., et al., *SHP2 and SOCS3 contribute to Tyr-759-dependent attenuation of interleukin-6 signaling through gp130*. *Journal of Biological Chemistry*, 2003. **278**(1): p. 661-671.
307. Williams, J.J., K. Munro, and T.M. Palmer, *Role of ubiquitylation in controlling suppressor of cytokine signalling 3 (SOCS3) function and expression*. *Cells*, 2014. **3**(2): p. 546-562.
308. Piessevaux, J., et al., *The many faces of the SOCS box*. *Cytokine & growth factor reviews*, 2008. **19**(5-6): p. 371-381.
309. Williams, J.J. and T.M. Palmer, *Unbiased identification of substrates for the Epac1-inducible E3 ubiquitin ligase component SOCS-3*. *Biochem Soc Trans*, 2012. **40**(1): p. 215-8.
310. Sasaki, A., et al., *Cytokine-inducible SH2 protein-3 (CIS3/SOCS3) inhibits Janus tyrosine kinase by binding through the N-terminal kinase*

- inhibitory region as well as SH2 domain.* Genes to Cells, 1999. **4**(6): p. 339-351.
311. Babon, J.J., et al., *The structure of SOCS3 reveals the basis of the extended SH2 domain function and identifies an unstructured insertion that regulates stability.* Molecular cell, 2006. **22**(2): p. 205-216.
  312. Bergamin, E., J. Wu, and S.R. Hubbard, *Structural basis for phosphotyrosine recognition by suppressor of cytokine signaling-3.* Structure, 2006. **14**(8): p. 1285-1292.
  313. Babon, J.J. and N.A. Nicola, *The biology and mechanism of action of suppressor of cytokine signaling 3.* Growth Factors, 2012. **30**(4): p. 207-219.
  314. Yasukawa, H., et al., *The JAK-binding protein JAB inhibits Janus tyrosine kinase activity through binding in the activation loop.* The EMBO journal, 1999. **18**(5): p. 1309-1320.
  315. Babon, J.J., et al., *Suppression of cytokine signaling by SOCS3: characterization of the mode of inhibition and the basis of its specificity.* Immunity, 2012. **36**(2): p. 239-250.
  316. Nicholson, S.E., et al., *Suppressor of cytokine signaling-3 preferentially binds to the SHP-2-binding site on the shared cytokine receptor subunit gp130.* Proceedings of the National Academy of Sciences, 2000. **97**(12): p. 6493-6498.
  317. De Souza, D., et al., *SH2 domains from suppressor of cytokine signaling-3 and protein tyrosine phosphatase SHP-2 have similar binding specificities.* Biochemistry, 2002. **41**(29): p. 9229-9236.
  318. Dunn, S.L., et al., *Feedback inhibition of leptin receptor/Jak2 signaling via Tyr1138 of the leptin receptor and suppressor of cytokine signaling 3.* Molecular endocrinology, 2005. **19**(4): p. 925-938.
  319. Hörtnner, M., et al., *Suppressor of cytokine signaling-3 is recruited to the activated granulocyte-colony stimulating factor receptor and modulates its signal transduction.* The Journal of Immunology, 2002. **169**(3): p. 1219-1227.
  320. Ram, P.A. and D.J. Waxman, *SOCS/CIS protein inhibition of growth hormone-stimulated STAT5 signaling by multiple mechanisms.* Journal of Biological Chemistry, 1999. **274**(50): p. 35553-35561.
  321. Emanuelli, B., et al., *SOCS-3 is an insulin-induced negative regulator of insulin signaling.* Journal of Biological Chemistry, 2000. **275**(21): p. 15985-15991.
  322. Yamamoto, K., et al., *SOCS-3 inhibits IL-12-induced STAT4 activation by binding through its SH2 domain to the STAT4 docking site in the IL-12 receptor  $\beta$ 2 subunit.* Biochemical and biophysical research communications, 2003. **310**(4): p. 1188-1193.
  323. Kershaw, N.J., et al., *SOCS3 binds specific receptor–JAK complexes to control cytokine signaling by direct kinase inhibition.* Nature Structural and Molecular Biology, 2013. **20**(4): p. 469.
  324. White, C.A. and N.A. Nicola, *SOCS3: An essential physiological inhibitor of signaling by interleukin-6 and G-CSF family cytokines.* Jak-Stat, 2013. **2**(4): p. e25045.
  325. Babon, J.J., et al., *Secondary structure assignment of mouse SOCS3 by NMR defines the domain boundaries and identifies an unstructured insertion in the SH2 domain.* The FEBS journal, 2005. **272**(23): p. 6120-6130.

326. Linossi, E.M. and S.E. Nicholson, *The SOCS box—adapting proteins for ubiquitination and proteasomal degradation*. IUBMB life, 2012. **64**(4): p. 316-323.
327. Babon, J.J., et al., *The SOCS box domain of SOCS3: structure and interaction with the elonginBC-cullin5 ubiquitin ligase*. Journal of molecular biology, 2008. **381**(4): p. 928-940.
328. Ehltling, C. and D. Häussinger, *Sp3 is involved in the regulation of SOCS3 gene expression*. Biochemical Journal, 2005. **387**(3): p. 737-745.
329. Qin, H., et al., *Molecular mechanism of lipopolysaccharide-induced SOCS-3 gene expression in macrophages and microglia*. The Journal of Immunology, 2007. **179**(9): p. 5966-5976.
330. Ehltling, C., et al., *Regulation of suppressor of cytokine signaling 3 (SOCS3) mRNA stability by TNF- $\alpha$  involves activation of the MKK6/p38MAPK/MK2 cascade*. The Journal of Immunology, 2007. **178**(5): p. 2813-2826.
331. Wong, P.K., et al., *SOCS-3 negatively regulates innate and adaptive immune mechanisms in acute IL-1–dependent inflammatory arthritis*. The Journal of clinical investigation, 2006. **116**(6): p. 1571-1581.
332. Lejeune, D., J.-B. Demoulin, and J.-C. Renauld, *Interleukin 9 induces expression of three cytokine signal inhibitors: cytokine-inducible SH2-containing protein, suppressor of cytokine signalling (SOCS)-2 and SOCS-3, but only SOCS-3 overexpression suppresses interleukin 9 signalling*. Biochemical Journal, 2001. **353**(1): p. 109-116.
333. Cassatella, M.A., et al., *Interleukin-10 (IL-10) selectively enhances CIS3/SOCS3 mRNA expression in human neutrophils: evidence for an IL-10–induced pathway that is independent of STAT protein activation*. Blood, 1999. **94**(8): p. 2880-2889.
334. Bjørnbæk, C., et al., *Identification of SOCS-3 as a potential mediator of central leptin resistance*. Molecular cell, 1998. **1**(4): p. 619-625.
335. Jegalian, A.G. and H. Wu, *Regulation of Socs gene expression by the proto-oncoprotein GFI-1B two routes for stat5 target gene induction by erythropoietin*. Journal of Biological Chemistry, 2002. **277**(3): p. 2345-2352.
336. Ma, Z., et al., *Mutations of HNF-1 $\beta$  inhibit epithelial morphogenesis through dysregulation of SOCS-3*. Proceedings of the National Academy of Sciences, 2007. **104**(51): p. 20386-20391.
337. Qin, H., et al., *TGF- $\beta$  promotes Th17 cell development through inhibition of SOCS3*. The Journal of Immunology, 2009. **183**(1): p. 97-105.
338. Sasaki, A., et al., *The N-terminal truncated isoform of SOCS3 translated from an alternative initiation AUG codon under stress conditions is stable due to the lack of a major ubiquitination site, Lys-6*. Journal of Biological Chemistry, 2002.
339. Piessevaux, J., et al., *Functional cross-modulation between SOCS proteins can stimulate cytokine signalling*. Journal of Biological Chemistry, 2006.
340. Kiu, H.I.U., et al., *Regulation of Multiple Cytokine Signalling Pathways by SOCS3 is Independent of SOCS2*. Growth factors (Chur, Switzerland), 2009. **27**(6): p. 384-393.

341. Lucet, I.S., et al., *The structural basis of Janus kinase 2 inhibition by a potent and specific pan-Janus kinase inhibitor*. *Blood*, 2006. **107**(1): p. 176-183.
342. Hu, H. and S.-C. Sun, *Ubiquitin signaling in immune responses*. *Cell research*, 2016. **26**(4): p. 457.
343. Kamura, T., et al., *VHL-box and SOCS-box domains determine binding specificity for Cul2-Rbx1 and Cul5-Rbx2 modules of ubiquitin ligases*. *Genes & development*, 2004. **18**(24): p. 3055-3065.
344. Johnston, J.A., *Are SOCS suppressors, regulators, and degraders?* *Journal of leukocyte biology*, 2004. **75**(5): p. 743-748.
345. Zhang, J.-G., et al., *The SOCS box of suppressor of cytokine signaling-1 is important for inhibition of cytokine action in vivo*. *Proceedings of the National Academy of Sciences*, 2001. **98**(23): p. 13261-13265.
346. Boyle, K., et al., *The SOCS box of suppressor of cytokine signaling-3 contributes to the control of G-CSF responsiveness in vivo*. *Blood*, 2007. **110**(5): p. 1466-1474.
347. Boyle, K., et al., *Deletion of the SOCS box of suppressor of cytokine signaling 3 (SOCS3) in embryonic stem cells reveals SOCS box-dependent regulation of JAK but not STAT phosphorylation*. *Cellular signalling*, 2009. **21**(3): p. 394-404.
348. Orr, S.J., et al., *SOCS3 targets Siglec 7 for proteasomal degradation and blocks Siglec 7-mediated responses*. *J Biol Chem*, 2007. **282**(6): p. 3418-22.
349. Irandoust, M.I., et al., *Suppressor of cytokine signaling 3 controls lysosomal routing of G-CSF receptor*. *The EMBO journal*, 2007. **26**(7): p. 1782-1793.
350. Wolfler, A., et al., *Site-specific ubiquitination determines lysosomal sorting and signal attenuation of the granulocyte colony-stimulating factor receptor*. *Traffic*, 2009. **10**(8): p. 1168-79.
351. van de Geijn, G.-J.M., J. Gits, and I.P. Touw, *Distinct activities of suppressor of cytokine signaling (SOCS) proteins and involvement of the SOCS box in controlling G-CSF signaling*. *JOURNAL OF LEUKOCYTE BIOLOGY.*, 2004. **76**: p. 237-244.
352. van de Geijn, G.-J.M., et al., *G-CSF receptor truncations found in SCN/AML relieve SOCS3-controlled inhibition of STAT5 but leave suppression of STAT3 intact*. *Blood*, 2004. **104**(3): p. 667-674.
353. Kawaguchi, T., et al., *Hepatitis C virus down-regulates insulin receptor substrates 1 and 2 through up-regulation of suppressor of cytokine signaling 3*. *The American journal of pathology*, 2004. **165**(5): p. 1499-1508.
354. Ionomou, M. and D.N. Saunders, *Systematic approaches to identify E3 ligase substrates*. *Biochem J*, 2016. **473**(22): p. 4083-4101.
355. Meierhofer, D., et al., *Quantitative analysis of global ubiquitination in HeLa cells by mass spectrometry*. *J Proteome Res*, 2008. **7**(10): p. 4566-76.
356. Williams, J.J.L., et al., *Interaction of suppressor of cytokine signalling 3 with cavin-1 links SOCS3 function and cavin-1 stability*. *Nature Communications*, 2018. **9**: p. 168.
357. Krump-Konvalinkova, V., et al., *Establishment and characterization of an angiosarcoma-derived cell line, AS-M*. *Endothelium*, 2003. **10**(6): p. 319-28.

358. Smith, P.K., et al., *Measurement of protein using bicinchoninic acid*. Anal Biochem, 1985. **150**(1): p. 76-85.
359. Livak, K.J. and T.D. Schmittgen, *Analysis of relative gene expression data using real-time quantitative PCR and the 2(-Delta Delta C(T)) Method*. Methods, 2001. **25**(4): p. 402-8.
360. Estep, J.A., et al., *Immunoblot screening of CRISPR/Cas9-mediated gene knockouts without selection*. BMC Mol Biol, 2016. **17**: p. 9.
361. Carroll, D., *Genome engineering with targetable nucleases*. Annual review of biochemistry, 2014. **83**: p. 409-439.
362. Gaj, T., C.A. Gersbach, and C.F. Barbas, 3rd, *ZFN, TALEN, and CRISPR/Cas-based methods for genome engineering*. Trends Biotechnol, 2013. **31**(7): p. 397-405.
363. Ahmad, G. and M. Amiji, *Use of CRISPR/Cas9 gene-editing tools for developing models in drug discovery*. Drug Discov Today, 2018. **23**(3): p. 519-533.
364. Malina, A., et al., *Repurposing CRISPR/Cas9 for in situ functional assays*. Genes & development, 2013. **27**(23): p. 2602-2614.
365. David, F. and V. Siewers, *Advances in yeast genome engineering*. FEMS Yeast Res, 2015. **15**(1): p. 1-14.
366. Sander, J.D. and J.K. Joung, *CRISPR-Cas systems for editing, regulating and targeting genomes*. Nat Biotechnol, 2014. **32**(4): p. 347-55.
367. Ishino, Y., et al., *Nucleotide sequence of the iap gene, responsible for alkaline phosphatase isozyme conversion in Escherichia coli, and identification of the gene product*. Journal of bacteriology, 1987. **169**(12): p. 5429-5433.
368. Mojica, F.J., et al., *Biological significance of a family of regularly spaced repeats in the genomes of Archaea, Bacteria and mitochondria*. Molecular microbiology, 2000. **36**(1): p. 244-246.
369. Lander, E.S., *The Heroes of CRISPR*. Cell, 2016. **164**(1-2): p. 18-28.
370. Bolotin, A., et al., *Clustered regularly interspaced short palindrome repeats (CRISPRs) have spacers of extrachromosomal origin*. Microbiology, 2005. **151**(8): p. 2551-2561.
371. Danese, S., E. Dejana, and C. Fiocchi, *Immune regulation by microvascular endothelial cells: directing innate and adaptive immunity, coagulation, and inflammation*. J Immunol, 2007. **178**(10): p. 6017-22.
372. Chi, J.T., et al., *Endothelial cell diversity revealed by global expression profiling*. Proc Natl Acad Sci U S A, 2003. **100**(19): p. 10623-8.
373. Unger, R.E., et al., *In vitro expression of the endothelial phenotype: comparative study of primary isolated cells and cell lines, including the novel cell line HPMEC-ST1.6R*. Microvasc Res, 2002. **64**(3): p. 384-97.
374. Krump-Konvalinkova, V., et al., *Stable knock-down of the sphingosine 1-phosphate receptor S1P1 influences multiple functions of human endothelial cells*. Arterioscler Thromb Vasc Biol, 2005. **25**(3): p. 546-52.
375. Voyta, J.C., et al., *Identification and isolation of endothelial cells based on their increased uptake of acetylated-low density lipoprotein*. J Cell Biol, 1984. **99**(6): p. 2034-40.
376. Gordon, P.B., Sussman, II, and V.B. Hatcher, *Long-term culture of human endothelial cells*. In Vitro, 1983. **19**(9): p. 661-71.

377. Sanjana, N.E., O. Shalem, and F. Zhang, *Improved vectors and genome-wide libraries for CRISPR screening*. Nat Methods, 2014. **11**(8): p. 783-784.
378. Shalem, O., et al., *Genome-scale CRISPR-Cas9 knockout screening in human cells*. Science, 2014. **343**(6166): p. 84-87.
379. Santa Cruz Biotechnology Inc. *SOCS-3 CRISPR/Cas9 KO Plasmid (h2): sc-400455-KO-2*. 2018 [cited 2018 October, 10]; Available from: <https://datasheets.scbt.com/sc-400455-KO-2.pdf>.
380. Ran, F.A., et al., *Genome engineering using the CRISPR-Cas9 system*. Nat Protoc, 2013. **8**(11): p. 2281-2308.
381. Santa Cruz Biotechnology Inc. *Contact Santa Cruz Biotechnology*. 2018 [cited 2018 October, 10]; Available from: <https://www.scbt.com/scbt/customer-care/contact-us>.
382. Genetics Home Reference. *SOCS3 suppressor of cytokine signaling 3 [Homo sapiens (human)]*. 2018 [cited 2018 November, 29]; Available from: <https://ghr.nlm.nih.gov/gene/SOCS3#location>.
383. Shakhbazau, A., et al., *Transfection efficiencies of PAMAM dendrimers correlate inversely with their hydrophobicity*. Int J Pharm, 2010. **383**(1-2): p. 228-35.
384. Fass, D.M., J.E. Butler, and R.H. Goodman, *Deacetylase activity is required for cAMP activation of a subset of CREB target genes*. J Biol Chem, 2003. **278**(44): p. 43014-9.
385. Kamezaki, K., et al., *Roles of Stat3 and ERK in G-CSF signaling*. Stem Cells, 2005. **23**(2): p. 252-63.
386. Koeberlein, B., et al., *Hepatitis B virus overexpresses suppressor of cytokine signaling-3 (SOCS3) thereby contributing to severity of inflammation in the liver*. Virus Res, 2010. **148**(1-2): p. 51-9.
387. Uto-Konomi, A., et al., *Dysregulation of suppressor of cytokine signaling 3 in keratinocytes causes skin inflammation mediated by interleukin-20 receptor-related cytokines*. PLoS One, 2012. **7**(7): p. e40343.
388. Yasukawa, H., et al., *Suppressor of cytokine signaling-3 is a biomechanical stress-inducible gene that suppresses gp130-mediated cardiac myocyte hypertrophy and survival pathways*. J Clin Invest, 2001. **108**(10): p. 1459-67.
389. Yajima, T., et al., *Absence of SOCS3 in the cardiomyocyte increases mortality in a gp130-dependent manner accompanied by contractile dysfunction and ventricular arrhythmias*. Circulation, 2011. **124**(24): p. 2690-701.
390. O'shea, J.J. and P.J. Murray, *Cytokine signaling modules in inflammatory responses*. Immunity, 2008. **28**(4): p. 477-487.
391. Schwartz, A.L. and A. Ciechanover, *The ubiquitin-proteasome pathway and pathogenesis of human diseases*. Annu Rev Med, 1999. **50**: p. 57-74.
392. Turriziani, B., A. von Kriegsheim, and S.R. Pennington, *Protein-Protein Interaction Detection Via Mass Spectrometry-Based Proteomics*. Adv Exp Med Biol, 2016. **919**: p. 383-396.
393. Sampieri, C.L., et al., *Activation of p38 and JNK MAPK pathways abrogates requirement for new protein synthesis for phorbol ester mediated induction of select MMP and TIMP genes*. Matrix Biol, 2008. **27**(2): p. 128-38.

394. Grollman, A.P. and M.T. Huang, *Inhibitors of protein synthesis in eukaryotes: tools in cell research*. Fed Proc, 1973. **32**(6): p. 1673-8.
395. Serezani, C.H., et al., *Cyclic AMP: master regulator of innate immune cell function*. Am J Respir Cell Mol Biol, 2008. **39**(2): p. 127-32.
396. Conti, M. and J. Beavo, *Biochemistry and physiology of cyclic nucleotide phosphodiesterases: essential components in cyclic nucleotide signaling*. Annu Rev Biochem, 2007. **76**: p. 481-511.
397. Walsh, D.A., J.P. Perkins, and E.G. Krebs, *An adenosine 3',5'-monophosphate-dependant protein kinase from rabbit skeletal muscle*. J Biol Chem, 1968. **243**(13): p. 3763-5.
398. Shabb, J.B., *Physiological substrates of cAMP-dependent protein kinase*. Chem Rev, 2001. **101**(8): p. 2381-411.
399. Sassone-Corsi, P., *Transcription factors responsive to cAMP*. Annu Rev Cell Dev Biol, 1995. **11**: p. 355-77.
400. Delghandi, M.P., M. Johannessen, and U. Moens, *The cAMP signalling pathway activates CREB through PKA, p38 and MSK1 in NIH 3T3 cells*. Cell Signal, 2005. **17**(11): p. 1343-51.
401. Mayr, B. and M. Montminy, *Transcriptional regulation by the phosphorylation-dependent factor CREB*. Nat Rev Mol Cell Biol, 2001. **2**(8): p. 599-609.
402. de Rooij, J., et al., *Epac is a Rap1 guanine-nucleotide-exchange factor directly activated by cyclic AMP*. Nature, 1998. **396**(6710): p. 474-7.
403. Kawasaki, H., et al., *A family of cAMP-binding proteins that directly activate Rap1*. Science, 1998. **282**(5397): p. 2275-9.
404. Woolson, H.D., et al., *Selective inhibition of cytokine-activated extracellular signal-regulated kinase by cyclic AMP via Epac1-dependent induction of suppressor of cytokine signalling-3*. Cell Signal, 2009. **21**(11): p. 1706-15.
405. Lignitto, L., et al., *Control of PKA stability and signalling by the RING ligase praja2*. Nat Cell Biol, 2011. **13**(4): p. 412-22.
406. Aboulaich, N., et al., *Vectorial proteomics reveal targeting, phosphorylation and specific fragmentation of polymerase I and transcript release factor (PTRF) at the surface of caveolae in human adipocytes*. Biochem J, 2004. **383**(Pt 2): p. 237-48.
407. Bai, L., et al., *Regulation of cellular senescence by the essential caveolar component PTRF/Cavin-1*. Cell Res, 2011. **21**(7): p. 1088-101.
408. Jansa, P., et al., *The transcript release factor PTRF augments ribosomal gene transcription by facilitating reinitiation of RNA polymerase I*. Nucleic Acids Res, 2001. **29**(2): p. 423-9.
409. Aboulaich, N., et al., *Association and insulin regulated translocation of hormone-sensitive lipase with PTRF*. Biochem Biophys Res Commun, 2006. **350**(3): p. 657-61.
410. Anthonsen, M.W., et al., *Identification of novel phosphorylation sites in hormone-sensitive lipase that are phosphorylated in response to isoproterenol and govern activation properties in vitro*. J Biol Chem, 1998. **273**(1): p. 215-21.
411. Shen, W.J., et al., *Mutational analysis of structural features of rat hormone-sensitive lipase*. Biochemistry, 1998. **37**(25): p. 8973-9.
412. Hunter, T., *The Croonian Lecture 1997. The phosphorylation of proteins on tyrosine: its role in cell growth and disease*. Philos Trans R Soc Lond B Biol Sci, 1998. **353**(1368): p. 583-605.

413. Ley, R., et al., *Extracellular signal-regulated kinases 1/2 are serum-stimulated "Bim(EL) kinases" that bind to the BH3-only protein Bim(EL) causing its phosphorylation and turnover.* J Biol Chem, 2004. **279**(10): p. 8837-47.
414. Gonzalez, G.A. and M.R. Montminy, *Cyclic AMP stimulates somatostatin gene transcription by phosphorylation of CREB at serine 133.* Cell, 1989. **59**(4): p. 675-80.
415. Kuo, A., et al., *Caveolin-1 regulates lipid droplet metabolism in endothelial cells via autocrine prostacyclin-stimulated, cAMP-mediated lipolysis.* Journal of Biological Chemistry, 2018. **293**(3): p. 973-983.
416. Rothberg, K.G., et al., *Caveolin, a protein component of caveolae membrane coats.* Cell, 1992. **68**(4): p. 673-82.
417. Kovtun, O., et al., *Cavin family proteins and the assembly of caveolae.* J Cell Sci, 2015. **128**(7): p. 1269-1278.
418. Ludwig, A., B.J. Nichols, and S. Sandin, *Architecture of the caveolar coat complex.* J Cell Sci, 2016: p. jcs. 191262.
419. Yeow, I., et al., *EHD proteins cooperate to generate caveolar clusters and to maintain caveolae during repeated mechanical stress.* Current Biology, 2017. **27**(19): p. 2951-2962. e5.
420. Melo, A.A., et al., *Structural insights into the activation mechanism of dynamin-like EHD ATPases.* Proceedings of the National Academy of Sciences, 2017. **114**(22): p. 5629-5634.
421. Stoeber, M., et al., *Oligomers of the ATPase EHD2 confine caveolae to the plasma membrane through association with actin.* The EMBO journal, 2012. **31**(10): p. 2350-2364.
422. Senju, Y., et al., *Essential role of PACSIN2/syndapin-II in caveolae membrane sculpting.* Journal of cell science, 2011: p. jcs. 086264.
423. Strålfors, P., *Caveolins and caveolae, roles in insulin signalling and diabetes,* in *Caveolins and Caveolae.* 2012, Springer. p. 111-126.
424. Garcia-Cardena, G., et al., *Targeting of nitric oxide synthase to endothelial cell caveolae via palmitoylation: implications for nitric oxide signaling.* Proceedings of the National Academy of Sciences, 1996. **93**(13): p. 6448-6453.
425. Melo, R.C., et al., *Pre-embedding immunogold labeling to optimize protein localization at subcellular compartments and membrane microdomains of leukocytes.* Nat Protoc, 2014. **9**(10): p. 2382-94.
426. Palade, G.E. and R.R. Bruns, *Structural modulations of plasmalemmal vesicles.* J Cell Biol, 1968. **37**(3): p. 633-49.
427. Stan, R.V., *Structure of caveolae.* Biochim Biophys Acta, 2005. **1746**(3): p. 334-48.
428. Sowa, G., *Caveolae, caveolins, cavins, and endothelial cell function: new insights.* Front Physiol, 2012. **2**: p. 120.
429. Dwane, S. and P.A. Kiely, *Tools used to study how protein complexes are assembled in signaling cascades.* Bioeng Bugs, 2011. **2**(5): p. 247-59.
430. Hill, M.M., et al., *Co-regulation of cell polarization and migration by caveolar proteins PTRF/Cavin-1 and caveolin-1.* PLoS One, 2012. **7**(8): p. e43041.
431. Davalos, A., et al., *Quantitative proteomics of caveolin-1-regulated proteins: characterization of polymerase i and transcript release*

- factor/CAVIN-1 IN endothelial cells. Mol Cell Proteomics, 2010. 9(10): p. 2109-24.*
432. Heinrich, P.C., et al., *Principles of interleukin (IL)-6-type cytokine signalling and its regulation. Biochem J, 2003. 374(Pt 1): p. 1-20.*
  433. Borish, L.C. and J.W. Steinke, 2. *Cytokines and chemokines. J Allergy Clin Immunol, 2003. 111(2 Suppl): p. S460-75.*
  434. Kaptein, A., V. Paillard, and M. Saunders, *Dominant negative stat3 mutant inhibits interleukin-6-induced Jak-STAT signal transduction. J Biol Chem, 1996. 271(11): p. 5961-4.*
  435. Head, B.P., H.H. Patel, and P.A. Insel, *Interaction of membrane/lipid rafts with the cytoskeleton: impact on signaling and function: membrane/lipid rafts, mediators of cytoskeletal arrangement and cell signaling. Biochim Biophys Acta, 2014. 1838(2): p. 532-45.*
  436. Diaz, O., et al., *Disruption of lipid rafts stimulates phospholipase d activity in human lymphocytes: implication in the regulation of immune function. J Immunol, 2005. 175(12): p. 8077-86.*
  437. Podar, K., et al., *Essential role of caveolae in interleukin-6- and insulin-like growth factor I-triggered Akt-1-mediated survival of multiple myeloma cells. J Biol Chem, 2003. 278(8): p. 5794-801.*
  438. Mukhopadhyay, S., et al., *Cytoplasmic provenance of STAT3 and PY-STAT3 in the endolysosomal compartments in pulmonary arterial endothelial and smooth muscle cells: implications in pulmonary arterial hypertension. Am J Physiol Lung Cell Mol Physiol, 2008. 294(3): p. L449-68.*
  439. Yuan, K., et al., *Elevated inflammatory response in caveolin-1-deficient mice with Pseudomonas aeruginosa infection is mediated by STAT3 protein and nuclear factor kappaB (NF-kappaB). J Biol Chem, 2011. 286(24): p. 21814-25.*
  440. Holland, S.M., et al., *STAT3 mutations in the hyper-IgE syndrome. N Engl J Med, 2007. 357(16): p. 1608-19.*
  441. Kreins, A.Y., et al., *Human TYK2 deficiency: Mycobacterial and viral infections without hyper-IgE syndrome. J Exp Med, 2015. 212(10): p. 1641-62.*
  442. Ernst, M. and B.J. Jenkins, *Acquiring signalling specificity from the cytokine receptor gp130. Trends Genet, 2004. 20(1): p. 23-32.*
  443. Stark, G.R. and J.E. Darnell, Jr., *The JAK-STAT pathway at twenty. Immunity, 2012. 36(4): p. 503-14.*
  444. Canoy, D., *Distribution of body fat and risk of coronary heart disease in men and women. Curr Opin Cardiol, 2008. 23(6): p. 591-8.*
  445. Ding, S.Y., et al., *Pleiotropic effects of cavin-1 deficiency on lipid metabolism. J Biol Chem, 2014. 289(12): p. 8473-83.*
  446. Harding, I.C., et al., *Pro-atherosclerotic disturbed flow disrupts caveolin-1 expression, localization, and function via glycocalyx degradation. J Transl Med, 2018. 16(1): p. 364.*
  447. Back, M., et al., *Inflammation and its resolution in atherosclerosis: mediators and therapeutic opportunities. Nat Rev Cardiol, 2019.*
  448. Pavlides, S., et al., *Atherosclerosis, caveolae and caveolin-1. Adv Exp Med Biol, 2012. 729: p. 127-44.*
  449. Insull, W., Jr., *The pathology of atherosclerosis: plaque development and plaque responses to medical treatment. Am J Med, 2009. 122(1 Suppl): p. S3-S14.*

450. Frank, P.G., et al., *Genetic ablation of caveolin-1 confers protection against atherosclerosis*. *Arterioscler Thromb Vasc Biol*, 2004. **24**(1): p. 98-105.
451. Fernandez-Hernando, C., et al., *Genetic evidence supporting a critical role of endothelial caveolin-1 during the progression of atherosclerosis*. *Cell Metab*, 2009. **10**(1): p. 48-54.
452. Fernandez-Hernando, C., et al., *Endothelial-specific overexpression of caveolin-1 accelerates atherosclerosis in apolipoprotein E-deficient mice*. *Am J Pathol*, 2010. **177**(2): p. 998-1003.
453. Feron, O., et al., *Hydroxy-methylglutaryl-coenzyme A reductase inhibition promotes endothelial nitric oxide synthase activation through a decrease in caveolin abundance*. *Circulation*, 2001. **103**(1): p. 113-8.
454. Alicea-Velazquez, N.L. and T.J. Boggon, *The use of structural biology in Janus kinase targeted drug discovery*. *Curr Drug Targets*, 2011. **12**(4): p. 546-55.
455. Suessmuth, Y., et al., *A new polycythaemia vera-associated SOCS3 SH2 mutant (SOCS3F136L) cannot regulate erythropoietin responses*. *Br J Haematol*, 2009. **147**(4): p. 450-8.
456. Moshapa, F.T., K. Riches-Suman, and T.M. Palmer, *Therapeutic Targeting of the Proinflammatory IL-6-JAK/STAT Signalling Pathways Responsible for Vascular Restenosis in Type 2 Diabetes Mellitus*. *Cardiol Res Pract*, 2019. **2019**: p. 9846312.
457. Mahony, R., et al., *SOCS3 revisited: a broad regulator of disease, now ready for therapeutic use?* *Cell Mol Life Sci*, 2016. **73**(17): p. 3323-36.
458. Zhang, W.N., et al., *CUEDC2 (CUE domain-containing 2) and SOCS3 (suppressors of cytokine signaling 3) cooperate to negatively regulate Janus kinase 1/signal transducers and activators of transcription 3 signaling*. *J Biol Chem*, 2012. **287**(1): p. 382-92.

ARTICLE

DOI: 10.1038/s41467-017-02585-y

OPEN

# Interaction of suppressor of cytokine signalling 3 with cavin-1 links SOCS3 function and cavin-1 stability

Jamie J.L. Williams<sup>1</sup>, Nasser Alotaiq<sup>2</sup>, William Mullen<sup>2</sup>, Richard Burchmore<sup>3</sup>, Libin Liu<sup>4</sup>, George S. Baillie<sup>2</sup>, Fred Schaper<sup>5</sup>, Paul F. Pilch<sup>4</sup> & Timothy M. Palmer<sup>1</sup>

Effective suppression of JAK-STAT signalling by the inducible inhibitor “suppressor of cytokine signalling 3” (SOCS3) is essential for limiting signalling from cytokine receptors. Here we show that cavin-1, a component of caveolae, is a functionally significant SOCS3-interacting protein. Biochemical and confocal imaging demonstrate that SOCS3 localisation to the plasma membrane requires cavin-1. SOCS3 is also critical for cavin-1 stabilisation, such that deletion of SOCS3 reduces the expression of cavin-1 and caveolin-1 proteins, thereby reducing caveola abundance in endothelial cells. Moreover, the interaction of cavin-1 and SOCS3 is essential for SOCS3 function, as loss of cavin-1 enhances cytokine-stimulated STAT3 phosphorylation and abolishes SOCS3-dependent inhibition of IL-6 signalling by cyclic AMP. Together, these findings reveal a new functionally important mechanism linking SOCS3-mediated inhibition of cytokine signalling to localisation at the plasma membrane via interaction with and stabilisation of cavin-1.

<sup>1</sup>School of Pharmacy and Medical Sciences, University of Bradford, Bradford BD7 1DP, UK. <sup>2</sup>Institute of Cardiovascular and Medical Sciences, University of Glasgow, Glasgow G12 8QQ, UK. <sup>3</sup>Polyomics Facility, University of Glasgow, Glasgow G12 8QQ, UK. <sup>4</sup>Departments of Biochemistry and Medicine, Boston University School of Medicine, Boston MA 02118, USA. <sup>5</sup>Department of Systems Biology, Institute for Biology, Otto-von-Guericke-University Magdeburg 39106 Magdeburg, Germany. Correspondence and requests for materials should be addressed to J.J.L.W. (email: [jj.l.williams@bradford.ac.uk](mailto:jj.l.williams@bradford.ac.uk)) or to T.M.P. (email: [T.Palmer1@bradford.ac.uk](mailto:T.Palmer1@bradford.ac.uk))

Cytokines control many important biological responses, including haematopoiesis, T-cell differentiation and expansion, and inflammatory status<sup>1,2</sup>. Multiple temporally distinct inhibitory mechanisms operate to ensure signalling responses downstream of activated cytokine receptors are transient in nature. Therefore, sustained pathway activation perpetuates chronic inflammatory conditions such as rheumatoid arthritis and colitis, haematological malignancies such as polycythemia vera, and also solid tumour development<sup>3–5</sup>.

Several cytokine receptors, including gp130 (the signal transducing component of the interleukin-6 (IL-6) signalling complex), activate receptor-associated Janus kinases (JAKs) which then trigger receptor engagement with proteins such as signal transducer and activators of transcription (STATs), particularly STAT3. Phosphorylated STATs can then dimerise and translocate to the nucleus, where they function as transcription factors by binding to specific promoter elements and recruiting transcriptional co-activators<sup>1,2</sup>.

“Suppressors of cytokine signalling” (SOCS) proteins comprise a family of eight related members (cytokine-inducible SH2-containing protein (CIS), SOCS1–7) identified initially by their role as cytokine-inducible negative feedback inhibitors of signal propagation from specific cytokine receptors<sup>6</sup>. SOCS3 is recruited to activated cytokine receptors following the formation of a SOCS3 interaction motif upon phosphorylation of key Tyr residues by cytokine-activated JAKs. SOCS3 terminates signalling from gp130 by binding via a central SH2 domain to PTyr759, allowing it to interact with and inhibit adjacent receptor-bound JAKs via its kinase inhibitory region (KIR) thereby preventing the recruitment and tyrosine phosphorylation of STATs<sup>7</sup>. The C-terminal SOCS box domain directs SH2 domain-bound interacting proteins for ubiquitylation due to its ability to bind elongin B and C, Cullin family member Cul5, and RING (Really Interesting New Gene) finger protein Rbx2<sup>7</sup>. Following SOCS3-dependent ubiquitylation, targets such as FAK1 can be degraded either by the proteasome<sup>8,9</sup> or, in the case of the granulocyte colony-stimulating factor receptor (G-CSFR), by trafficking into lysosomal compartments following internalisation<sup>10</sup>. However, despite advances in our molecular understanding of how SOCS3 interacts with cytokine receptors and JAKs, the extent to which other cellular proteins regulate SOCS3 function is unclear. Recently, CUE domain-containing 2 (CUEDC2) was identified as a novel SOCS3-interacting protein that could enhance its interaction with elongin C<sup>11</sup>. Such observations raise the possibility that additional protein interactors may be required to maximise the ability of SOCS3 to regulate signalling.

Cavin-1 (alternatively known as polymerase I and transcript release factor (PTRF)) is an abundant component of caveolae, which function as specialised lipid raft microdomains within the plasma membrane. Caveolae were first identified by electron microscopy as 50–100 nm flask-shaped plasma membrane invaginations<sup>12</sup> and are now known to play critical roles in controlling endocytosis, sphingolipid metabolism, and compartmentalisation of signalling pathways<sup>13</sup>. Cavin-1, which is one of a family of four related proteins (cavins 1 to 4), is recruited by one or more “caveolin” proteins (caveolins 1 to 3) to the plasma membrane during the latter stages of caveola biogenesis, and is thought to be essential for caveola formation by stabilising caveolin proteins at the plasma membrane<sup>14</sup>.

While some studies have demonstrated localisation of cytokine receptors and JAKs in lipid raft microdomains<sup>15–18</sup>, little is known about the impact of caveolin expression/function on JAK–STAT signalling and no studies have specifically examined a role for cavins. In this study, we identify a novel interaction between SOCS3 and cavin-1. This interaction is not only required for optimal SOCS3-mediated inhibition of IL-6-mediated

JAK–STAT signalling but also for effective stabilisation of cavin-1 and hence caveolin-1. Therefore, our findings define a new relationship between SOCS3 and cavin-1 in which each partner plays previously unappreciated roles in maintaining effective inhibition of JAK–STAT signalling (cavin-1), cavin-1 expression, and caveola stability (SOCS3).

## Results

**Cavin-1 as a SOCS3-regulated ubiquitylated protein.** As well as inhibiting cytokine receptor signalling by inhibiting the Tyr kinase activity of receptor-bound JAKs<sup>19</sup>, SOCS3 can also control the stability of SH2 domain-bound proteins as part of an elongin/cullin/SOCS3 (ECS<sup>SOCS3</sup>) E3 ubiquitin ligase complex<sup>6,7,20</sup>. While several ubiquitinated substrates of SOCS3 are known, the full spectrum has yet to be identified. Thus, we pursued an experimental approach to elaborate on SOCS3 function by investigating SOCS3-regulated proteins. Since there is no consensus sequence for ubiquitylation, we used a stable isotopic labelling of amino acids in cell culture (SILAC)/mass spectrometry approach to compare ubiquitinomes from wild-type SOCS3<sup>+/+</sup> (WT) and SOCS3<sup>-/-</sup> murine embryonic fibroblast (MEF) cell lines expressing equivalent levels of a tandem affinity purification-compatible tagged ubiquitin transgene following SOCS3 induction (Supplementary Fig. 1). Using this approach, ubiquitylated proteins regulated by SOCS3 would be predicted to be enriched in WT but not SOCS3<sup>-/-</sup> MEFs.

A ubiquitin transgene containing a tandem hexahistidine and biotin tag (HB-Ub) was used to allow two-step tandem affinity purification of the ubiquitinome via sequential Ni-NTA and streptavidin affinity chromatography under fully denaturing conditions necessary to inactivate deubiquitinases and prevent co-purification of non-covalently interacting ubiquitin-binding proteins<sup>21,22</sup>. Stable HB-Ub-expressing WT and SOCS3<sup>-/-</sup> MEFs were generated via retrovirus-mediated gene transfer and assessed by immunoblotting for equivalent expression levels of the HB-Ub transgene. SOCS3 was induced by elevation of intracellular cyclic adenosine monophosphate (cAMP) levels with forskolin (50  $\mu$ M), a direct activator of adenylyl cyclase. To increase the probability of detecting proteins whose ubiquitylation was SOCS3 dependent, protein tyrosine phosphatases were inhibited using a combination of sodium orthovanadate and H<sub>2</sub>O<sub>2</sub> to preserve the PTyr status of potential substrates and maximise interaction with the SOCS3 SH2 domain<sup>23</sup>, while the ubiquitinome was preserved using proteasome inhibitor MG132. Tandem affinity-purified ubiquitinomes from WT and SOCS3<sup>-/-</sup> MEFs were then analysed using an Orbitrap Velos FTMS and data processed using the MaxQuant computational platform<sup>24</sup> (170). Under these conditions, MaxQuant detected cavin-1 (O54724) with a log<sub>2</sub>(normalised H L<sup>-1</sup>) = 1.37 (5 unique peptides, count ratio of 6). This suggested that cavin-1 was a ubiquitylated protein specifically depleted in SOCS3<sup>-/-</sup> MEFs.

**SOCS3 enhances cavin-1 stability.** Our proteomics screen suggested that SOCS3 regulates cavin-1 stability. To examine this, we compared the ability of increasing levels of SOCS3 to trigger the proteasomal degradation of co-transfected cavin-1 and FAK1, a previously characterised substrate of ECS<sup>SOCS3</sup><sup>8,9</sup>. Consistent with previous work, increased SOCS3 expression triggered a decrease in FAK1 levels that could be rescued by inclusion of proteasome inhibitor MG132. In contrast, levels of cavin-1 were not altered even at the highest level of SOCS3 expression and were not increased by proteasome inhibitor MG132 (Fig. 1a). To determine whether SOCS3 could regulate levels of endogenous cavin-1, we assessed the effects of SOCS3 deletion on cavin-1 expression levels in MEFs. Immunoblotting of whole-cell extracts

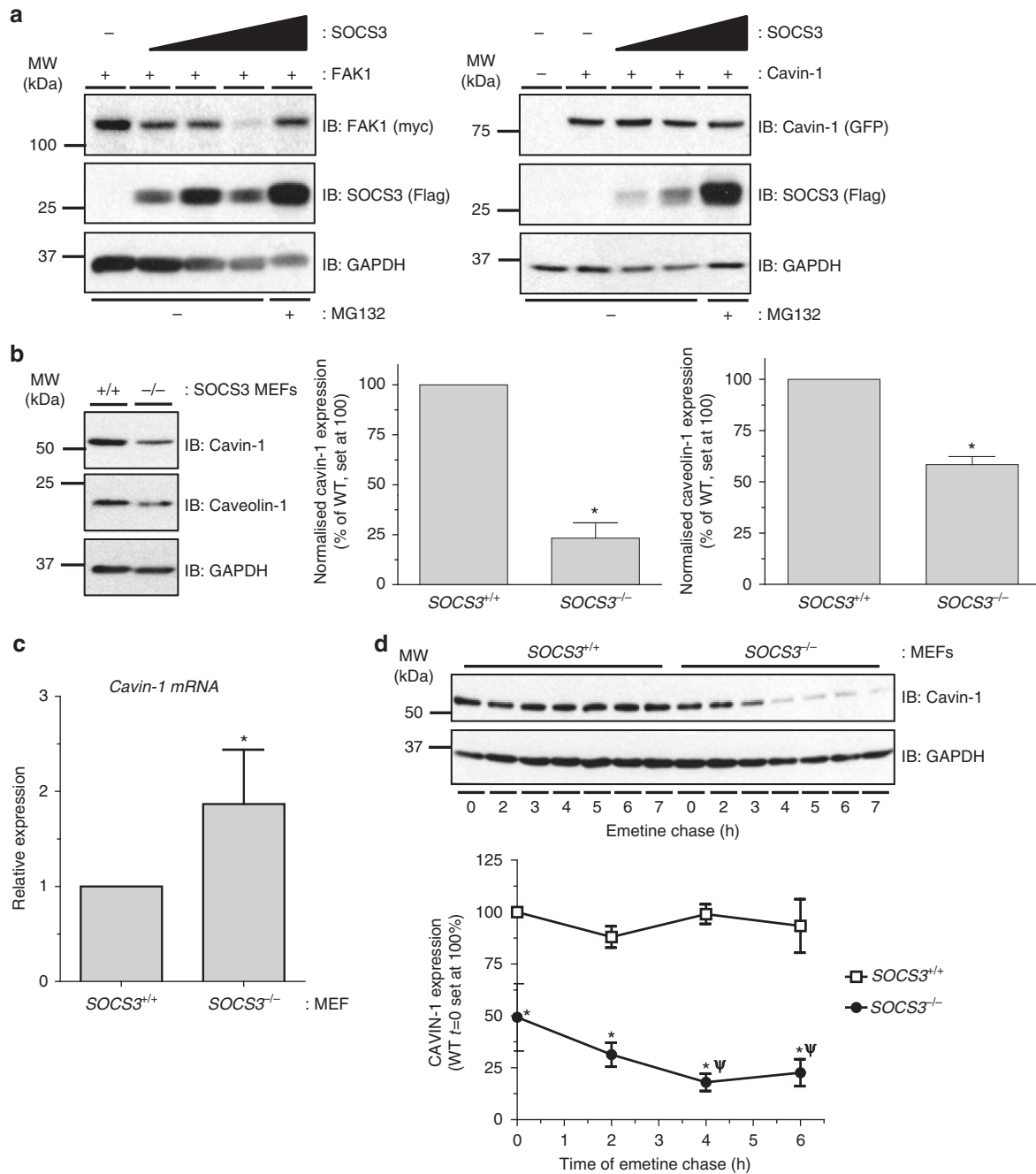


**Fig. 1** Cavin-1 stability is enhanced in the presence of SOCS3. **a** HEK293 cells co-transfected with fixed amounts of either myc-tagged FAK1 or GFP-cavin-1 expression constructs and increasing levels of Flag-SOCS3 were treated with or without proteasome inhibitor MG132 (6 μM) as indicated. Detergent-soluble whole-cell lysates were analysed by SDS-PAGE and immunoblotting. **b** Detergent-soluble whole-cell lysates prepared from SOCS3<sup>+/+</sup> (+/+) and SOCS3<sup>-/-</sup> (-/-) MEFs equalised for protein content were analysed by SDS-PAGE and immunoblotting. **c** Quantitative real-time PCR of cavin-1 mRNA levels in WT (SOCS3<sup>+/+</sup>) and SOCS3<sup>-/-</sup> MEFs. Data are presented as mean ± standard error for N = 3 experiments. **d** Upper: Protein-equalised soluble cell extracts from SOCS3<sup>+/+</sup> and SOCS3<sup>-/-</sup> MEFs chased for the indicated times in serum-free medium with protein synthesis inhibitor emetine (100 μM) were analysed by SDS-PAGE and immunoblotting with the indicated antibodies. Lower: Quantitation of cavin-1 levels in SOCS3<sup>+/+</sup> and SOCS3<sup>-/-</sup> MEFs is also shown. Results are presented as mean values ± standard error for N = 3 experiments. \*P < 0.05 vs. corresponding treatment in SOCS3<sup>+/+</sup> MEFs, ΨP < 0.05 vs. t = 0

revealed that levels of cavin-1 protein were significantly reduced in SOCS3<sup>-/-</sup> MEFs versus WT cells. This reduction occurred under conditions in which cavin-1 mRNA levels were significantly increased in SOCS3<sup>-/-</sup> MEFs versus WT cells (Fig. 1b, c). The decrease in cavin-1 protein was paralleled by a similar decrease in caveolin-1 expression levels (Fig. 1b), which is consistent with previous studies showing that loss of cavin-1 triggers

reductions in all three caveolin isoforms<sup>14</sup>. We then measured the half-lives of cavin-1 protein in WT and SOCS3<sup>-/-</sup> MEFs by monitoring time-dependent changes in cavin-1 expression in whole-cell extracts following inhibition of protein synthesis with emetine<sup>25</sup>. For these experiments, cells were also pre-treated with forskolin (Fsk) to elevate cAMP levels and increase SOCS3 expression in WT MEFs<sup>26,27</sup>. Direct comparison of cavin-1

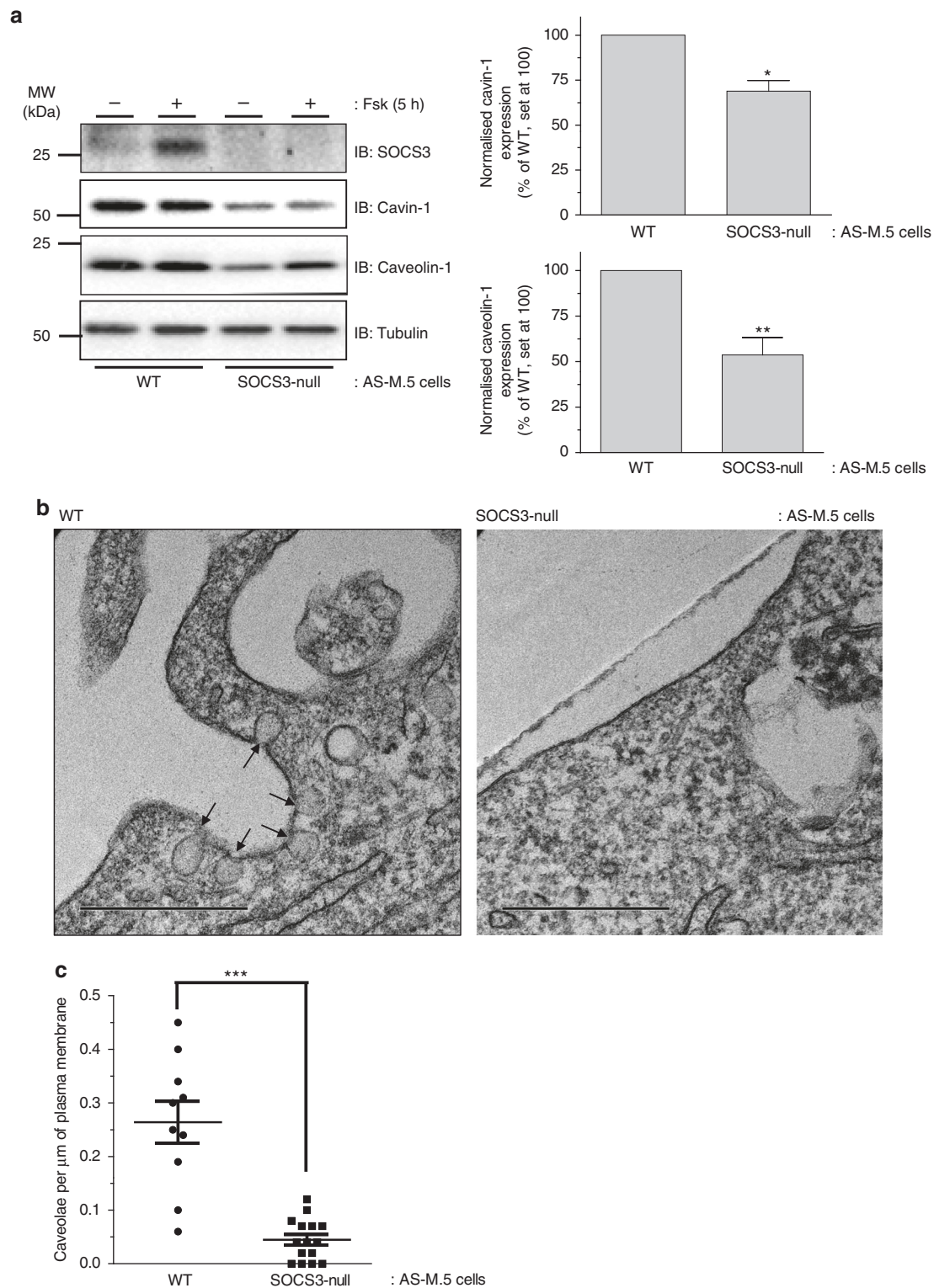


**Fig. 2** Effect of SOCS3 deletion on caveola abundance in endothelial cells. **a** Upper: Detergent-soluble whole-cell lysates from WT and SOCS3-null AS-M.5 human angiosarcoma-derived ECs treated with either vehicle or 50  $\mu\text{M}$  Fsk for 5 h were equalised for protein content for SDS-PAGE for immunoblotting with the indicated antibodies. Lower: Quantitation of cavin-1 and caveolin-1 protein levels in unstimulated AS-M.5 cells is presented as mean  $\pm$  standard error for  $N=3$  experiments. \* $P < 0.05$ , \*\* $P < 0.01$  vs. WT cells. **b** Transmitting electron microscopy (TEM) was performed on WT and SOCS3-null AS-M.5 cells as indicated. Cell surface caveolae (indicated by the arrows) were readily detectable in WT cells (left panel). In contrast, plasma membranes from SOCS3-null cells were flat and caveolae density was significantly reduced compared to WT cells (right panel). Scale bar = 0.5  $\mu\text{m}$ . **c** Quantitation of caveola density (number of caveolae per  $\mu\text{m}$  of plasma membrane) in WT and SOCS3-null AS-M.5 cells. \*\*\* $P < 0.0001$  vs. WT cells

stability in WT versus SOCS3<sup>-/-</sup> MEFs demonstrated that the absence of SOCS3 significantly reduced the half-life from >8 h (WT MEFs) to 2 h (SOCS3<sup>-/-</sup> MEFs; Fig. 1d). Thus, in contrast to the well-defined role of SOCS3 in destabilising target proteins by targeting them for ubiquitylation and proteasomal degradation, the presence of SOCS3 stabilised cavin-1.

**Effect of SOCS3 deletion on caveola abundance.** Our data thus far suggested that SOCS3 was an important regulator of caveolin-1 abundance via stabilisation of cavin-1. Homozygous deletion of the cavin-1 gene in mice results in marked reductions in the expression of all caveolin isoforms and a lack of detectable caveolae in multiple cell types, including endothelial cells (ECs) in which caveolae are especially abundant<sup>14</sup>.

To examine the impact of SOCS3 on caveola abundance, clustered regularly interspaced short palindromic repeats (CRISPR)/Cas9 technology was used to generate SOCS3-null AS-M.5 human angiosarcoma-derived immortalised ECs<sup>28</sup>. Treatment of WT AS-M.5 cells with cAMP-elevating agent Fsk was able to promote SOCS3 induction similar to that observed in MEFs and primary EC lines as previously reported<sup>26,27</sup>. However, this effect was lost in SOCS3-null AS-M.5 cells, while Nur77, a well-characterised cAMP-inducible gene product<sup>29</sup>, was detectable in both WT and SOCS3-null AS-M.5 cells following Fsk treatment (Fig. 2a, Supplementary Fig. 2). Similar to MEFs (Fig. 1b), SOCS3 deletion significantly reduced cavin-1 and caveolin-1 protein levels in AS-M.5 whole-cell extracts (Fig. 2a), demonstrating that this effect is independent of the cell system being investigated.

We then used transmission electron microscopy (TEM) to assess any consequences of the observed changes in cavin-1 and caveolin-1 expression on the abundance of cell surface caveolae. Caveolae were readily detectable in WT AS-M.5 cells as plasma membrane-localised flask-shaped invaginations ranging from 50 to 100 nm in diameter (Fig. 2b). In contrast, these were barely detectable in SOCS3-null cells (Fig. 2b, c). Therefore, significant reductions in cavin-1 and caveolin-1 protein levels triggered by the loss of SOCS3 in endothelial cells are translated into significantly reduced numbers of cell surface caveolae.

**Cavin-1 interacts with SOCS3 via a SH2 domain PEST sequence.** To assess whether SOCS3 could directly interact with cavin-1, co-immunoprecipitation (co-IP) experiments were performed in lysates isolated from transfected HEK293 cells transiently expressing Flag-SOCS3 and myc-cavin-1. These experiments demonstrated that myc-cavin-1 was present in anti-Flag antibody immunoprecipitates only when co-expressed with Flag-SOCS3, indicating the two proteins formed a complex (Fig. 3a). Similar results were obtained using Flag-cavin-1 and HA-SOCS3 (Supplementary Fig. 3), indicating that the effect was independent of the combination of tags used. Analysis of lysates and unbound samples from the experiments demonstrated that under conditions in which SOCS3 could be fully precipitated from lysates, a proportion of cavin-1 remained unbound, suggesting that not all available cavin-1 could interact with SOCS3 under these conditions (Supplementary Fig. 4). To assess the interaction of endogenously expressed SOCS3 and cavin-1, WT and SOCS3-null AS-M.5 cells were stimulated with Fsk prior to IP of cavin-1 and analysis by immunoblotting. These experiments demonstrated that immunoreactive SOCS3 was specifically enriched in cavin-1 IPs from WT AS-M.5 cells (Fig. 3b), consistent with the co-IP data from experiments using transfected cells (Fig. 3a).

To identify the regions within SOCS3 that are important for SOCS3/cavin-1 interaction, we initially utilised a panel of Flag-

tagged N- and C-terminal SOCS3 truncation mutants<sup>30,31</sup> for their ability to co-IP green fluorescent protein (GFP)-tagged cavin-1<sup>32</sup> as compared to WT SOCS3. Interestingly, all of the truncation mutants tested were able to co-IP GFP-cavin-1 to the same extent as full-length WT SOCS3 (Fig. 3c), suggesting that a region within the SH2 domain present in each of the mutants was necessary for SOCS3 binding to cavin-1. To test this, we expressed full-length SOCS3 (residues 1–225) and the region of the SOCS3 SH2 domain (residues 46–142, termed SOCS3 ΔSH2) required for cavin-1 binding (Fig. 3d) as GFP-tagged fusion proteins and compared their ability to co-IP myc-tagged cavin-1 in transfected HEK293 cells. As a negative control, we used a GFP fusion protein containing residues 177–225 of the SOCS box that we identified as dispensable for cavin-1 interaction (Fig. 3c). Similar to WT SOCS3-GFP, SOCS3 ΔSH2-GFP was able to co-IP myc-tagged cavin-1 above the non-specific levels observed with the SOCS3 SOCS box-GFP fusion and cavin-1 alone, albeit not to the same extent as WT SOCS3-GFP (Fig. 3d, lane 2 versus lane 8). Therefore, these data showed that residues 46–142 within the SOCS3 SH2 domain were both necessary and sufficient for SOCS3 interaction with cavin-1.

As many SOCS3 binding partners, including gp130, CD33 and FAK1, must be Tyr phosphorylated in order to interact with SOCS3, we pursued three experimental approaches to examine whether or not the PTyr-binding pocket within the SOCS3 SH2 domain was required for interaction with cavin-1. First, we treated transfected HEK293 cells with protein Tyr phosphatase inhibitor sodium orthovanadate in the presence or absence of hydrogen peroxide<sup>23</sup>. These experiments demonstrated that the isolation of GFP-cavin-1 in anti-Flag (SOCS3) immunoprecipitates was not altered by increases in global Tyr phosphorylation levels (Fig. 4a), suggesting that cavin-1 formed a complex with SOCS3 via a mechanism that did not require prior Tyr phosphorylation. Secondly, we tested R71K-mutated SOCS3, in which the conserved PTyr binding site within the SOCS3 SH2 domain is disrupted<sup>30,31</sup>, for its ability to form a complex with cavin-1. Co-IP assays revealed that a R71K-mutated SOCS3 bound cavin-1 equivalently to WT SOCS3 (Fig. 4b), again supporting the concept that cavin-1 interacted with the SOCS3 SH2 domain in a manner independent of its capacity to bind Tyr-phosphorylated ligands. Finally, N-terminally biotinylated peptides encompassing the Tyr759 motif of gp130 in phosphorylated (PTyr759 peptide) and non-phosphorylated (Tyr759 peptide) forms were used as bait to test the effect of cavin-1 co-expression on the ability of SOCS3 to be precipitated in peptide pull-down assays. As reported by others<sup>30</sup>, SOCS3 specifically associated with the PTyr759 peptide under these conditions. Using a maximally effective concentration of peptide (100 nM), co-expression with cavin-1 did not reduce the ability of SOCS3 to precipitate with PTyr759 peptide (Fig. 4c). Taken together, these data demonstrated that cavin-1 interacted with the SOCS3 SH2 domain at a location distinct from the well-defined PTyr-binding pocket.

The region of the SOCS3 SH2 domain identified in the studies above consists of two structurally distinct components. Firstly, residues 46–127 comprise of β-sheet and α-helical regions that form part of the PTyr-binding pocket common to all SH2 domains. Secondly, residues 128–142 form part of an unstructured PEST sequence insert that links the SH2 domain helix B with BG loop and βG strand motifs (residues 166–185)<sup>33</sup>. PEST motifs are unstructured hypermobile regions that have roles in multiple cellular processes by controlling protein–protein interactions and protein turnover<sup>34,35</sup>. We noted the presence of a PEST sequence within the classic SH2 domain structure is also displayed by CIS but none of the other SOCS family proteins<sup>33</sup>. Having excluded the PTyr-binding functionality for SH2 domain



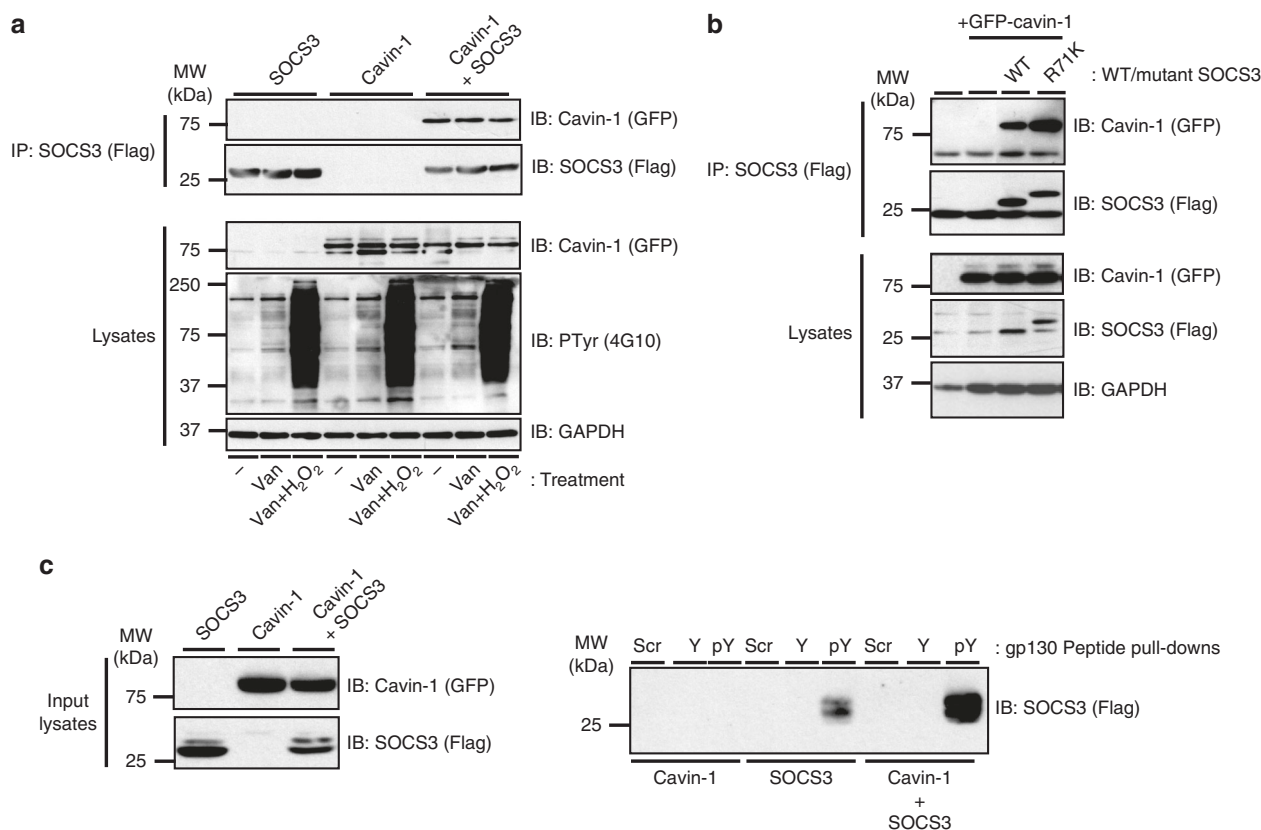


**Fig. 4** Cav1-SOCS3 interaction occurs independently of the PTyr binding capacity of the SH2 domain. **a** HEK293 cells transfected with expression constructs encoding Flag-SOCS3 and GFP-tagged cavin-1 as indicated were treated with or without Tyr phosphatase inhibitors sodium orthovanadate (Van; 1 mM) for 1.5 h and then hydrogen peroxide (H<sub>2</sub>O<sub>2</sub>; 0.2 mM) for an additional 30 min prior to harvesting. Protein-equalised soluble cell extracts were then processed by IP with anti-Flag M2-agarose beads prior to SDS-PAGE and immunoblotting with the indicated antibodies. Whole-cell lysates from the samples used in the IP were also fractionated by SDS-PAGE for immunoblotting in parallel. **b** Protein-equalised soluble cell extracts from HEK293 cells transfected with expression constructs encoding either WT or R71K-mutated Flag-SOCS3 and GFP-tagged-cavin-1 as indicated were processed by IP with anti-Flag M2-agarose beads prior to SDS-PAGE and immunoblotting with the indicated antibodies. Whole-cell lysates from the samples used in the IP were also fractionated by SDS-PAGE for immunoblotting in parallel. **c** Protein-equalised soluble cell extracts from HEK293 cells transfected with expression constructs encoding WT Flag-SOCS3 and GFP-tagged cavin-1 as indicated were incubated with 100 nM N-terminally biotinylated peptides corresponding to the Tyr759 motif of gp130 in its phosphorylated (pY) or non-phosphorylated (Y) forms or a scrambled control (Scr) and streptavidin-agarose beads prior to SDS-PAGE and immunoblotting with the indicated antibodies. Whole-cell lysates from the samples used in the pull-down were also fractionated by SDS-PAGE for immunoblotting in parallel

PEST sequence was sufficient to confer interaction with cavin-1. Bioinformatic analysis using ePESTfind (<http://emboss.bioinformatics.nl/cgi-bin/emboss/pepfind>) identified human Grap2 as a candidate SH2 domain-containing protein that lacked a detectable PEST sequence. In addition, Grap2 was unable to form a complex with cavin-1 upon co-expression in transfected HEK293 cells (Fig. 5d). Therefore, Pro129-Arg163 from SOCS3 was transplanted onto the central Grap2 SH2 domain and the resulting chimera (Grap2-S3PEST) assessed for its ability to form a complex with co-expressed cavin-1 in transfected HEK293 cells. These experiments demonstrated that insertion of SOCS3 PEST sequence was sufficient to confer an ability to bind cavin-1 on the resulting Grap2-S3PEST chimera, albeit to a much weaker extent than WT SOCS3 (Fig. 5d).

**Multiple cavin-1 regions required for SOCS3 interaction.** To examine whether SOCS3 interacts directly with cavin-1, peptide arrays of overlapping 25-mer peptides sequentially shifted by five amino acids and spanning the full-length cavin-1 open reading frame were overlaid with purified recombinant SOCS3 and visualised by probing with anti-SOCS3 antibodies (Fig. 6a). Dark spots represent positive areas of SOCS3 interaction. Using this

approach we found that SOCS3 could interact strongly with two distinct regions spanning >70 amino acids within the cavin-1 open reading frame: an N-terminal region spanning residues 75–152 and a C-terminal region encompassing residues 200–295. To validate the importance of these regions in controlling interaction with SOCS3 in intact cells, we generated a panel of myc epitope-tagged N- and C-terminal truncation mutants of cavin-1 (Fig. 6b) and tested their ability to co-IP Flag-SOCS3 upon co-expression in transfected HEK293 cells. All the truncated cavin-1 mutants expressed comparably to WT cavin-1 except for the C1 construct encoding residues 1–75 (Fig. 6c). These experiments demonstrated that, compared with WT cavin-1, each of the N-terminal and C-terminal truncation mutants was compromised in its capacity to co-IP with SOCS3. In conjunction with data from the peptide array experiments, our findings demonstrate that multiple SOCS3 binding interfaces within cavin-1 were required for optimal interaction with SOCS3.

**Cavin-1 promotes SOCS3 localisation to the plasma membrane.** Cavin-1 is required for stabilisation and maturation of caveolae at the plasma membrane, although it is also present with caveolin-1 in non-lipid raft fractions<sup>37</sup>. SOCS3 is thought to be

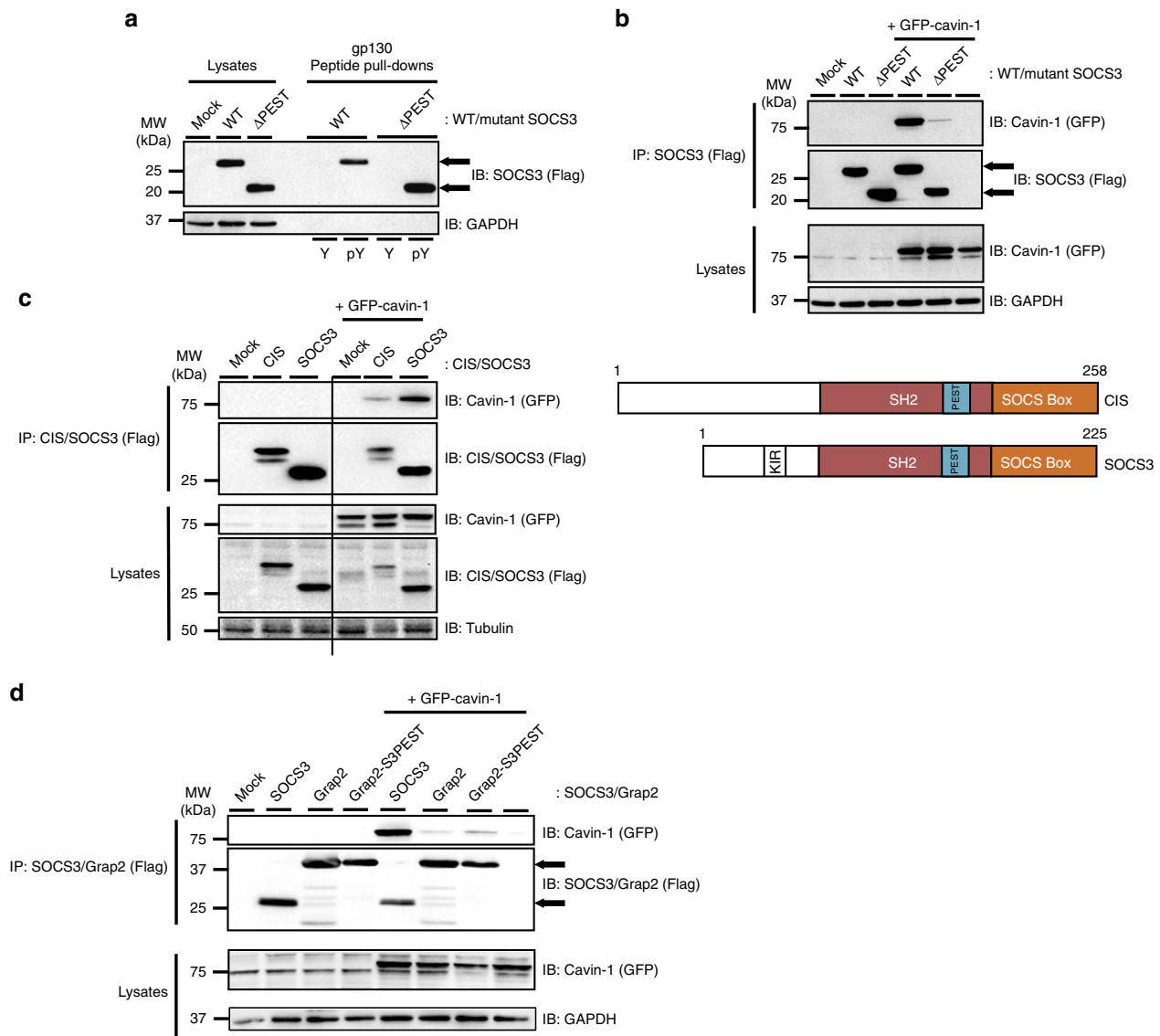


**Fig. 5** Cav1-SOCS3 interaction requires the SOCS3 SH2 PEST motif. **a** Protein-equalised soluble cell extracts from HEK293 cells transfected with expression constructs encoding either WT or  $\Delta$ PEST Flag-SOCS3 were incubated with 100 nM N-terminally biotinylated peptides corresponding to the Tyr759 motif of gp130 in its phosphorylated (pY) or non-phosphorylated (Y) forms and streptavidin-agarose beads prior to loading with whole-cell lysate samples for SDS-PAGE and immunoblotting with the indicated antibodies. **b** Protein-equalised soluble cell extracts from HEK293 cells transfected with expression constructs encoding either WT or  $\Delta$ PEST Flag-SOCS3 and GFP-tagged cavin-1 as indicated were processed by IP with anti-Flag M2-agarose beads prior to SDS-PAGE and immunoblotting with the indicated antibodies. Whole-cell lysates from the samples used in the IP were also fractionated by SDS-PAGE for immunoblotting in parallel. **c** Upper, Protein-equalised soluble cell extracts from HEK293 cells transfected with or without the indicated CIS and SOCS3 expression constructs and GFP-tagged cavin-1 as indicated were processed by IP with anti-Flag M2-agarose beads prior to SDS-PAGE and immunoblotting with the indicated antibodies. Lower, Schematic of CIS and SOCS3. **d** Protein-equalised soluble cell extracts from HEK293 cells transfected with or without the indicated SOCS3 and Grap2 expression constructs and GFP-tagged cavin-1 as indicated were processed by IP with anti-Flag M2-agarose beads prior to SDS-PAGE and immunoblotting with the indicated antibodies. Whole-cell lysates from the samples used in the IP were also fractionated by SDS-PAGE for immunoblotting in parallel

recruited to activated cytokine receptors at the plasma membrane following the formation of a SOCS3 interaction motif upon phosphorylation of key Tyr residues by cytokine-activated JAKs<sup>19</sup>. Therefore, to examine a role for cavin-1 in controlling SOCS3 localisation, we used confocal microscopy to assess the effect of cavin-1 deletion on the subcellular distribution of a SOCS3-GFP fusion protein expressed in transfected cells plated at low density. A transfected SOCS3-GFP construct was used for these experiments as we failed to specifically detect endogenous SOCS3 staining in WT MEFs over and above background

staining in SOCS3<sup>-/-</sup> MEFs in confocal imaging experiments using three separate commercially available antibodies. In transfected WT MEFs, two populations of SOCS3-GFP-derived fluorescence were detectable: a punctate intracellular pool and a plasma membrane-localised pool (Fig. 7a). Endogenous cavin-1 was localised predominantly at the plasma membrane of the trailing edge of the cells as described by others<sup>38</sup>. Merging of the images revealed co-localisation of SOCS3-GFP and cavin-1 specifically at the plasma membrane (Fig. 7a). Analysis of SOCS3-GFP/cavin-1 staining produced Pearson's correlation coefficient

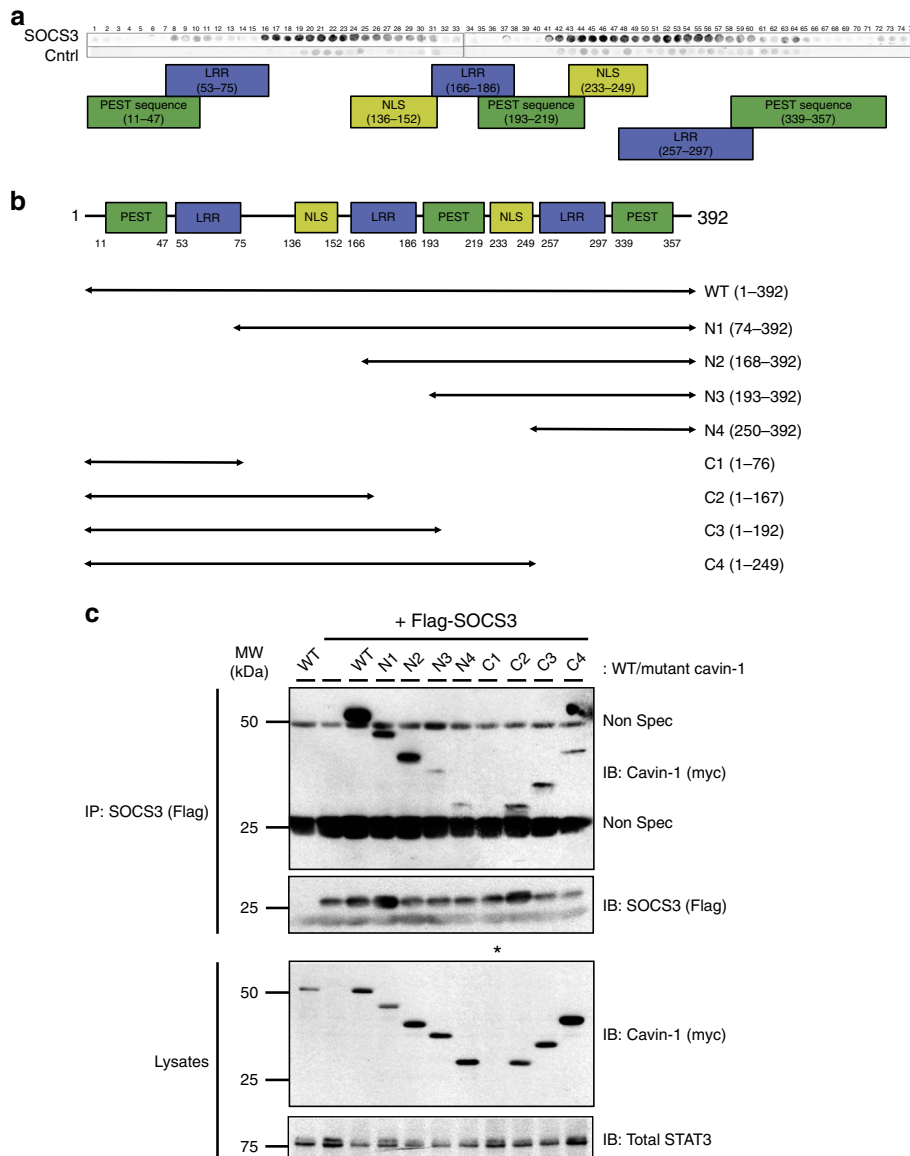


**Fig. 6** SOCS3 interacts with multiple regions within cavin-1. **a** An immobilised library of 25-mer peptides sequentially shifted by 5 amino acids along the entire cavin-1 open reading frame was overlaid with either purified SOCS3 or a negative control (Cntrl). Dark spots represent areas of interaction between SOCS3 and peptides within the cavin-1 peptide array. The domain structure of murine cavin-1 is indicated below the overlay. **b** Schematic representation of the N- and C-terminally truncated myc-tagged cavin-1 mutants used for co-IP experiments. **c** Protein-equalised soluble cell extracts from HEK293 cells transfected with expression constructs encoding either myc-tagged WT cavin-1 or the indicated truncation mutants and Flag-tagged SOCS3 as indicated were processed by IP with anti-Flag M2-agarose beads prior to SDS-PAGE and immunoblotting with the indicated antibodies. Whole-cell lysates from the same samples used in the IP were also fractionated by SDS-PAGE for immunoblotting in parallel. \*Indicates that expression of the C1 cavin-1 mutant was not detectable; Non Spec refers to immunoglobulin-derived non-specific staining

values of >0.90 at the plasma membrane, indicative of a high degree of co-localisation (Fig. 7b). Conversely, in *cavin-1*<sup>-/-</sup> MEFs SOCS3-GFP was undetectable at the plasma membrane and only present within a punctate intracellular pool (Fig. 7a). Importantly, transient co-expression of SOCS3-GFP with co-transfected cavin-1-mCherry into *cavin-1*<sup>-/-</sup> MEFs was able to restore their co-localisation at the plasma membrane (Fig. 7c). Expression of GFP alone in WT MEFs did not produce any detectable co-localisation with cavin-1, and its distribution was similar in both WT and *cavin-1*<sup>-/-</sup> MEFs (Supplementary Fig. 5A, B).

Additionally, subcellular fractionation experiments demonstrated that cavin-1 was mainly present in membrane and cytoplasmic fractions. This mirrored the subcellular distribution

of SOCS3 in WT MEFs following induction by Fsk treatment for 5 h. Interestingly, cavin-1 deletion shifted the distribution of SOCS3 predominantly to the cytoplasm (Fig. 7d). Thus, the presence of cavin-1 was important for localising endogenous SOCS3 to the membrane fraction, consistent with our confocal imaging experiments using SOCS3-GFP (Fig. 7a-c). Subcellular fractionation experiments also demonstrated that SOCS3 deletion produced a comparable reduction in caveolin-1 expression at the membrane as deletion of cavin-1, indicative of an indirect role for SOCS3 in maintaining caveolin-1 expression via stabilisation of cavin-1 (Fig. 7d). This change was specific for caveolin-1 as levels of the membrane marker flotillin were unaffected by deletion of either SOCS3 or cavin-1 (Fig. 7d). Therefore, together these data indicate that cavin-1 co-localised with a plasma membrane pool

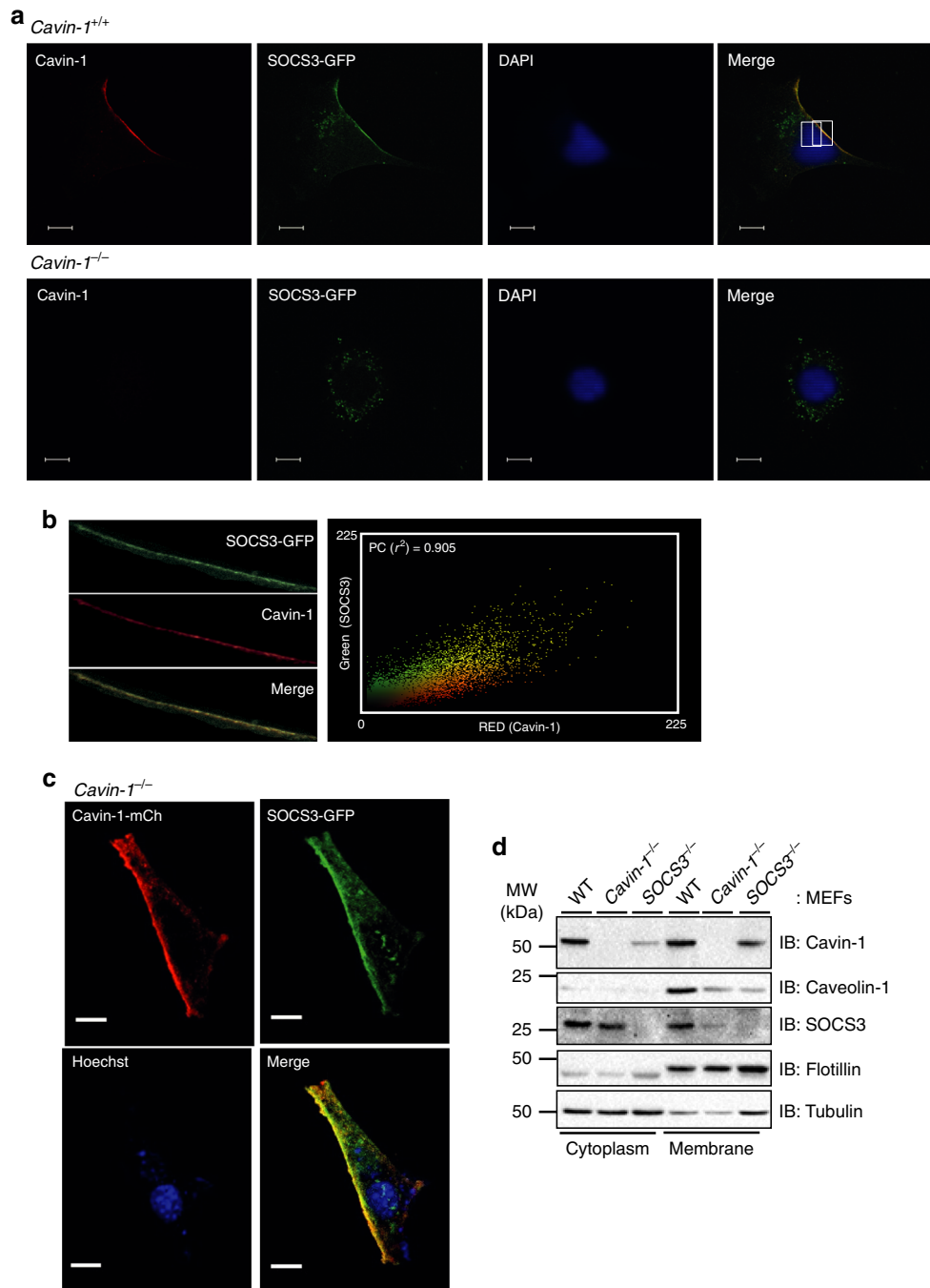


**Fig. 7** Cavin-1 drives SOCS3 localisation to the plasma membrane. **a** WT (*cavin-1*<sup>+/+</sup>) and *cavin-1*<sup>-/-</sup> MEFs transiently expressing SOCS3-GFP (green) were stained with DAPI prior to being fixed, solubilised, and stained with anti-cavin-1 antibody (red) before mounting for imaging by confocal microscopy. Areas of red and green overlap are yellow. Scale bar = 10  $\mu$ m. **b** Pearson's correlation coefficient value ( $r^2$ ) measured from the intensity values located within the rectangular region on the plasma membrane superimposed on the merged cavin-1/SOCS3-GFP image from WT MEFs. **c** *Cavin-1*<sup>-/-</sup> MEFs transiently co-expressing SOCS3-GFP (green) and cavin-1-mCh (red) were stained with Hoechst 33342 prior to being fixed for imaging by confocal microscopy. Areas of red and green overlap are yellow. Scale bar = 10  $\mu$ m. **d** WT, SOCS3<sup>-/-</sup>, and *cavin-1*<sup>-/-</sup> MEFs were pre-incubated with Fsk (50  $\mu$ M) for 5 h to induce SOCS3 prior to subcellular fractionation and analysis by SDS-PAGE and immunoblotting with the indicated antibodies

of SOCS3 in intact cells and was an important determinant of SOCS3 localisation to the plasma membrane.

**Cavin-1 limits IL-6-stimulated Tyr705 STAT3 phosphorylation.** While some studies have demonstrated localisation of cytokine receptors and JAKs in lipid raft microdomains<sup>15–18</sup>, relatively little is known about the impact of caveolin expression/

function on JAK–STAT signalling and no studies have specifically examined a role for caveins. Our data suggested that cavin-1 and SOCS3 interacted directly and co-localised at the plasma membrane, while SOCS3 was mainly cytosolic in the absence of cavin-1. To examine any functional impact of cavin-1 on cytokine signalling, we examined the effects of cavin-1 deletion in MEFs on IL-6-mediated activation of STAT3, as determined by phosphorylation at Tyr705 which is required for STAT3 to form

transcriptionally active complexes<sup>39</sup>. While stimulation of both WT and *cavin-1*<sup>-/-</sup> MEFs with a sIL-6R $\alpha$ /IL-6 *trans*-signalling complex triggered a transient increase in STAT3 phosphorylation on Tyr705, the response was greater and more sustained in *cavin-1*<sup>-/-</sup> MEFs, being detectable at the 60 and 120 min time points in *cavin-1*<sup>-/-</sup> but less pronounced in WT cells (Fig. 8a). Interestingly, Tyr705 phosphorylation was specifically enhanced as STAT3 phosphorylation on Ser727 (which is mediated by several candidate Ser/Thr kinases<sup>40</sup>) was unaffected by *cavin-1* deletion. Moreover, the increase in IL-6 signalling occurred despite reduced levels of JAK1 in *cavin-1*<sup>-/-</sup> MEFs, although this reduction did not reach statistical significance (Fig. 8a). Other cytokine receptor complexes that utilise gp130 include those for leukaemia inhibitory factor (LIF) and oncostatin M (OSM): LIF signals via gp130/LIF receptor (LIFR) heterodimers, while OSM signals downstream using either LIFR/gp130 or OSM receptor/gp130 complexes<sup>41</sup>. As observed with sIL-6R $\alpha$ /IL-6, Tyr705 phosphorylation of STAT3 in response to either LIF or OSM was greater in *cavin-1*<sup>-/-</sup> versus WT MEFs at 60 min (Fig. 8b). Taken together, these data suggested that loss of *cavin-1* compromised one or more inhibitory mechanisms responsible for suppressing gp130- and JAK-mediated Tyr phosphorylation of STAT3.

Previous studies have demonstrated that depletion or loss of SOCS3 results in prolonged activation of STAT3 in response to specific cytokines<sup>42–44</sup>, similar to the effect observed upon *cavin-1* deletion. We have shown previously that the ability of cAMP to inhibit IL-6 signalling in vascular ECs, MEFs, and COS cells has an absolute requirement for Epac1-dependent induction of SOCS3<sup>26,27,45</sup>. Given the importance of *cavin-1* in localising SOCS3 to the plasma membrane and the sustained phosphorylation of STAT3 on Tyr705 observed following sIL-6R $\alpha$ /IL-6 stimulation of *cavin-1*<sup>-/-</sup> MEFs, we examined the impact of *cavin-1* deletion on the inhibitory effect of cAMP which has previously been shown to be SOCS3 dependent<sup>26,45</sup>. These experiments demonstrated that while pre-treatment of WT MEFs with cAMP-elevating drug Fsk (50  $\mu$ M) significantly inhibited sIL-6R $\alpha$ /IL-6-stimulated Tyr705 phosphorylation of STAT3, this effect was lost in *cavin-1*<sup>-/-</sup> MEFs even though Fsk in combination with sIL-6R $\alpha$ /IL-6 produced equivalent levels of SOCS3 in WT and *cavin-1*<sup>-/-</sup> MEFs (Fig. 8c). These results also did not reflect a non-specific reduction in cAMP responsiveness following loss of *cavin-1* as Fsk could trigger the accumulation of cAMP target gene *Nur77* equivalently in both WT and *cavin-1*<sup>-/-</sup> MEFs (Supplementary Fig. 6). Therefore, the presence of *cavin-1* was necessary for SOCS3-mediated inhibition of IL-6 signalling by cAMP.

## Discussion

The importance of SOCS3 in limiting downstream signalling from cytokine receptor complexes that utilise gp130, as well as the leptin receptor *Obrb* and the G-CSFR, is well established<sup>6,7</sup>. However, relatively little is known about how SOCS3 interaction with other intracellular proteins can impact on its ability to inhibit signalling. As part of a study to identify SOCS3-regulated substrates, we performed “stable isotopic labelling of amino acids in cell culture” (SILAC) analysis of ubiquitinome profiles in WT and *SOCS3*<sup>-/-</sup> MEFs stably expressing a tandem affinity purification (TAP)-tagged ubiquitin transgene<sup>46</sup>. Using this approach, the caveola scaffolding protein *cavin-1* was identified as a ubiquitinated protein whose levels were stabilised in WT cells. We have demonstrated that *cavin-1* can interact with SOCS3 and that the absence of SOCS3 results in increased turnover of *cavin-1* and a parallel reduction in cellular levels of caveolin-1 and cell surface caveolae. We have also demonstrated that *cavin-1* is important for effective SOCS3-mediated suppression of

JAK–STAT signalling in response to sIL-6R $\alpha$ /IL-6 *trans*-signalling complexes.

The importance of caveolae and other lipid raft microdomains for maintaining signalling from the plasma membrane has been demonstrated for a variety of systems, including endothelial nitric oxide synthase and Src<sup>47,48</sup>. In comparison, relatively little information is available on how they regulate JAK–STAT pathway activation. Localisation of JAK–STAT signalling components, including gp130, receptors for growth hormone, ciliary neurotrophic factor and LIF, and JAK2 to lipid rafts has been determined by biochemical fractionation of cell extracts<sup>15–18,49–52</sup>. However, the functional consequences appear to be context dependent, such that raft disruption by treatment with cholesterol-depleting agents like  $\beta$ -cyclodextrin or homozygous deletion of caveolin-1 can either inhibit<sup>15,16,49</sup> or enhance<sup>52,53</sup> downstream signalling. Thus, Lisanti and colleagues<sup>52</sup> have examined the effects of manipulating caveolin-1, and demonstrated that caveolin-1 can suppress prolactin receptor-mediated JAK2-dependent phosphorylation and activation of STAT5a in murine mammary epithelial cells *in vitro*, consistent with observations that caveolin-1 deletion *in vivo* enhances prolactin receptor signalling<sup>53</sup>. The mechanism proposed was via a direct interaction between caveolin-1 and JAK2, although no evidence of a direct effect of caveolin-1 on JAK2 Tyr kinase activity was presented<sup>52</sup>. Other studies have specifically examined the importance of caveolae for gp130 function, demonstrating that a significant proportion of cellular gp130 resides in detergent-resistant lipid rafts and can co-IP with caveolin-1. In addition, cholesterol depletion with  $\beta$ -cyclodextrin has been shown to trigger the re-distribution of gp130 to non-raft fractions and attenuate the ability of IL-6 to stimulate STAT3 phosphorylation on Tyr705<sup>16</sup>. In contrast, others have found that both gp130 and STAT3 are localised to lipid rafts<sup>15</sup> and demonstrated an inverse relationship between caveolin-1 expression and STAT3 activation<sup>54</sup>. Therefore, while a weak association between membrane microdomains and JAK–STAT signalling modules has been made, the molecular mechanisms responsible for this interaction remain unclear.

Our data would suggest a novel route through which caveola accessory protein *cavin-1* can modulate cytokine receptor signalling via interaction with the inhibitory regulator SOCS3. While SOCS3 expression is induced in response to many stimuli, conditional gene targeting strategies have revealed that sensitivity to SOCS3 is restricted to a panel of plasma membrane-localised cytokine receptors<sup>6,7,41</sup>. Consistent with another study<sup>38</sup>, we found that while *cavin-1* was localised to the plasma membrane in WT MEFs, it was not distributed uniformly, instead localising to the trailing edge of migrating cells. Importantly, a significant proportion of SOCS3-GFP co-localised to the same plasma membrane compartment in WT but not *cavin-1*<sup>-/-</sup> MEFs. Together with data showing that *cavin-1* could co-IP with SOCS3 and that purified SOCS3 could interact with multiple *cavin-1*-derived peptides *in vitro*, we propose that *cavin-1* binds SOCS3 directly and that this contributes to efficient SOCS3 recruitment to the plasma membrane where it can effectively bind and inhibit cytokine receptors such as gp130. A key aspect of this model (Fig. 9) is that SOCS3 can still bind Tyr phosphorylated peptide *in vitro* in the presence of *cavin-1*. Interestingly, the SOCS3 SH2 domain appeared to fulfil both PTyr and *cavin-1* binding functions as *cavin-1* interaction required the PEST motif present within the SOCS3 SH2 domain, which we and others have shown to be dispensable for PTyr binding<sup>33,36</sup>. In some respects, this is similar to the recently described interaction between SOCS3 and CUEDC2, which also binds the SH2 domain and enhances SOCS3-mediated inhibition of JAK1–STAT3 activation by IL-6<sup>11</sup>. Since CUEDC2 potentiates SOCS3 function it would be

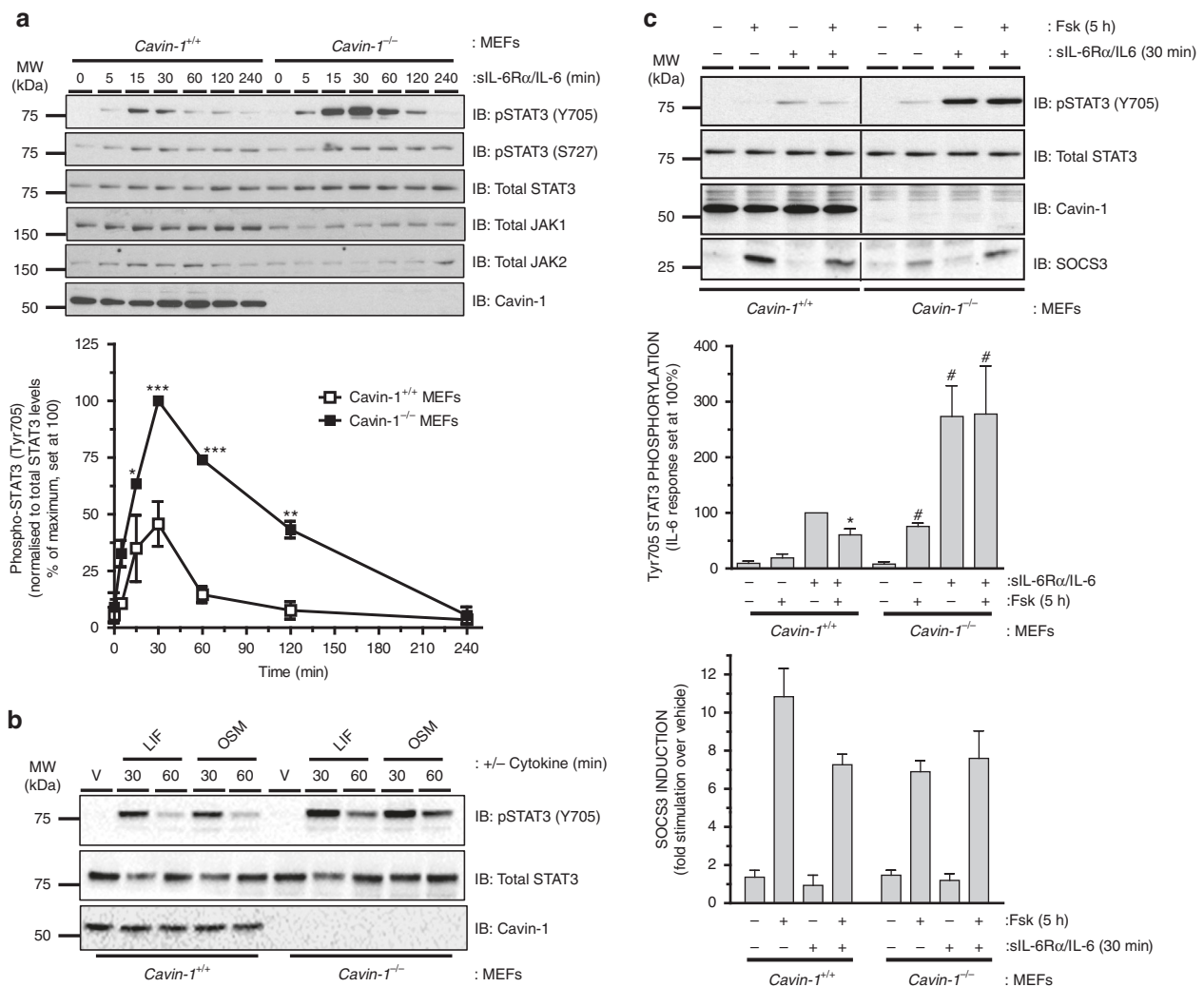


**Fig. 8** Cav-1 limits Tyr705 phosphorylation of STAT3 via SOCS3. **a** Upper: Protein-equalised soluble cell extracts from *cavin-1<sup>+/+</sup>* and *cavin-1<sup>-/-</sup>* MEFs treated for the indicated times with sIL-6Rα/IL-6 (25 and 5 ng ml<sup>-1</sup>) were fractionated by SDS-PAGE prior to immunoblotting with the indicated antibodies. Quantitation of normalised Tyr705 phospho-STAT3 in *cavin-1<sup>+/+</sup>* and *cavin-1<sup>-/-</sup>* MEFs are presented as mean values ± standard error for *N* = 3 experiments. \**P* < 0.05, \*\**P* < 0.01, \*\*\**P* < 0.001 vs. corresponding treatment in *cavin-1<sup>+/+</sup>* MEFs. **b** Protein-equalised soluble cell extracts from *cavin-1<sup>+/+</sup>* and *cavin-1<sup>-/-</sup>* MEFs treated for 30 and 60 min with leukaemia inhibitory factor (LIF; 0.5 nM), oncostatin M (OSM; 10 ng ml<sup>-1</sup>) or vehicle (V) were fractionated by SDS-PAGE prior to immunoblotting with the indicated antibodies. **c** Upper: WT (*cavin-1<sup>+/+</sup>*) and *cavin-1<sup>-/-</sup>* MEFs were pre-incubated with or without Fsk (50 μM) for 5 h prior to treatment with or without sIL-Rα/IL-6 (25 and 5 ng ml<sup>-1</sup>) for 30 min. Cell extracts were analysed by SDS-PAGE and immunoblotting with the indicated antibodies. Lower: Quantitation of normalised Tyr705 phospho-STAT3 and SOCS3 in *cavin-1<sup>+/+</sup>* and *cavin-1<sup>-/-</sup>* MEFs is presented as mean ± standard error for *N* = 3 experiments, \**P* < 0.05 vs. sIL-6Rα/IL-6 treatment in *cavin-1<sup>+/+</sup>* MEFs, #*P* < 0.05 vs. vehicle treatment in *cavin-1<sup>-/-</sup>* MEFs.

anticipated that, like cav-1, its interaction with the SH2 domain must be independent of PTyr binding, suggesting it may also involve the PEST sequence. However, in contrast to cav-1, CUEDC2 localises to the cytoplasm and nucleus<sup>55</sup>. Nevertheless, our observations and those of Zhang et al.<sup>11</sup> raise the possibility that multiple proteins may bind within the SOCS3 SH2 domain to facilitate localisation with Tyr phosphorylated binding partners in distinct subcellular compartments. In this regard, it should be noted that confocal imaging and subcellular fraction experiments detected SOCS3 in the cytoplasm as well as the plasma membrane, and that cav-1 deletion resulted in the specific loss of the plasma membrane pool.

To date, we are only aware of one other study which has examined the impact of the PEST sequence on SOCS3 function<sup>36</sup>. However, these experiments were performed in HEK293 cells co-transfected to express a STAT3-responsive reporter gene and increasing amounts of either WT or ΔPEST SOCS3. The authors

noted that at maximal levels of WT and ΔPEST SOCS3 expression, both constructs abolished LIF-stimulated activation of STAT3. However, upon normalising SOCS3 function with the expression levels of WT and ΔPEST SOCS3, they also noted that at submaximal expression levels the functionality of ΔPEST SOCS3 was less than that of WT SOCS3. Thus, they concluded that WT SOCS3 is slightly more efficient at inhibiting STAT3 activation<sup>36</sup>. Others have shown that low expression levels of SOCS3 inhibit signalling via interaction with gp130 followed by inhibition of JAK activity, whereas overexpression SOCS3 can inhibit gp130 signalling independently of interaction with the SOCS3 binding site and works instead via direct inhibition of JAK1<sup>19,56</sup>. These data would also suggest that any functional deficits in ΔPEST SOCS3 in localising to gp130 would be overcome by its overexpression. In contrast, our functional experiments examining signalling from endogenous proteins suggest an important aspect of SOCS3 PEST motif function is an interaction

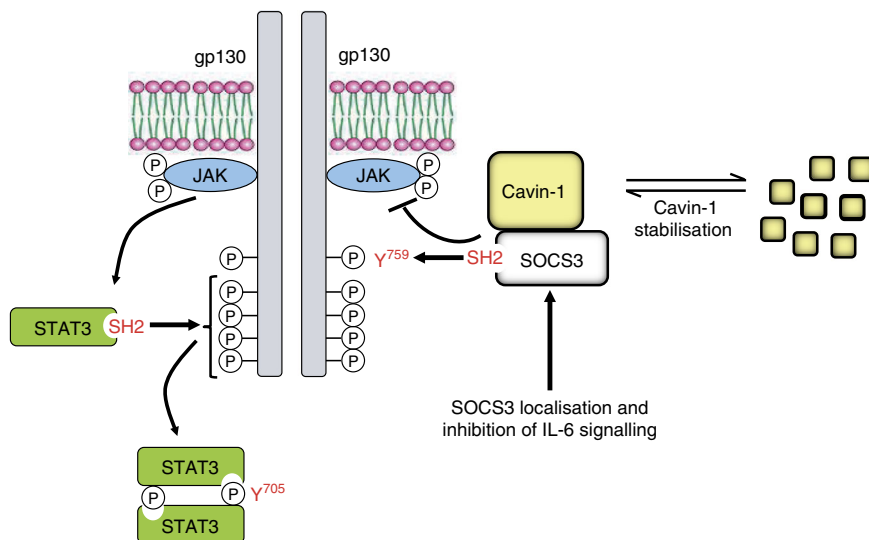


**Fig. 9** Model of novel functional interactions between SOCS3 and cavin-1

with cavin-1 that is critical for effective regulation of JAK–STAT signalling. The effects on signalling of reconstituting *cavin-1*<sup>-/-</sup> MEFs with mutated cavin-1 that fails to interact with SOCS3 but retains the ability to stabilise caveolin-1 would be very informative in dissecting whether cavin-1 is essential for SOCS3 function or simply enhances it through facilitating recruitment to the plasma membrane. It would also be important to assess any functional consequences of SOCS3 on gp130 ubiquitylation<sup>57</sup> and receptor trafficking<sup>10</sup> in order to fully assess the impact of cavin-1 on SOCS3 function.

While this adds an extra layer of regulation for SOCS3, our study has also identified a previously unknown mechanism by which SOCS3 can regulate cavin-1 function by enhancing its stability and, as a consequence, maintaining expression levels of caveolin-1 and cell surface caveolae. Similar observations have recently been reported for Eps15 homology domain-containing protein 2 (EHD2) which, to our knowledge, is the only other example of a cavin-1-interacting protein that regulates caveola stability, although a direct effect on cavin-1 turnover has not been examined<sup>58</sup>. More generally, our findings also raise the possibility that cavins constitute a new class of SOCS3-interacting proteins. While the presence of cavin-1 and caveolin-1 is sufficient to generate caveolae in many cell types<sup>59</sup>, MEFs also express cavin-2 and cavin-3. Elegant biochemical and biophysical studies have demonstrated that cavins assemble into oligomeric complexes both in cells and in vitro<sup>60,61</sup>. While each of the cavins is detectable on individual caveolae<sup>59</sup>, cavin-2 and cavin-3 appear to form distinct hetero-oligomeric complexes with cavin-1 rather than with each other<sup>60</sup>. Thus, it would be anticipated that SOCS3 should interact with both cavin-1/cavin-2 and cavin-1/cavin-3 oligomers and therefore distribute itself uniformly around caveolar bulbs similarly to cavin-1<sup>61</sup>. As the SOCS3 PEST sequence was necessary for cavin-1 interaction, it would also be informative to assess what extent this property is shared among similar sequences present in other SOCS family members. Analysis of the SOCS family revealed that CIS, which like SOCS3 can also interact with cavin-1, contains a PEST motif located in its SH2 domain, while SOCS1, SOCS5, and SOCS7 each have one or more PEST sequences located within their N-terminal domains. In contrast, no PEST motifs are found in SOCS2, SOCS4, and SOCS6. Given the distinct roles of different SOCS family members in regulating signalling<sup>62</sup>, the functional significance of the identified PEST motifs and their roles in determining the

localisation of individual SOCS proteins via distinct protein interactions warrant further investigation.

Finally, our findings may have implications in the context of how cavin-1 and SOCS3 dysfunction can trigger disease. Several inactivating frameshift mutations within exon 2 of the cavin-1 gene that result in the production of altered cavin-1 proteins have been identified in patients with general lipodystrophy, muscular dystrophy, and insulin resistance<sup>63–66</sup>. In each case, a lack of functional cavin-1 is associated with the downregulation and/or mislocalisation of all three caveolin subtypes in skeletal muscle and an absence of cell surface caveolae in patient-derived fibroblasts<sup>64</sup> and skeletal muscle<sup>63</sup>. As multiple regions within cavin-1 are required for optimal binding of SOCS3, the mutated cavin-1 proteins identified in patients with congenital generalised lipodystrophy would be predicted to be compromised in their ability to interact with SOCS3, thereby resulting in enhanced IL-6 responses. In this regard, cardiac-specific homozygous deletion of murine *SOCS3* results in contractile dysfunction and the occurrence of a variety of ventricular arrhythmias<sup>67</sup>, the latter of which is also observed in patients with inactivating cavin-1 mutations<sup>64</sup>. Finally, a F136L germline *SOCS3* mutation found in a subset of polycythemia vera patients has been shown to display an impaired capacity to inhibit erythropoietin receptor–JAK2 signalling<sup>68</sup>. As F136 is located within the PEST insert we have identified as critical for cavin-1 interaction, this mutation may alter cavin-1 binding to SOCS3 to block its inhibitory effects on JAK–STAT signalling. Based on our findings, future studies will therefore need to examine how cavin-1 and/or SOCS3 mutations identified in patients interact to trigger defective regulation of signalling in these pathologies.

## Methods

**Cell culture and transfection.** HEK293 cells were obtained from the European Collection of Authenticated Cell Cultures (ECACC) through Sigma. Immortalised *SOCS3*<sup>-/-</sup> and *cavin-1*<sup>-/-</sup> MEFs and the corresponding WT cell lines have been described previously<sup>59,69</sup>. HEK293 cells and MEFs were maintained in Dulbecco's modified Eagle's medium (DMEM) supplemented with 10% (v/v) foetal bovine serum (FBS), 1 mM L-glutamine, 100 U ml<sup>-1</sup> penicillin and 100 μM streptomycin. AS-M.5 human angiosarcoma-derived ECs generously provided by Dr Vera Krump-Konvalinkova and Professor Charles Kirkpatrick (Johannes Gutenberg University of Mainz, Germany)<sup>28</sup> were cultured in endothelial growth medium-2 supplemented with 2% (w/v) FBS, hydrocortisone, ascorbate, and recombinant growth factors as recommended by the supplier (Lonza). HEK293 cells at 80% confluence on poly-D-lysine-coated dishes were transfected with 2–8 μg of complementary DNA (cDNA) per 100 mm dish using PolyFect transfection reagent (Qiagen) as per THE manufacturer's instructions.

For SILAC experiments, MEFs were grown in either heavy SILAC DMEM ( $^{13}\text{C}_6$ -arginine,  $^{13}\text{C}_6$ -lysine; R6K6) or control SILAC DMEM ( $^{12}\text{C}_6$ -arginine,  $^{12}\text{C}_6$ -lysine; R0K0) (Dundee Cell Products, UK) supplemented with 10% (v/v) dialysed calf serum, 100 U ml $^{-1}$  penicillin, 100  $\mu\text{M}$  streptomycin, 4  $\mu\text{g}$  ml $^{-1}$  puromycin, 200 mg l $^{-1}$  L-proline and 1  $\mu\text{M}$  D-biotin. Arginine can be metabolised from  $^{13}\text{C}_6$ -arginine to an isotope of the non-essential amino acid  $^{13}\text{C}_5$ -proline via the arginase pathway thus complicating data analysis<sup>70</sup>. As such, media were supplemented with L-proline (200 mg l $^{-1}$ ) to prevent arginine conversion. Furthermore, as overexpression of the HB-Ub-tag reduces the availability of cellular D-biotin<sup>21</sup>, growth medium was supplemented with D-biotin (1  $\mu\text{M}$ ) to prevent saturation of *in vivo* biotinylation by excessive HB-Ub-tag expression. Plat-E retroviral packaging cells were maintained in DMEM supplemented with 10% (v/v) FBS, 100 U ml $^{-1}$  penicillin, 100  $\mu\text{M}$  streptomycin, 1  $\mu\text{g}$  ml $^{-1}$  puromycin, 10  $\mu\text{g}$  ml $^{-1}$  blasticidin, and 1 mM glutamine.

**Constructs.** Murine Grap2 (cat no. MR204666) and murine CIS (cat no. MR203328) in pCMV6-Entry were from Origene. Human SOCS3 CRISPR/Cas9 knockout (KO) and human SOCS3 HDR plasmids (cat. no. sc-400455) were from Santa Cruz Biotechnology. Expression constructs for Flag-tagged WT murine SOCS3 (hereafter termed pcDNA3/Flag-SOCS3), the truncation mutants  $\Delta\text{N}20$ ,  $\Delta\text{N}36$ ,  $\Delta\text{C}40$ , and  $\Delta\text{C}84$ , R71K-mutated SOCS3, and the  $\Delta\text{PEST}$  mutant SOCS3 (generously provided by Dr Jeff Babon, Walter and Eliza Hall Institute of Medical Research, Australia) have all been described previously<sup>30,31,33,71</sup>. N-terminally GFP-tagged murine cavin-1 has been described previously<sup>32</sup> while a cavin-1-mCherry expression construct was generously provided by Dr Ben Nichols (MRC Laboratory of Molecular Biology, Cambridge, UK).

Full-length murine WT SOCS3,  $\Delta\text{SH}2$  SOCS3 (amino acids 46–142), and SOCS3 box domain-only (amino acids 177–225) GFP fusion proteins were generated by PCR amplification and sub-cloning in-frame with the GFP open reading frame in pEGFP-N1 (Clontech). The following primers were used to generate PCR products using pcDNA3/Flag-SOCS3 as the template prior to digestion with the indicated restriction enzymes for sub-cloning:-

Forward primers: WT (GAA GAA GAA TTC GCC ACC ATG GTC ACC CAC AGC AAG), SOCS box only (GAA GAA GAA TTC GCC ACC ATG GTA CTG AGC CGA CCT CTC), SH2 domain only (GAA GAA GAA TTC GCC ACC ATG TTC TAG TGG AGC GGC GTG). *EcoRI* sites for sub-cloning underlined, initiating Met codon in italics. Reverse primers: WT and SOCS box only (TT CTC GGG ATC CGC AAG TGG AGC ATC ATA CTG ATC CAG G).  $\Delta\text{SH}2$  SOCS3 (TTC TCG GGA TCC GCT TCC GTG GGT GGC AAA G). *BamHI* sites for sub-cloning underlined.

Myc-tagged WT murine cavin-1 and the truncation mutants N1 (amino acids 74–392), N2 (amino acids 168–392), N3 (amino acids 193–392), N4 (amino acids 250–392), C1 (amino acids 1–76), C2 (amino acids 1–167), C3 (amino acids 1–192), and C4 (amino acids 1–249) were generated by PCR amplification and sub-cloning in-frame with the C-terminal myc epitope (EQKLISEEDL) in pcDNA3.1/mycHis A(-) (Invitrogen). The following primers were used to generate PCR products using pEGFP-C1/cavin-1 as the template prior to digestion with the indicated restriction enzymes and sub-cloning:-

Forward primers: WT, C1, C3, C3 and C4 constructs (GGA GAA CCT CTA GAC GCC ACC ATG GAG GAT GTC ACG CTC), N1 (GGA GAA CCT CTA GAC GCC ACC ATG CAA GCC CAG CTG GAG), N2 (GGA GAA CCT CTA GAC GCC ACC ATG CTG AGC GTC AGC AAG TCG), N3 (GGA GAA CCT CTA GAC GCC ACC ATG CGG CCC GAG GAT GAC ACC), N4 (GGA GAA CCT CTA GAC GCC ACC ATG ACG CGT GAG AAC CTG GAG). *XbaI* sites for sub-cloning underlined, initiating Met codon in italics. Reverse primers: C1 (TTC TCG GAT CCA CTG GCG TTG GGT CAG CTG), C2 (TTC TCG GAT CCA TTT GGC CGG CAG CTT GAC), C3 (TTC TCG GAT CCA CTC GCC CTC GTC CAG CTC), C4 (TTC TCG GAT CCA GCG CAC CTT GGT CTT CTC). WT, N1, N2, N3, and N4 constructs (TTC TCG GAT CCA GTC GCT GTC GCT CTT GTC). *BamHI* sites for sub-cloning underlined.

A mutated Grap2(SOCS3-PEST) in which residues 129–163 encompassing the SOCS3 PEST sequence were inserted between amino acids 149–150 within the Grap2 ORF in pCMV6-Entry was synthesised by GeneArt<sup>TM</sup>. All constructs were verified by sequencing to ensure the absence of additional unanticipated mutations.

**Retroviral delivery of a His<sub>6</sub>+biotin Ub (HB-Ub) transgene.** Using Lipofectamine2000 (Invitrogen), Plat-E retroviral packaging cells in 10 cm dishes at approximately 80% confluence were transfected with a HB-Ub-expressing plasmid kindly donated by Professor Peter Kaiser (University of California at Irvine, USA)<sup>22</sup>. Following incubation in media without antibiotic selection, retrovirus-containing media were collected following two sequential incubation periods, one of 24 h at 37 °C and a second of 24 h at 32 °C.

**Retroviral-mediated generation of cell lines.** MEFs in 10 cm dishes at approximately 40% confluence were transduced with 2 ml of retrovirus containing media in a final volume of 4 ml DMEM supplemented with 10% (v/v) FBS, 1 mM glutamine, and 10  $\mu\text{g}$  ml $^{-1}$  polybrene. After 12 h, the media were replaced with DMEM supplemented with 10% (v/v) FBS, 1 mM L-glutamine and 100 U ml $^{-1}$  penicillin, 100  $\mu\text{M}$  streptomycin and 1  $\mu\text{g}$  ml $^{-1}$  puromycin to select for positive clones. Following dilution and re-plating, positive clones were expanded and HB-

Ub-expressing clones identified by immunoblotting whole-cell extracts with a polyHis antibody.

**Tandem affinity purification.** SOCS3<sup>+/+</sup> and SOCS3<sup>-/-</sup> MEFs were harvested in lysis buffer (8 M urea, 300 mM NaCl, 50 mM NaH<sub>2</sub>PO<sub>4</sub>, 0.5% (v/v) NP-40, pH 8.0) supplemented with 1 mM phenylmethylsulfonyl fluoride (PMSF). Following sonication (3  $\times$  10 s pulses, with a 10 s rest phase, at 40% amplitude), supernatants were isolated by centrifugation at 21,000 $\times$ g for 30 min at room temperature (RT) and equalised for protein content. Lysates from SOCS3<sup>+/+</sup> and SOCS3<sup>-/-</sup> MEFs were mixed in a 1:1 ratio before incubation with 30  $\mu\text{l}$  of 50% (v/v) Ni<sup>2+</sup>-NTA-Sepharose beads per milligram of protein and rotated overnight at RT. Beads were isolated by centrifugation at 100 $\times$ g for 1 min and then washed sequentially, once with 20 bead volumes of buffer A (8 M urea, 300 mM NaCl, 50 mM NaH<sub>2</sub>PO<sub>4</sub>, 0.5% (v/v) NP-40, pH 8.0) supplemented with 1 mM PMSF and 10 mM imidazole and twice with 20 bead volumes of buffer B (8 M urea, 300 mM NaCl, 50 mM NaH<sub>2</sub>PO<sub>4</sub>, 0.5% (v/v) NP-40, pH 6.3) supplemented with 10 mM imidazole and 1 mM PMSF. Beads were isolated by centrifugation at 100 $\times$ g for 1 min and bound proteins eluted twice with 5 bead volumes of elution buffer (8 M urea, 200 mM NaCl, 50 mM NaH<sub>2</sub>PO<sub>4</sub>, 2% (w/v) SDS, 10 mM EDTA, 100 mM Tris, 500 mM imidazole, pH 8.0) supplemented with 1 mM PMSF.

Eluate from the Ni affinity chromatography step was directly added to 10  $\mu\text{l}$  of 50% (v/v) streptavidin-Sepharose beads per milligram of initial protein lysate and rotated overnight at RT. Beads isolated by centrifugation at 100 $\times$ g for 1 min at RT were washed sequentially, twice with 25 bead volumes of buffer C (8 M urea, 200 mM NaCl, 2% (w/v) SDS, 100 mM Tris, pH 8.0) and twice with 25 bead volumes of buffer D (8 M urea, 1.2 M NaCl, 0.2% (w/v) SDS, 100 mM Tris, 10% (v/v) ethanol, 10% (v/v) isopropanol, pH 8.0). Bound proteins were eluted with one bead volume of aqueous biotin (50 mM) at 95 °C for 5 min. Following isolation by centrifugation at 100 $\times$ g for 1 min at RT, eluate was concentrated using Amicon 10K Ultra-2 Centrifugal Filter Devices (Millipore) as per the manufacturer's instructions.

**In-gel trypsin digestion.** Sodium dodecyl sulphate-polyacrylamide gel electrophoresis (SDS-PAGE)-fractionated TAP eluate was stained with InstantBlue (Expedition) prior to manual sectioning into several manageable gel slices. Individual gel slices were washed sequentially with 500  $\mu\text{l}$ , 100 mM ammonium bicarbonate and then 500  $\mu\text{l}$ , 50% (v/v) acetonitrile/ammonium bicarbonate (100 mM) for 30 min with shaking. The samples were reduced with the addition of 150  $\mu\text{l}$  100 mM ammonium bicarbonate and 10  $\mu\text{l}$  45 mM dithiothreitol for 30 min at 60 °C. Samples were cooled to RT before alkylation using 10  $\mu\text{l}$  100 mM iodoacetamide in the dark for 30 min at RT. Gel pieces were then washed in 500  $\mu\text{l}$  50% (v/v) acetonitrile/ammonium bicarbonate (100 mM) for 1 h with shaking at RT. Following treatment with 50  $\mu\text{l}$  acetonitrile for 10 min, the solvent was discarded and the gel pieces dried using a vacuum centrifuge for 1 h. Gel slices were fully rehydrated in trypsin suspended in 1 ml 25 mM ammonium bicarbonate and incubated overnight at 37 °C after which the supernatant was transferred to a fresh 96-well plate without disturbing the gel pieces. Residual digested protein was extracted by using 20  $\mu\text{l}$  5% (v/v) formic acid for 20 min at RT with shaking followed by the addition of 40  $\mu\text{l}$  acetonitrile for a further 20 min with shaking at RT. Pooled extracts were dried using a SpeedVac centrifugal evaporator before resuspension in 10  $\mu\text{l}$  dH<sub>2</sub>O prior to mass spectrometry.

**Liquid chromatography and mass spectrometry.** Samples were analysed on a Dionex Ultimate 3000 RSLC Nano flow system (Dionex). The samples (5  $\mu\text{l}$ ) were loaded onto a Dionex 100  $\mu\text{m}$   $\times$  2 cm 5  $\mu\text{m}$  C18 Nano trap column at a flow rate of 5  $\mu\text{l}$  min $^{-1}$  by the Ultimate 3000 RS autosampler (Dionex). The composition of the loading solution was 0.1% formic acid and acetonitrile (98:2). Once loaded onto the column, the sample was then washed off into an Acclaim PepMap 75  $\mu\text{m}$   $\times$  15 cm, 2  $\mu\text{m}$  100 Å C18 Nano column at a flow rate of 0.3  $\mu\text{l}$  min $^{-1}$ . The trap and nano flow column were maintained at 35 °C in an Ultimate 3000 Rapid Separation LC system (Thermo Fisher). The samples were eluted with a gradient of solvent A: 0.1% formic acid (solvent A) versus acetonitrile (solvent B) starting at 1% B rising to 15% then to 45% B over 50 and then 90 min. The column was washed using 90% B before being equilibrated prior to the next sample being loaded.

Column eluate was directed to a Proxeon Nano spray electrospray ionisation (ESI) source (Thermo Fisher) operating in positive ion mode and then into an Orbitrap Velos FTMS. The ionisation voltage was 2.5 kV and the capillary temperature was 230 °C. The mass spectrometer was operated in tandem mass spectrometry (MS/MS) mode scanning from 300 to 2000 amu. The top 20 multiply charged ions were selected from each full scan for MS/MS analysis, the fragmentation method was CID at 35% collision energy. The ions were selected for MS<sup>2</sup> using a data-dependent method with a repeat count of 1 s and repeat and exclusion time of 15 s. Precursor ions with a charge state of 1 were rejected. The resolution of ions in the first stage (MS<sup>1</sup>) was 60,000 and 7500 for the second stage (CID MS<sup>2</sup>). Data were acquired using Xcalibur v.2.1 (Thermo Fisher).

**Analysis of LC-MS/MS.** Post-LC-MS/MS analysis was performed using MaxQuant v.1.11.36<sup>72</sup> and searched with Andromeda search engine<sup>73</sup> against the IPI mouse.v3.80 Fasta formatted database (release February 2011). Phosphorylation (S, T, Y), ubiquitination (GlyGly), and oxidation (Met) were set as variable

modifications, whereas carbamidomethylation (Cys) was set as fixed modification. The peptides used for protein quantification were set to unique and razor and minimum ratio count set to 1. Requantify was set to "TRUE" for deep searching of paired SILAC peaks. "Labelled amino acid filtering" was set to "FALSE" to improve analysis using R6K6 SILAC labelling. All other options were set to default.

**CRISPR/Cas9 generation of SOCS3-null AS-M.5 EC lines.** Using SuperFect transfection reagent (Qiagen), AS-M.5 cells in 6 cm dishes at approximately 80% confluence were co-transfected with human SOCS3 CRISPR/Cas9 KO and human SOCS3 HDR plasmids. Following dilution and re-plating, positive clones were isolated by selection in medium supplemented with puromycin (2  $\mu\text{g ml}^{-1}$ ). SOCS3-null clones were identified by immunoblotting whole-cell extracts with SOCS3 antibody following cellular treatment with Fsk (50  $\mu\text{M}$ , 5 h) to induce SOCS3 gene expression<sup>26,45</sup>.

**Antibodies.** The following antibodies were obtained from the indicated suppliers: anti-Flag M2 antibody (Sigma F3165, 1 in 1000), anti-HA HA-7 antibody (Sigma H9658, 1 in 1000), PTRF/cavin-1 (Abcam ab48824, 1 in 1000), caveolin-1 (BD Biosciences 610059, 1 in 1000) and anti-phosphotyrosine monoclonal antibody 4G10 (Millipore 05-321, 1 in 1000), GAPDH (Abcam, ab8245, 1 in 20,000), anti-myc 9E10 (ascites generated by ProSci, 1 in 2000), anti- $\alpha$ -tubulin 12G10 (DSHB 12G10, 1 in 10,000), SOCS3 (M20; Santa Cruz sc-7009, 1 in 500), STAT3 (EPR787Y; Abcam ab68153, 1 in 1000), phospho-STAT3 (Tyr705) (3E2; Cell Signaling 9138L, 1 in 1000), phospho-STAT3 (Ser727) (6E4; Cell Signaling 9136, 1 in 1000), JAK1 (BD Transduction Laboratories 610232, 1 in 1000), JAK2 (D2E12; Cell Signaling 3230, 1 in 1000), and flotillin-1 (BD Transduction Laboratories 610821, 1 in 500). Sheep polyclonal anti-GFP serum was generously provided by Professor Graeme Milligan (University of Glasgow, UK) and was used in a 1 in 2000 dilution.

**Immunoblotting.** Cell lysates were prepared as described previously<sup>74</sup>. Cells were washed twice with ice-cold phosphate-buffered saline (PBS) and lysed by scraping into lysis buffer (50 mM HEPES pH 7.4, 150 mM sodium chloride, 1% (v/v) Triton X-100, 0.5% (v/v) sodium deoxycholate, 0.1% (w/v) SDS, 10 mM sodium fluoride, 5 mM EDTA, 10 mM sodium phosphate, 0.1 mM PMSF, 10  $\mu\text{g ml}^{-1}$  benzamide, 10  $\mu\text{g ml}^{-1}$  soybean trypsin inhibitor, 2% (w/v) EDTA-free complete protease inhibitor cocktail (Sigma)). After 30 min on ice, lysates were vortexed and cleared by centrifugation. Equivalent amounts of protein, as determined by bicinchoninic acid protein assay, were resolved by SDS-PAGE, transferred to a nitrocellulose membrane, and analysed by immunoblotting as previously described<sup>26,74,75</sup>. Uncropped immunoblots used to generate Figs. 1b and 5b are shown in Supplementary Figure 7.

**RNA analysis.** Total RNA extraction from MEFs grown in 60 mm dishes was carried out using a miRNeasy Mini Kit (Qiagen) according to the manufacturer's instructions. The cDNA was generated from 1  $\mu\text{g}$  total RNA using 200 U SuperScript™ II Reverse Transcriptase (Invitrogen) following the manufacturer's instructions with 100 ng random hexamers, 2.5 mM of each dNTP and 40 U RNaseOUT (Invitrogen) in a final volume of 20  $\mu\text{l}$ . Real-time quantitative PCRs were performed on a MX3000 system (Stratagene) using Power SYBR® Green PCR Master Mix (Applied Biosystems) in a final volume of 10  $\mu\text{l}$  containing 1  $\mu\text{l}$  cDNA, 0.5 mM of each primer, and 1x Power SYBR® Green PCR Master Mix. The murine *cavin-1* primers used were GCAAGGTCAGCGTCAAC (forward primer) and CCGGACGCTTGACTTCA (reverse primer). GAPDH primers used for normalisation were GGCTGGCATTGCTCTCAA (forward primer) and GCTGTAGCCGTATTTCATTGTC (reverse primer). Primers were purchased from Dharmacon.

**Co-immunoprecipitation and peptide pull-down assays.** For co-IP assays, either transfected cells or WT and SOCS3-null AS-M.5 cells were harvested in ice-cold PBS, pelleted by centrifugation at 1000 $\times$ g for 5 min at 4 °C, and lysed in co-IP buffer (50 mM HEPES, pH 7.4, 120 mM NaCl, 5 mM EDTA, 10% (v/v) glycerol, 1% (v/v) Triton X-100, 5 mM NaF, 1 mM sodium orthovanadate, 10  $\mu\text{g ml}^{-1}$  benzamide, 0.1 mM PMSF, 10  $\mu\text{g ml}^{-1}$  soybean trypsin inhibitor, 2% (w/v) EDTA-free complete protease inhibitor cocktail). Following solubilisation by incubation for 1 h at 4 °C with rotation, lysates were centrifuged at 21,000 $\times$ g for 15 min at 4 °C and the supernatant equalised for protein content and volume. Non-specifically binding proteins were removed from soluble fractions by a 1 h pre-clearing step using 40  $\mu\text{l}$  of 50% (v/v) slurry of protein G-Sepharose 4B FF beads (Sigma) re-suspended in 100  $\mu\text{l}$  2% (w/v) IgG-free bovine serum albumin (BSA). Following sedimentation of protein G-Sepharose beads by brief centrifugation, pre-cleared lysates were incubated overnight at 4 °C with rotation with either 40  $\mu\text{l}$  fresh protein G-Sepharose beads pre-equilibrated with 2% (w/v) IgG-free BSA and anti-cavin-1 antibody or 40  $\mu\text{l}$  pre-conjugated anti-Flag M2-agarose beads (Sigma). Immune complexes were then isolated by brief centrifugation and washed three times with 1 ml of co-IP buffer. Following removal of the final wash, protein complexes were eluted for analysis by SDS-PAGE by the addition of 40  $\mu\text{l}$  of electrophoresis sample buffer containing 12% (w/v) SDS and incubation for 30 min at 65 °C followed by a further 5 min at 95 °C.

For peptide pull-down assays, protein-equalised soluble extracts from transfected HEK293 cells were incubated with 100 nM N-terminally biotinylated peptides (Severn Biotech, UK) and streptavidin-agarose prior to isolation of complexes by brief centrifugation and washing as described above. The peptides used had the following amino acid sequences: Tyr759 (Y), biotin-TSSTVQYSTVVHSG; and PTyr759 (pY), biotin-TSSTVQpYSTVVHSG. Samples were then eluted for analysis by SDS-PAGE and immunoblotting as described above.

**Peptide array overlays.** Arrays were produced by automatic SPOT synthesis and synthesised on continuous cellulose membrane supports on Whatman 50 cellulose membranes using Fmoc-chemistry with the AutoSpot-Robot ASS 222 (Intavis Bioanalytical Instruments AG) as we have previously described<sup>76</sup>. Following blocking of non-specific protein binding sites by incubation in tris-buffered saline with Tween-20 (TBST; 50 mM Tris pH 7.5, 150 mM NaCl, 0.1% (v/v) Tween 20) containing 5% (w/v) BSA, membranes were overlaid with 10  $\mu\text{g ml}^{-1}$  purified recombinant Trx-polyHis-tagged SOCS3 (Sino Biological Inc.) diluted in TBST-5% (w/v) BSA. After washing in TBST, bound SOCS3 was detected by probing overlays with anti-SOCS3 antibody followed by IRDye-conjugated secondary antibody prior to visualisation using a LI-COR Odyssey Sa imaging system. As a negative control, identical arrays were identically treated in parallel minus recombinant SOCS3.

**Subcellular fractionation.** Confluent 10 cm dishes of WT, *cavin-1*<sup>-/-</sup>, and SOCS3<sup>-/-</sup> MEFs were used to prepare subcellular fractions using a Subcellular Protein Fractionation Kit (Thermo Scientific) in accordance with the the manufacturer's instructions.

**Confocal microscopy.** For analysis of endogenous *cavin-1* and transfected SOCS3-GFP, WT, and *cavin-1*<sup>-/-</sup> MEFs in 10 cm dishes were transiently transfected with or without SOCS3-GFP expression constructs. The following day, cells were split onto glass coverslips and left for a further 24 h. Cells were then washed with PBS and fixed with 3% (w/v) paraformaldehyde (PFA) in PBS for 25 min. After washing with PBS and quenching residual PFA with 20 mM glycine in PBS, cells were permeabilised with 0.1% (v/v) Triton X-100 and non-specific binding sites blocked by a 30 min of incubation at RT in PBS containing 3% (w/v) BSA and 10% (v/v) donkey serum. Cells were then incubated with rabbit anti-cavin-1 antibody (Abcam ab48824, 1 in 100 dilution) for 90 min at RT. Cells were washed with PBS containing 0.1% (v/v) Triton X-100, 1% (w/v) BSA, and 10% (v/v) donkey serum prior to incubation with Alexa Fluor 594-conjugated donkey anti-rabbit IgG (Life Technologies A21207, 1 in 200 dilution) for 1 h at RT. Finally, the cells were washed with PBS, mounted in ProLong® Gold anti-fade reagent containing nuclear stain 4',6-diamidino-2-phenylindole (DAPI), and visualised using a LSM510 laser scanning confocal imaging system (Carl Zeiss). Images were analysed by Meta-morph software to generate Pearson's correlation coefficients.

For experiments involving co-expression of SOCS3-GFP and *cavin-1*-mCherry in *cavin-1*<sup>-/-</sup> MEFs, cells at 80–90% confluence on 6 cm dishes were transfected with 1  $\mu\text{g}$  of each construct using PolyFect transfection reagent as per the manufacturer's instructions. The following day, cells were seeded into  $\times 16$  Lab-Tek chamber slides (Fisher Scientific) at a density of  $5 \times 10^4$  cells per chamber and cultured for a further 24 h. Cells were then washed twice with Hanks' balanced salt solution with  $\text{Ca}^{2+}/\text{Mg}^{2+}$  and 0.2% (w/v) sucrose to preserve morphology before fixing by incubation with 4% (w/v) PFA at RT for 20 min in the dark. After removal of fixative and two washes with PBS, nuclei were stained with 10  $\mu\text{g ml}^{-1}$  Hoechst 33342 (Life Technologies) prior to imaging using a VivaTome spinning disk confocal microscope (Carl Zeiss). Images were analysed using Fiji ImageJ and the Coloc 2 plugin.

**Transmission electron microscopy.** WT and SOCS3-null AS-M.5 cells were seeded at a density of  $1 \times 10^6$  cells per ml into 6-well plates and onto Thermanox coverslips (13 mm diameter) for culturing to confluency. The cells were then fixed in 1.5% (w/v) glutaraldehyde in 0.1 M sodium cacodylate buffer at 4 °C for 1 h. Following three washes in 0.1 M sodium cacodylate buffer in 2% (w/v) sucrose, the cells were incubated with 1% (w/v) osmium tetroxide/0.1 M sodium cacodylate for 1 h, washed three times in distilled water, and incubated in 0.5% (w/v) uranyl acetate in the dark for 1 h. Following two rinses in distilled water, cells were dehydrated in stepwise alcohol increments (30–100% (v/v)) and incubated overnight in a 1:1 mix of propylene oxide/TAAB aldehyde Epon 812 resin. The propylene oxide was then allowed to evaporate to leave pure resin, which was changed twice before the sample was embedded in fresh resin which was allowed to polymerise at 60 °C for 48 h. Ultrathin sections were cut using a Leica Ultracut UCT and a Diatome diamond knife, contrast stained with aqueous 2% (w/v) methanolic uranyl acetate and Reynolds lead citrate, and viewed using a LEO 912AB TEM (Carl Zeiss) at an accelerating voltage of 120 kV. TIF images were captured using an Olympus Soft Imaging System and image contrast modified using Adobe Photoshop CS.

**Statistics.** Statistical significance was assessed either by one-way analysis of variance or unpaired *t*-tests with an  $\alpha$  probability of 0.05. At least three separate experiments were used for analysis.

**Data availability.** All the data that support the findings of this study are available from the corresponding author upon reasonable request.

Received: 24 July 2015 Accepted: 11 December 2017

Published online: 12 January 2018

## References

- O'Shea, J. J. et al. The JAK-STAT pathway: impact on human disease and therapeutic intervention. *Annu. Rev. Med.* **66**, 311–328 (2015).
- Eulendorf, R. et al. Interleukin-6 signalling: more than Jaks and STATs. *Eur. J. Cell Biol.* **91**, 486–495 (2012).
- Quintás-Cardama, A., Kantarjian, H., Cortes, J. & Verstovsek, S. Janus kinase inhibitors for the treatment of myeloproliferative neoplasias and beyond. *Nat. Rev. Drug Discov.* **10**, 127–140 (2011).
- O'Shea, J. J., Kontzias, A., Yamaoka, K., Tanaka, Y. & Laurence, A. Janus kinase inhibitors in autoimmune diseases. *Ann. Rheum. Dis.* **72**, ii111–ii115 (2013). Suppl 2.
- Yu, H., Lee, H., Herrmann, A., Buettner, R. & Jove, R. Revisiting STAT3 signalling in cancer: new and unexpected biological functions. *Nat. Rev. Cancer* **14**, 736–746 (2014).
- Linossi, E. M., Babon, J. J., Hilton, D. J. & Nicholson, S. E. Suppression of cytokine signaling: the SOCS perspective. *Cytokine Growth Factor Rev.* **24**, 241–248 (2013).
- Babon, J. J., Varghese, L. N. & Nicola, N. A. Inhibition of IL-6 family cytokines by SOCS3. *Semin. Immunol.* **26**, 13–19 (2014).
- Liu, E., Côté, J.-F. & Vuori, K. Negative regulation of FAK signaling by SOCS proteins. *EMBO J.* **22**, 5036–5046 (2003).
- Niwa, Y. et al. Methylation silencing of SOCS-3 promotes cell growth and migration by enhancing JAK/STAT and FAK signalings in human hepatocellular carcinoma. *Oncogene* **24**, 6406–6417 (2005).
- Wölfler, A. et al. Site-specific ubiquitination determines lysosomal sorting and signal attenuation of the granulocyte colony-stimulating factor receptor. *Traffic* **10**, 1168–1179 (2009).
- Zhang, W.-N. et al. CUEDC2 (CUE domain-containing 2) and SOCS3 (suppressors of cytokine signaling 3) cooperate to negatively regulate Janus kinase 1/signal transducers and activators of transcription 3 signaling. *J. Biol. Chem.* **287**, 382–392 (2012).
- Palade, G. Fine structure of blood capillaries. *J. Appl. Phys.* **24**, 1424 (1953).
- Parton, R. G. & del Pozo, M. A. Caveolae as plasma membrane sensors, protectors and organizers. *Nat. Rev. Mol. Cell Biol.* **14**, 98–112 (2013).
- Liu, L. et al. Deletion of Cavin/PTRF causes global loss of caveolae, dyslipidemia, and glucose intolerance. *Cell Metab.* **8**, 310–317 (2008).
- Sehgal, P. B., Guo, G. G., Shah, M., Kumar, V. & Patel, K. Cytokine signaling: STATs in plasma membrane rafts. *J. Biol. Chem.* **277**, 12067–12074 (2002).
- Podar, K. et al. Essential role of caveolae in interleukin-6- and insulin-like growth factor I-triggered Akt-1-mediated survival of multiple myeloma cells. *J. Biol. Chem.* **278**, 5794–5801 (2003).
- Elsasser, T. H. et al. Caveolae nitration of Janus kinase-2 at the 1007Y-1008Y site: coordinating inflammatory response and metabolic hormone readjustment within the somatotrophic axis. *Endocrinology* **148**, 3803–3813 (2007).
- Lee, M. Y., Ryu, J. M., Lee, S. H., Park, J. H. & Han, H. J. Lipid rafts play an important role for maintenance of embryonic stem cell self-renewal. *J. Lipid Res.* **51**, 2082–2089 (2010).
- Kershaw, N. J. et al. SOCS3 binds specific receptor-JAK complexes to control cytokine signaling by direct kinase inhibition. *Nat. Struct. Mol. Biol.* **20**, 469–476 (2013).
- Babon, J. J. et al. The SOCS box domain of SOCS3: structure and interaction with the elonginBC-cullin5 ubiquitin ligase. *J. Mol. Biol.* **381**, 928–940 (2008).
- Tagwerker, C. et al. A tandem affinity tag for two-step purification under fully denaturing conditions: application in ubiquitin profiling and protein complex identification combined with in vivo cross-linking. *Mol. Cell Proteom.* **5**, 737–748 (2006).
- Meierhofer, D., Wang, X., Huang, L. & Kaiser, P. Quantitative analysis of global ubiquitination in HeLa cells by mass spectrometry. *J. Proteome Res.* **7**, 4566–4576 (2008).
- Hecht, D. & Zick, Y. Selective inhibition of protein tyrosine phosphatase activities by H<sub>2</sub>O<sub>2</sub> and vanadate in vitro. *Biochem. Biophys. Res. Commun.* **188**, 773–779 (1992).
- Cox, J. & Mann, M. MaxQuant enables high peptide identification rates, individualized p.p.b.-range mass accuracies and proteome-wide protein quantification. *Nat. Biotechnol.* **26**, 1367–1372 (2008).
- Ley, R. et al. Extracellular signal-regulated kinases 1/2 are serum-stimulated “Bim(EL) kinases” that bind to the BH3-only protein Bim(EL) causing its phosphorylation and turnover. *J. Biol. Chem.* **279**, 8837–8847 (2004).
- Sands, W. A., Woolson, H. D., Milne, G. R., Rutherford, C. & Palmer, T. M. Exchange protein activated by cyclic AMP (Epac)-mediated induction of suppressor of cytokine signaling 3 (SOCS-3) in vascular endothelial cells. *Mol. Cell Biol.* **26**, 6333–6346 (2006).
- Woolson, H. D., Thomson, V. S., Rutherford, C., Yarwood, S. J. & Palmer, T. M. Selective inhibition of cytokine-activated extracellular signal-regulated kinase by cyclic AMP via Epac1-dependent induction of suppressor of cytokine signalling-3. *Cell. Signal.* **21**, 1706–1715 (2009).
- Krump-Konvalinkova, V. et al. Establishment and characterization of an angiosarcoma-derived cell line, AS-M. *Endothelium* **10**, 319–328 (2009).
- Fass, D. M., Butler, J. E. F. & Goodman, R. H. Deacetylase activity is required for cAMP activation of a subset of CREB target genes. *J. Biol. Chem.* **278**, 43014–43019 (2003).
- Lehmann, U. et al. SHP2 and SOCS3 contribute to Tyr-759-dependent attenuation of interleukin-6 signaling through gp130. *J. Biol. Chem.* **278**, 661–671 (2003).
- Sasaki, A. et al. Cytokine-inducible SH2 protein-3 (CIS3/SOCS3) inhibits Janus tyrosine kinase by binding through the N-terminal kinase inhibitory region as well as SH2 domain. *Genes Cells* **4**, 339–351 (1999).
- Hill, M. M. et al. PTRF-Cavin, a conserved cytoplasmic protein required for caveola formation and function. *Cell* **132**, 113–124 (2008).
- Babon, J. J. et al. Secondary structure assignment of mouse SOCS3 by NMR defines the domain boundaries and identifies an unstructured insertion in the SH2 domain. *FEBS J.* **272**, 6120–6130 (2005).
- Sandhu, K. S. & Dash, D. Conformational flexibility may explain multiple cellular roles of PEST motifs. *Proteins Struct. Funct. Bioinforma.* **63**, 727–732 (2006).
- Sue, S.-C. & Dyson, H. J. Interaction of the IkappaBalpha C-terminal PEST sequence with NF-kappaB: insights into the inhibition of NF-kappaB DNA binding by IkappaBalpha. *J. Mol. Biol.* **388**, 824–838 (2009).
- Babon, J. J. et al. The structure of SOCS3 reveals the basis of the extended SH2 domain function and identifies an unstructured insertion that regulates stability. *Mol. Cell* **22**, 205–216 (2006).
- Hansen, C. G. & Nichols, B. J. Exploring the caves: caveolins and caveolae. *Trends Cell Biol.* **20**, 177–186 (2010).
- Hill, M. M. et al. Co-regulation of cell polarization and migration by caveolar proteins PTRF/Cavin-1 and caveolin-1. *PLoS ONE* **7**, e43041 (2012).
- Kaptein, A., Paillard, V. & Saunders, M. Dominant negative stat3 mutant inhibits interleukin-6-induced Jak-STAT signal transduction. *J. Biol. Chem.* **271**, 5961–5964 (1996).
- Decker, T. & Kovarik, P. Serine phosphorylation of STATs. *Oncogene* **19**, 2628–2637 (2000).
- Heinrich, P. C. et al. Principles of interleukin (IL)-6-type cytokine signalling and its regulation. *Biochem. J.* **374**, 1–20 (2003).
- Croker, B. A. et al. SOCS3 negatively regulates IL-6 signaling in vivo. *Nat. Immunol.* **4**, 540–545 (2003).
- Lang, R. et al. SOCS3 regulates the plasticity of gp130 signaling. *Nat. Immunol.* **4**, 546–550 (2003).
- Brender, C. et al. Suppressor of cytokine signaling 3 regulates CD8 T-cell proliferation by inhibition of interleukins 6 and 27. *Blood* **110**, 2528–2536 (2007).
- Yarwood, S. J., Borland, G., Sands, W. A. & Palmer, T. M. Identification of CCAAT/enhancer-binding proteins as exchange protein activated by cAMP-activated transcription factors that mediate the induction of the SOCS-3 gene. *J. Biol. Chem.* **283**, 6843–6853 (2008).
- Tagwerker, C. et al. A tandem affinity tag for two-step purification under fully denaturing conditions: application in ubiquitin profiling and protein complex identification combined with in vivo cross-linking. *Mol. Cell Proteom.* **5**, 737–748 (2006).
- García-Cardena, G. et al. Dissecting the interaction between nitric oxide synthase (NOS) and caveolin: functional significance of the nos caveolin binding domain in vivo. *J. Biol. Chem.* **272**, 25437–25440 (1997).
- Li, S., Couet, J. & Lisanti, M. P. Src tyrosine kinases, alpha subunits, and h-ras share a common membrane-anchored scaffolding protein, caveolin. caveolin binding negatively regulates the auto-activation of src tyrosine kinases. *J. Biol. Chem.* **271**, 29182–29190 (1996).
- Buk, D. M. et al. Polarity and lipid raft association of the components of the ciliary neurotrophic factor receptor complex in Madin-Darby canine kidney cells. *J. Cell Sci.* **117**, 2063–2075 (2004).
- Yanagisawa, M., Nakamura, K. & Taga, T. Roles of lipid rafts in integrin-dependent adhesion and gp130 signalling pathway in mouse embryonic neural precursor cells. *Genes Cells* **9**, 801–809 (2004).
- Yang, N., Huang, Y., Jiang, J. & Frank, S. J. Caveolar and lipid raft localization of the growth hormone receptor and its signaling elements: impact on growth hormone signaling. *J. Biol. Chem.* **279**, 20898–20905 (2004).
- Park, D. S. et al. Caveolin-1-deficient mice show accelerated mammary gland development during pregnancy, premature lactation, and hyperactivation of the Jak-2/STAT5a signaling cascade. *Mol. Biol. Cell* **13**, 3416–3430 (2002).

53. Sotgia, F., Schubert, W., Pestell, R. G. & Lisanti, M. P. Genetic ablation of caveolin-1 in mammary epithelial cells increases milk production and hyper-activates STAT5a signaling. *Cancer Biol. Ther.* **5**, 292–297 (2006).
54. Mukhopadhyay, S. et al. Cytoplasmic provenance of STAT3 and PY-STAT3 in the endolysosomal compartments in pulmonary arterial endothelial and smooth muscle cells: implications in pulmonary arterial hypertension. *Am. J. Physiol. Lung Cell. Mol. Physiol.* **294**, L449–L468 (2008).
55. Zhang, P.-J. et al. CUE domain containing 2 regulates degradation of progesterone receptor by ubiquitin-proteasome. *EMBO J.* **26**, 1831–1842 (2007).
56. Schmitz, J., Weissenbach, M., Haan, S., Heinrich, P. C. & Schaper, F. SOCS3 exerts its inhibitory function on interleukin-6 signal transduction through the SHP2 recruitment site of gp130. *J. Biol. Chem.* **275**, 12848–12856 (2000).
57. Lin, Q. et al. The HECT E3 ubiquitin ligase NEDD4 interacts with and ubiquitinates SQSTM1 for inclusion body autophagy. *J. Cell Sci.* **130**, 3839–3850 (2017).
58. Morén, B. et al. EHD2 regulates caveolar dynamics via ATP-driven targeting and oligomerization. *Mol. Biol. Cell* **23**, 1316–1329 (2012).
59. Bastiani, M. et al. MURC/Cavin-4 and cavin family members form tissue-specific caveolar complexes. *J. Cell Biol.* **185**, 1259–1273 (2009).
60. Gambin, Y. et al. Single-molecule analysis reveals self assembly and nanoscale segregation of two distinct cavin subcomplexes on caveolae. *Elife* **3**, e01434 (2014).
61. Ludwig, A. et al. Molecular composition and ultrastructure of the caveolar coat complex. *PLoS Biol.* **11**, e1001640 (2013).
62. Subramaniam, P. S. & Johnson, H. M. Lipid microdomains are required sites for the selective endocytosis and nuclear translocation of IFN- $\gamma$ . Its receptor chain IFN- Receptor-1, and the phosphorylation and nuclear translocation of STAT1. *J. Immunol.* **169**, 1959–1969 (2002).
63. Hayashi, Y. K. et al. Human PTRF mutations cause secondary deficiency of caveolins resulting in muscular dystrophy with generalized lipodystrophy. *J. Clin. Invest.* **119**, 2623–2633 (2009).
64. Rajab, A. et al. Fatal cardiac arrhythmia and long-QT syndrome in a new form of congenital generalized lipodystrophy with muscle rippling (CGL4) due to PTRF-CAVIN mutations. *PLoS Genet.* **6**, e1000874 (2010).
65. Dwianingsih, E. K. et al. Child with asymptomatic elevation of serum creatine kinase shows PTRF-CAVIN mutation matching with congenital generalized lipodystrophy type 4. *Mol. Genet. Metab.* **101**, 233–237 (2010).
66. Ardisson, A. et al. Novel PTRF mutation in a child with mild myopathy and very mild congenital lipodystrophy. *BMC Med. Genet.* **14**, 89 (2013).
67. Yajima, T. et al. Absence of SOCS3 in the cardiomyocyte increases mortality in a gp130-dependent manner accompanied by contractile dysfunction and ventricular arrhythmias. *Circulation* **124**, 2690–2701 (2011).
68. Suessmuth, Y. et al. A new polycythaemia vera-associated SOCS3 SH2 mutant (SOCS3F136L) cannot regulate erythropoietin responses. *Br. J. Haematol.* **147**, 450–458 (2009).
69. Kawaguchi, T. et al. Hepatitis C virus down-regulates insulin receptor substrates 1 and 2 through up-regulation of suppressor of cytokine signaling 3. *Am. J. Pathol.* **165**, 1499–1508 (2004).
70. Bendall, S. C. et al. Prevention of amino acid conversion in SILAC experiments with embryonic stem cells. *Mol. Cell Proteom.* **7**, 1587–1597 (2008).
71. Nicholson, S. E. et al. Mutational analyses of the SOCS proteins suggest a dual domain requirement but distinct mechanisms for inhibition of LIF and IL-6 signal transduction. *EMBO J.* **18**, 375–385 (1999).
72. Cox, J. & Mann, M. MaxQuant enables high peptide identification rates, individualized p.p.b.-range mass accuracies and proteome-wide protein quantification. *Nat. Biotechnol.* **26**, 1367–1372 (2008).
73. Cox, J. et al. Andromeda: a peptide search engine integrated into the MaxQuant environment. *J. Proteome Res.* **10**, 1794–1805 (2011).
74. Rutherford, C. et al. Regulation of cell survival by sphingosine-1-phosphate receptor S1P1 via reciprocal ERK-dependent suppression of Bim and PI-3-kinase/protein kinase C-mediated upregulation of Mcl-1. *Cell Death Dis.* **4**, e927 (2013).
75. Safhi, M. M. A., Rutherford, C., Ledent, C., Sands, W. A. & Palmer, T. M. Priming of signal transducer and activator of transcription proteins for cytokine-triggered polyubiquitylation and degradation by the A2A adenosine receptor. *Mol. Pharmacol.* **77**, 968–978 (2010).
76. Brown, K. M. et al. Phosphodiesterase-8A binds to and regulates Raf-1 kinase. *Proc. Natl. Acad. Sci. USA* **110**, E1533–E1542 (2013).

## Acknowledgements

The authors thank Drs Aki Yoshimura, Jeff Babon, and Ben Nichols for provision of expression constructs, Dr John Pediani for assistance with confocal imaging, and Mrs Margaret Mullin for assistance with TEM. This work was supported by project grants to T.M.P. from the Chief Scientist Office (ETM/226), British Heart Foundation (PG12/1/29276, PG 14/32/30812), and a National Health Service Greater Glasgow and Clyde Research Endowment Fund (2011REFCH08). P.F.P. was supported by the National Institutes of Health grant DK097708. J.J.L.W. was supported by a doctoral training studentship from the Biotechnology and Biological Sciences Research Council Doctoral Training Programme in Biochemistry and Molecular Biology at the University of Glasgow (BB/F016735/1). N.A. was supported by a Saudi Government PhD Scholarship. This work was also supported in part by equipment grants to T.M.P. from Diabetes UK (BDA 11/0004309) and Alzheimer's Research UK (ARUK-EG2016A-3).

## Author contributions

J.J.L.W. designed and performed all the experiments except where indicated. Generation of the WT and SOCS3-null AS-M.5 cells and the data presented in Figs. 1b, c, 2b, c and 7a–c and Supplementary Figs. 2, 5 and 6 were performed by N.A. Supplementary Figure 3 was generated by L.L. under the supervision of P.F.P. P.F.P. also provided technical advice on use of the *cavin-1*<sup>-/-</sup> MEFs. The proteomics experiments that resulted in the initial identification of cavin-1 were carried out under the supervision of W.M. and R.B. G.S.B. supervised the design and synthesis of the peptide array experiments. F.S. devised the peptide pull-down experiments and provided advice on use of several of the mutated SOCS3 constructs. T.M.P. conceived and designed the study, supervised the data analysis, and wrote the paper with input from all authors.

## Additional information

**Supplementary Information** accompanies this paper at <https://doi.org/10.1038/s41467-017-02585-y>.

**Competing interests:** The authors declare no competing financial interests.

**Reprints and permission** information is available online at <http://npg.nature.com/reprintsandpermissions/>

**Publisher's note:** Springer Nature remains neutral with regard to jurisdictional claims in published maps and institutional affiliations.



**Open Access** This article is licensed under a Creative Commons Attribution 4.0 International License, which permits use, sharing, adaptation, distribution and reproduction in any medium or format, as long as you give appropriate credit to the original author(s) and the source, provide a link to the Creative Commons license, and indicate if changes were made. The images or other third party material in this article are included in the article's Creative Commons license, unless indicated otherwise in a credit line to the material. If material is not included in the article's Creative Commons license and your intended use is not permitted by statutory regulation or exceeds the permitted use, you will need to obtain permission directly from the copyright holder. To view a copy of this license, visit <http://creativecommons.org/licenses/by/4.0/>.

© The Author(s) 2018